Magnetostriction in transition metal - metalloid metallic glasses

Thomas, Andrew P.

Award date:
1991

Awarding institution:
University of Bath

Magnetostriction in Transition Metal - Metalloid Metallic Glasses

Submitted by Andrew P. Thomas

for the degree of PhD

of the University of Bath

1991

A. Thomas

ProQuest LLC
789 East Eisenhower Parkway
P.O. Box 1346
Ann Arbor, MI 48106-1346

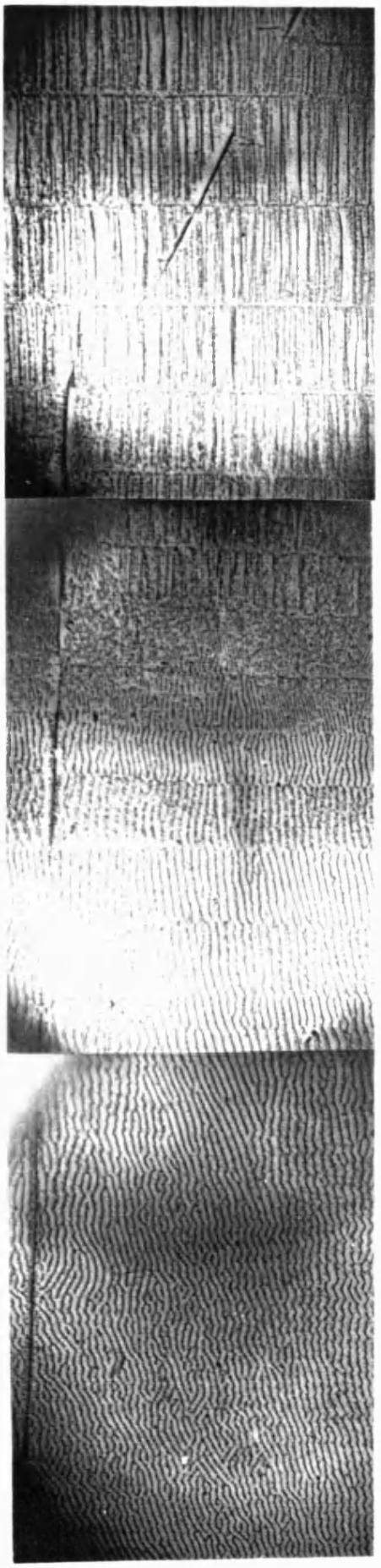

PREFACE

Parts of this work, or work related to it, have been published or are to be published in the following papers:

Squire P.T., M.R.J. Gibbs and A.P. Thomas, "Magnetostriction of Obliquely Annealed Metallic Glass", *J. Magn. Magn. Mat.* 83 (1990) 179.

Thomas A.P., M.R.J. Gibbs and P.T. Squire, "Dependence of Magnetostriction on Induced Anisotropy in Metallic Glasses", *IEEE Trans. Mag.* MAG-26 (1990) 1406.

Thomas A.P. and M.R.J. Gibbs, "Anisotropy and Magnetostriction in Metallic Glasses", to be published in *J. Magn. Magn. Mat.* (1991).

Thomas A.P., M.R.J. Gibbs, J.H. Vincent and S.J. Ritchie, "Technical Magnetostriction Parameters for Application of Metallic Glass", to be published in *J. Appl. Phys.* in the proceedings of INTERMAG/MMM'91, Pittsburgh USA (1991).

Thomas A.P., M.R.J. Gibbs, J.H. Vincent and S.J. Ritchie, "Magnetostriction in Surface Crystallised Fe- and Fe-Ni based Metallic glasses", to be published in *IEEE Trans. Mag.* in the proceedings of INTERMAG/MMM'91, Pittsburgh USA (1991).

Squire P.T., A.P. Thomas, M.R.J. Gibbs and M. Kuzminski, "Domain Studies of Field-Annealed Amorphous Ribbon", to be published in *J. Magn. Magn. Mat.* in the proceedings of ICM'91, Edinburgh (1991).

Pankhurst Q.A., M.R.J. Gibbs and A.P. Thomas, "Moment Distribution in $Fe_{78}B_{13}Si_{19}$ Ribbons by Mössbauer Spectroscopy", to be published in *J. Magn. Magn. Mat.* in the proceedings of ICM'91, Edinburgh (1991).

Gibbs M.R.J., "The Effect of Large Spread in Moment Directions on Anisotropy and Magnetostriction in Amorphous Alloys", *Proc. 5th Int. Conf. Physics of Magnetic Materials*, Madralin near Warsaw, Poland (World Scientific, 1990) 242.

I would like to express my sincere thanks to Dr. Mike Gibbs for his constant help and guidance throughout the project. I am also very grateful to Mr. P.T. Squire, Dr. S.M. Sheard and Mr. J.H. Vincent for valuable discussions, and to Mr. M. Tatar for continued technical support.

The project was funded by an SERC research grant and was sponsored by GEC-Marconi Hirst Reasearch Centre.

ABSTRACT

The project is concerned with an investigation of certain magnetostrictive properties of iron and iron-nickel based metallic glasses in relation to the macroscopic magnetic anisotropy induced by a range of different anneals. The specific properties investigated were the magnetostrictive strain, λ_e, and certain magnetostrictive response parameters such as $\left|\frac{d\lambda}{dH}\right|_{max}$.

A review is made of theoretical models concerned with the prediction of the magnetostriction, and its behaviour, of materials with amorphous structure, and of magnetostriction measurement techniques applied to metallic glasses.

Measurements of magnetostrictive, magnetic and magnetelastic properties, and domain studies were made on field annealed samples where the easy axis of the induced anisotropy was at various oblique angles to the magnetisation direction. The results are compared with the predictions of one particular theoretical model concerned with samples which have an amorphous structure and obliquely induced anisotropy. Modifications required in the model are identified.

From these measurements, the angular spread in the magnetisation vector was estimated. This spread and its effect on the magnetostriction are discussed. It was concluded that the spread at atomic scales is significantly higher than previously predicted.

The magnetostrictive strain, response parameters and anisotropy constant were measured for different transverse anneal conditions. Two processes of induction of anisotropy by field anealing were identified, only one of which effected change in the magnetostriction. It was concluded that a high anisotropy constant is not essential for maximum λ_e, rather that the anisotropy be sufficiently developed to produce a uniaxial character. The anneal conditions necessary to maximise the response are discussed, with a view to optimising suitability as transducer material.

The development of λ_e by way of partial crystallisation of the metallic glass is investigated. It was concluded that partial crystallisation can provide a viable method of production of low field, good stability transducer material.

Table of Contents

1 Introduction

1.1 Aim of Study

The project has been concerned with the investigation of magnetostriction and magnetostrictive response in transition metal-metalloid (TM-M) alloys with an amorphous structure. The amorphous structure was obtained in these materials by rapid quenching from the liquid state, and as such they are termed metallic glasses. The alloys used in this work were iron and iron-nickel based. The magnetostriction and magnetostrictive response are important for the classification of perfomance and calibration in transducers. They were measured on metallic glasses with uniaxial magnetic anisotropy induced by either field annealing or by the introduction of a stress field by partial surface crystallisation. The project was divided into three parts.

1. Oblique angle field annealing. The magnetostriction parameters were measured with respect to the angle between the induced magnetic easy axis and the applied field. The results were compared with a theoretical model in order to determine the angular magnetic moment dispersion and the extent to which magnetisation occurs by moment rotation rather than domain wall movement.

2. Transverse field annealing. The magnetostriction and response were measured for samples transversely field annealed for a range of anneal times and temperatures, resulting in transversely induced magnetic easy axes with different anisotropy constants. The variation of parameters with field anneal was investigated to achieve optimum conditions for transducer applications.

3. Controlled partial crystallisation. It has been established that this induces a magnetic anisotropy with the easy axis normal to the ribbon plane in material with positive λ_s, such that the magnitude of the anisotropy constant is directly related to the

coercivity. Similar measurements to those on the transversely field annealed material were taken on samples annealed for a range of times at temperatures close to their crystallisation temperatures, and considered with respect to the extent of crystallisation in terms of the coercivity or X-ray diffraction peak areas.

In this chapter metallic glasses and the reasons for their investigation are discussed, and parameters and terms used in this study are defined. Chapter two is concerned with the structure of amorphous materials, magnetostriction and magnetic anisotropy in more detail. Chapter three covers the experimental methods and procedures. The results are presented in the subsequent chapters and the final chapter includes an overall discussion of the results and the conclusions.

1.2 Magnetic and Magnetostrictive Properties

All the relevant magnetic parameters used in this study can be derived from the magnetisation (hysteresis or M-H) curve or the magnetostriction λ-H curve. Figure 1.1 shows the main parameters. All parameters are given in S.I. units in this study (except anneal time and temperature, which are given in minutes and °C).

Saturation Magnetisation, M_s: This is simply the magnetisation at saturation. This corresponds to the state where all moments within the material are aligned as far as possible with the applied magnetic field, H, so that further increase in H has no effect on M.

Saturation Induction, B_s: The induction is given by $B=\mu_0(H+M)$ so that strictly B does not reach a maximum value with increasing H. However, since $M_s>>H$ in magnetically soft ferromagnetic material, it is a good approximation to put $B_s=\mu_0 M_s$.

Susceptibility, χ : The susceptibility at any point on the M-H curve is simply defined as M/H. The differential susceptibility is given by the gradient of the curve, dM/dH,

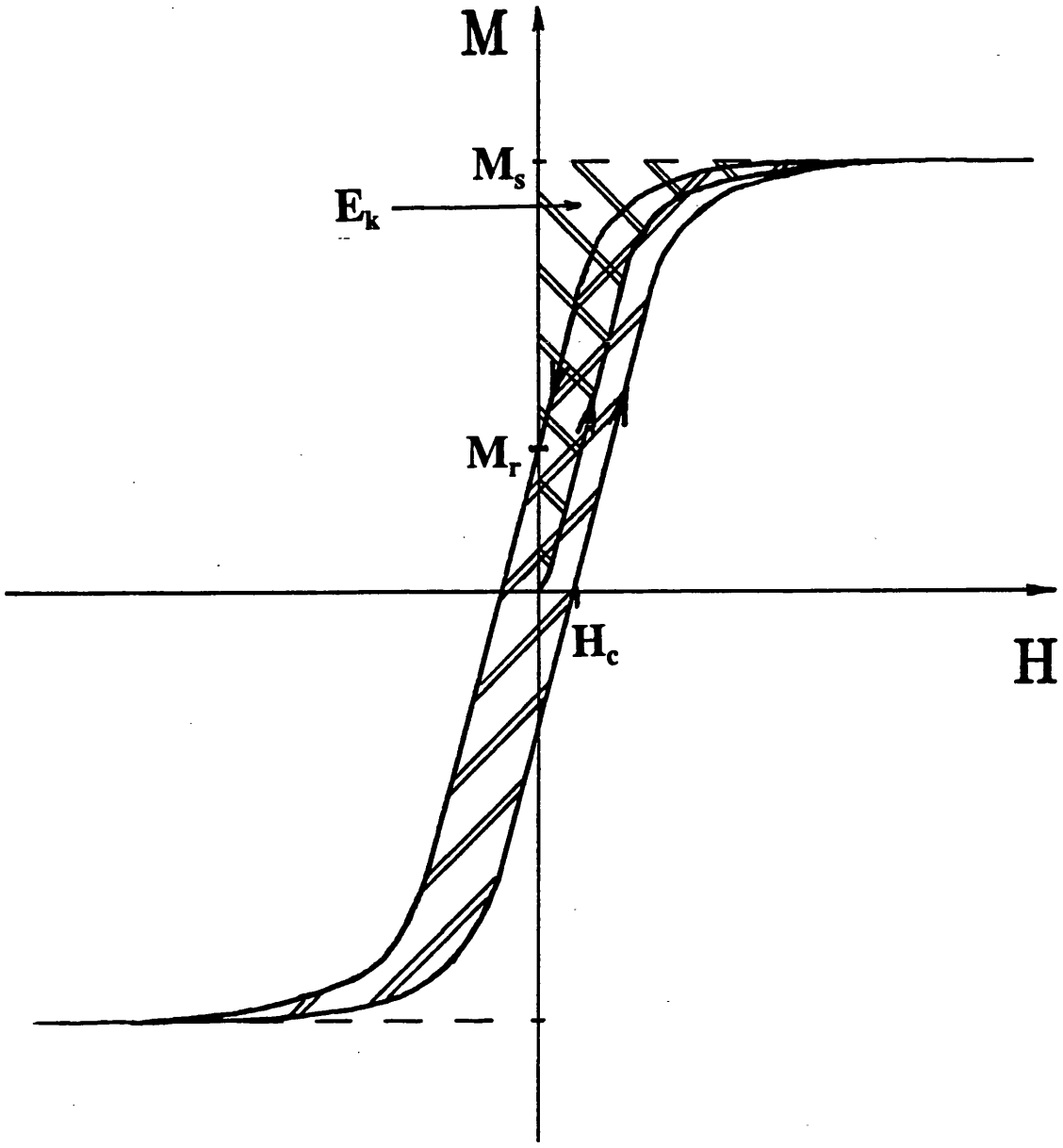

Figure 1.1 : Hysteresis curve and it's main parameters. The path of magnetisation from the demagnetised state to saturation and the major M-H loop is shown by the bold line. The saturation magnetisation, M_s, is shown, as are the crossing points of the loop at zero M and H; the remanence, M_r, and the coercivity, H_c. The hashed area between the ordinate and the curve is the anisotropy energy density, E_k, and the alternately hashed area within the loop is the energy density loss per cycle.

which becomes zero at saturation. The initial susceptibility, χ_0, is the susceptibility at M≈0. However a linear hysteresis plot with some non-zero coercivity does not have constant susceptibility, and χ can even become negative, but does have constant differential susceptibility. In this study, therefore, χ was taken to be the differential susceptibility and χ_0 to be that at M=0 ($H=\pm H_c$). This was very close to the initial susceptibility because the materials used had very small coercivities.

Anisotropy Field, H_k: This is the applied field at which saturation is achieved. It has been shown [e.g. Fähnle and Kronmüller 1978, Fähnle and Egami 1982, Garoche and Malozemoff 1984, Vázquez *et al* 1989] that in most cases in amorphous alloys the approach to saturation follows an inverse power law such that $(M_s-M)\propto H^{-n}$ (or the sum of terms with different exponents). Thus H_k can be difficult to quantify. In many cases it can be estimated by assuming a purely linear M-H loop for the region $M<M_s$, with gradient χ_0, and extrapolating to saturation, so that $H_k\approx M_s/\chi_0$.

Coercivity, H_c: The coercive field is the field required to achieve zero magnetisation from a magnetised state in the opposite direction. The coercivity is the coercive field on the major hysteresis loop between the saturated states.

Magnetic Anisotropy Energy, E_k: This is generally defined as the magnetisation energy per unit volume of the material

$$E_k = \int_0^{M_s} \mu_0 H dM = \int_0^{H_k} \mu_0 (M_s - M) dH . \qquad 1.1$$

and is the energy per unit volume required to rotate the magnetisation into the applied field direction. It is termed the anisotropy energy in materials where this magnetisation energy density is direction dependent, with the minimum occurring in a direction termed the magnetic easy axis. The variation with respect to the angle between the easy axis

and the direction of magnetisation, ϕ, is generally expressed as a series of powers of $\sin(\phi)$ so that the energy, E_k, is at a minimum when the magnetisation is collinear with the easy axis. It is limited to even powers due to symmetry. Thus

$$E_k = K_0 + K_1 \sin^2\phi + K_2 \sin^4\phi + \ldots, \qquad 1.2$$

where K_n are constants. K_0 is the isotropic term. The second order term represents uniaxial anisotropies. The fourth and higher order terms represent non-uniaxial (biaxial, etc) anisotropies and are generally small and so are neglected.

Some workers (e.g. Nielson and co-workers [Nielson 1985]) modified the definition of E_k to the difference in E_k in a material before and after induction of a magnetic anisotropy, so that negative E_k tended to indicate magnetisation along an anisotropic easy axis and positive E_k along a hard axis.

The moments were notionally fully aligned along the anneal field direction during induction of anisotropy in this study (by field anneal). There is no isotropic term in E_k in this case since there is no degree of isotropy in the moment direction. The work in turning the moments from an isotropic distribution was done in aligning the moments during the anneal and hence the isotropic term K_0 drops out from E_k. Therefore E_k measured in this project was given by $E_k=K_1\sin^2(\phi)$, giving the energy density required to fully align the local magnetisation into the applied field direction from the induced easy axis.

In this study K_L is referred to as the anisotropy constant at a local scale (over which the short range order is defined - see chapter 2). K_u refers to the corresponding macroscopic volume average value of a sample.

Loss (Hysteresis): This is the loss in energy per unit volume when the material is taken round the hysteresis loop, and is represented by the area inside the loop.

Shape Demagnetisation effect: When a sample of magnetic material is positioned within a magnetic field, it becomes magnetised. Free poles are formed on a surface where

there is a discontinuity in the component of magnetisation normal to the surface, as is the case at the ends of the sample, due to the difference in magnetisation between it and the surrounding environment. These free poles set up a field which acts in the opposite direction to the applied field within the sample, which has the effect of partially demagnetising it. This demagnetising field is proportional to the magnetisation of the sample, i.e.

$$H_d = DM, \qquad 1.3$$

where D is the demagnetisation factor. D is determined by the geometry of the sample. The demagnetising field is only uniform within ellipsoidal samples. In rectangular samples, H_d is greater at the ends than it's bulk.

The total internal magnetic field within a sample is the sum of the applied and the demagnetising fields, i.e.

$$\begin{aligned} H_i &= H_a - H_d \qquad 1.4 \\ &= H_a - DM \\ &= H_a - D\chi H_i \\ &= \frac{H_a}{(1 + D\chi)}. \end{aligned}$$

In this study, the samples used were long and thin, to maximise the sample magnetisation and minimise surface area of the ends as far as possible. Consequently, the internal fields were significantly less than the applied field. The magnetic parameters presented in this study were corrected for the shape demagnetising field, and hence were the intrinsic properties of the material independent of sample geometry.

Magnetostriction: When a material is magnetised, it can undergo a change in its dimensions. This phenomenon is termed magnetostriction. It can be divided into two types - linear and volume.

The volume magnetostriction, ω, is the isotropic change in volume, $\Delta V/V$. This occurs at large applied fields beyond saturation and is due to the field overcoming thermal spin disorder. The forced linear magnetostrictive strain is then approximately one third of the fractional volume change. The volume magnetostriction is generally very small in TM-based alloys ($\omega \sim 10^{-12}$) and Cullity [1972] stated that "it has no bearing on the behaviour of practical magnetic materials in ordinary fields". It is of negligible effect in this study and is disregarded.

Linear magnetostriction, λ, is the spontaneous uniaxial strain due to magnetisation, $\Delta l/l$. A typical plot of the field dependence of λ is shown in figure 1.2. The linear strain is directly related to the magnetisation and reaches a maximum at M_s (corresponding to H_k, where this can be defined, on the λ-H plot). As discussed in chapter 2, it occurs as a result of structural deformation due to rotation of magnetic moments as the material is magnetised.

The saturation magnetostriction constant, λ_s, is the strain of a material, measured in the direction of magnetisation, with initially randomly orientated moments, when magnetised to saturation. It is an intrinsic property of the material. Typical values are approximately -7×10^{-6} and -34×10^{-6} for polycrystalline Fe and Ni. Giant magnetostriction materials have been developed, such as Terfenol™, which have values of λ_s of some 10^{-3}.

Spontaneous linear magnetostrictive strain is elastic so that the volume of the material remains almost constant. Therefore when a sample of material with isotropic magnetostriction constant (such as polycrystalline or amorphous material) and random moment directions is saturated, the magnetostrictive strain at an angle θ to the direction of magnetisation, $\lambda(\theta)$, is given by

$$\lambda(\theta) = \frac{3}{2}\lambda_s\left(\cos^2\theta - \frac{1}{3}\right). \qquad 1.5$$

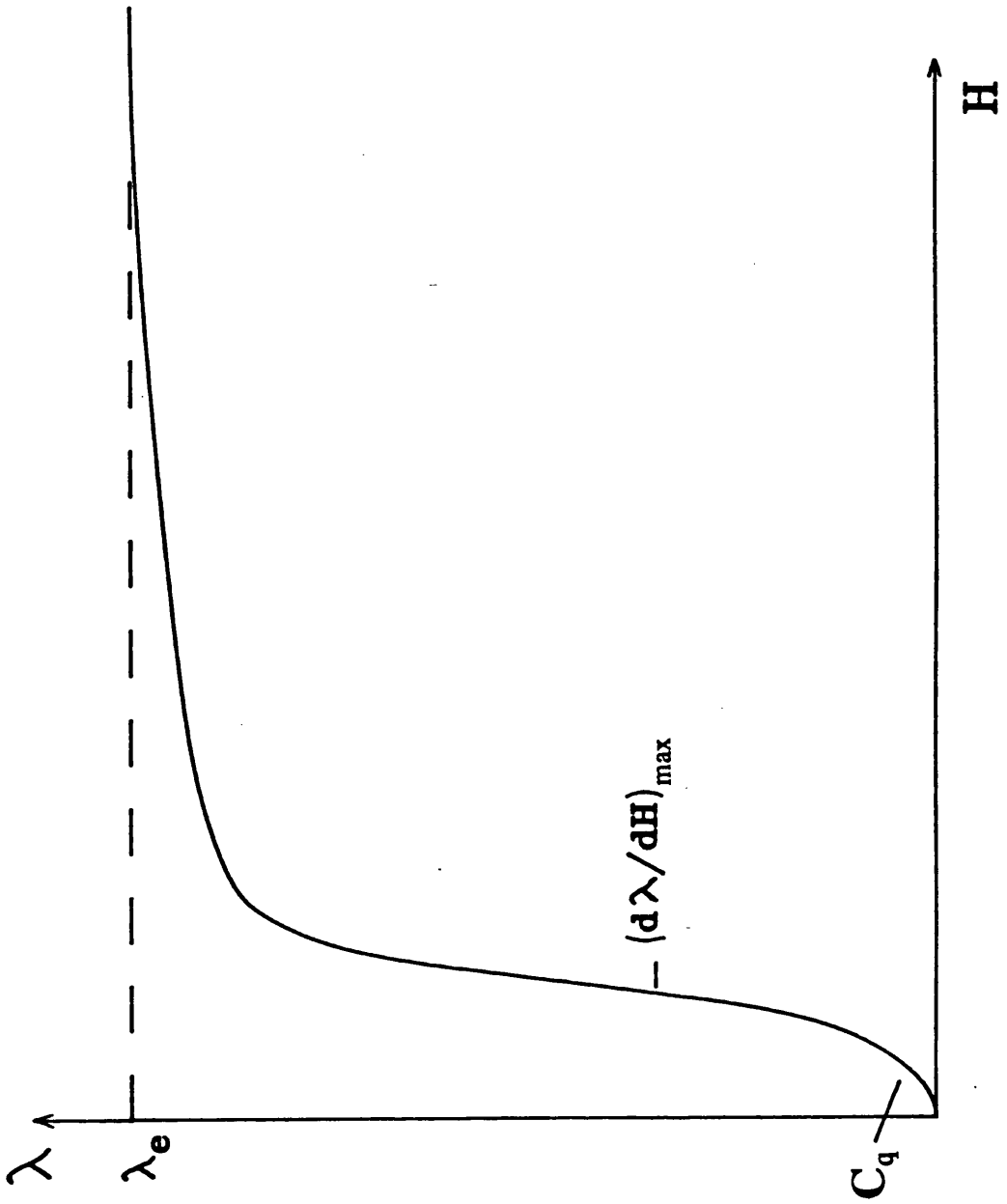

Figure 1.2 : λ-H plot and the main parameters. The engineering magnetostriction, λ_e, is the magnetostriction at saturation. The maximum gradient, $d\lambda/dH$, occurs at the inflection. Where the curve can be approximated by a quadratic at low H, C_q is the λ-H quadratic coefficient.

Thus the change in strain between longitudinally and transversely saturated material is $3\lambda_s/2$.

The engineering magnetostriction, λ_e, is defined as the difference in strain of the material before and after the application of a magnetic field which has the effect of rotating the magnetisation vector from an angle θ_i to the applied field direction to a final angle θ_f [Bucholtz *et al* 1986], so that

$$\lambda_e = \frac{3}{2}\lambda_s(\cos^2\theta_f - \cos^2\theta_i)\,. \qquad 1.6$$

Quadratic coefficients of λ-H and λ-M, C_q and C_Q: In the theoretical case where magnetisation proceeds purely by moment rotation from a transverse direction, it has been shown that λ varies quadratically with H and M [Livingston 1982] (see chapter 2). For cases where the initial magnetisation direction is not transverse, the quadratic relationship becomes an approximation [Squire 1990]. C_q and C_Q are defined as the constants of proportionality of the λ-H and λ-M quadratic components. In practical cases involving amorphous alloys this model holds well at low M and H. However, the approach to saturation of M and λ slows with respect to H (see the section on H_k for references) because of fluctuations in local properties within the material due to intrinsic defects and inhomogeneities within the material, and to variations in the internal field due to the shape of the sample [e.g. Kronmüller 1981b, Livingston 1982]. Consequently the model breaks down at the approach to saturation. The variation of λ with H can often be approximated by a polynomial (even orders only due to the symmetry of the λ-H plot). The higher order terms act as corrections from the quadratic, and are often small in well field annealed samples, i.e.

$$\lambda = C_1H^2 + C_2H^4 + \ldots \qquad 1.7$$

Maximum λ-H gradient, dλ/dH(max): In the model above, the λ-H gradient is proportional to H up to a maximum at H_k, and is zero where $H>H_k$. However, in real materials the gradient decreases on the approach to saturation. Consequently the maximum gradient occurs at an inflection well below saturation (figure 1.2). The region around the inflection can generally be closely approximated by a linear λ-H relationship.

The quadratic coefficients and maximum gradient are potentially useful parameters inasmuch as the magnetostrictive response, dλ/dH, can be described with respect to small changes in the applied field by a single parameter, either at low M, or at the λ-H inflection by the application of a bias field.

ΔE effect: The structural changes due to magnetostriction cause changes in the elastic moduli. ΔE is defined as the difference between the Young's modulus at an applied field, H, and that at saturation, and can be given by

$$\frac{\Delta E}{E_s} = \frac{E_s - E}{E_s} = 1 - \frac{E}{E_s}, \qquad 1.8$$

[Squire 1990]. It is generally a small effect but has been shown to be large in Fe-based amorphous alloys [e.g. Berry and Pritchet 1976, Arai and Tsuya 1978, Squire and Gibbs 1989] with values of up to 0.8. An expression for the variation of E in obliquely field annealed material was derived by Squire [1990]. This effect has been utilised for transducer applications [Squire and Gibbs 1987b].

Magnetoelastic Coupling Coefficient, k: This is a measure of the fraction of transfer of energy between elastic and magnetic energy when a material is magnetised. The expression for k in material with transverse anisotropy was derived by Spano *et al* [1982]

$$k = \left[1 + \left(\frac{\mu_0 M_s H_k^3}{9\lambda_s^2 E_M H^2}\right)\right]^{-\frac{1}{2}}, \qquad 1.9$$

(from Livingston [1982]), where E_M is Young's modulus at constant M. This is typically less than 0.3 in most crystalline materials [Livingston 1982], but has been measured to be over 0.9 in Fe-based amorphous alloys [Modzelewski *et al* 1981] and as high as 0.98 and 0.95 in METGLAS 2605SC [Spano *et al* 1982, Wùn-Fogle *et al* 1986]. This reflects the high efficiency these materials exhibit as magnetoelastic (or piezomagnetic) transducers.

1.3 Metallic Glasses

Metallic glasses are a class of amorphous alloys that are formed by quenching from the liquid phase so rapidly that atoms do not have time to arrange themselves into energetically favourable crystalline lattices. The glass phase is therefore a metastable one, the stability depending primarily on the composition. The stability of the structure is often significantly improved by the addition of solute atoms in the alloy or metal. These stabilise the amorphous phase by occupying positions in the structure such as to require significant structural rearrangement to attain crystallisation, and to inhibit atomic interdiffusion. Other methods of formation of amorphous materials include sputtering and chemical deposition. These, however, are not considered here. Reviews of the methods of metallic glass formation are given by Liebermann [Chapter 3 from Luborsky 1983] and Moorjani and Coey [1984]. The most common method of manufacture is melt spinning. All samples used in this study were melt spun. The alloy is melted, generally by rf inductive heating. It is then brought into contact, through a nozzle, with a rotating wheel with good thermal conductivity and high thermal mass. This rapidly solidifies the material and drags it away from the nozzle, forming a long thin ribbon. The rotational velocity of the wheel, the pressure on the melt through the nozzle and the distance between the nozzle and the wheel can be controlled to produce a uniform thickness and surface

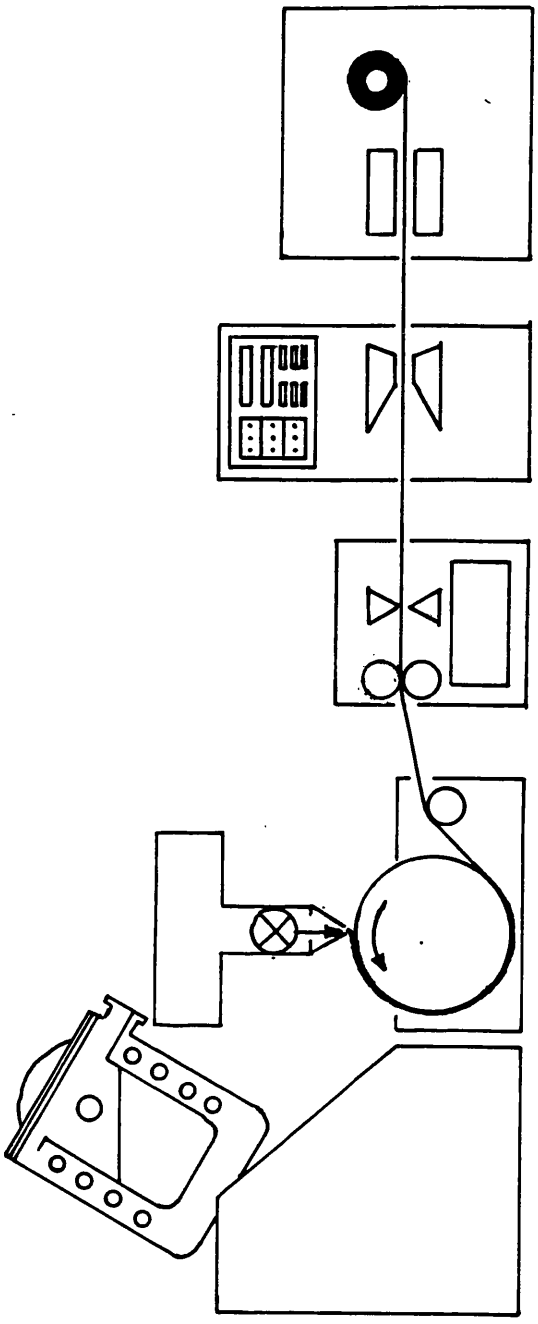

Figure 1.3 : Schematic diagram of the melt-spinning process used by Allied-Signal. The melt is pumped onto the revolving wheel at a controlled rate, and rapidly solidifies. The solid ribbon flies off the wheel and passes through a roller assembly which measures the thickness. This information is used to constantly adjust the rate of extrusion, so controlling the ribbon thickness.

finish (a schematic diagram of the system used by Allied-Signal is shown in figure 1.3). The velocity of the wheel is high to produce the required quenching rate of 10^5-$10^6 Ks^{-1}$ and the ribbon is produced at a rate of approximately 30 ms^{-1}. The process can be done in a vacuum or inert atmosphere to avoid oxidation during the process. The resulting ribbon is generally a few centimetres wide and some tens of micrometres thick.

Ferromagnetic amorphous alloys have been of great interest because they exhibit excellent soft magnetic properties compared with similar polycrystalline materials. These are discussed in the next section. These alloys are comprised of various 4f rare-earth metals (RE) and/or early 3d transition metals (TM), specifically Fe, Ni and Co, along with approximately 15-20% metalloid (M) atoms (mainly P, B, Si, C). The metalloids act as solute atoms, improving the glass stability. As well as favourable magnetic properties they also exhibit other advantageous mechanical properties. All of these result from the absence of grain boundaries which occur in polycrystalline alloys. Among the mechanical properties, metallic glasses have very high yield strengths (up to 4500MPa) and hardness. They tend to be very flexible in the as cast or flash annealed state, although can become very brittle after extensive heat treatment. They can be very resistant to corrosion since there are no grain boundaries which can be preferentially oxidised. Another important advantage of the amorphous alloys is that they are stable over wide ranges of compositions, so it is often possible to tailor the composition to achieve required material parameters, particularly when combined with controlled heat treatments. Also the manufacturing process is very cheap. The main disadvantage is that the ribbons must be very thin to achieve the quench rates required. This, together with the brittleness of heat-treated ribbons, means that they do not lend themselves to many potential applications. The maximum thickness and width of commercially available ribbons are at present approximately 30μm and 200mm. A review of reviews on amorphous alloys is given by Luborsky [1983].

1.4 Magnetic and Magnetostrictive Properties of Amorphous Alloys

The absence of any long range order in amorphous structures results in the cancelling out of the randomly oriented local crystal fields on a macroscopic scale. The absence of a macroscopic crystal field is the main reason for the soft magnetic properties exhibited by ferromagnetic amorphous alloys. The susceptibility of these alloys are far greater than the corresponding crystalline phases, without significant decrease in M_s. χ_0 was measured in this study to be of the order of 10^4 and 10^3 in longitudinally field annealed Fe and Fe-Ni based alloys (after correcting for the shape demagnetisation effect), with anisotropy fields of some $10^2 Am^{-1}$ and correspondingly low anisotropy energies. It can be as high as 10^6 in Fe-based alloys when annealed in a toroidal form such that shape demagnetisation is completely removed. Since the structure contains no grain boundaries to act as domain wall pinning sites, the hysteresis is also far lower, with H_c typically below $1 Am^{-1}$ in stress relieved material. The amorphous structure is effective in scattering conduction electrons, resulting in high electrical resistivities. This is an advantage in soft magnetic materials on account of the lower eddy currents which result due to domain wall movement, suppressing the wall movement, so reducing the susceptibility, especially in ac applications. Higher electrical resistivity leads to lower eddy currents.

As a result of the manufacturing process, the air cooled and wheel cooled sides are different, as shown by optical micrographs [e.g. Lemcke 1989]. The air cooled side is shinier, i.e. has lower surface roughness than the wheel cooled side. The surface features are different in that they are of the form of small asperities in the case of the former, and tend to be pits on the latter caused by bubbles of air and vapour trapped between the material and the wheel. These features tend to be anisotropic, lying along the ribbon axis because of the nature of ribbon formation. The surface features on the air side are due to uneven ribbon thickness. These therefore lead to regions of non-uniform thermal mass,

which in turn lead to non-uniform quench rates, with material at asperities cooling at slower rates. The material around air bubbles on the wheel side are insulated from the wheel and consequently also cool at slower rates. Regions of slower quench rates undergo thermal contraction at slower rates. As a result, stresses are induced between regions of different quench rates. The profile of stresses within as cast ribbons are discussed and shown diagrammatically by Hodson [1986]. These degrade the soft magnetic properties of the material if the magnetostriction constant is non-zero. The randomness in the stress induced easy axes causes maze domain structures as illustrated by domain patterns of as cast ribbons [Leamy *et al* 1975, Schroeder 1978, Livingston 1979], figure 1.4. The presence of internal stress in a non-zero magnetostriction material can be reflected in the coercivity, H_c. Stresses induce easy axes of magnetisation through magnetoelastic coupling. The moments within a domain wall lie in intermediate directions between the directions of magnetisation of the domains. If the moments within a wall tend to lie in the same direction as the easy axis induced by a stress at a region in the material then the wall tends to be pinned at that region due to the reduction in the magnetic anisotropy energy. Thus domain walls are pinned at or away from these regions of stress (depending on the direction of the easy axis relative to that of the domain wall), giving rise to hysteresis in the M-H loop. In an unstressed amorphous alloy, no such pinning sites should occur, since the easy axis of magnetisation, which is determined predominantly by the structure, is random in direction over length scales smaller than that of the domain wall width, with the result that the coercivity should be close to zero. The coercivity is non-zero in fully stress relieved material (such that there is no domain wall pinning by local stress fields) as a result of a number of factors discussed in Kronmüller [1981a], the most predominant of which is surface irregularities. In that paper, it was calculated that this coercivity has an upper limit of approximately 0.5 Am^{-1} for a typical Fe-Ni-P-B ribbon.

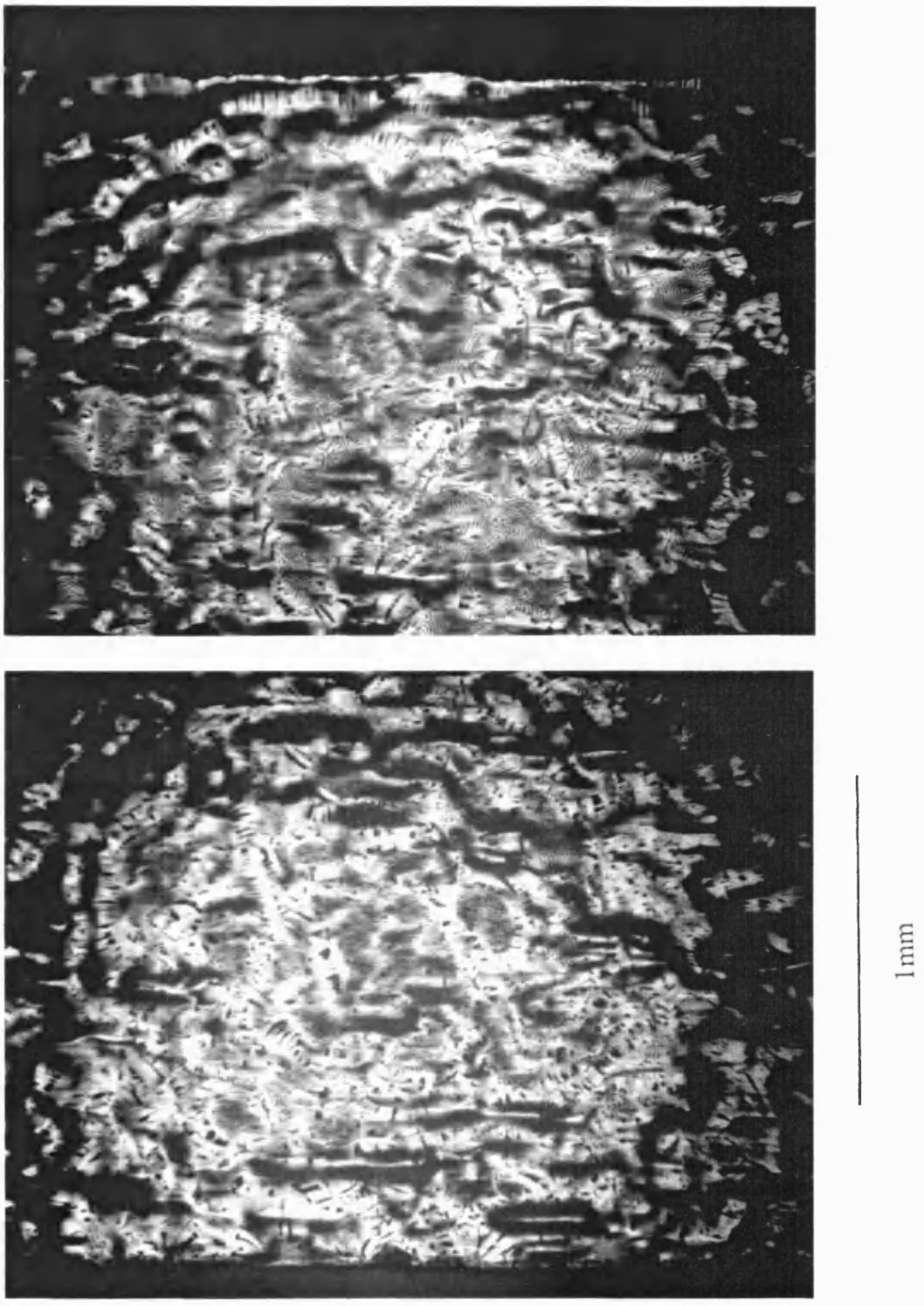

Figure 1.4 : Photograph of typical Bitter domain pattern of as cast ribbon of Fe-Ni based alloy. The maze patterns are caused by surface closure domains which occur at regions with a component of magnetisation out of the ribbon plane. The radial patterns are caused by induced anisotropy around localised stress centres.

The magnetostriction constants, λ_s, for Fe-Ni-Co based binary alloys are compared with those for the corresponding crystalline phases in O'Handley [1977a]. They are of the same order, $\sim 10^{-5}$-10^{-6}, reflecting similarities in the structure at atomic scales. Because of the higher susceptibilities, however, the magnetostrictive response of the former tend to be correspondingly higher than the latter. The low anisotropy energy is primarily the reason for the very high magnetoelastic coupling constant of the amorphous materials.

1.5 Applications

The relatively high magnetostriction constant and the low anisotropy constant resulting in the very high magnetoelastic coupling coefficient make these materials very suitable for transducer applications. At present the most common transducer materials are piezoelectric ceramics, such as lead zirconate titanate (PZT), which has an electromechanical coupling coefficient of approximately 0.6. The giant magnetostriction RE-TM alloys, such as Terfenol™, have magnetomechanical coupling of around 0.65. Amorphous ferromagnetic materials can have values of k which are significantly greater than this, particularly TM-M alloys. Some reported values of k of several of the more common TM-M alloys are given in table 1.1.

Alloy	k	Reference
METGLAS 2605SC	>0.9	Allied-Signal
	>0.9	Modzelewski *et al* 1981
	0.95	Wun-Fogle *et al* 1986
	0.969	Clark and Wun-Fogle 1989
	0.98	Spano *et al* 1982
METGLAS 2605S2	0.93	Allied-Signal
	>0.9	Anderson 1982
	0.93	Wun-Fogle *et al* 1986
	0.935	Clark and Wun-Fogle 1989
METGLAS 2605S3 ($Fe_{77}C_2Si_5B_{16}$)	0.85	Allied-Signal
	>0.9	Anderson 1982
METGLAS 2605CO ($Fe_{67}Co_{18}Si_{11}B_{14}$)	0.76	Allied-Signal
	0.71	Modzelewski *et al* 1981
	0.79	Clark and Wun-Fogle 1989
METGLAS 2826MB	0.5	Anderson 1982

Table 1.1: Reported values of the magnetomechanical coupling coefficient, k.

A wide range of stress, pressure, strain and field sensors have been proposed or developed. For example, Squire and Gibbs [1987] utilised the change in elastic moduli to relate the magnetic field to the velocity of shear waves along a TM-M amorphous

ribbon. Bucholtz *et al* [1987] developed a potential magnetometer based on the direct measurement of magnetostrictive strain. Work has been done at Bath University on the development of sonar transducers [Gibbs *et al* 1986, Rees *et al* 1989]. A full review of the sensing applications of metallic glasses is covered by Hernando *et al* [1988] and Gibbs and Squire [1989].

Since, as stated, these materials are suitable for transducer applications because of the high λ_s and low K_u, it was suggested that λ_s/K_u might be used as a rough figure of merit for transducer suitability [Lord 1988]. Wun-Fogle *et al* [1986] found that a high value of λ_s^2/K_u^3, while necessary, was not the only factor in determining the coupling constant in a given material, and that sample thickness and surface roughness were also significant factors. There is a trend for λ_s and K_u to be roughly related in many materials. For instance, in RE-TM based alloys, such as Terfenol™, λ_s is typically of the order of 10^{-3} and K_u of the order of $10^5 Jm^{-3}$, giving a figure of merit of $10^{-8} J^{-1}m^3$. The corresponding figures for an Fe-Ni based alloy are $\lambda_s \sim 10^{-5}$ and $K_u \sim 10^3 Jm^{-3}$, also giving a figure of merit of $10^{-8} J^{-1}m^3$. Thus, although it gives an indication of transducer suitability generally, it does not differentiate between the range of operation. RE-TM alloys exhibit very large magnetostriction, but require a relatively large energy input to attain it, making them more suitable for transmitters than for receivers, and for sensors of large strains, fields, etc.

Although it is magnetostrictive transducer applications that are important in this study, there are a wide range of other applications for amorphous metals, most of which require low magnetostriction. As such, they are not reviewed here, but are covered fully in Luborsky [1983] and Moorjani and Coey [1984].

2 Theory and Literature Survey

2.1 Structure of Amorphous Materials

O'Handley [1987] stated "Magnetism - even in 3d alloys - is predominantly a local phenomenon determined by the immediate environment about potentially magnetic atoms". Consequently, it is important to determine and classify the structure of the material at an atomic (local) scale.

Amorphous structures exhibit inherent randomness by their nature. This randomness leads to intrinsic random spatial fluctuations of material parameters which depend implicitly on the structure. In crystal lattices, there is no such random structural variation, and consequently their material parameters are effectively single-valued. This is not the case for amorphous structures. The structural and material parameters are better described by distributions about the mean values, with some finite standard deviation dependent on the extent of randomness in the structure.

The most important description of the physical structure is the radial distribution function (RDF). It is determined experimentally using X-ray, neutron or electron diffraction techniques, and is simply the probability function of atomic spacing. A typical RDF for Fe- and Fe-Ni based alloys is shown in figure 1.1 [from Aur *et al* 1982 and Egami 1984]. All RDFs of these alloys show a similar basic form, i.e. a main first peak at ~0.25nm followed by two second peaks close together at ~0.42 and 0.50nm, with smaller peaks at ~0.2nm intervals becoming less distinct, up to 7-8 peaks at ~1.5nm. Beyond this the randomness of the structure averages the RDF out to a steady value. The areas under the peaks are related to the number of atoms within that range of atomic spacings. The discrete nature of the first few peaks indicate a distinct structural order at very short ranges over a few atomic spacings, with similar nearest neighbour spacing to that of the corresponding crystalline phase. This is known as the short range order (SRO)

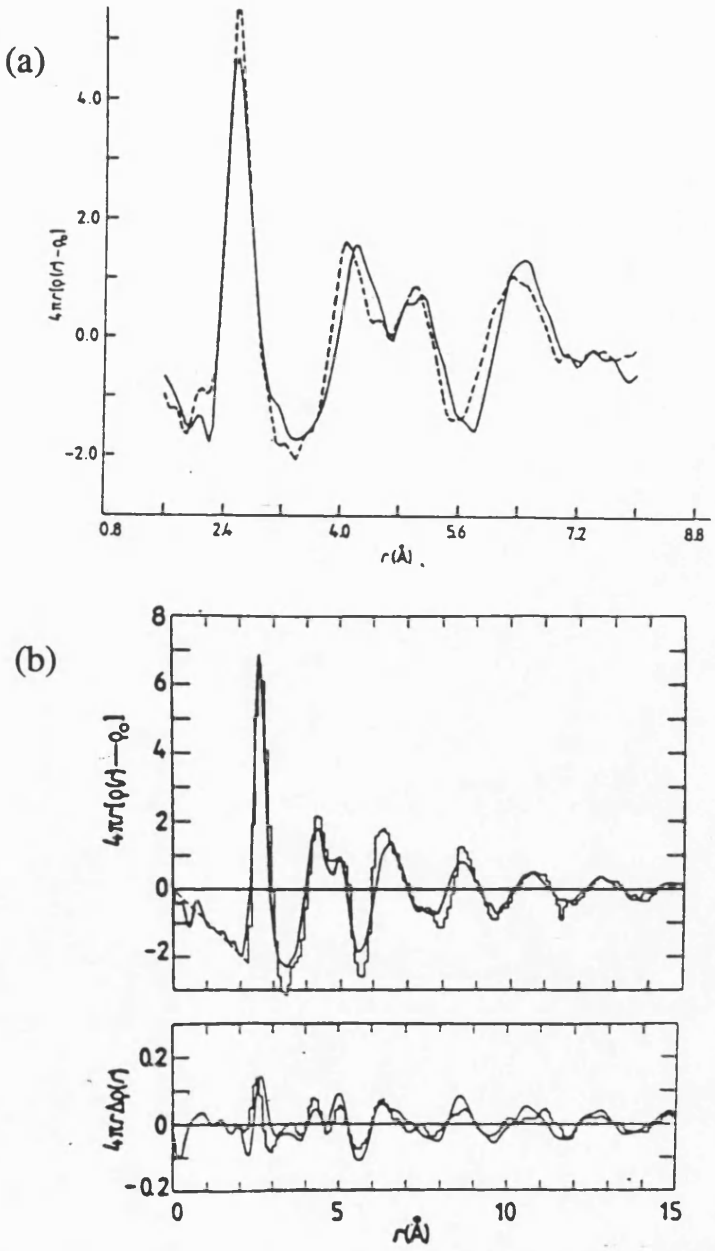

Figure 2.1: a) Reduced RDF for $Fe_{75}B_{25}$ (– – – –) and $Fe_{75}Si_{15}B_{10}$ (———) reproduced from Aur *et al* [1982]. The differences in spacings of the peaks is due to the difference in size of the metalloid atoms. b) The solid curve is the reduced RDF of $Fe_{40}Ni_{40}P_{14}B_6$, and the histogram is that of amorphous Fe (from a paper cited in Egami [1978]), reproduced from Egami [1978]. The lower plot in (b) shows the difference in the RDF due to annealing, causing relief of quenched in stresses. From this it can be seen that annealing causes the RDF peaks to become more distinct, resulting from increased short range order. In all alloys shown, the first peak occurs at approximately 0.25nm. The higher order peaks occur at approximately 0.2nm intervals, and the RDF averages out to a steady value at about 1.5nm (7-8 peaks).

of the structure. Integration of the first peak yields the number of nearest neighbours (coordination number). It has been measured at 10-12 atoms in most amorphous structures. The change in the RDF due to annealing is also shown in figure 2.1 [from Egami 1984] and demonstrates that the SRO is changed if quenched-in stresses are relieved and some degree of atomic rearrangement occurs.

A number of models have been put forward to describe the structure. These are reviewed in Egami [1984]. Possibly the most used model is based on the dense random packed (DRP) hard sphere structure [Bernal and Mason 1960], which had a similar RDF to that seen in materials by Cargill [1970]. The atomic potential was developed to improve on the hard sphere. The "soft sphere" DRP model gave a higher packing fraction, close to that of the fcc structure and therefore with a similar density. A Lennard-Jones type potential was used, although this is not critical. Egami [1984] stated that "as long as the potential is reasonably chosen, the salient features of the model seem to be the same". Other types of models have assumed a structure based on structural units such as isocahedra or Bernal polyhedra.

Becker [1978] showed that the arrangement of Fe and Ni (and P) atoms could be closely simulated by the DRP model, with the B (and other metalloids such as Si and C) atoms taking interstitial sites. It is these smaller atoms filling the Bernal holes that are too small for metal atoms that give the structure its stability by restricting atomic rearrangement, with the greatest stability at 15-20 atomic percent of the total composition. Because of the nature of these holes, there are relatively few M-M pairs, increasing the Fe content and the structural order around each B atom. The results of SRO studies by Mössbauer and NMR were reviewed by Durand [1980]. He found from these studies (see also Durand and Pannisod [1983]) that the local order seen from the metalloid sites was very strong and resembled that in the crystalline phase. Egami [1984] suggested that the local symmetry about these sites was due to the local topology rather

than by directional chemical bonding, so that there appeared to be higher symmetry about the Bernal holes that are occupied by M atoms than about metal atom sites. The SRO about TM sites is less clearly defined, with larger fluctuations. This implies strong TM-M bonding, with weaker TM-TM bonds and rare M-M bonds. Egami [1984] stated that the correct interpretation of the RDF was that the atomic environment in amorphous alloys was close to that of the DRP model but deviated slightly towards that in crystalline alloys. As shown by NMR, this is especially evident around metalloid atoms. The support for and against crystalline SRO was reviewed in O'Handley [1987]. He put the case for two types of amorphous materials - those whose SRO was close to that of a crystalline phase and those with a SRO unlike any crystalline phase. He discussed the particular case of $Fe_{1-x}B_x$, and concluded that it may be of the latter type.

The probes used in the techniques mentioned, such as an X-ray, electron or neutron beam, covered macroscopic regions of the material and the results obtained are volume averages in the form of distributions, and as such were insensitive to detail at local scale. Fluctuations in the local structure were reflected by the spread in the distribution.

2.1.1 CSRO and TSRO

The SRO has been split into two subdivisions; the geometrical or topological and chemical short range order, TSRO and CSRO respectively by Egami [1978, 1981] where they were fully defined and discussed. The TSRO describes the numbers and spacings of atoms regardless of their type. The ordering of like or unlike pairs of atoms is described by the CSRO. It was seen, for instance, that the CSRO is increased about B atoms in $(Fe\text{-}Ni\text{-}Co)_{80}B_{20}$ alloys, as discussed in the previous section. Consequently, the RDF reflects the TSRO, inasmuch as the RDF is the result of the weighted sum of partial atomic pair RDFs. However, it can be deconvoluted into the component partial functions

by a number of methods that alter the weighting factors of different atomic species, so yielding information on the CSRO. This is covered more fully by Wagner (Chapter 5 of Luborsky [1983]). The scale over which the SRO is evident, i.e. the atomic scale involving a single atom site and its nearest neighbours, is often referred to as the "local" scale.

During an anneal the atoms tend to adjust their positions slightly into arrangements with lower potential energy, dictated by the local stresses (whether mechanical or due to magnetoelastic effects) present during the anneal. These involve small topological changes in the structure and these tend to include low activation energy events since there exist a number of stable or metastable atomic sites due to the non-uniqueness of the structure, in contrast to crystalline structures where there are distinct potential wells at each lattice site. Higher temperature anneals allow higher degrees of atomic inter-diffusion and long range diffusion of defect structures. This can lead to pair ordering, i.e. changes in the CSRO. Since they require a greater degree of atomic rearrangement, CSRO changes generally involve higher activation energies than purely TSRO changes. CSRO changes, however, must by their nature involve changes in TSRO, although the opposite is not necessarily true. Thus the two types of SRO are inherently inter-related and the distinction is an arbitrary one. Both kinds of structural change lead to changes in structure-sensitive material parameters which can be both reversible and irreversible, as defined by Kronmüller *et al* [1984]. They stated that reversible relaxation processes are thought to be due to short range atomic rearrangements, and their activation energy spectrum is largely lower than that for irreversible processes (with some overlap), which include long range diffusional processes. The discussion of activation energies and comparison of reversible and irreversible changes is covered in Hygate and Gibbs [1987] and Kronmüller [1984].

2.1.2 Significance of SRO

Changes in the positions of the peaks in the RDF lead to changes in the material density. Since the atomic spacings given by the RDF peaks of the amorphous and crystalline phases are similar in most materials, so are their densities. Cargill [1975] measured only a few percent difference in density on crystallisation of the amorphous alloys. Properties that are dependent primarily on the volume average of the atomic spacing, such as the Curie temperature, T_c, and the saturation magnetisation, M_s, are insensitive to the structure of the material, only to the density. Therefore the amorphous and crystalline phases of an alloy have similar values for these parameters. Properties which are dependent on fluctuations in the structure, such as magnetic anisotropy, exchange fluctuations and local magnetostriction are more sensitive to the SRO. These parameters are characterised better by some measure of the width of the distribution of some local quantity, such as the first RDF peak. These parameters are far more dependent on factors such as composition, temperature, applied stress and field.

Characterisation of the SRO is of critical importance since it is this which dictates the behaviour of the anisotropy and magnetostriction. The local magnetostriction constant at a given site, λ_L, is related to the strain dependence of the local anisotropy constant, i.e. $\lambda_L \propto dK_L/d\varepsilon$. It is dependent on the interaction of orbital moments between nearest neighbours (i.e. orbit-lattice coupling). The local magnetostrictive strain due to an applied field is further dependent on the strength and direction of the local magnetisation. This in turn depends on the spin-spin (exchange) interactions between nearest neighbours (and so on the SRO), and the magnitude and direction of the local K_L, which is dominated by the local crystal field. The local K_L is hence also sensitive to the SRO. (It has been established that the SRO in amorphous alloys is close to that for

crystalline alloys. Therefore the local crystal field is of the same order as that of the crystalline phase. While this is the macroscopic value in crystal lattices, it rapidly averages to zero over greater volumes and is effectively zero over lengths >1.5nm).

2.2 Magnetostriction

As described in the previous section the local magnetostriction is inherently dependent on the structure at a local scale regardless of the long range nature. As mentioned, it is best described in the form of distributions in magnitude and direction. The macroscopic value is some volume average over the whole structure. The origin of the local magnetostriction is discussed in this section. Theoretical models concerning predictions of its magnitude and its behaviour with respect to composition and application of stress and field are reviewed. This is followed by a review of models for its volume average to obtain λ_s, and for the behaviour of the magnetostrictive strain of a sample of material of known λ_s.

2.2.1 Origin of Magnetostriction

Magnetostriction and anisotropy are intrinsically related, the former being the strain derivative of the latter. They both have their origin in spin-orbit coupling. Vonsovsky [1940] calculated magnetostriction constants based on a spin-orbit coupling model and found the results to agree with experiment within an order of magnitude. Kittel [1949] established that magnetostriction would be zero where the anisotropy is independent of strain. Two models for the cause of magnetostriction were proposed by Callen and Callen [1963, 1965], termed the one-ion and two-ion models. It is the one-ion magnetostriction that has its origin in spin-orbit coupling. Ions with incomplete outer electron shells or

sub-shells have non-zero magnetic moments and the shape of the shells exhibit some physical asymmetry. Such asymmetry is uniaxial so that the shape of the ions can be considered to have changed from spherical to ellipsoidal (this is a simplification because only s-subshells are spherical, and the shape is also affected by the delocalisation of electrons in the d-band). As mentioned in section 2.1, the short range order in amorphous TM-M alloys is close to that of the crystal phase, which leads to local crystal (or ligand) fields of the same order of magnitude as in the crystalline phase, although they average to zero over macroscopic distances. Because of the interactions between neighbouring atoms that arise from these local crystal fields the orbital motion of the electrons are strongly tied to the local atomic structure. Hence the electron shells are quenched into position by strong orbit-lattice coupling, where "lattice" in this context refers to the structure at the local level. When a magnetic field is applied, the moments tend to align towards the direction of the field. This has the effect of rotating the electron shells due to spin-orbit coupling, which results in some distortion of the structure due to the orbit-lattice coupling. The orbit-lattice coupling is far greater than the spin-orbit coupling in 3d metal alloys, so the resulting spin-lattice coupling is very weak and its magnitude is highly dependent on that of the spin-orbit coupling. As a consequence of the weak coupling, large moment rotations result in small distortions in the structure. This is manifested in the form of small saturation magnetostriction constants - of the order of 10^{-5}-10^{-7} in the case of most TM-M alloys. If the asymmetry of the outer shell is such that it has a long axis parallel to the moment, then the ion can be considered to have distorted from a sphere into a prolate ellipsoid, which induces a tensile strain in the moment direction, resulting in a positive magnetostriction constant. Similarly, ions with an oblate ellipsoidal overall shape lead to negative magnetostriction.

The two ion model is dictated by various anisotropic strain-dependent spin-spin interactions between pairs of ions, such as dipolar and exchange interactions.

2.2.1.1 Temperature and Composition Dependence

The contributions towards the magnetostriction from the two sources (one-ion and two-ion) are dependent on the relevant ions. Also they were shown by Callen and Callen [1963, 1965] to have different temperature variations. O'Handley [1978] gave the expression:

$$\lambda_s(T) = C_1 \hat{I}_{\frac{5}{2}}(X) + C_2 m(T)^2 . \qquad 1.1$$

The first term is the contribution from uniaxial one-ion magnetostriction. $\hat{I}_{5/2}(X)$ is a hyperbolic Bessel function, where the argument X is defined by the temperature dependence of the saturation magnetisation such that

$$\hat{I}_{\frac{3}{2}}(X) = \frac{M_s(T)}{M_s(0)} = m(T) . \qquad 1.2$$

The second term of equation 2.1 is the contribution from the two-ion model. O'Handley measured these contributions in a range of TM-M alloys and found that for Fe- and Fe-Ni based alloys the contribution due to single ions was positive and was predominant, with only a small two-ion contribution, i.e. $C_1>0$ and $C_2\sim0$. For Co-rich alloys the predominant one-ion contribution was negative and that of the two-ion was positive, partially cancelling each other, i.e. $C_1<0$ and $C_2>0$. As a result, a Co-Fe based alloy has zero magnetostriction at a certain Co:Fe ratio at a given temperature (approximately 93:7 at room temperature, O'Handley [1977]), but deviates from zero as the temperature is varied (figure 7 from O'Handley [1978]) or when an external stress is applied [Fähnle and Egami 1982]. The magnetostriction of a Fe-Co alloy can be described by combining the two one-ion contributions linearly and adding the two-ion term approximately linearly with Co content (the terms should be added quadratically at higher Co concentrations where only Co-Co interactions are significant).

The compositional dependence of λ_s at room temperature was mapped for the $(Fe\text{-}Ni\text{-}Co)_{80}B_{20}$ ternary system [O'Handley 1978]. A comparison of λ_s between amorphous and polycrystalline Fe-Ni and Fe-Co based alloys is given in O'Handley [1977]. Although there is some correlation between the variation of λ_s with composition in the case of Fe-Co, there is little between the Fe-Ni alloys. The main reason is differences in the local structure, since λ_s is strongly coupled to this. In the crystalline phase this structure is simply the lattice and is easily characterised. In amorphous alloys, however, it is neither as simple nor as homogeneous, but from the above evidence it can be inferred that the lattice structure of the Fe-Co, which is of hcp or fcc type, is closer to the apparent local structure of the corresponding amorphous alloys than the Fe-Ni lattice, which is of bcc type. This is illustrated by the coordination numbers of the structures. The hcp and fcc lattices have a coordination number of 12, while that of bcc is 8. As mentioned in section 2.1, the coordination number of most amorphous structures has been measured to be approximately 12. From this it can be inferred that λ_s is dependent primarily on the nature of the local structure, dictated by the SRO, and the presence or absence of long range order was found to have negligible effect on it [Tsuei and Lilienthal 1976].

2.2.2 Theoretical Models

Theoretical prediction of the intrinsic local magnetostriction constant is very difficult. The models reviewed in the following subsection are concerned with the prediction of the temperature and field dependence of λ_s(local) from local material and electronic properties, generally obtained from studies on corresponding crystalline

phases. Those in the next subsection deal with models for the volume averaging of λ_s(local) to obtain the macroscopic value. In the third subsection the magnetostriction parameters of a sample are obtained from the macroscopic properties such as λ_s and K_u.

2.2.2.1 Temperature and Field Dependence

A number of existing theoretical models were reviewed by Lachowicz and Szymczak [1984]. They largely divided these into one- and two-ion models following the models proposed by Callen and Callen, discussed in the previous section. These models were originally applied to crystalline lattices, but were extended to amorphous structures by O'Handley [1978]. As Lachowicz and Szymczak [1984] stated, this theory was of a phenomenological nature. It predicted the field and temperature dependence of the magnetostriction rather than its actual value with respect to composition. Szymczak and Zuberek [1981, 1982, 1983] also considered the field and temperature dependence of the magnetostriction by way of the magnetoelastic parameters. The local magnetostriction constant is related to the local magnetoelastic coefficient, B_1, by

$$\lambda = -\frac{2}{3}\left(\frac{B_1}{C_{11}-C_{12}}\right), \qquad 1.3$$

where C_{ij} are elastic moduli [Kittel 1949], and the magnetoelastic coefficient is the strain derivative of the macroscopic magnetic anisotropy [O'Handley 1987],

$$B_i = \frac{\partial E_k}{\partial \varepsilon_i}. \qquad 1.4$$

They used three different models for magnetostriction to consider its behaviour: the pair-ordering model, the random anisotropy model, and the columnar structure model. The third one pertains to the perpendicular anisotropy in amorphous RE-TM films and will not be considered here. The pair-ordering model involved two-ion pseudo-dipolar

interactions. Since the structural anisotropy parameter, which is a measure of the fractional anisotropy in atomic spacing, is small (of the order of 10^{-2}-10^{-3} in field annealed TM-M alloys [e.g. Fähnle and Furthmüller 1990]), the magnetoelastic properties depend mainly on isotropically distributed ion-pairs, giving a single isotropic magnetoelastic tensor component. The authors then derived the expression for this component with respect to the field and temperature using the theory from Callen and Callen [1963, 1965]. The random anisotropy model involved the volume average of the local magnetoelastic tensor in a system where the local magnetisation direction was a result of the competition between exchange interactions and randomly orientated local anisotropy. Given the local magnetoelastic tensor components the authors calculated the local magnetoelastic energy term, U_{me}. After averaging over all U_{me} the effective magnetoelastic tensor had isotropic properties, and it was shown that the relevant component of this tensor, B_{eff}, was some linear combination of the local magnetoelastic tensor components. In both models the temperature and field dependence of the amorphous alloys were of complicated forms, different from that predicted by Callen and Callen for crystalline structures. The authors stated that the relative importance of the models was not known, but that all mechanisms are coincident in a material to differing extents and that it is possible in principle to separate the contributions by the measurement of the field and temperature dependence of λ. Szymczak [1987] used the two models discussed to investigate the stress dependence of magnetostriction of amorphous alloys and found good agreement with experimental results.

The one-ion model proposed by Suzuki and Egami [1983] worked on the basis of the point charge model. They used the calculation of single-ion local anisotropy from the point charge model to obtain its variation with respect to strain to derive the volume averaged magnetostriction constant. They obtained the result that λ_s is zero in the unscreened point charge model in an isotropic structure. However, if the charges were

screened then the potential, f(R), had some screening term, g(R), such that

$$f(R) = \frac{g(R)}{R^3}, \qquad 1.5$$

where negative g(R) corresponds to screening and positive g(R) to anti-screening. The authors obtained a simple expression for the magnetostriction constant:

$$\lambda_s = -\sqrt{\frac{1}{30\pi}} C_\gamma^{-1} \langle \sum_j g'(R_{ij})\, R_{ij}^{-2} \rangle, \qquad 1.6$$

where C is the elastic modulus. Therefore λ_s is positive for screened point charges and negative for anti-screened. The effect exactly cancels for unscreened charges and λ_s becomes zero. Egami [1984] stated that for the electrons in the d subshells, screening corresponded to the Fermi energy being towards the bottom of the band.

Apart from the pseudo-dipolar pair ordering model, Szymczak [1978] had also proposed a model for a dipolar mechanism for magnetostriction in amorphous ferrimagnetic RE-TM alloys. The two-ion contribution is more significant in these alloys, but only has a second order effect on the one-ion contribution in TM-M alloys.

A model for magnetostriction was put forward by O'Handley and Berger [1978] in relation to the electronic structure. It was based on the premise that magnetostriction is primarily dependent on the orbital character of the electrons at the Fermi level, ε_F [Berger 1965]. The angular momentum at the Fermi level, $\langle l_z \rangle$, is approximately proportional to the product of the density of states at ε_F and its derivative with respect to energy:

$$\langle l_z \rangle_{\varepsilon_F} \propto \frac{\delta N(\varepsilon)}{\delta \varepsilon}\bigg|_{\varepsilon_F} N(\varepsilon_F). \qquad 1.7$$

The authors pointed out that the d band in amorphous TM-M alloys was split due to the combination of essentially different bands arising from each component TM species, and that the compositions of the alloys in the $(Fe\text{-}Ni\text{-}Co)_{80}B_{20}$ series where λ_s

vanished were those where the orbital angular momentum was zero. This occurred where the Fermi level lay between the two split bands, i.e. where $N(\varepsilon_F)=0$, or, if some overlap between the bands existed, at the minimum so that the slope with respect to energy was zero [O'Handley, from Luborsky 1983]. The model was developed to predict the composition of zero magnetostrictive alloys in the Co-T-B system, where T represented Fe, Mn, Cr and V [O'Handley and Sullivan 1981]. They found good agreement with experimental results after accounting for the positive two-ion magnetostriction component in the Co-rich alloys and modifications to the model to include virtual-bound-states. Egami [1984] cited evidence that $N(\varepsilon_F)$ was asymmetrical with respect to energy, with the maximum close to the top of the band and that ε_F is below this in Fe-based alloys, so that λ_s is positive. ε_F is above the maximum for Co and Ni alloys leading to negative λ_s. The variation in magnetostriction in Fe-Co and Fe-Ni alloys is approximately linear with increasing Fe content, and zero λ_s occurs at some intermediate composition. This model was geared more toward the explanation of the complex and technologically important case of zero magnetostriction than toward the prediction of λ_s with respect to composition, field and temperature. A limitation of the model was that it did not account for two-ion contributions and as such, predictions based on it will be in error to some extent, depending on this contribution, although it has met with reasonable success in the prediction of the composition of zero-magnetostrictive alloys [O'Handley 1987].

Intrinsic defects in the structure set up local stress tensors. The magnetic after-effect (i.e. the change in certain magnetic properties with time, which occurs after heat treatment, as fully described and discussed by Kronmüller and Moser in Luborsky [1983]) is based on magnetostrictive coupling between these stresses and the magnetisation. Allia *et al* [1983] showed that the permeability after-effect was related to the saturation magnetostriction, the magnetostriction constant and the second moment

of the shear stresses by

$$\frac{\Delta\mu}{\mu} \propto \frac{\lambda_s^2}{M_s}\langle\sigma^2\rangle . \qquad 1.8$$

This relationship was found to agree well with experimental results. They showed that the after-effect did not vanish for some near zero λ_s alloys. Therefore the local magnetostriction is not necessarily zero in such alloys, and the macroscopic value is some volume average, which can cancel to zero.

2.2.2.2 Volume Average of Local λ_s

O'Handley and Grant [1985] considered the macroscopic magnetostriction constant of a polycrystalline material where the crystallites were independent and randomly oriented and λ_s of the crystalline phase was known. They showed that the macroscopic value was some linear combination of the magnetostriction coefficients of the crystal structure. They then considered an amorphous alloy to behave like a random array of very small uniaxial particles, approximately 1nm in size, each with its own easy axis and anisotropy energy (citing the temperature dependence of λ_s [O'Handley 1978] as support for this assumption). When an external field was applied, the moment in each particle would rotate towards the field direction, causing the easy axis to attempt to align with the moment, so causing it to strain. The macroscopic λ_s would, in a similar way to the polycrystalline material, be some non-zero combination of the coefficients of the uniaxial particles. In this case the macroscopic λ_s would vanish only if the coefficients were zero. Therefore the model contradicted the result of Allia and Vinai [1982] and Fähnle and Egami [1982] that the macroscopic magnetostriction vanished due to the cancellation of randomly oriented strains. The authors considered only non-interacting, non-rotating, isolated structural units with random easy axes, although they added in a

footnote that when an additional factor involving some interaction between neighbouring sites was introduced, as in the model by Fähnle and Egami, this would allow zero magnetostriction due to volume averaging. They stated "the magnetostrictive strain at one site depends not only on the direction of magnetisation at that site (as we have assumed) but also upon its direction at neighbouring sites."

Fähnle and Egami [1982] proposed a similar phenomenological model involving a one-ion anisotropy mechanism for magnetostriction. This model dealt with the volume average of the magnetostrictive strains within a structure with local units which were strongly coupled together due to their elastic constants and with random anisotropy direction with a narrow distribution in its magnitude, particularly in terms of its field and temperature dependence. It was stated that this model was able to explain observed values of magnetostriction in TM-M amorphous alloys, although other mechanisms could not be excluded. This is a reflection of the predominance of the one-ion mechanism in these alloys. They stated the important fact that, whereas crystalline materials exhibit zero magnetostriction only when the strain derivative of the anisotropy coefficients are zero (as stated by Kittel [1949]), the magnetostriction in amorphous structures vanish when the volume average of the strain derivative of the single-ion anisotropy coefficients is zero, even if these local strain derivatives are non-zero.

Fähnle and co-workers have developed a comprehensive model for the magnetostriction of amorphous alloys and have discussed the results in the context of experimental results. This work is reviewed by Fähnle *et al* [1990], which lists the publications resulting from it. As with O'Handley and Grant they made the assumption that the material consisted of an array of local structural units each with their own anisotropy energy and easy axis. These could be grains within a polycrystalline material, or clusters of atoms and their nearest neighbours in amorphous structures with shapes based on Bernal polyhedra. The exact nature of the structural unit, however, was not

critical to the results of the model. Therefore this theory is applicable both to amorphous alloys and to polycrystalline materials. The model was a development of that of O'Handley and Grant inasmuch as the structural units were coupled together via the elastic interactions, so the strains of the units are different from those if they were isolated. The authors stated that as a consequence the calculation of the macroscopic λ_s from the local magnetostriction tensors becomes "rather complicated", and the calculation of the local parameters from the macroscopic value becomes "terribly complicated".

When a field is applied to a structure as described in the model, the structural units tend to reduce their anisotropy energy by two processes. One is for their easy axes to rotate into the field direction by rotation of the whole unit (reorientation process). Because of the elastic constraints on each unit by its neighbours this rotation is small in practice, and it was shown that the contribution to λ_s from rigid unit rotation is very small [Furthmüller *et al* 1987]. The other process was termed the conventional mechanism. A unit would reduce the anisotropy constant by undergoing spontaneous magnetostrictive strains to modify the easy axis direction by way of shear deformations of atoms within the units, and also by modification of the anisotropy energy strength. The principle of shear deformation induced easy axis rotation is illustrated in figure 1.2 (from Furthmüller *et al* [1987]). There were basically two different methods of summation of the elastically coupled local strains to obtain an expression for the macroscopic magnetostriction; the incompatibility method and the balance of forces method. These are fully discussed in Furthmüller *et al* [1987].

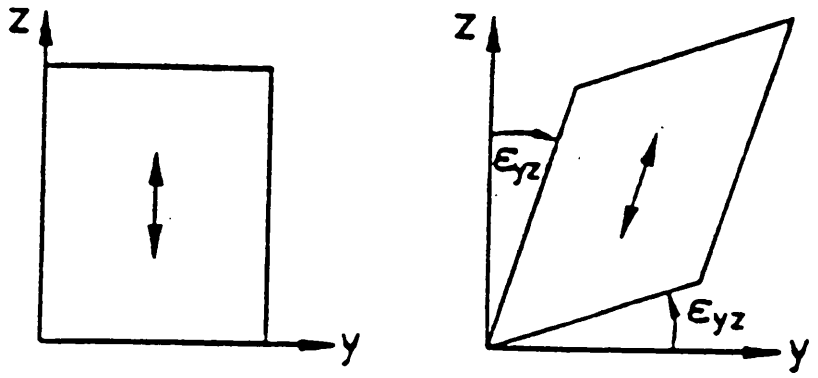

Figure 2.2: Rotation of easy axis by shear deformation. This shows schematically how the magnetisation direction of a local structural unit can be rotated by the shear stresses (reproduced from Furthmüller and Fähnle [1988])

The incompatibility method [Fähnle and Furthmüller 1988] required a gedanken experiment beginning with the structure in its initial state. The exchange interactions are removed and the structural units "cut" from each other, removing the elastic interactions (figure 1.3). The material is then fully magnetised. In this method the reorientation mechanism is forbidden, otherwise all units would simply undergo rigid rotations so that their easy axes lay in the field direction at this point. The units then reduce their anisotropy energy by the conventional mechanism, causing the units to undergo magnetostrictive strains, which because of the random nature of the structure, would all be different, and the units naturally would not fit back together again. To restore the compatibility of the material the units are strained by elastic interactions. This is arrived at by the minimisation of the sum of the anisotropy and elastic energy densities. The macroscopic magnetostriction is related to the average local strain tensor, so that where the elastic interactions are zero, it is related only to the mean magnetostrictive strain, as predicted in the non-interacting model of O'Handley and Grant. The intrinsic fluctuations in the elastic and magnetostrictive properties in the material lead to a distribution in the local unit strain, $\varepsilon_{ij}(\mathbf{r})$, which was calculated in the form of a perturbation series, which modified the results of the summation. The result of the calculation taking into account only the zeroth order in the series (i.e. taking only the mean values for the material properties and ignoring the fluctuations) was the same as that for the non-interacting model. This is because the effect of the elastic couplings averages out macroscopically. The value of the macroscopic λ_s was calculated for Co and Gd using the material parameters of the crystalline phases. They found that in the case of Co (which is of importance here because the relevant crystalline material parameters are similar to those of Fe and Ni) the modification of λ_s due to the inclusion of the first and second orders of the perturbation series was of the order of 1-10% depending on the local magnetostriction values. Therefore the effect of the elastic couplings was fairly small

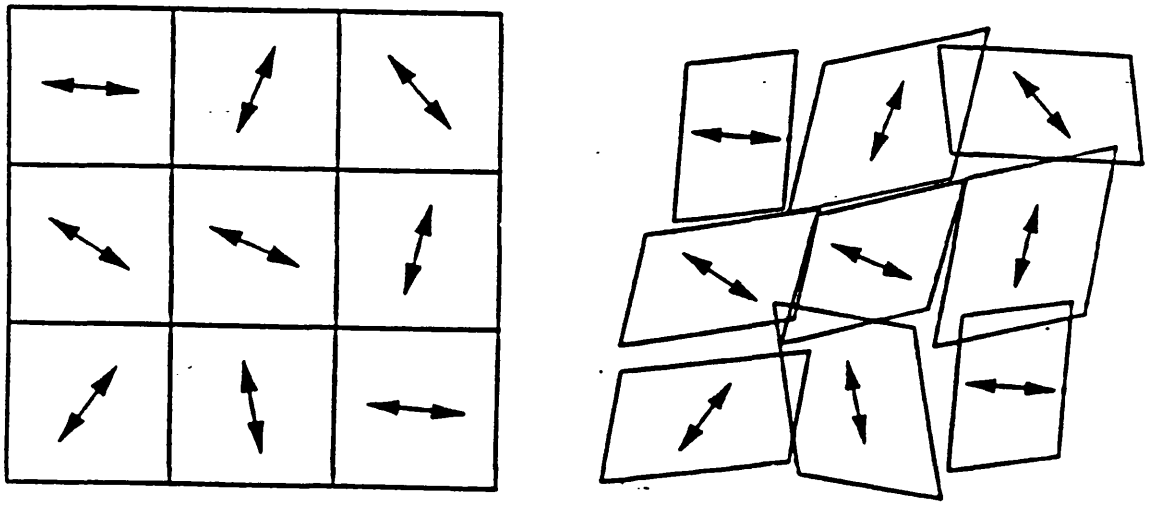

Figure 2.3: Start point for the gedanken experiment leading to the compatability method for the formulation of λ_s, reproduced from Fähnle *et al* [1990]. a) The local structural units are coupled together and have random easy axis directions. b) The elastic coupling is "removed", allowing each local unit to spontaneously strain along the easy axes. The method then allows for this assembly to be magnetised (without rigid rotation of the units), followed by the re-introduction of the elastic coupling.

and the non-interacting model is a good approximation. The coupling effects reduced the value of λ_s due to elastic strains partially cancelling the local magnetostriction. This had a greater effect so that the O'Handley and Grant model gave a poor approximation, though of the right order of magnitude. The authors pointed out that these results did not necessarily represent the values for Co- and Gd-based alloys, but reflected the values for materials with similar material parameters as crystalline Co and Gd.

The balance of force method [Furthmüller *et al* 1986] required a different starting point for the gedanken experiment. The reference state of the material is that state where the structural units have their local magnetisation "switched off" and hence without magnetostrictive deformation. When magnetised, the units are subjected to three concurrent sets of forces. The magnetostrictive forces and the forces inducing the reorientation mechanism act to minimise the anisotropy energy, and the elastic forces act to minimise the elastic energy of the structure. The total energy, is minimised with respect to the field to achieve equilibrium (compatibility). Because of intrinsic fluctuations in the anisotropy and the elastic and magnetoelastic parameters, the result is modified by a perturbation series, in a similar way to the compatibility method. This method has an advantage over the other one in that the reorientation mechanism is included. The contributions of the two mechanisms were investigated [Furthmüller *et al* 1987] and it was concluded that the reorientation mechanism had at most a negligibly small contribution.

The macroscopic magnetostriction constant was calculated from the local parameters of Co and Gd using the balance of forces method to the second order of the perturbation series and was compared to the corresponding results from the incompatibility method, in Furthmüller *et al.* There was good agreement between the methods when the contributions from the perturbation series were included, especially in the case of Gd.

By "playing around with local material parameters" they constructed two classes of materials. Class 1 materials were those whose macroscopic magnetostriction, λ_s, is of the same order of magnitude as λ_s(local), i.e. the higher order perturbation components due to elastic coupling are small and the results of the summation are close to that of O'Handley and Grant. They believed Fe-Ni alloys to be of this type. The class 2 materials were those whose λ_s(local) is greater than the macroscopic value due to partial cancellation of the higher order terms (in the incompatibility method). It was possible, according to the models, for a material to exhibit zero macroscopic λ_s while being strongly magnetostrictive on a local scale. They stated that since there are in principle infinitely many sets of local material parameters leading to class 2 materials and these parameters could be tailored by alloying, it may be possible to imagine this situation in real amorphous ferromagnetic alloys of totally different compositions (including Fe-based alloys). A series of Co-rich TM-M alloys exhibit near-zero magnetostriction, which could occur either due to near-zero local values or by the cancellation of the volume average due to the effect of elastic couplings. However, the temperature dependence of the one- and two-ion contributions indicate that the latter is the case and are therefore class 2 materials.

The effect of field and stress annealing were discussed in the context of the model [Fähnle *et al* 1990], particularly in relation to the class 2 materials. Also, the influence of non-local elastic behaviour was calculated [Beuerle and Fähnle 1990]. It was concluded that this effect was not significant in strongly magnetostrictive materials such as Fe-Ni-B alloys and low magnetostrictive class 1 alloys, but became more important for the class 2 alloys.

2.2.2.3 Sample Magnetostriction Parameters

The models reviewed in this section are phenomenological and discuss the magnetomechanical properties of a sample of amorphous metal ribbon given its macroscopic magnetostriction and anisotropy properties, taking account of the domain structure within the sample.

Livingston assumed a first order uniaxial anisotropy across the width of the ribbon (such as would be induced by stress or field annealing), with a resulting coherent transverse domain structure as shown schematically in figure 1.4, when in the absence of field or stress. Application of a field, H, along the ribbon longitudinal axis has the effect of rotating the magnetisation direction within each domain by an angle $(90-\theta)^{\circ}$. Due to symmetry, the magnetisation along the field axis is the same for each domain, so there is no domain wall movement. It was found from minimisation of energy that the field is related to the magnetisation along the field axis:

$$\frac{M}{M_s} = \frac{H}{H_k} = \cos\theta \qquad (H \le H_k), \tag{1.9}$$

(H_k - anisotropy field). The resulting M-H plot is purely linear between saturation in one direction and that in the opposite direction, with the susceptibility given by

$$\chi = \frac{M}{H} = \frac{M_s}{H_k} \tag{1.10}$$

$$= \frac{\mu_0 M_s^2}{2K_u}.$$

The rotation of moments through 90° induces the maximum magnetostrictive strain of $3\lambda_s/2$. The strain induced along the axis in which the field is applied, λ, as given in equation 1.5, becomes

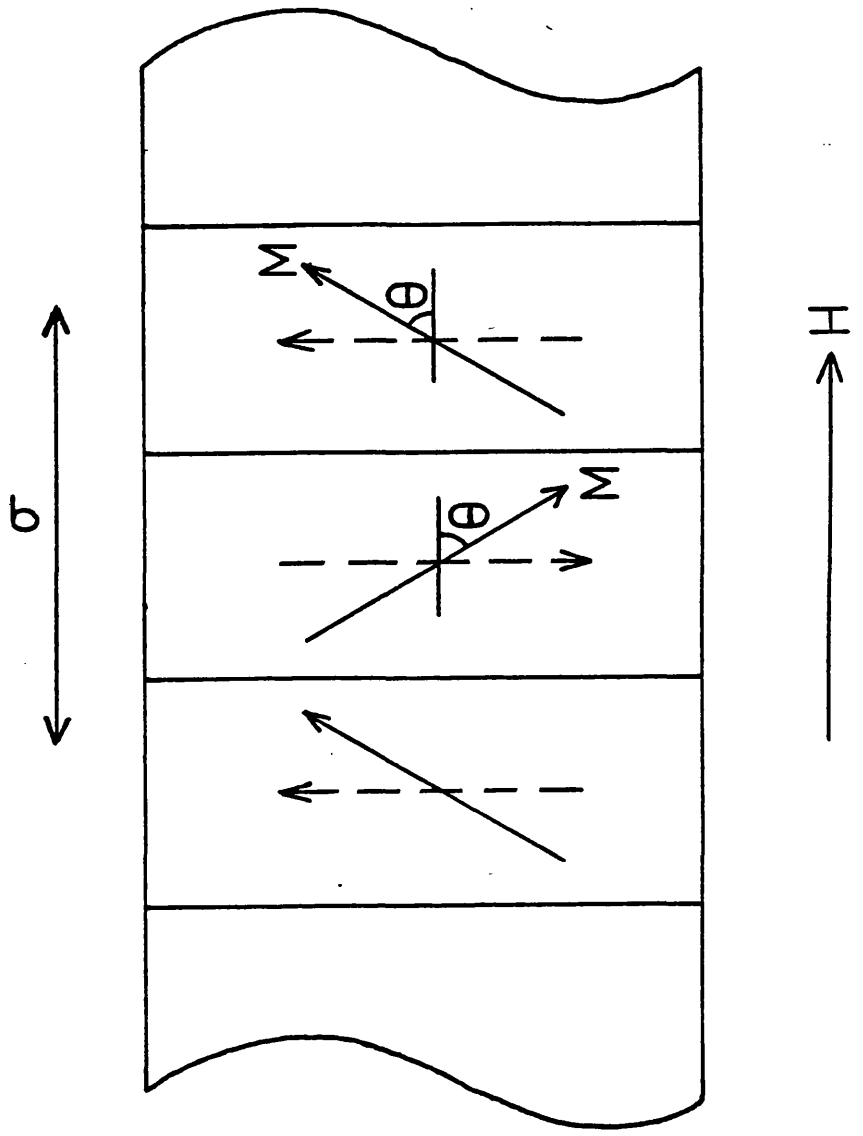

Figure 2.4: Schematic representation of the domain structure of the ribbon with transversely induced anisotropy (after Livingston [1982]). Due to symmetry, the domain walls are evenly spaced and are static with respect to applied field and/or stress. Magnetisation in the applied field direction occurs by rotation of the domain magnetisations.

$$\lambda = \frac{3\lambda_s}{2}\left(\cos^2\theta - \frac{1}{3}\right) = \frac{3\lambda_s}{2}\left(\frac{H^2}{H_k^2} - \frac{1}{3}\right). \qquad 1.11$$

The variation of M and λ were shown graphically as functions of applied field and stress. The magnetomechanical coupling, d, which is the field derivative of the strain was shown to be a maximum at H_k,

$$d_{max} = \frac{3\lambda_s}{H_k} = \frac{3\lambda_s M_s}{2K_u}. \qquad 1.12$$

The expressions were modified by replacing the field, H, with a reduced value, H_σ, to account for stresses along the axis which alter the apparent anisotropy constant. However, the effect of stress has been ignored in this study in the case of M and λ_s.

The effect of magnetisation on the Young's modulus, E, was also considered. The normalised change in E with respect to H was shown to be

$$\frac{\Delta E}{E} = \frac{E_M - E}{E} = \frac{9\lambda_s^2 E_M H^2}{M_s H_{k\sigma}^3}. \qquad 1.13$$

E_M is the Young's modulus of the material in a magnetised state. The magnetoelastic coupling factor, k, was given by

$$k = d\left(\frac{E}{\chi}\right)^{\frac{1}{2}} = \left(1 + \frac{\mu_0 M_s H_k^3}{9\lambda_s^2 E_M}\right)^{-\frac{1}{2}} \quad (0 \le k \le 1). \qquad 1.14$$

It can be seen from the above expressions that the reason for the very high magnetoelastic coupling coefficients seen in some amorphous alloys, particularly the Fe and Fe-Ni based ones, [e.g. Modzelewski *et al* 1981, Spano *et al* 1982, Kabacoff 1982, Wun-Fogle *et al* 1986] is their very low macroscopic anisotropy constants, represented in equation 2.14 by low H_k, while the saturation magnetisation, magnetostriction and elastic constants are similar to those of crystalline materials of similar compositions. This allows a higher degree of moment rotation at lower fields.

Equation 2.11 leads to the important result that the macroscopic magnetostriction of amorphous alloys with uniaxial transverse anisotropy is proportional to the square of the applied field and therefore also to the square of the magnetisation:

$$\lambda = C_q H^2 = C_Q M^2 . \qquad 1.15$$

where

$$C_Q = \frac{3\lambda_s \chi_0^2}{2M_s^2}, \qquad 1.16$$

and

$$C_q = \frac{3\lambda_s}{2M_s^2}. \qquad 1.17$$

Thus the magnetostrictive strain and the applied field are related by way of a single parameter (which is potentially useful in transducer applications). It was found in this study that this is a good approximation at low magnetisation.

The main limitation of the model is the assumption of a purely uniaxial transverse anisotropy within an homogeneous, stress-free material, leading to the domain structure shown in figure 2.4. This is an ideal case, with inhomogeneities arising predominantly from internal stresses due to the ribbon quenching or from bending and twisting [Livingston and Morris 1984]. Livingston emphasised that it was important to remove such stresses by annealing, but at a temperature well below the crystallisation temperature to avoid significant crystallisation. Also the effect of the shape of the sample should be taken into account since the internal field is not constant throughout the sample if it is non-elliptical. These inhomogeneities lead to a rounding of the knees of the M-H and λ-H plots at the approach to saturation [Spano *et al* 1982, This thesis, figures 5.1 and 3.9].

Inhomogeneities are never fully removed. Very small scale stress fields can exist around defects which occur due to the random nature of the structure. Therefore there

are intrinsic fluctuations in the local anisotropy constants and exchange interactions, even if the quenched in macroscopic stresses were fully relieved. This leads to distributions in the magnitude and direction of K_u and hence in local magnetisation. It is possible to quantify the effect of these deviations from the transverse direction on the magnetostrictive strain using the model by Squire [1990] which was developed to allow for anisotropy induced at some angle, θ, to the applied field direction (see below). Another limitation of the Livingston model arises due to the fact that it was found that the moment rotation model breaks down as the ribbon thickness increases because of the increased fractional volume occupied by domain walls as the domains become narrower [Wun-Fogle *et al* 1986]. Notable differences in the magnetoelastic coupling constant and fit to the model were measured in METGLAS 2605S2 ribbon between 10μm and 20μm thick.

The Squire model was similar to that of Livingston in that it assumed an homogeneous material with a uniaxial induced anisotropy. The direction of easy axis was some angle, θ, to the direction of magnetisation, with a resulting domain structure as shown in figure 1.5, comprising two sets of domains - those with their magnetisation at an acute angle to the applied field direction and those at an obtuse angle, separated by straight 180° domain walls. Application of a field applied along the ribbon longitudinal axis caused magnetisation by way of both domain wall movement and moment rotation within the domains. The domain walls move so that the domains with their moment direction at an acute angle to the field direction grow at the expense of those with their moment direction at an obtuse angle. The angles of both sets of domains rotate towards the field direction as H is increased. The model made the assumption that at some field strength the moments of the domains with their direction of magnetisation oriented away from the field direction flip to reduce magnetostatic and wall energy, suddenly making the material a single domain. The field strength at which this occurs, and whether these

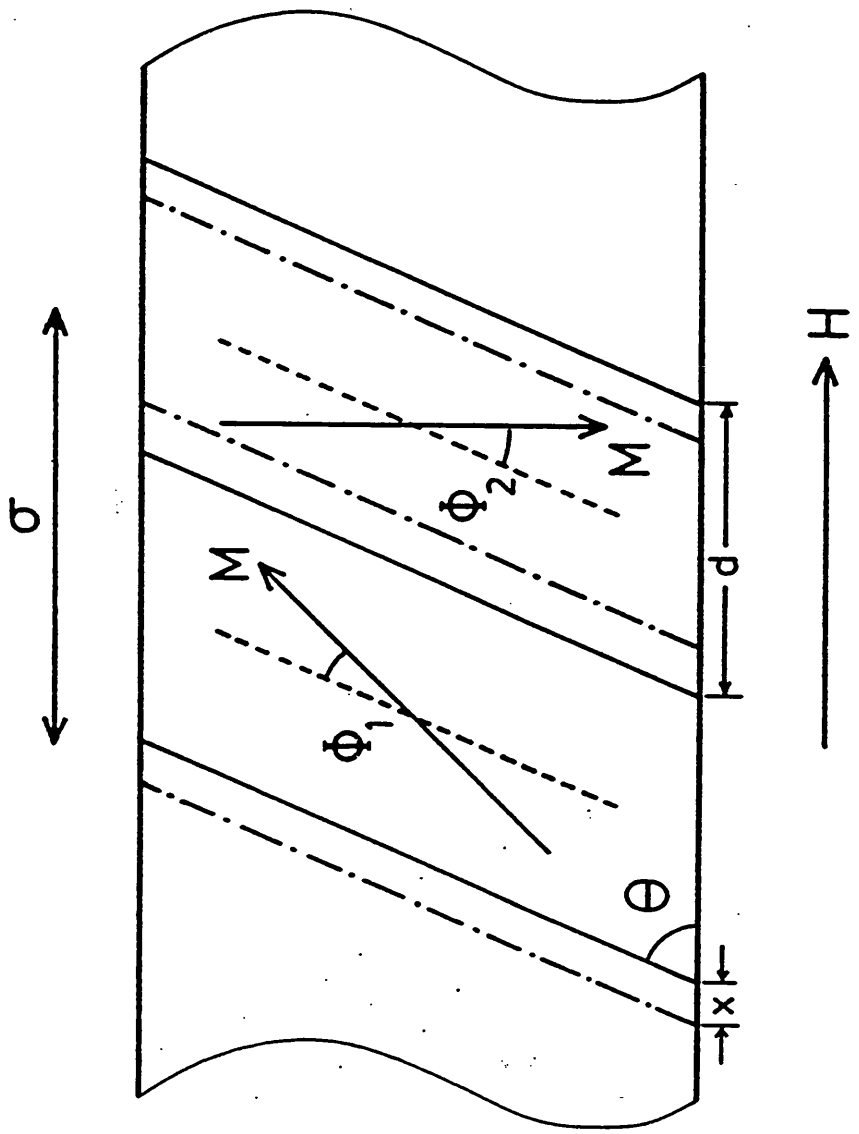

Figure 2.5: Schematic representation of the domain structure of the ribbon with anisotropy induced at an oblique angle, θ, to the applied field direction (reproduced from Squire [1990]). Magnetisation in the field direction occurs both by magnetisation rotation and by domain wall movement.

domains disappear due to wall movement before moment flipping can occur, is dependent on the angle θ as well as the material parameters. The sample is then a single domain and further magnetisation then occurs by moment rotation alone.

This model therefore predicted the behaviour of various magnetic and magnetoelastic properties with respect to anisotropy angle, θ, as well as to applied field and stress by minimisation of the total energy density. Some of the expressions become complex but reduce to those of the Livingston model where $\theta=90°$. Squire showed that the magnetisation, M, was linear with H only in the case of $\theta=0$ and 90°. The variation is shown for a series of θ in figure 1.6 (from the paper) in the absence of stress, γ. The initial susceptibility, χ_0, ($\gamma=0$) was given by the expression

$$\chi_0 = \left(\frac{\mu_0 M_s^2}{2K_u}\right)(\sin^2\theta + c\cos^2\theta), c = \left(\frac{\chi_{\theta=0}}{\chi_{\theta=90}}\right), \qquad 1.18$$

where the ratio of χ_0 for transverse and longitudinal anisotropy, c, is an empirically derived factor. χ_0 is shown as a function of θ for a series of γ in figure 1.7 (from the paper) for c=10.

The expression for λ was derived by the addition of the fractional contributions of the two sets of domains, and a series of λ-H plots are shown for different θ (again from the paper, with $\gamma=0$) in figure 1.8. At $\theta=90°$ the expression reduces to that given in equation 2.11, while at $\theta=0$ λ_e is clearly zero since magnetisation occurs by 180° domain wall movement only. Although λ is proportional to H^2 only in the case $\theta=90°$, the relationship can be approximated to a quadratic, with the coefficient given by

$$C_q = \frac{3}{8} f(\theta)\left(\frac{\mu_0 M_s}{K_u}\right)^2 \lambda_s, \qquad 1.19$$

where

$$f(\theta) = \frac{1}{2}[(c-1)\sin^2 2\theta - 2\sin^2\theta\cos 2\theta]\,. \qquad 1.20$$

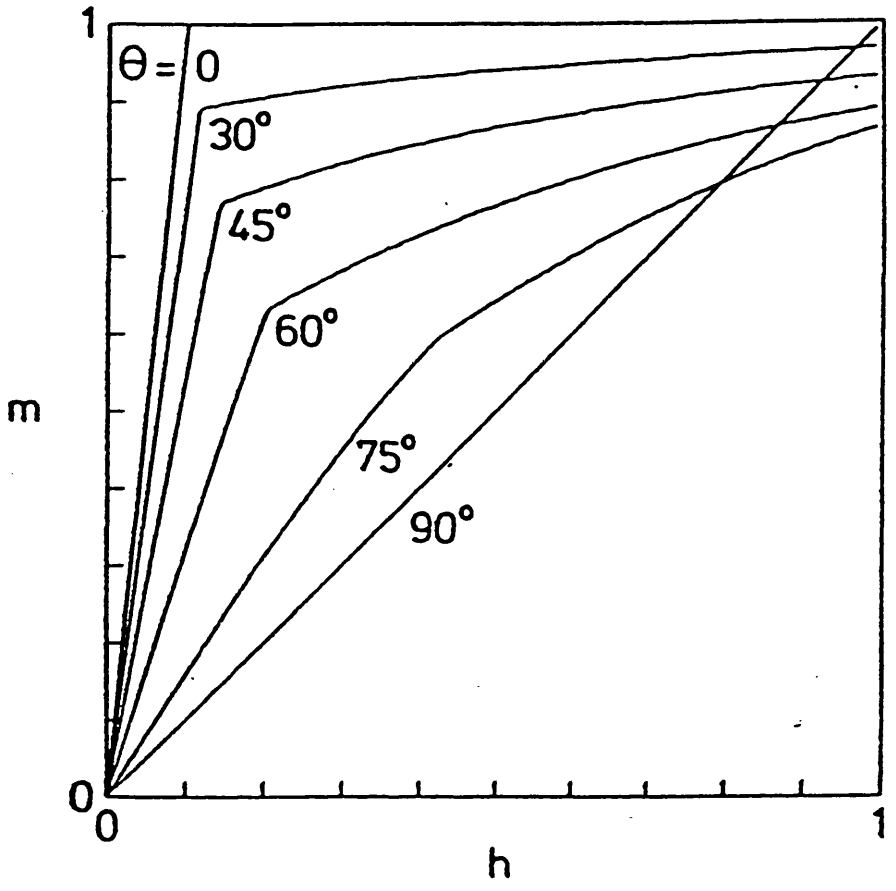

Figure 2.6: Magnetisation curves for a series of angle of uniaxial anisotropy, θ (reproduced from Squire [1990]). The discontinuities are due to the abrupt end of domain wall movement. At higher fields, the ribbon is notionally a single domain, so that further magnetisation occurs by magnetisation rotation alone.

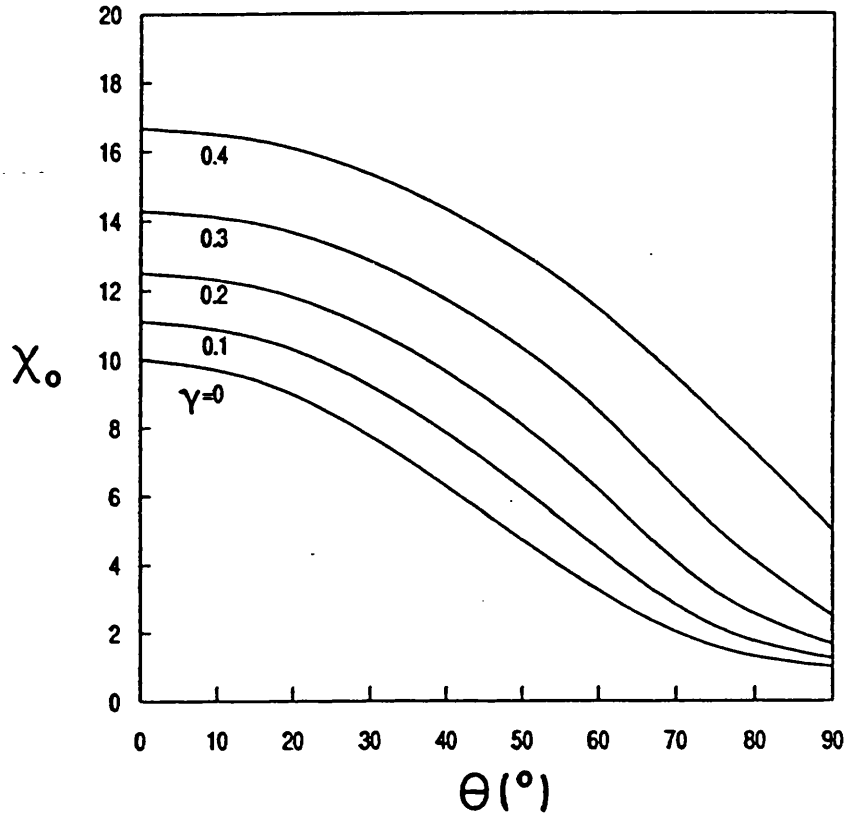

Figure 2.7: Variation of initial susceptibility with angle of uniaxial anisotropy (for a series of applied stresses), assuming a ratio *c* of 10 (reproduced from Squire [1990]).

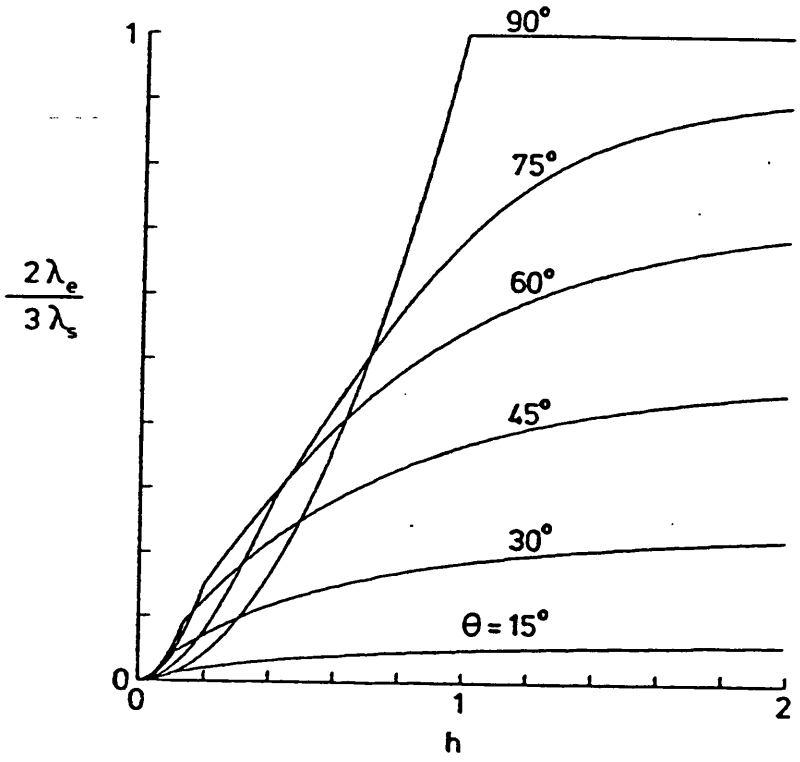

Figure 2.8: Normalised λ-H curves for a series of angle of uniaxial anisotropy angle (reproduced from Squire [1990]).

The λ-M quadratic was given by a similar expression:

$$C_Q = \frac{3}{2}\left(\frac{\lambda_s}{M_s^2}\right) q(\theta), \qquad 1.21$$

where

$$q(\theta) = \frac{f(\theta)}{2(\sin^2\theta + c\cos^2\theta)^2}. \qquad 1.22$$

Squire also derived an expression for the variation in Young's modulus as a function of θ, K_u, λ_s and γ. A series of normalised E-H plots for different θ are shown in figure 1.9 (figure 12 from the paper). The ΔE effect is greatest at $\theta = 90°$, with E reaching a minimum at H_k. At $\theta < 45°$ E(H=0) is at a minimum and E increases monotonically to the saturation value with increasing H.

An investigation of the behaviour of these parameters, in the absence of stress, was made in this study on a number of Fe and Fe-Ni amorphous alloys. The results were compared with the predictions from this model, and are discussed in chapter 4.

The M-H, λ-H and E-H plots exhibited discontinuities caused by the abrupt end to domain wall movement and by moment flipping, at the point where the material became a single domain and further magnetisation was due solely to magnetisation rotation. These were most evident in the E-H plots at high θ. They were not seen in experimental results for two reasons. Firstly because moment flipping does not occur in practice. This is because there is an additional constraint on the rotation of the domain magnetisations. If the magnetisation vectors of the two sets of adjacent domains rotate at different rates with respect to H, a difference in the components of magnetisation normal to the domain walls occurs at the walls interfacing the domains. This results in free poles being set up at the walls, increasing the demagnetising field in the domains with the greater rate of magnetisation rotation and *vice versa*. Therefore the magnetisation vectors of adjacent domains are coupled to each other, in such a way that the rates of magnetisation rotation

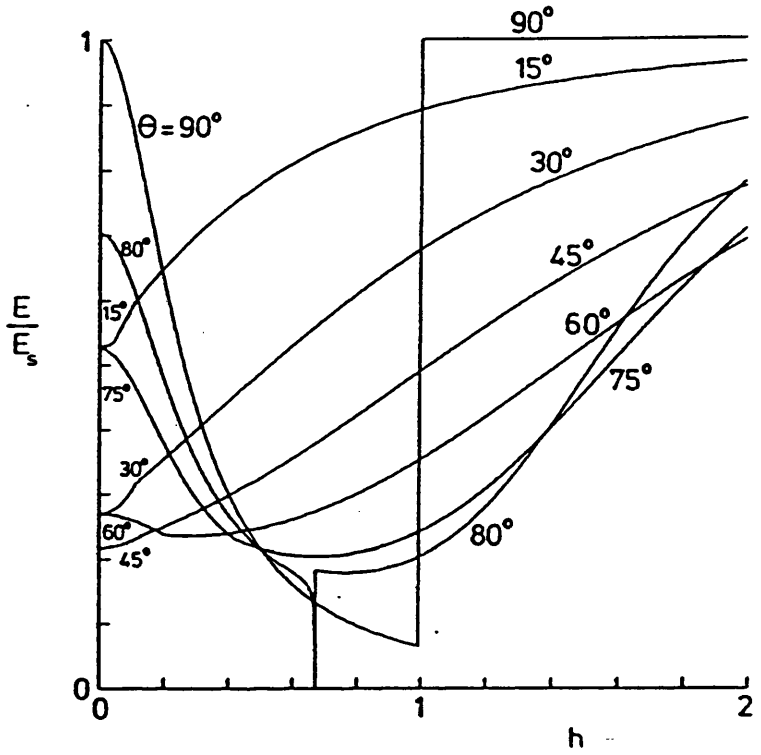

Figure 2.9: Normalised variation of Young's modulus with applied field for a series of angle of uniaxial anisotropy (K_u=100Jm^{-1}, λ_s=40×10^{-6}, reproduced from Squire [1990]). Note that the maximum ΔE occurs at θ=90°. The value of H at which the minimum occurs approaches zero as θ approaches 45°. For θ<45°, the minimum is at H=0 and ΔE decreases as θ approaches zero.

are kept as equal as possible to minimise the demagnetisation energy density, i.e. $d\psi_1/dH=d\psi_2/dH$. This was confirmed from studies of the domain structures for ranges of H in chapter 4. The coupling of the magnetisation directions of the two sets of domains prohibits spin flipping. Secondly, the discontinuities were smoothed out because the domain walls did not all meet at exactly the same applied field strength, so there was no abrupt end to wall movement. This was partly because of wall pinning and bowing due to intrinsic structural defects, and partly because the assumption made in the model that the domain walls can be modelled by a single potential is not an accurate one, and there were fluctuations in the wall potential and so in the extent of wall movement, resulting in irregularities in them (as well as fluctuations in the internal field arising from non-uniform demagnetisation in non-elliptical samples). These factors are addressed in chapter 4.

2.3 Measurement of Magnetostriction

A number of different methods have been used to obtain λ_s experimentally. Many of these were reviewed by Lachowicz and Szymczak [1984]. They could be divided into two classes: direct strain measurement, and indirect measurement by way of the variation of susceptibility with applied stress. The former are considered first.

2.3.1 Direct Strain Measurement

The easiest and most direct method of measurement of strain is the strain gauge. It is the method used to obtain manufacturers' data (Allied-Signal, Vacuumschmelze). O'Handley [1978] obtained magnetostriction values for a range of alloys in the $(FeNiCo)_{80}B_{20}$ ternary system and measured the variation of temperature of λ_s of these

materials using metal foil and semiconductor strain gauges bonded onto the samples with polyamide adhesive, with the gauge acting as one branch of an a.c. bridge arrangement. The magnetostriction constant, λ_s, of a ribbon was obtained by measuring the strain parallel and perpendicular to the saturating field. λ_s is then given by

$$\lambda_s = \frac{2}{3}(\varepsilon_{\parallel} - \varepsilon_{\perp}) \qquad 1.23$$

where $\varepsilon_{\parallel}$ and $\varepsilon_{\perp}$ are the strain measured parallel and perpendicular to the direction of magnetisation, respectively. Butler *et al* [1988] used strain gauges to measure λ_s on various RE-FeB alloys. They measured the strain of a METGLAS 2605SC ribbon by bonding a single gauge to it, and repeated the measurement after bonding an additional gauge to the opposite face. The readings gave the same result and both agreed with the manufacturer's data. It should not be inferred from this, however, that the bonding has a negligible effect on the strain. The additional bond had little effect on λ, and the agreement with the manufacturer's data reflected the similarity in the methods of measurement.

Datta *et al* [1984] measured λ_s on METGLAS 2605S2 using both a strain gauge bonded to the sample with low melting wax, and a piezoelectric sensor. They found the data from the gauge to be variable, and suggested that it was due to the stress caused by the gauge mounting. The piezoelectric transducer, however, was not bonded to the material but sat on it under its own weight with the piezoelectric element as one leg of a tripod arrangement. The strain was measured with the sample subjected to a 60Hz a.c. magnetising field of over 1.6T. The transducer was calibrated using material of a known λ_s, usually measured with a strain gauge, causing the data obtained using this method to be subject to the same limitations as the strain gauge method, as well as to those peculiar to this method itself. They obtained a value for maximum strain, λ_e, for transversely field annealed METGLAS 2605S2 (T_a=400°C, t_a=120min, H=10 Oe) of 40ppm, so that λ_s

=27ppm.

Bucholtz and co-workers measured magnetostrictive strain directly using a bulk-optic Michelson interferometer [Bucholtz *at al* 1986, 1987]. This entailed bonding an optical fibre onto the sample using low modulus epoxy resin. Sample strain then caused a change in the path length of light through this fibre which was measured with the interferometer. It was stated that flat samples have severe limitations for use with the long fibres that were needed for the accuracy required. Therefore the ribbon samples were wound into multilayer toroids, the layers being bonded together with the same epoxy resin, and 15-17m of the fibre was wound around its circumference. This assembly was then field annealed such that the induced easy axis lay along the circumference. Strain was measured with respect to applied field, H, along the cylinder axis (see figure 1.10). They measured the magnetostrictive strain at saturation, λ_s, of transversely field annealed METGLAS 2605S2 with respect to annealing field, time and temperature. They obtained a maximum asymptotic value of λ_s=37ppm at large fields, times and temperatures in the range of approximately 380-450°C (higher temperatures induce significant crystallisation, degrading the value of λ_s of the samples), corresponding to a value of $\lambda_s \approx$24ppm. They also derived the moment spread from λ_s using the same principle as used in this study, and measured the corresponding λ-H quadratic coefficients. These results are discussed and compared with results presented in this thesis in chapter 4.

The effect on λ_s of bonding samples was investigated using a model system by Gibbs *et al* [1987]. It was found that thin coatings (a few tens of micrometres) of cyanoacrylate suppressed the strain by 25-50%. This was an improvement on that of Bucholtz *et al* [1985], who found that it was suppressed by a factor of six due to bonding on to a 1mm layer of epoxy resin.

The three-terminal capacitance dilatometer has been used by some workers [Jergel

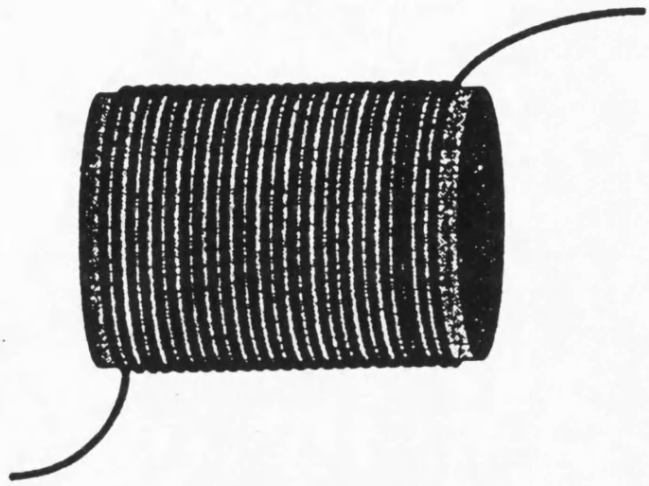

Figure 2.10: Configuration of a optical fibre magnetometer (reproduced from Bucholtz *et al* [1987]). The amorphous ribbon is wound into a multi-layered toroid, the layers being bonded together with epoxy. The fibre is wrapped around the outside a number of times and is bonded in position. The whole is then annealed to induce a uniaxial anisotropy in the circumferential direction, so that maximum response is to fields along the toroid axis. The toroid configuration has the advantage of the lack of shape demagnetisation, and the mechanical stability of the toroid is improved by the winding of multiple layers. The main disadvantage is the requirement for the bonding of the layers and the fibre, which degrades the magnetostrictive response.

et al 1989, Ishio and Kadowaki 1989, Jagielinski 1981, Tsuya *et al* 1975]. A sample is fixed in contact with one plate of a capacitor. A strain in the sample can be measured by the change in the capacitance. The capacitance cell developed by Ishio and Sato [1988] enables a single layer of ribbon to be measured, rather than requiring a number of layers to be bonded together. The authors measured λ_s for $Fe_{80}B_{20}$ to be 39ppm, which agreed well with measurements from other techniques. This method has been found to be most suitable for materials without near zero λ_s, i.e. for $\lambda_s > 10^{-7}$. A similar method is the cantilever-capacitance method [Klokholm 1976] which was designed specifically for thin films deposited onto thin substrates, mounted in a capacitor in a similar way to the previous arrangement. The substrate is non-magnetic, so when the thin film strains they are forced to bend. The resulting deflection causes a change in capacitance. This cantilever arrangement was also used by other workers who measured the deflection by an interferometer or a tunnelling probe, or by the deflection of a laser beam. These are discussed in Tam and Schroeder [1989].

When a magnetostrictive ribbon is subjected to an axial and a transverse magnetic field simultaneously (the transverse field produced by current flowing along it) it undergoes magnetostrictive torsional strain. This is known as the Wiedemann effect. This is due to the fields combining to rotate the moments into a helical path, so inducing strain in this orientation. This effect was fully discussed by Liniers *et al* [1985]. The relationship between λ_s and the torsional strain per unit length, ξ, was derived and a comparison between theory and experiment was made, giving an overall agreement. It was shown that λ_s is approximated by the expression

$$\lambda_s = \frac{\xi_{max} a}{2}, \qquad 1.24$$

where a is the ribbon thickness. They obtained a value of λ_s for METGLAS 2605SC of 28ppm. One limitation was that the technique was not suitable for materials with high

anisotropies since the field produced by the current flowing through the sample was not sufficient to fully rotate the moments. Therefore it was not suitable for as-cast ribbons because of the high anisotropies induced by the quenched in stresses. The same limitation applied to stress and/or field annealed samples with a high induced K_u. The other limitation is the thickness of the ribbon. The results become susceptible to large errors when the cross-sectional area of the ribbon is less than $10^{-8}m^2$. This technique for measurement of λ_s was described by Núñez de Villalicencio *et al* [1986] and was used to measure λ_s and K_u of various stress relieved (T_a=320°C, t_a=60min) TM-M alloys. λ_s measurements included 22ppm for METGLAS 2605SC, 12ppm for METGLAS 2826 and 13ppm for $Fe_{40}Ni_{40}B_{20}$, although the final value was subject to some error. It should be noted that it is arguable that all the alloys were fully stress relieved after the anneal, particularly those whose T_x is significantly higher than 380°C, such as 2605SC (T_x=480°C). Vázquez *et al* [1986] used this technique in the study of the temperature dependence of some Fe-Ni alloys near ferromagnetic phase transitions, leading to the exponent of the $\lambda(T)$-$M(T)$ power law.

Brizzolara *et al* [1989] introduced a magnetometer based on the magnetostrictive response of an Fe-based amorphous ribbon, namely METGLAS 2605SC. They utilised the quadratic λ-H relationship for material with transverse uniaxial anisotropy (equation 2.11), so that the magnetostrictive response, $d\lambda/dH$, of the transversely field annealed ribbon (T_a=390°C, t_a=10min, H_a>1kOe) was proportional to the applied field. This device was adapted to measure the magnetostriction of ribbon samples directly [Brizzolara and Colton 1990]. The strain of the sample was measured using a tunnelling tip. A schematic diagram from the paper is shown in figure 1.11. A small potential difference was applied between the tip and the sample. The current flowing (tunnelling) across a gap between the two varies exponentially and is highly sensitive to the gap width. This current was used in a feedback configuration to drive a piezoelectric shifter whose response had been

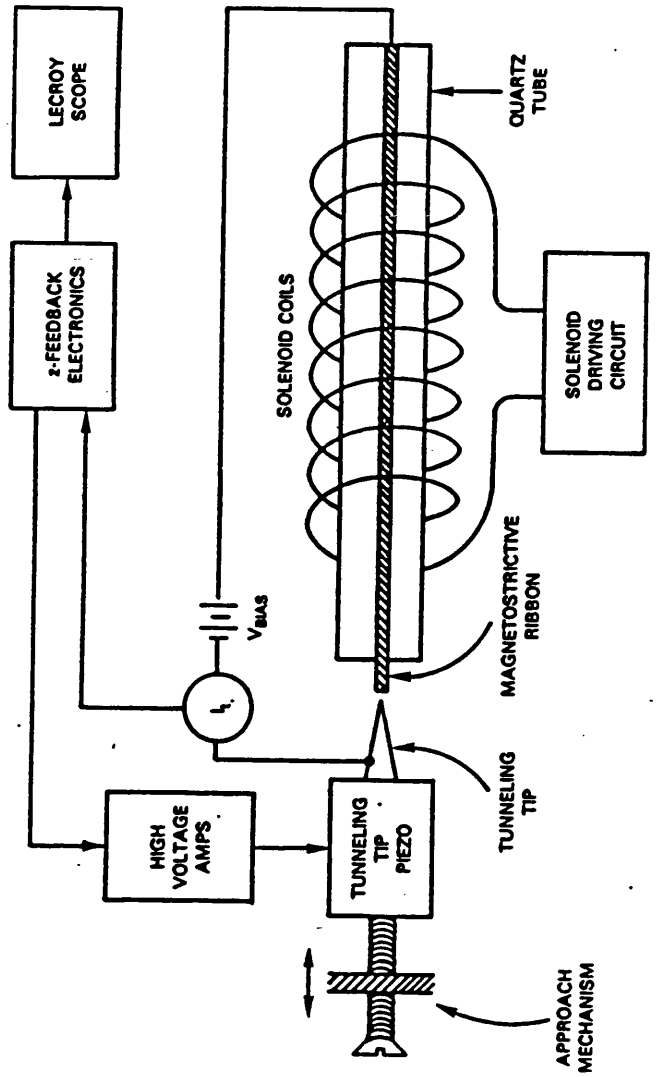

Figure 2.11: Schematic diagram of the tunneling-tip strain detector (reproduced from Brizzolara and Colton [1990]). The current through the tip is highly sensitive to distance of the gap between the sample and the tip, so that the tip can be kept at a constant distance from the sample end. The strain is measured from the movement of the piezoelectric shifter (on which the tip is mounted) which is required to keep the gap size constant. This is done by putting the tip current into a feedback or "constant current" configuration.

determined interferometrically. Thus the gap width could be precisely controlled. The sample was placed in a quartz tube so that it was supported along its edges. It rested on a thin layer of light machine oil, allowing it to slide freely. A gold sputtered aluminium tag was bonded to the end of the sample to provide a good tunnelling surface. The quartz tube was situated coaxially inside a solenoid where fields up to $\pm 40 kAm^{-1}$ were applied at a frequency range of 0.1-10Hz. Because of the length of the solenoid, measurements were initially limited to short samples, approximately 10-20mm in length, leading to relatively high demagnetising fields. It was later replaced by a pair of Helmholtz coils allowing longer samples to be used. The accuracy of the device was investigated by measuring crystalline nickel and iron. They measured λ_s for transverse field annealed METGLAS 2605SC and METGLAS 2714A ($Co_{66}Fe_4Ni_1B_{14}Si_{15}$) to be 27(±1)ppm and 0.19(±0.02)ppm respectively. The METGLAS 2605SC sample had dimensions 6×2.6×0.025mm, and hence suffered a significant demagnetising effect.

The λ_s-H plot of this sample from the paper is shown in figure 1.12a. From this it can be seen that the sample was not fully saturated by the field applied by the solenoid. After accounting for the demagnetising factor such that

$$H_{int} = H_{ext} - H_D = H_{ext} - \frac{1}{D}, \qquad 1.25$$

(where H_{int} and H_{ext} are internal and external applied fields respectively) it was found that the maximum internal applied field, H_{int}, was $80Am^{-1}$. The maximum strain obtained from the λ-H plot was approximately 262nm (obtained from the figure) which corresponded to λ_s=44ppm (the authors claimed 40ppm in the paper). Figure 2.12b shows a typical λ-H plot for the same alloy transversely field annealed under almost identical conditions, measured during this project on the optical-fibre dilatometer on a sample with dimensions 55×5×0.025mm (K_u was in close agreement with that of the METGLAS 2605SC samples used by Brizzolara *et al*, namely $38Jm^{-3}$ [Spano *et al* 1982]). The plot

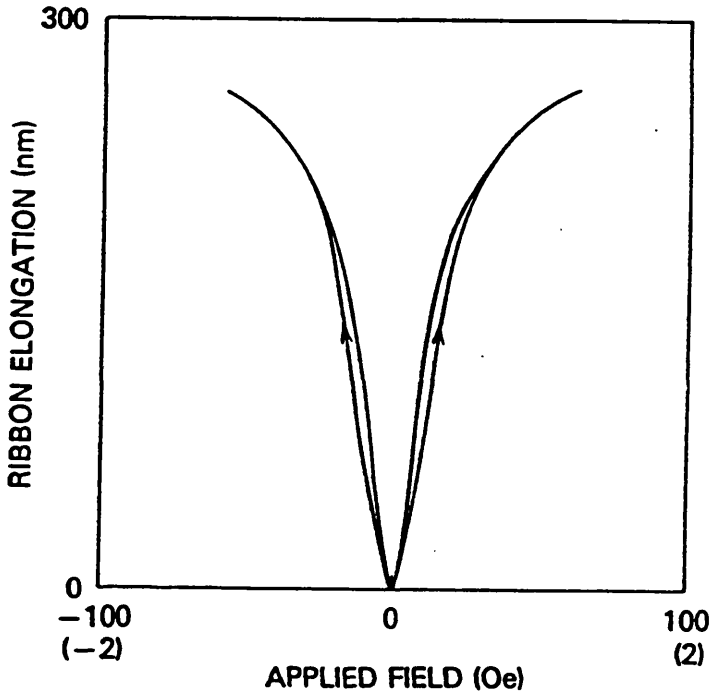

(a)

Figure 2.12: Comparison of λ-H plots of METGLAS 2605SC obtained from a) the tunneling-tip strain detector [Brizzolara and Colton 1990] and b) the optical fibre dilatometer used in this study. In (a), the figures in brackets represent the internal field, so that the maximum internal applied field was 1Oe≈80Am^{-1}. The sample used was 6mm long, so 300nm represents strain of 50ppm. In (b) the vertical lines represent the same internal field of 80Am^{-1}. It should be noted that there is some uncertainty in the internal field due to it's non-uniformity within non-elliptical samples.

(q)

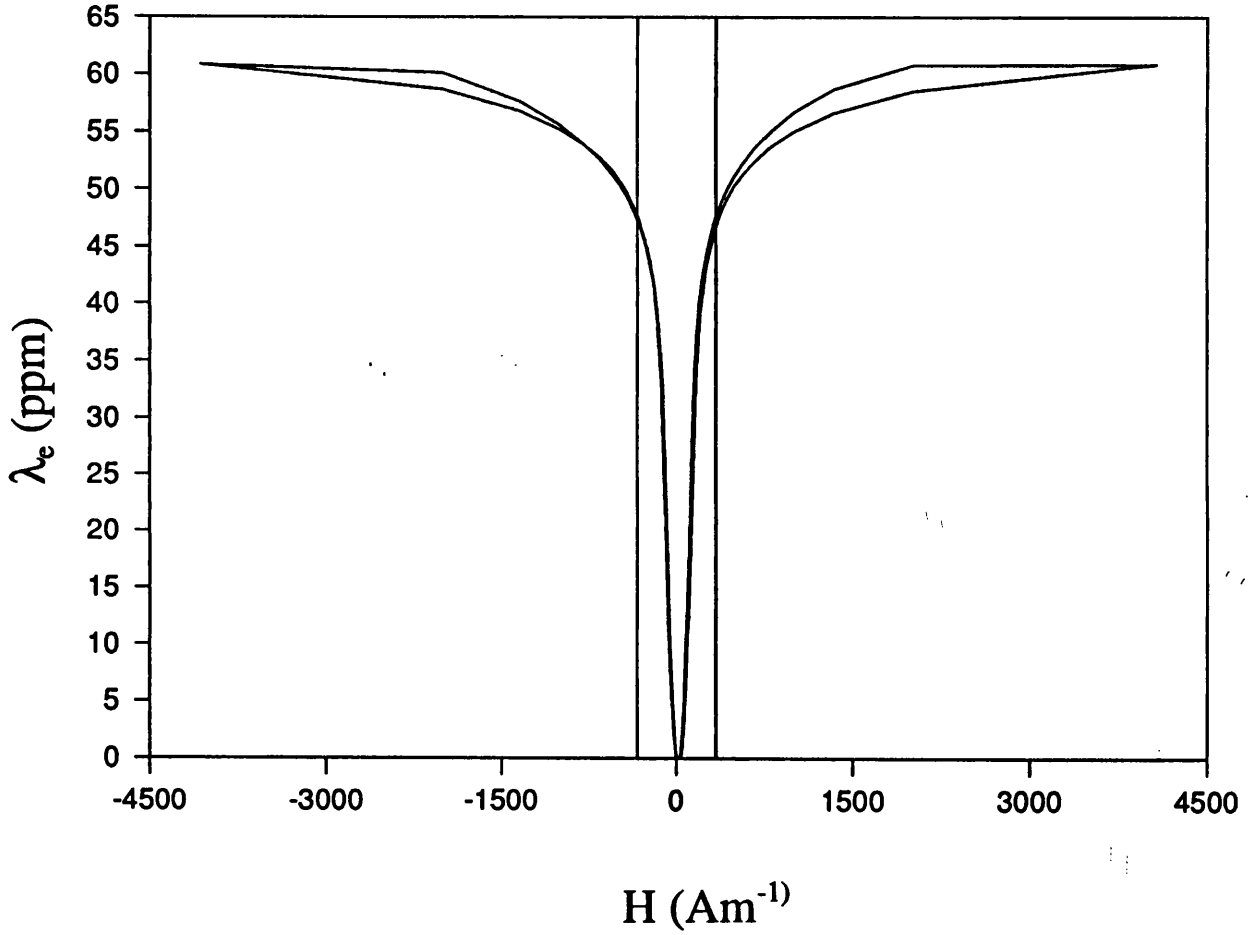
65
60
55
50
45
40
35
30
25
20
15
10
5
0
λ_e (ppm)
-4500
-3000
-1500
0
1500
3000
4500
H (Am^{-1})

shows that the sample was almost fully saturated and the maximum strain was measured to be approximately 61ppm. However, the applied field which corresponded to an internal field of $80Am^{-1}$, which is indicated by vertical lines on the plot does not saturate the material. The strain at this field was well below that at saturation and was found to be approximately 47ppm, in fairly good agreement with that obtained by Brizzolara and Colton. The two λ-H_{int} plots appear very similar. For these reasons it was thought that the tunnelling tip strain detector gave results similar to those of the optical-fibre dilatometer. It is worth noting that this device works on a similar set-up to the modified dilatometer system currently being developed at Bath, i.e. an unbonded sample free to strain, measured by a non-contacting transducer in a feedback arrangement. It is the only other non-contacting, low frequency (quasi-dc), direct strain measurement system at present. The comparison between the data from the two systems was conveyed to the authors in a private communication, together with a suggestion that they repeat the measurements on a sample of much lower shape demagnetising factor. In their reply, they suggested that the difference in the strain measurements might be due to the lack of precision inherent in estimating internal fields. They re-stated that the strain measured on the sample was 40ppm, not 44ppm. Although they had also measured the strain on a longer (8mm) sample to be λ_e=46ppm, there was large uncertainty in the measurement. They stated that as they were no longer in this field of work, they were unable to take further readings, and so could neither corroborate nor refute the results of λ_e=60ppm.

2.3.2 Indirect Measurement

Indirect measurements of λ_s have often been favoured for the ease of sample preparation and the lack of necessity to load or bond the material which, in the case of thin amorphous ribbons, can severely suppress the strain. Also measurement of λ_s with

respect to variations in temperature and applied stress are often more straightforward. Most indirect measurement systems made utilise the linear variation of some magnetic parameter with applied stress.

Spano *et al* [1982] measured the variation of initial susceptibility of two amorphous alloys, where

$$\frac{1}{\chi_0}=\frac{2\mu_0 K_u}{M_s^2}+\left(\frac{3\mu_0\lambda_s}{M_s^2}\right)\sigma. \qquad 1.26$$

From this they obtained values of λ_s and K_u for transversely field annealed METGLAS 2605SC (T_a=390°C, t_a=10min) of 27ppm and 38Jm^{-3} respectively. They also obtained a value of the magnetoelastic coupling factor, k, of 0.98, the highest recorded for any material. No linear behaviour was observed for METGLAS 2605CO.

This method has been used extensively by Hernando and co-workers in their investigation of near-zero magnetostrictive Co-based alloys. This work is not of direct relevance and is not reviewed here. Other workers to use this method include Warlimont and Hilzinger [1981] and O'Dell [1981].

Clark and Wun-Fogle [1989] termed the magnetostrictive response, $d\lambda/dH$, the magnetostrictivity, d. They showed that, in the case of single-vector magnetisation rotation, this is given by

$$d=\left[s^M\left(\frac{\chi^\sigma}{\chi^\varepsilon}\right)(\chi^\sigma-\chi^\varepsilon)\right]^{\frac{1}{2}}, \qquad 1.27$$

where s^M is the compliance at constant M, the value of which was obtained from the manufacturer. χ^σ and χ^ε are the susceptibility at constant stress and strain respectively. Therefore, by measurement of these susceptibilities they obtained d with respect to H, the integral of which gave the λ-H plot, corrected for the sample shape demagnetisation factor. They measured four different transversely field annealed alloys which included METGLAS 2605SC and METGLAS 2605S2, and obtained values of λ_s of 44ppm and

48ppm respectively.

A common technique is the small-angle magnetisation rotation (SAMR) method. It was introduced for amorphous alloys by Narita *et al* [1980] where it is fully described. A schematic is shown in figure 1.13. A sample is positioned within two orthogonal fields. The larger, dc field, parallel to the sample axis, was produced by a long solenoid. A pair of coils within the solenoid produced a smaller field across the sample width, driven by an ac source. The sample was also subjected to a controlled stress along its axis. The larger field had the effect of aligning the magnetisation along the sample axis while the smaller field caused a deviation of the magnetisation direction of a few degrees away from this axis at the frequency of the ac source. This small change in M along the sample axis was picked up by a search coil in the form of an ac signal voltage with twice the frequency of the transverse applied field. If the stress, σ, were altered, the signal voltage would change due to the change in anisotropy. An adjustment in the dc bias field, $\Delta H_{\parallel}$, which had the effect of returning the signal voltage to its original value would then be proportional to λ_s, the relationship given by the expression

$$\lambda_s = \left(\frac{M_s}{3\sigma}\right)\Delta H_{\parallel} . \qquad 1.28$$

This expression was modified for non-uniform magnetisation rotation and surface irregularities. Using this technique they measured λ_s of METGLAS 2605 and METGLAS 2826 to be 34.6ppm and 12.3ppm respectively with errors less than 5%. The authors claimed a sensitivity of approximately 2×10^{-7} for METGLAS 2826 ribbon. This has shown to be a useful technique for low λ_s alloys and is possibly the most commonly used. However, it was pointed out that it was less suitable for high λ_s materials [e.g. Hernando *et al* 1986] because the relatively large local anisotropies resulting from internal stresses cause relatively greater fluctuations in magnetisation and so a slower approach to saturation. This then requires larger bias fields with the result that the output

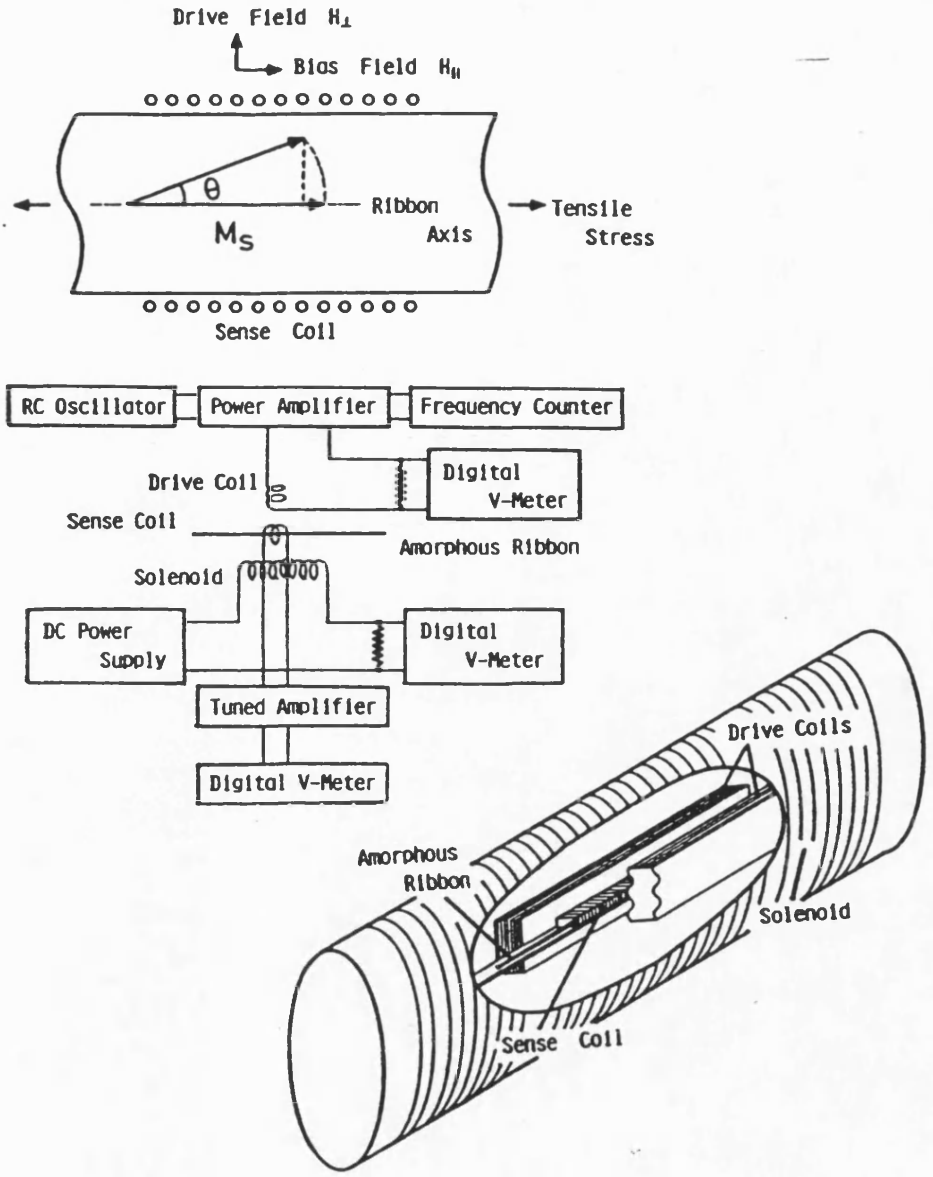

Figure 2.13: Principle and schematic diagram of the Small Angle Magnetisation Rotation measurement apparatus (reproduced from Narita *et al* [1980]). A small perpendicular ac field rotates the magnetisation of the magnetised sample, causing an ac variation in the emf of the search coils. A tensile stress, σ, is applied, causing a change in the uniaxial anisotropy, and so the degree of magnetisation rotation. The bias field provided by the solenoid is altered until the ac variation in the search coils (i.e. the degree of rotation) is returned to its original value. This compensation field, ΔH, is directly related to λ_s, i.e.

$$\lambda_s = \Delta H\left(\frac{M_s}{3\sigma}\right).$$

signal approaches its detection limit, although this can partly be overcome by using higher frequency ac fields. By careful experimental procedure to avoid some of the causes of internal stresses, including pre-annealing and particular attention to the sample holder, Sanchez *et al* [1988] measured λ_s on METGLAS 2826 and obtained a value of 10ppm at room temperature. Kraus [1989] modified this technique so that the bias field was in the transverse direction. He claimed a sensitivity of 10^{-8}, and that the technique was suitable for both low and high λ_s materials. However it also depended on the trade-off between high bias field to attain low spread in magnetisation and the decrease in sensitivity at high fields.

2.4 Anisotropy

The anisotropy energy density, E_k, is defined in chapter 1. The following subsection is concerned with its sources. It can be induced by stress and/or field annealing. The induction by field annealing is discussed in the subsequent subsection.

2.4.1 Sources of Anisotropy

It is established that there a number of different types of magnetic anisotropy which can be classified as: crystal, shape, stress, induced and exchange. The crystal anisotropy is the only intrinsic one. The others are extrinsic or induced. The crystal anisotropy is generally predominant in crystalline material. The absence of long range crystal anisotropy in amorphous materials thus enables the anisotropy to be largely tailored.

1. Crystal anisotropy

This single-ion anisotropy term arises from weak spin-orbit and strong orbit-lattice (or orbit-structure) coupling. When a field is applied it tends to turn the spins in the

incomplete outer shell of each ion, which are weakly coupled to the electron orbits. These, however, are strongly coupled to the structure. Thus the orbits are quenched in position and the spins are effectively coupled to the structure. If the crystal field is large so that the coupling is strong, more energy is required to turn the spins away from the crystal field, leading to a large anisotropy energy. The magnetic interactions in amorphous ferromagnets are discussed by Nayar and Batra [1990] and are compared with those in crystals.

In amorphous structured materials the macroscopic volume average crystal anisotropy vanishes, and its contribution to the macroscopic value of E_k can be neglected. However, as discussed in section 2.1.2, the local crystal field can be significant, and can be comparable to that in the corresponding crystal lattice of similar composition. Because of the random nature of the structure, the easy axis direction of the local anisotropies tend to be random (in the absence of any other source of anisotropy). This has a profound effect on the angular spread of moments inasmuch as it is directly dependent on the local anisotropy constants and exchange interactions. This is discussed more fully in section 2.6.

2. Shape anisotropy

This is determined by the ease of magnetisation in different directions due to the demagnetising effect of the shape of the sample. This can be tailored by using suitably shaped samples. It is given by

$$E_{shape} = \frac{1}{2}\mu_0 D M^2, \qquad 1.29$$

where D is the demagnetising factor, defined in chapter 1.

3. Stress anisotropy

Stress anisotropy arises in non-zero magnetostrictive materials via the magnetoelastic effect. In the same way that magnetising a material causes it to strain,

applying a stress (and therefore a strain via the elastic moduli) causes change in the magnetisation energy density and rotation of moments. In a positively magnetostrictive material a tensile stress causes the easy axis to align with the stress. The change in anisotropy energy density resulting from an applied stress is given by

$$E_\sigma = -\frac{3}{2}\lambda_s \sigma \cos^2\theta, \qquad 1.30$$

where θ is the resulting angle between the spontaneous magnetisation and the direction in which the strain is measured. It is the internal stresses that occur in as-cast amorphous ribbons as a result of the manufacturing processes that produce large anisotropies which result in the various maze and radial domain patterns [e.g. Fujimori *et al* 1976]. It is necessary to relieve these stresses by annealing to make it magnetically softer and improve the material's properties. Internal stresses can easily produce unwanted anisotropies making the material magnetically harder. This is the predominant cause of anisotropy in TM based metallic glasses [e.g. O'Handley 1975]. Because of this much work has been done on zero and near-zero magnetostrictive alloys in applications other than transducers (e.g. Hernando and co-workers).

4. Induced anisotropy

There are three main types of induced anisotropy. That caused by irradiation will not be considered here. The other two are caused by field and stress annealing. Field, or magnetic, annealing is the most commonly used method of inducing anisotropy. The material is annealed below the Curie temperature within a magnetic field great enough to achieve saturation. This has the effect of rearranging the structure to minimise the energy density with the magnetisation in the applied field direction, so that when the material is cooled the moments largely remain in this direction. Hence it is recoverable by annealing under similar conditions in the absence of a field. Stress annealing induces an anisotropic easy axis by way of the magnetoelastic effect. The tensile stress causes

atomic bonds to become more aligned in the stress direction. During the anneal the strained material rearranges its structure by thermally activated deformations to form bonds with a more isotropic distribution. Upon cooling and removal of the applied stress the bonds parallel to the stress direction contract and the distribution of atomic spacing becomes anisotropic. Hence back stresses are produced in the material which are compressive in the applied stress direction, causing a hard magnetic anisotropic axis in this direction in positively magnetostrictive materials. Since the deformations can be some combination of elastic, anelastic and plastic, it is not fully recoverable upon further annealing, although it is difficult to differentiate between the contributions. A lot of work has been done on stress annealing, especially on near-zero λ_s Co rich alloys (e.g. Nielson and co-workers). The effect is not negligible in these materials because although the magnetostriction is macroscopically near-zero, this is not necessarily the case at the local scale (see section 2.2). However, it is not of direct relevance in this study so is not covered further. Annealing in the presence of stress and field has been reported to induce K_u greater than the sum of those induced by the two types of anneals separately, and that K_u reduced to that induced by stress annealing alone after relaxation [Vázquez *et al* 1987].

Surface crystallisation can produce a stress field which induces an anisotropy within a nonzero magnetostrictive material. This is discussed in section 2.5.

2.4.2 Induction of Anisotropy by Magnetic Annealing

Anisotropies other than the crystal and shape anisotropies are the result of pair ordering, i.e. the directional ordering of different types of pairs of atoms due to interactions (including dipolar, pseudo-dipolar and exchange interactions) between their spins. If, because of these interactions, moments prefer to orient along the axes of a given

type of atom pair, then these pairs will tend to align with an applied field, resulting in small distortions in the structure in the form of the two-ion magnetostriction contribution. These distortions are elastic and the structure returns to its original configuration upon removal of the field. If, however, the field is applied at an elevated (anneal) temperature allowing rearrangement of atomic positions, pair ordering can occur to a greater degree and can largely become frozen in upon return to a lower (ambient) temperature. Hence work on anisotropy induced by field annealing has shown that its development is due predominantly to directional pair ordering [Luborsky and Walter 1977], and is governed by thermal activation processes and that the driving force results from the magnetic interaction energies between the magnetisation and the atom pair [Fujimori, from Luborsky 1983, Kronmüller *et al* 1984]. The kinetics of the development of K_u are shown in Kronmüller *et al* [1984] and in Chambron and Chamberod [1980]. Kronmüller *et al* showed, using the model of thermally activated alignment of mobile atom pairs [Gibbs *et al* 1983], that K_u increases linearly with log time and they obtained activation energy spectra for the alignment of pairs in a Co-Ni-Fe based alloy. By comparing the spectra of as-cast and stress relieved samples, they were able to classify the processes into "reversible" and "irreversible" annealing processes and obtain energy spectra for each.

The directional ordering of pairs of atoms can be regarded as an increase in chemical or compositional short range order (CSRO). However, the structural ordering has been measured from diffraction techniques to be very low. Corrections of 1-2% in the RDF are generally enough to explain measured values of K_u [Cargill and Mizoguchi 1979]. This is consistent with the conclusion of Slonczewski [from Rado and Suhl 1963] who found that the preference of like atoms for the local magnetisation direction or that of solute atoms for certain interstitial sites is never more than about 1%, and also with the finding that the anisotropy parameter (anisotropy in the angular distribution of atom pairs) is of the order of 1% in field annealed amorphous alloys [e.g. Szymczak 1987,

Fähnle and Furthmüller 1990].

Increase in the anneal temperature increases the disorder due to the effects of entropy, so decreasing K_u. Chambron and Chamberod [1980] found that the fully developed anisotropy, $K_u(t_a=\infty)$ was approximately inversely proportional to the anneal temperature (the measured variation for VAC0040 in this study is shown in figure 5.3). The temperature and composition dependences were better described by the directional ordering theory [Néel 1954, Taniguchi and Yamamoto 1954, Slonczewski (from Rado and Suhl 1963)]. If a binary alloy of *a* and *b* atoms with respective relative atomic fractions C_a and C_b is annealed at a temperature, T_a, for a period long enough to achieve equilibrium (manifested by steady K_u with time), then the theory predicts that the anisotropy is given by

$$K_u = \frac{A f(c)}{T_a}\left(\frac{M_s(T)}{M_s(0)}\right)^2\left(\frac{M_s(T_a)}{M_s(0)}\right)^2, \qquad 1.31$$

where $M_s(T)$, $M_s(T_a)$ and $M_s(0)$ are the saturation magnetisations at the measuring and anneal temperatures and at 0K respectively. A is some constant that is dependent on the atomic arrangement and range of interactions considered and $f(c)$ is a function dependent on the concentration of the two metal atoms. In the case of ideal solutions where nonmagnetic interactions are zero, this is given by

$$f(c) = \frac{N n C_a^2 C_b^2}{2}, \qquad 1.32$$

where *N* and *n* are the number of atoms per unit volume and the number of possible orientations of a pair within a structure. A slightly more complex expression was derived for the case where nonmagnetic interaction is nonzero.

Luborsky and Walter [1977] measured the field anneal induced anisotropy for the range of binary alloys $(Fe_xNi_{1-x})_{80}B_{20}$ for a series of anneal temperatures, and found good agreement between the anneal temperature dependence of K_u and that predicted by the

above expressions when normalised to give the best fit.

Luborsky and Walter found that the induced anisotropy after accounting for temperature, $K'_u=Af(c)$, was at a maximum with respect to composition where x=0.5. This is consistent with the prediction of the directional order theory if the pair ordering is due to Fe-Ni pairs. They also found that K_u did not vanish at x=1, i.e. for the single metal alloy, as the model predicted, but was of the order of 25% of the maximum value and was almost temperature independent. They concluded that this discrepancy was due to some kind of interstitial ordering involving the B atoms or to Fe-Fe pair ordering with respect to the Fe-B matrix. Further investigation on $(Fe_xNi_{1-x})_{80}P_{14}B_6$ [Luborsky and Walter 1977] showed that there existed a monatomic contribution at high Fe concentration ($x\approx1$) which decreased as x decreased. They concluded that this contribution was due to the ordering of metalloid atoms with respect to the SRO of the Fe atomic structure. The dependence of K_u on T_a at x=1 ($Fe_{80}P_{14}B_6$) also indicates some directional ordering involving the metalloids. This temperature dependence is far less evident in the $Fe_{80}B_{20}$ alloy implying that there is a pair ordering contribution due to the P atoms which are too large to occupy interstitial sites, and occupy DRP atom sites in the structure, and that the term due to interstitial ordering of the B atoms is less temperature dependent. Similar nonzero K_u was found in $(Fe_xCo_{1-x})_{78}B_{12}Si_{10}$ at x=0 and 1 by Fujimori *et al* [1976] and was attributed to some cause other than pair ordering.

Becker [1978] introduced a third process for the induction of K_u by magnetic annealing, along with directional pair ordering and interstitial ordering. He proposed a single ion contribution which could be accounted for by the selective replacement of single atoms in the DRPHS structure such as to bias the distribution of local anisotropies. He claimed that the K_u of Fe-only alloys could be explained by this model and the fact that these alloys can be magnetically annealed is a consequence of the presence of substitutional P atoms in the DRHPS structure.

2.5 Partial Crystallisation

Annealing at temperatures close to the crystallisation temperature produces the nucleation and growth of small crystallites. These tend to nucleate in regions of higher atomic mobility allowing structural rearrangement at lower temperatures, such as at the surfaces [Pregger and Kramer 1989]. In rapidly quenched ribbons as used in this study, they also tended to nucleate at sites where the material quench rate was slowest, since more time was allowed for atomic ordering in these regions. This is generally on the wheel cooled side where air or vapour was trapped between the ribbon and wheel causing a small bubble which partially insulated the ribbon from the ribbon [Hodson 1986] and, on the air side, it was at the asperities where the ribbon was thickest and so had maximum thermal mass, hence slowest quench rate, that crystallites tended to nucleate. The crystallisation was slightly more pronounced on the wheel side of the ribbon studied by Ok and Morrish [1981] because of more nucleation sites. The nucleation was examined by electron or optical microscopy of sections of various TM-M ribbons [Lemcke 1989, Herzer and Hilzinger 1986]. It was found that the crystalline phase in $Fe_{78}B_9Si_{13}$ was α-Fe, was nucleated at the surfaces, and the growth was dendritic with the growth axis along the [100] direction. The crystallite growth was textured with the dendrites normal to the wheel cooled surface and at an oblique angle (50-60°) to the air cooled side.

Crystallisation has the effect of reducing the magnetic softness of the material due both to the introduction of grain boundaries and amorphous-crystalline phase interfaces which act as domain wall pinning sites and to the introduction of randomly oriented crystal fields which do not average to zero above atomic scales. The crystalline phase is of a higher density and as it grows it tends to expel metalloid atoms producing a metalloid-rich interface. Using Mössbauer studies, Ok and Morrish [1981] proposed that, due to the crystallites' greater density, the partially crystallised surface regions

contract causing a compressive stress in the bulk of the material and tensile stress in the crystallised regions themselves (figure 8 from the paper). They confirmed this by the removing the surface layers and they observed Mössbauer spectra of stress relieved material and curling of the ribbon resulting from the stress relief. In positively magnetostrictive material this induces anisotropy easy axes perpendicular to and parallel to the surface in the bulk and surface layers respectively.

Using this proposal as a basis, they calculated the internal stresses. From this they derived an expression for the induced anisotropy,

$$K_u = \frac{K_{max}\alpha\delta}{d} \qquad 1.33$$

in the bulk of the material, where δ is the total thickness of the crystallised surface layers, α is the fractional volume of crystallites within these surface layers, d is the ribbon thickness and K_{max} is given by

$$K_{max} = \frac{\lambda_s E}{2(1-\nu)} \frac{\rho_{cr} - \rho_{am}}{\rho_{am}} \qquad 1.34$$

(E-Young's modulus, ν-Poisson's ratio, ρ_{cr} and ρ_{am} - density of amorphous and crystalline phases). Thus the anisotropy is directly proportional to the crystallised surface layer thickness. They measured the variation of K_u with δ on METGLAS 2605S2 and found good agreement between the model and the data. The expression for the coercivity was derived to be

$$H_c \propto \frac{K_u M_r}{M_s^2} \qquad 1.35$$

Since it was found that $M_r/M_s \propto \delta/d$,

$$H_c \propto \frac{K_{max}}{M_s} \propto \left(\frac{\delta}{\alpha}\right)^2 . \qquad 1.36$$

Hence H_c is proportional to δ^2. However, this quadratic relationship was shown to occur only for a range of low δ. Where this is the case, the coercivity is simply the "compensation" field required to rotate the bulk magnetisation in order to compensate for the significantly reduced change in magnetisation of the surface layers at low H (due to domain wall pinning). However, in ribbons with a greater degree of crystallisation, higher fields are required to achieve "compensation" in M from bulk magnetisation rotation, but the higher fields become sufficient to overcome wall pinning, thus causing Barkhausen jumps, so decreasing the apparent compensation field (i.e. H_c). Consequently the variation of H_c with δ deviates from a quadratic where the "compensation" field becomes greater than that required to overcome the pinning forces in the surface layers. This was found to be the case in METGLAS 2605S2 ribbon, where the data was in good agreement with the $H_c \propto \delta^2$ relationship for $\delta < 5\mu m$, but with further crysallisation H_c increased slower than δ^2.

Sheard *et al* [1989] compared the effects of both partial surface and bulk crystallisation on the magnetic properties of TM-M alloys. They concluded that the properties were insensitive to the type of crystallisation at low fractional crystallite volumes, but above 20% bulk crystallisation the effect of the random easy axes of the crystallites caused significant dispersion in the magnetisation direction distribution. They presented data in which the percentage of crystallisation by volume was approximately proportional to H_c, above ~20% by volume.

The induction of perpendicular anisotropy by controlled surface crystallisation to increase the engineering magnetostriction of TM-M ribbon samples was introduced by Gibbs *et al* [1988]. Values of λ_e of almost 60ppm were measured on partially crystallised METGLAS 2605SC samples with H_c of approximately $10Am^{-1}$. They suggested that this could be a viable method of induction of perpendicular anisotropy in metallic glasses, to optimise the magnetostriction for transducer purposes.

2.6 Moment Spread

It is established that magnetostrictive strain arises from rotation of magnetic moments, and hence that maximum strain results from maximum rotation of the moments, that is when all moments are rotated through 90° into the applied field direction. This can be achieved by the development of a uniaxial anisotropy in a direction orthogonal to the subsequent direction of magnetisation by, for instance, field annealing. The case where all moments are perfectly collinear in the induced easy axis direction in the demagnetised state is, however, an ideal one in amorphous alloys due to the inherently random nature of the structure. In such amorphous structures, where *a priori* no two atomic environments are topologically or chemically equivalent, there are distributions in local (short range) magnetic easy axis direction, and in local anisotropy energy density, although it is difficult to distinguish the two effects experimentally [Barandiarán *et al* 1989].

The moment orientations are determined by competing interactions; the exchange interaction aligning the spins and local anisotropy interactions turning the moments into the local easy axis directions [e.g. Coey 1978]. The balance between exchange and anisotropy forces results in an average moment direction with some distribution in orientation. The extent of this canting is determined predominantly by the ratio of the exchange stiffness parameter, A, and the local anisotropy, K_L.

The local anisotropies are dominated by the local crystal or ligand field due to the SRO and therefore the easy axes are random on a site to site basis. This leads to the random anisotropy model which is of particular importance in the study of 4f RE alloys whose local anisotropies are relatively very strong.

A distribution in atomic spacing is inherent in a disordered structure, as indicated by the width of the RDF. This leads to a distribution in spin-spin exchange interactions

as dictated by the Bethe-Slater curve. The topological and chemical disorder that causes distributions in exchange interactions, anisotropy energy density and easy axis direction similarly leads to variations in the magnitude and orientation of magnetic moments through weak lattice-moment interactions as well as due to partial delocalisation of the unpaired 3d electrons [Moorjani and Coey 1984]. Broad moment distributions have been observed via hyperfine interaction measurements in TM-M ferromagnetic alloys at low temperatures, although this distribution became narrow as the material approached its Curie temperature due to thermal averaging of the atomic environment by phonons, and also to local anisotropy decreasing faster than exchange as temperature increases [Coey 1978]. Ryan *et al* [1987] measured moment spreads of ~35° at x=0.88 and ~110° at x=0.93, with a correlation length of ~2.2nm. They found that by extrapolating the composition range Fe_xZr_{1-x} to amorphous pure Fe (x=1), hypothetically assuming that it could exist, the distribution in exchange interactions would be so great that the material would be speromagnetic. The distribution in exchange interactions could be so great in the Fe-Zr alloys that there could be some proportion of negative spin-spin interactions leading to antiferromagnetic local structural units. They stated that this "negative exchange is likely to be associated with shorter Fe-Fe bonds". Krey *et al* [1990] also considered the Fe-Zr alloys. They commented that the spatial fluctuations in the moment direction were compatible with those observed by Cowley *et al* [1988] in $Fe_{87}B_{17}$ and Melamud *et al* [1987] in $Fe_{78}B_{13}Si_9$ (see later), and arose from the "subtle interplay between the isotropic intra-atomic Coulomb interaction and the anisotropic kinetic terms in the electron Hamiltonian". Gang Xiao and Chien [1987] did a similar study using Fe_xRE_{1-x} (RE=Ti,Zr,Hf,Nb,Ta,Mo) and Fe_xM_{1-x} (M=B,Sb). They made similar conclusions to Ryan and Coey concerning Fe-RE but found that the Fe-M alloys had structures with narrow ferromagnetic interaction distributions and high mean moment per atom, similar to that of a bcc-like amorphous structure, exhibiting far less spero- or

asperomagnetism. The distribution of moments in TM-M alloys was estimated from the linewidths of hyperfine fields [Kaneyoshi and Tamura 1984]. A "rather broad" distribution of moments was measured, with some spins aligned antiferromagnetically. Again, this distribution was attributed to spatially varying short-range interaction due to the fluctuating environment.

The spatial fluctuation of moment direction as a result of competition between the exchange and local anisotropy was considered by Alben *et al* [1978]. They made the assumption for local moment materials that the orientational correlation length of the moments, L, was much longer than that of the anisotropy, d, which was expected to fluctuate approximately from site to site. Thus the fluctuation in moment direction takes the path of a random walk. Also they ignored the distribution in interactions and anisotropies, so leading to single valued parameters for A and K_L. From this, they obtained expressions for the average exchange energy density

$$E_{ex} \sim \frac{A}{L^2} \qquad 1.37$$

(A - exchange stiffness), and average anisotropy energy density

$$E_a \sim -K_L \left(\frac{d}{L}\right)^{\frac{3}{2}} \qquad 1.38$$

(K_L - local anisotropy). At minimum total energy,

$$\frac{d(E_{ex} + E_a)}{dL} = 0, \qquad 1.39$$

the expression for L becomes

$$L \sim \frac{16A^2}{9K_L^2 d^3} \qquad 1.40$$

and the resulting average energy density (E_{ex}+E_a) is then

$$E \sim \frac{-0.1K_L^4 d^6}{A^3}. \qquad 1.41$$

This holds where L>>d. For large K_L the moments follow the easy axes more closely, so L approaches d.

Using values of $A=10Jm^{-1}$ [Gyorgy 1978], $d\sim2.6\times10^{-10}m$ and $K_L\sim2\times10^5Jm^{-3}$ (estimated from the macroscopic anisotropy in uniaxial Fe-M crystals) as typical values for Fe-M alloys, they obtained values of $E\sim5\times10^{-5}Jm^{-3}$ and L~250μm (and L~0.5nm in RE-Fe alloys due to larger K_L). In reviewing this work O'Handley [1987] cited SEM pictures of ferromagnetic domains in TM-M amorphous alloys as support for this result [Leamy *et al* 1975, Hasegawa and Ranjan Ray 1978, Livingston and Morris 1985] where typical domain widths were of the order of L calculated above. Such a long correlation length implies very small spread around the average moment direction on a site to site scale.

However, there is evidence for larger moment spreads in TM-M alloys. Melamud *et al* [1987] used Mössbauer measurements to measure moment direction distributions with spreads of ±30-50° in field annealed METGLAS 2605S2. Savage and Spano [1982] reported measured in-ribbon-plane deviations of ±10° in transversely field annealed METGLAS 2605SC and ±30° in METGLAS 2605CO. This study was extended on METGLAS 2605SC [Methasiri *et al* 1985, Methasiri and Tang 1985] where the spread was found to decrease from ±18° to ±6° as the field anneal temperature was increased from 321°C to 403°C. Ito *et al* [1981] measured the local magnetisation direction to be Gaussian with a spread of ~45° in a Co-rich alloy. Bucholtz *et al* [1986] used magnetostriction measurements to obtain a value of spread of ±10° in transversely field annealed METGLAS 2605S2.

More recently Cowley *et al* [1988] have measured moment canting using neutron diffraction techniques at ILL. Measurements were taken on samples in the as-received

state in a field of 2T at 10K. Measurements at higher temperatures showed no significant difference implying the canting was not due to thermal fluctuations. They found that the canting in $Fe_{78}B_{12}Si_{10}$ (METGLAS 2605S2) was too small to be observed but could be seen in $Fe_{78}B_{17}$ and was substantially larger in two Fe-Ni based alloys, consistent perhaps with higher local anisotropies in the binary alloys. The data suggest that spin directions are nearly randomly distributed from site to site, and the maximum canting observed was estimated to be approximately ±50°, although the spread ranged from this maximum to almost zero for different samples. The atomic and magnetic structure in as-received material is not well characterised and further work is planned by the magnetic materials group at Bath on stress relieved and field annealed samples whose structure is more uniform and better characterised.

The observation that there is significant moment spread from site to site in TM-M amorphous alloys appears to directly challenge the conclusion of the Alben *et al* model, that moments have an orientational correlation length of ~250μm. Although domains have widths of $\sim 10^2$-10^3μm in these field annealed alloys, domain studies using the Bitter technique show a secondary wall system whose finely spaced walls lie across the larger domains, generally perpendicular to the main domain walls when in the demagnetised state [Smith *et al* 1988] (see section 4.2.3). The smaller domains have widths ~10-40μm although smaller domains would be difficult to see due to the size of the colloid. It has been suggested [Smith *et al* 1988] that this secondary wall system is consistent with dispersion in magnetisation vector within the larger domains (figure 4.12). These observations imply that domain pictures do not seem to support the 250μm correlation length, as suggested by O'Handley, but give an upper limit of this length at ~40μm.

If the calculated value of L=250μm is put into the expressions for average exchange and anisotropy energy densities, the total energy density, E, is calculated to be $\sim 10^{-5}$Jm^{-3}. As discussed in section 2.4, the total is more generally the sum of energy densities due

(in this case where there is no field anneal induced anisotropy) to a)exchange, E_{ex} b)crystal lattice anisotropy, E_{an} c)shape factor, E_{shape} d)directional ordering, $E_{d.o.}$ and e)stress induced anisotropy, E_σ:

$$E_k = E_{ex} + E_{an} + E_{shape} + E_{d.o.} + E_\sigma \qquad 1.42$$

If material is used in which in which the last two contributions are reduced to zero by full internal stress relief anneal in the absence of a magnetic field, and where the shape factor can be accounted for, the resulting average energy density, E_k, is given by the sum of the exchange and anisotropy contributions, $E_{ex}+E_a$. This (shape factor corrected) average energy density in fully stress relieved samples has been measured to be ~1-10Jm^{-3} in Fe-based alloys and ~10-20Jm^{-3} in Fe-Ni based alloys - significantly higher than that predicted in the model. Possible causes for this discrepancy are discussed by Gibbs [1990b]. It is possible that the moment correlation length is lower due to a higher K_L than derived from uniaxial Fe-M crystals. As Furthmüller *et al* [1987] pointed out, the coordination number in amorphous alloys is approximately 12, closer to that of hcp or fcc crystal structures than to bcc. Hence the value of K_u for the structural unit should be of the order of that in crystalline Co rather than Fe. This would give $K_u=10^5Jm^{-3}$. The correlation length, d, is estimated to be 1nm [O'Handley 1987, Gibbs 1990]. From this the moment correlation length was calculated to be L=20μm [Gibbs 1990]. Furthermore, at room temperature, where $T\sim T_c$, partial averaging of atomic positions by phonons imply some distribution in the exchange interaction (and so in M_s). The spread in this distribution is difficult to quantify, but Gibbs stated that it is not unreasonable to assume an order of magnitude variation in exchange stiffness, A, reducing the moment correlation length to L~200nm. This has the effect of making the model less accurate since the initial assumption that moment correlation length is much longer than that of local easy axis (L>>l) no longer holds. Consequently, the upper bound estimate for L is ~1mm, but the lower estimate is uncertain. It is concluded that the moment correlation

length is significantly shorter than previously proposed, and that the moment spread is correspondingly higher. There is evidence that this spread is significant even at high fields and low temperatures.

Studies on the magnetisation on the approach to saturation [Fähnle and Kronmüller 1978, Garoche and Mazelemoff 1984] indicated that moment dispersion is due to stress anisotropy around structural defects, resulting in spatially uncorrelated anisotropy $<10^6 Jm^{-3}$ in Fe-Ni-B thin films. However, they found that the spin canting, even with strong uniaxial anisotropy, is only a few degrees in fields of $\sim 80 kAm^{-1}$, in contrast with the findings of Melamud and Cowley *et al.* Fähnle [private communication, 1990] pointed out that spin cantings of the order of that found by these Mössbauer studies would indicate strongly damped spin waves and a large intrinsic coercive field, neither of which are seen. He suggested that they might arise from competing exchange interactions rather that from random local anisotropies.

Since magnetostrictive strain is a direct consequence of moment rotation, it can be seen that a spread in moment direction about a transverse macroscopic easy axis has the effect of reducing the macroscopic magnetostrictive strain of the material without affecting the magnetostriction constant, λ_s. Similarly, a spread about a longitudinal axis increases the strain (as described in equation 4.3).

It should be noted, however, that there is no contribution to λ_e by moments which are highly coupled into the structure by very strong local anisotropy since they are not able to rotate within the applied fields used in this study and that of Bucholtz. These moments are constrained by the local anisotropy to the (randomly oriented) local easy axis, and so can exhibit wide angular spread. This site-to-site spread is not evident in magnetostriction measurements, but has been seen by neutron scattering, even at very high applied fields and low temperatures [Cowley *et al* 1988], indicating that the applied fields used in this study had the effect of rotating only a small proportion of the moments.

Therefore the spread discussed in this study was not the absolute value, but an apparent one, reflecting only those moments that contributed to the magnetisation. This apparent spread was generally significantly less than the actual one.

3 Method and experimental procedure

3.1 Introduction

This chapter describes the methods used to measure the parameters that were investigated in this study. It begins by describing the equipment used to prepare the samples and to obtain the initial data; namely the annealing system, the magnetisation measurement system, the optical fibre dilatometer to measure magnetostriction, the ΔE measurement system, the Bitter technique used for domain studies and, briefly, the X-ray diffraction equipment. The subsequent section covers the methods used to extract the required information from the measured data.

3.2 Measurement of Data

This section describes the equipment and methods used in the acquisition of the measured data.

3.2.1 Preparation of Samples

Most material used in this work is commercially available. The alloys were obtained from Vacuumschmelze GmbH of Germany and the Allied-Signal of the USA. The melt-spun material was in the form of ribbons of various widths and thicknesses, and was stored in dessicators at all times when not in use. Relevant manufacturers' data on the alloys are given in table 3.1.

Samples were cut from the ribbons with sharp scissors, to dimensions of approximately 58×5mm. Care was taken to avoid edge cracks, nicks and buckling, since these could be sites of strong stresses. Also, if the samples were not flat, their strain

Alloy Trade Name	Composition	B_s (T)	T_c (°C)	T_x (°C)	λ_s (ppm)
METGLAS 2605S2	$Fe_{78}Si_9B_{13}$	1.58	415	550	27
METGLAS 2605SC	$Fe_{81}Si_{3.5}B_{13.5}C_2$	1.61	370	480	30
METGLAS 2826MB	$Fe_{40}Ni_{38}Mo_4B_{18}$	0.88	353	410	12
VAC0040	$Fe_{40}Ni_{40}B_{20}$	1.0	400	400	
VAC7505	$Fe_{78}Si_9B_{11}C_2$	1.5	420	500	30

Table 3.1: Manufacturers' data on the alloys used in this study.

could be restricted inside the dilatometer sample holders (section 3.2.3). Therefore the samples were rejected if they were not deemed to be suitable. They were cut so that their long axis was parallel to the original ribbon axis for convenience (this had the effect of reducing the demagnetisation due to the surface features, which were generally longitudinally oriented, although this should have a negligible effect). While handling the material, gloves were always worn and care was taken to ensure that the surfaces were not contaminated. Also, all samples were cleaned with acetone to remove grease and dirt before and after annealing. Since the wheel on a melt-spinner drags the material away from the nozzle at a high velocity as it solidifies, most quenched-in stresses are as a result of this and tend to lie along the ribbon axis. The largest component of the easy axis of quenched-in stress induced magnetic anisotropy, where it was evident, tended to be along this axis in much of the material as well (although there were also smaller transverse and perpendicular components), but this was notionally annealed out during stress-relief anneals.

All samples were stress relieved before magnetic annealing, to ensure that their properties were consistent with each other and independent of the manufacturing and

processing histories. Stress relief was achieved by annealing in a furnace in air in the absence of fields (other than ambient) at temperatures and for times chosen to yield minimum values of coercivity. However, annealing has the effect not only of relieving quenched-in stresses but also of promoting crystallisation, which degrades the properties of the amorphous structure by inducing stresses around the crystallised grains due to differences in density of the different phases [Ok and Morrish 1981] (see section 2.5). These two processes have opposite effects on the coercivity, so H_c of an amorphous alloy subjected to an isothermal anneal will initially decrease due to stress relief, and then begin to increase as crystallisation sets in. The relationship between extent of crystallisation and coercivity has been investigated by Herzer and Hilzinger [1986] and Sheard *et al* [1989]. The time at which the minimum in H_c occurs and the value of this minimum depend on the anneal temperature in relation to the crystallisation temperature of the material, T_x. Clearly zero coercivity is an ideal case and coercivity exists due to a number of sources as described in Kronmüller [1981a]. In the alloys studied, it was found that the samples had been stress relieved to a high degree without any noticeable crystallisation setting in where H_c was approximately $1 Am^{-1}$ or less.

A Eurotherm-controlled chamber furnace was available for annealing without applied field. An aluminium table of large thermal mass, with a piece of plate aluminium resting on top, was placed in the furnace and allowed to equilibrate at the required temperature. The temperature of the table was monitored using a chromel-alumel thermocouple junction bolted to it, sensed by a Digitron meter. The sample was placed on the table beneath the aluminium plate. Because of its small thermal mass and good heat conductivity, it can be assumed that it reached anneal temperature instantaneously.

The field-annealing equipment consisted of a large water-cooled electromagnet with iron cores (100mm in diameter and 100mm pole gap) driven by a Farnell constant current power supply, and a high-temperature hot-air blower, the outlet of which was

directed down a Pyrex tube which lay between the poles of the magnet. The sample was held between two circular plates of aluminium which were loosely clamped together. These were positioned horizontally in the tube directly between the centre of the poles. A chromel-alumel thermocouple was fixed to the plates and its temperature was read by a Digitron temperature measurement instrument.

For the initial part of the project, i.e. the oblique field anneals and the time-temperature studies on VAC0040, a current of 15A was passed through the electromagnet. Thereafter, this was increased to 25A, due to a more powerful supply becoming available. This did not increase the field proportionately because the iron cores were approaching saturation. The induction at a point centrally between the poles was measured, using a Gaussmeter, to be 0.4T with a current of 25A. The variation of field with current and with horizontal position between the poles is shown in figure 3.1. The start time of the anneal was the point at which the thermocouple temperature reached the anneal temperature. The time taken for anneal temperature to be achieved and for the subsequent cool (with the heater on the air blower turned off) are shown in the anneal temperature time-profile in figure 3.2.

3.2.2 Magnetisation Measurement System

The magnetic properties of the materials were derived from the relation between its magnetisation, M (or induction, B) and applied field, H, i.e. the hysteresis loop. This was measured using the computer controlled, quasi-DC, digital M-H measurement system, described in Squire *et al* [1988], and in full detail in Sheard [1989]. It operated on the principle of Faraday's law where a change in applied magnetic induction, B, along the axis of a conducting coil, induces an emf spike, V, across the coil such that

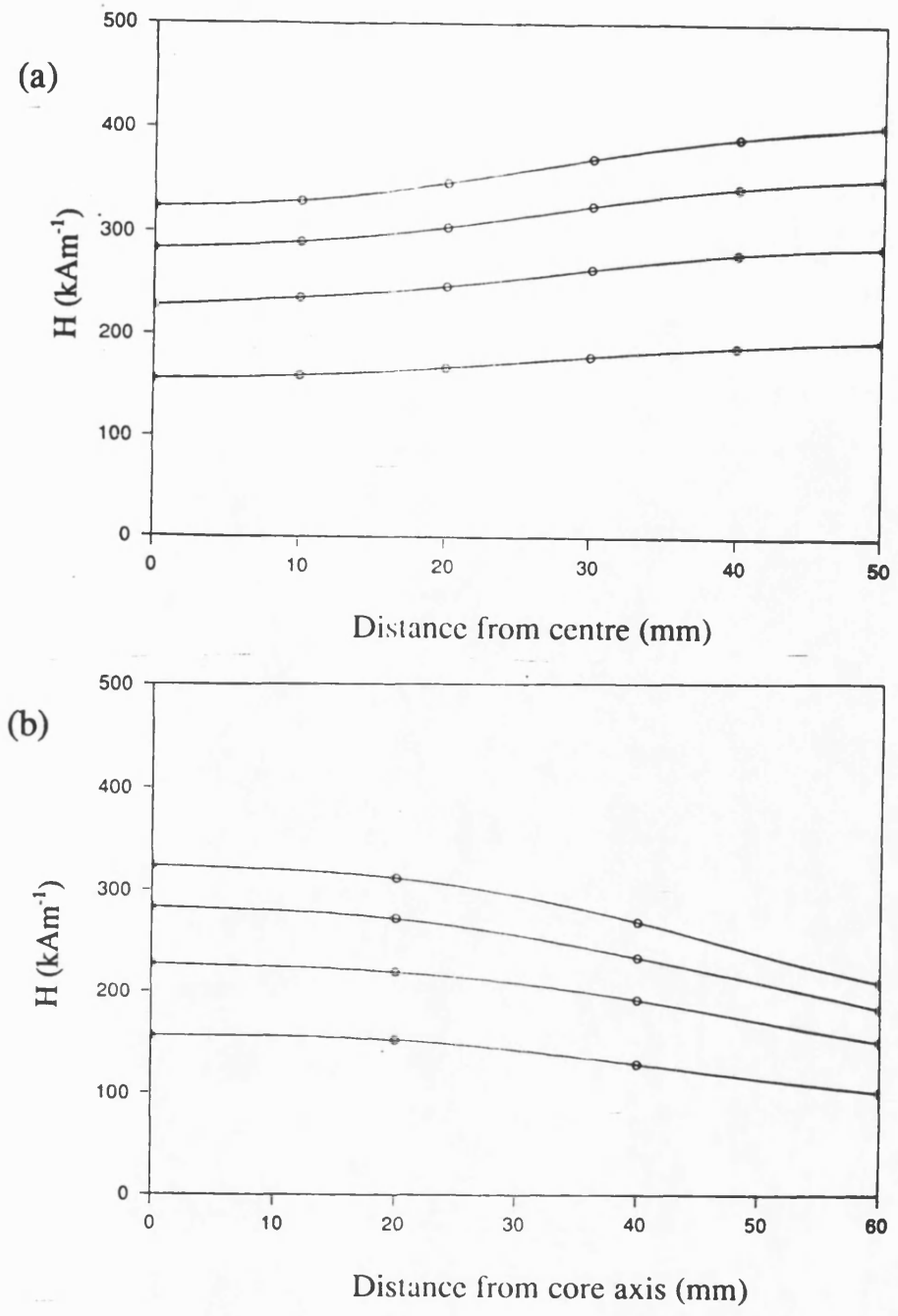

Figure 3.1: Measured field profiles between the cores of the field anneal electromagnet a) in the field direction b) transverse to the field direction, with driving currents of 25, 20, 15 and 10 Amps. The zero position was halfway between the cores, on their centre axis. Hence in (a) 50mm is directly next to one of the cores. The external field variation over a centrally placed sample 50mm long was approximately 6% and 10% during transverse and longitudinal field anneals respectively. The internal field variation would be less than this because the high permeability of the materials has the effect of making the flux density more uniform over the whole sample.

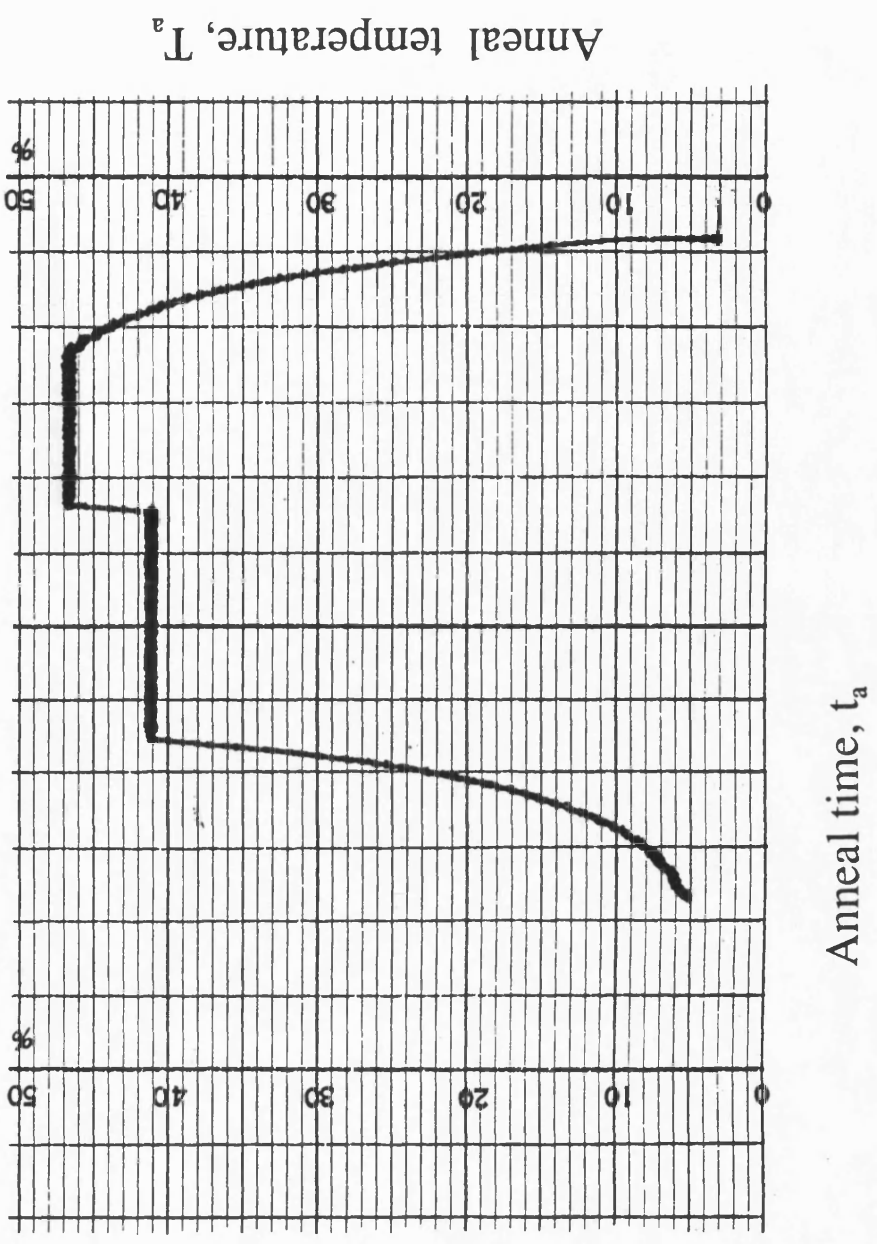

Figure 3.2: Typical field anneal time-temperature profile. The time axis leads from right to left in this diagram. One abscissa increment represents 5 minutes and one ordinate increment represents 10°C, with 0 at 0°C. The figure therefore represents a 10 minute anneal at 470°c followed by 15 minutes at 410°C.

$$V = nA\frac{dB}{dt}, \qquad 3.1$$

where A and n are the cross-sectional area and number of turns in the coil, respectively.

The system comprised a 1.5m×75mmI/D solenoid driven by a Kepco ±20A ±20V power amplifier, capable of producing up to 15kAm^{-1} along the solenoid axis. Within the solenoid were two identical search coils, 82mm in length with 40000 turns, positioned along the axis, 470mm from each other and each coil approximately equal distances from the ends of the solenoid (~400mm). This achieved flux distributions around each coil with a very high degree of uniformity when no samples were present. Thus, when the current through the solenoid was stepped, the resulting field step induced an emf spike across each of the search coils, the integral of which was proportional the change in induction, ΔB, of their environment. The search coils were arranged in a bridge which could be balanced so that the output emf was zero when the coils' environments were identical, such as when they were both empty (apart from air). This had the effect of cancelling any ambient fields or common-mode variations and interference. The sample to be measured was placed centrally inside one of the coils. The output emf was proportional to the change in induction of the sample and free space in the first coil minus the free space in the second:

$$\int V dt \propto \mu_0(H+M) - \mu_0 H \qquad 3.2$$

$$\propto \mu_0 M.$$

Consequently the time integral of the output emf was proportional to the change in magnetisation of the sample only.

The stepping of the current through the solenoid, and hence of the applied field, was controlled by the computer. Prior to starting the measurement, the computer sent maximum output signal to the input of the power amplifier via a D-A converter. The

power amplifier was operated in current mode so that the output current was proportional to the input voltage. The maximum required applied field could be set by adjustment of a potentiometer across the power amplifier input. In this study, this maximum field was determined by a rough trial-and-error, such that it was large enough to approximately saturate the sample without being so large that unnecessary data were collected at this state. Typical values for H_{max} for transversely field annealed metallic glasses used here were of the order of 8kA/m (a current of approximately 10A).

At this point, when instructed by the operator, the computer cycled the amplifier input signal from maximum positive to maximum negative voltage, and back to maximum positive, in discrete steps at constant software-specified time intervals, hence stepping the field from saturation in one direction along the solenoid axis to saturation in the opposite direction, and back again. The D-A converter had a time constant of approximately 1ms. Consequently, it can be assumed that the applied field had reached a steady state at approximately 5ms after the computer stepped the input signal (the power amplifier time constant was less than this, so was not a factor). As a result, the emf output spike was approximately 5ms full width, and the integrator was designed accordingly. A further 300-400ms pause (minimum) was required for the computer to input the signal from the integrator via an A-D converter, to process the data, and to reset the integrator before the next step.

If the applied field were cycled at a constant rate with respect to time, i.e. constant ΔH_{app} at each step, then much of the information on the M-H loop could be missed due to insufficient sampling in the case of magnetically soft material such as most amorphous alloys, since a large change in magnetisation would occur over a small range of H_{app}. Consequently, the sampling rate must be increased over the range where $\frac{dM}{dH}$ is significantly increased. Since the system was computer controlled, the manner in which H_{app} was cycled could be dictated very precisely. The input voltage to the power amplifier was

cycled in the form of a function defined in the computer program, so that the changes in H_{app} were large at large H/H_{max}, but decreased as H_{app} approached zero, where $\frac{dM}{dH}$ increased. The function used was based on tangent functions, specifically

$$\frac{H}{H_{max}} = \frac{\tan(2b\pi t/T)}{\tan(b\pi/2)}, \quad 0 < b < 1 \qquad 3.3$$

where t and T were the current step number and the total number of steps in the cycle, respectively, and the shape factor, b, was an operator specified parameter that dictated the rate at which ΔH_{app} varied with H_{app}. For stress relieved metallic glasses, 4kA/m was generally required to achieve a high degree of saturation, but approximately 90% of the change in magnetisation occurred within 50-100Am^{-1} of the demagnetised state, and in these cases, a shape factor of 0.9-0.99 was found to give optimum spacing of sampling points on the M-H loop.

Apart from optimising the sampling rate, this had a second advantage; that is, at low H_{app} where $\frac{dM}{dH}$ was large, the decrease in ΔM per step resulted in ΔM remaining low for each step. As stated, the steps occurred over a few milliseconds, with intervals of several hundred milliseconds. In this way large changes in M with respect to time were avoided, so avoiding rapid domain wall motion, which precipitate eddy currents around them, causing loss of magnetisation energy (hysteresis). Coercivities of less than 1Am^{-1} could be measured with reproducibility of approximately $\pm 0.2 Am^{-1}$. This was the justification for the descriptive term "quasi-DC".

A significant problem with DC magnetisation measurement systems to date is that the hysteresis loop is a closed loop, and all DC analogue integrator systems suffer from drift, which can be minimised but not removed. In this system, the field was cycled over a time period of at least a minute, but each measurement of ΔM was taken over the period of a field step, i.e. a few milliseconds. This drastically cut down the amount of drift. As the integrator was reset before each step, it was reasonable to assume that the drift during

each step period was similar, so that the drift in magnetisation was approximately constant with time. Using this assumption, each ΔM value was altered by an amount equal to the total drift between first and last M values divided by the number of steps per cycle. This was done by the computer after the cycle had been completed. Further, the software allowed any number of cycles (operator specified) to be measured and the mean values of M to be calculated. This acted as an added method of noise reduction in the cases where the drift in magnetisation readings was high and gave less confidence in the assumption of constant drift during each step.

Magnetisation was calculated by assuming that saturation of the sample was notionally achieved by the maximum applied field, and by normalising the M values measured (in arbitrary units) at $\pm H_{app}(max)$ to the manufacturers' values of $\pm M_s$.

Before measuring M-H loops, values for variables such as shape factor, b, and maximum applied field were ascertained by trial and error to optimise the number of points around the important region of low magnetisation while having enough data at larger fields to give information about the approach to saturation and to ensure that saturation was reached. In this study, four different M-H loops were measured for each sample, each one taken after removing and replacing the sample in a different orientation (e.g. upside-down, always with the long axis parallel to the solenoid axis). The main errors in the calculation of coercivity and susceptibility (see later) arose from variations in different M-H data sets rather than from errors in the calculation of the parameters from one data set alone. Where errors in such parameters are quoted, they arise from the standard deviation of the mean from the four different data sets for each sample. The error in the susceptibility data, then, is the standard deviation of the mean of eight gradients; two branches of each hysteresis curve.

3.2.3 Optical Fibre Dilatometer

This system measured change in length of a ribbon sample using the principle that when one end was fixed and the other end placed across the centre of a beam of light, the sample would block off more of the beam as it lengthened, reducing the amount of light picked up by a photodetector behind the sample (see figure 3.3). If the sample edge were close to the centre of the circular beam, the intensity of the beam were uniform over the whole beam, and the change in sample length Δl were much smaller than the diameter of the beam, D, then the change in transmitted power, P, is proportional to the extension of the sample. Specifically,

$$\frac{dP}{dl} = \frac{4P_0}{\pi D} = \text{constant}, \quad (l \ll D) \qquad 3.4$$

P_0 is the power transmitted by the total beam.

The system is fully described in Squire & Gibbs [1987]. A block diagram is shown in figure 3.4, taken from the paper.

The light beam source was an LED driven by a 10kHz AC supply. The light was directed into a beam splitter. The signal beam was directed along an optical fibre into an aluminium housing. At the end of the fibre a small lens was positioned to focus the emergent light into a parallel beam. This beam, a few millimetres long, was focussed by a similar lens onto the end of a optical fibre which directed the light into a photodetector. The ends of the optical fibres and lenses were arranged vertically in the housing so as to achieve mechanical stability. The other optical fibre from the beam splitter directed the light straight into a similar photodetector. The outputs of the two detectors were combined so that the output could be zeroed when the sample edge was central within the beam so cancelling any variation in source intensity (because of the low frequency of intensity variation, 10kHz, the phase difference due to different path lengths between

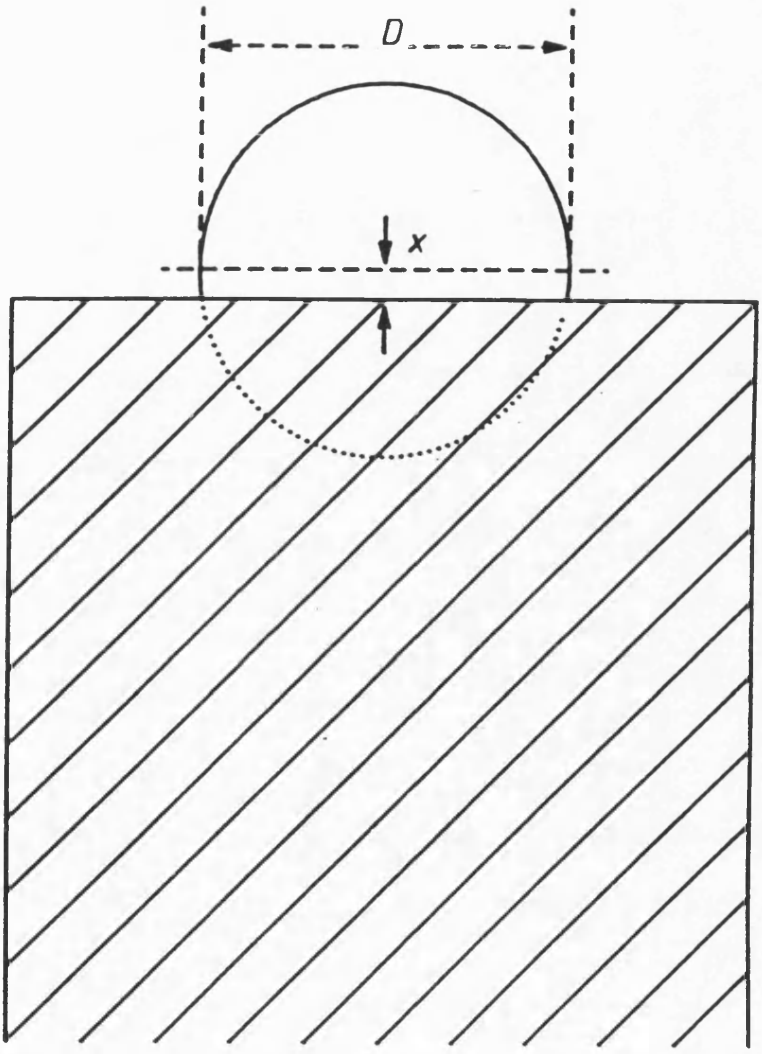

Figure 3.3: Schematic diagram of the sample end acting as a shutter across half of the beam of the optical fibre dilatometer (reproduced from Squire and Gibbs [1987]). If x<<D then the change in beam intensity picked up by the detector is approximately proportional to the strain, x.

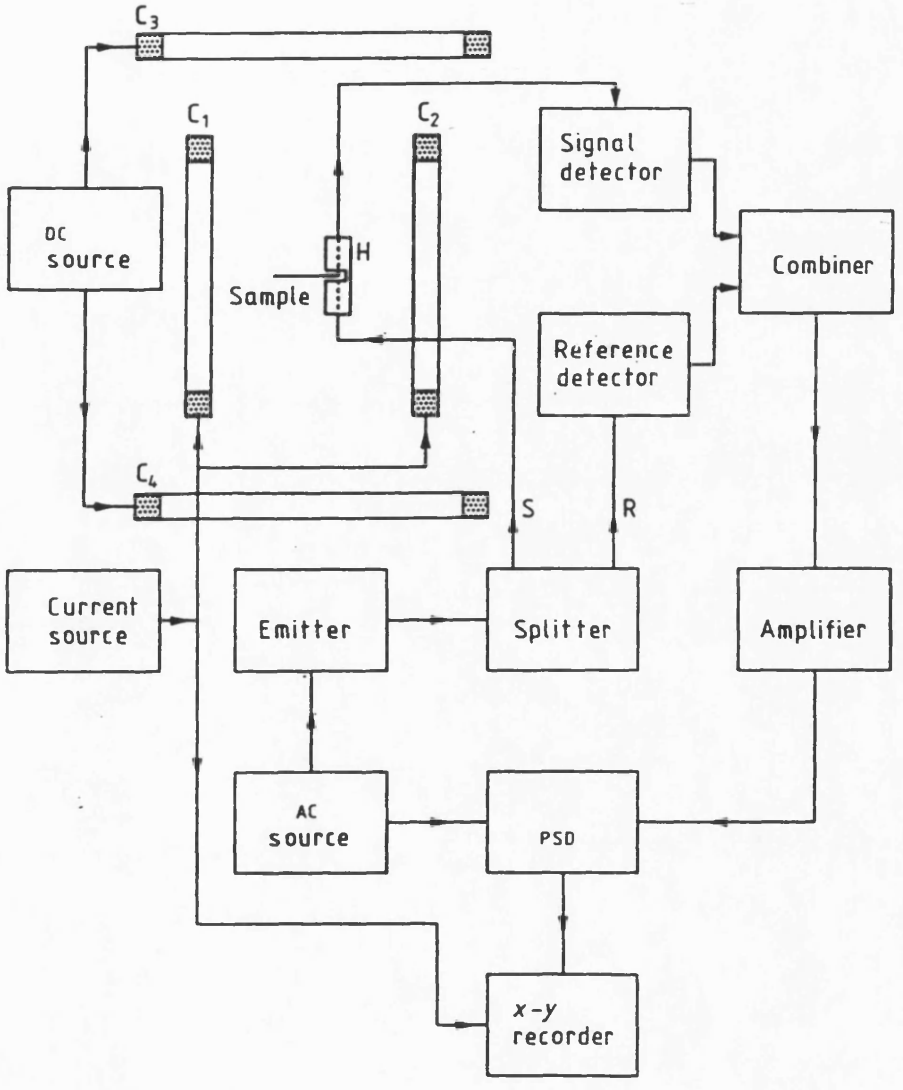

Figure 3.4: Block diagram of the optical fibre dilatometer apparatus (reproduced from Squire and Gibbs [1987]).

the two signals was negligible). This signal was amplified and fed into a phase sensitive detector (PSD) along with the LED supply voltage acting as the frequency reference. The phase of the signal voltage could be shifted until the signal and reference were in phase (this coincided with the maximum output voltage). They were then multiplied and the resulting signal was passed through a low pass filter to obtain a DC output, proportional to the signal voltage amplitude. During the project, the pre-amplifier, phase shifter, and the PSD were replaced by a lock-in amplifier (LIA), which was a single unit that performed the same tasks.

The sample to be measured was placed in a holder (see figure 3.5). The holder consisted of two clean glass slides separated by two non-magnetic spacers such as aluminium. The base slide was longer than the upper to allow part of the sample to protrude. The sample was placed in the holder and the protruding part would then be clamped down using "Tico pad" held down fast with masking tape. "Tico pad" was chosen because it was mechanically strong while elastic enough to avoid straining or damaging the sample when clamping it. Masking tape was found to be adequate as it was strong enough to hold the sample without creeping. For best results, the spacing of the slides was such that a) it was not so small that the movement or strain of the sample was not suppressed, i.e. that static friction was overcome by the forces causing the sample strain, and b) the spacing was not wide enough to allow vertical movement. This could cause flapping, where apparent strain decreases as the sample expands (see figure 3.11a and b).

In practice, it was found that the best spacing was generally 2-3 times the ribbon thickness, although this would increase for a sample that was not flat or that had nicks at the edges where it had been cut. As a rule of thumb, it was found that this occurred when there was a smooth sliding fit between the samples and the holder.

The sample and holder were placed horizontally on an aluminium block of large

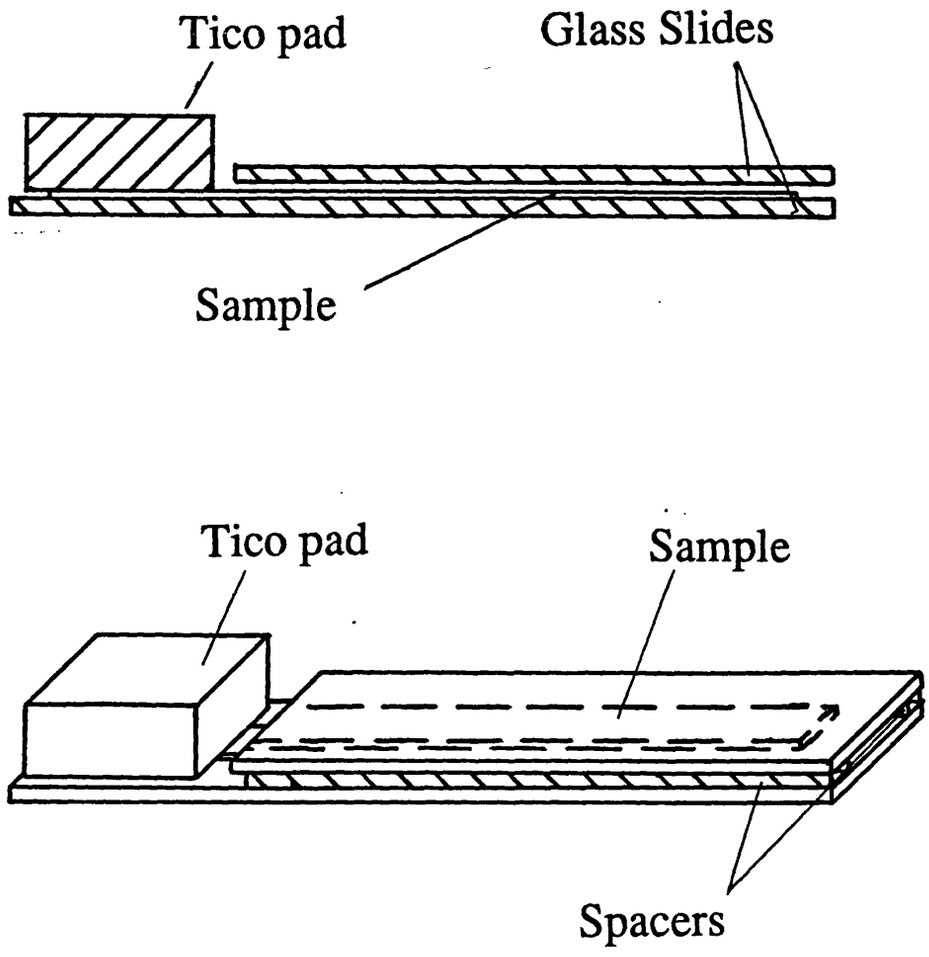

Figure 3.5: Sample holder for the optical fibre dilatometer.

thermal mass to stabilise temperature variations. The block was mounted on an x-table moved by turning a winder, one complete turn through 360° of which moved the table a distance of 12.5μm. The whole, including the aluminium housing containing the optical fibre assembly, resided in a polystyrene-lined box (to minimise temperature variations), supported on vibration dampers.

The sample was positioned with its long axis parallel to the direction of movement of the x-table and in line with the beam. The intensity of the beam picked up by the detector with respect to the relative position of the sample in the x-directon is given in figure 3.6 (from Squire & Gibbs 1987). It was found from this that the beam diameter was approximately 120μm. More importantly, the range where dP/dl=constant held to a high degree was 20-30μm across. The maximum strain expected from a 50mm sample of amorphous alloy would be less than 100ppm, i.e. less than 5μm; significantly smaller than the linear range of dP/dl.

The x-table was moved until the edge of the sample lay at the centre of the linear region of dP/dl, allowing for the reduction in beam intensity due to the glass holder. This corresponded to approximately half-way across the beam. This position was determined by finding the inflection in the intensity output with respect to the x-table position (see figure 3.6). The beam combiner was adjusted so that its output was zeroed, and the LIA amplification increased to the most suitable setting, such that the maximum input voltage corresponded approximately to the maximum strain to be measured. In this study this was ±1mV full scale input voltage. The LIA output, V_o, was ±10V full scale for all settings.

Having selected an amplification scale, the constant of proportionality between the LIA output voltage and the strain, C, was calibrated by measuring V_o with respect to relative position of the sample edge within the beam, l, (by movement of the x-table), which was linear over the whole range of l, and determining the gradient, dV_o/dl, so that

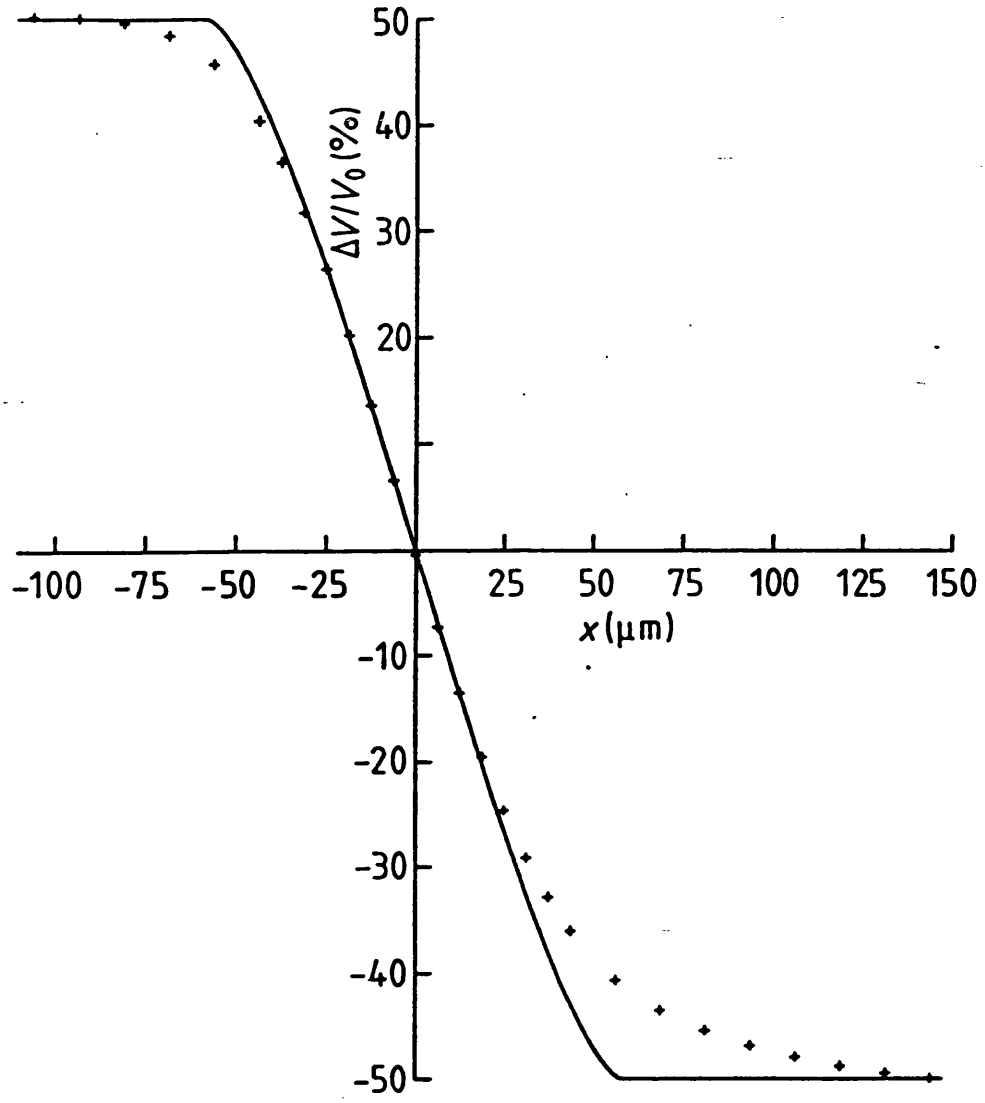

Figure 3.6: Variation of output signal of the optical fibre dilatometer with respect to the position of the sample end within the beam (reproduced from Squire and Gibbs [1987]). The linear region is over 10-20μm. Maximum extension expected from a 50mm sample is of the order of 3μm.

$$I = C V_o. \qquad 3.5$$

This calibration was done for each different sample holder and was repeated on a regular basis to allow for slight changes in C due to temporal variations in the instrumentation.

Magnetostriction was measured simply by measuring the strain of the sample with respect to field change only. The optical fibre assembly was surrounded by a pair of Helmholtz coils whose axis was in the x-direction, such that the sample lay at their centre, in a region of uniform flux density. The field was stepped in a similar way to the magnetisation rig. The computer software initiated each field step by changing the input signal to a power amplifier. The field was calibrated with respect to the current passing through the coils (which was measured by reading the voltage drop across a known resistance into the computer via an A-D converter) by measurement of the field using a Gaussmeter. This calibration was done each time the assembly was moved for any reason. At the end of each step, the LIA output voltage, V_o, was passed through an A-D converter and read by the computer. As with the DC magnetisation rig, the field was cycled from saturation in one direction to saturation in the opposite direction and back again. For the same reasons as the magnetisation rig, the results obtained could be termed quasi-DC. The maximum field attained was approximately 3.5kA/m during most of the project, but was increased to approximately 8kA/m for the crystallisation studies by the addition of more turns to the Helmholtz coils. Each coil comprised 400 turns of 1.5mm diameter copper wire, 20cm inner radius, their centres were 21cm apart. They were designed to have a resistance of 6Ω each so that when connected in parallel, they were of optimum load impedance to achieve maximum current from the Kepco ±12A ±36V power amplifier.

The profile of the field was approximated by a program, written by J. Freestone at Bath University, which used two methods to calculate the theoretical variation of field induced by Helmholtz coils. The method was firstly to determine the length of wire of

known cross-sectional area and resistivity to wind a pair of coils to a given resistance. Each coil was wound within a channel of square cross-section of known width. This determined the number of turns in the coils, n, and their mean radius, a. Parameters that could then be set included channel width, coil separation and current, I (the total field is optimum where the coil spacing is equal to the radius in the case of infinitesimally thin wires, and is close to optimum for coils with finite cross-sectional area). The first method calculated the total field due to two thin coils of radius a carrying a current nI, where the field at distance x along the coil axis by one of the coils is given by

$$H = \frac{nIa^2}{2(a^2+x^2)^{\frac{3}{2}}}, \qquad 3.6$$

such that, as mentioned, when x=a the field is constant between the coils. The second method used a more complex arrangement where current flowed through the whole square cross-sectional channel rather than through the actual arrangement of a coiled circular cross-sectional wire within the channel. This method is described fully in Zijlstra [1967]. The field profiles obtained from these two sets of calculations are shown in figure 3.7. The outer vertical lines signify the positions of the centres of the coils and the inner ones are the range over which the field variation is less than 1%. The two profiles appear very similar and the 1% range is the same for both. The difference in total field strength was thought to arise from the differences in the cross-sections of the coils used in the calculations and some correction for the packing fraction of the wire within the channel would increase the accuracy. The significant finding here is that the field was calculated to be constant to within 1% over a range of 134mm - far longer than any of the samples measured. The actual field profile along the coil axis where the samples were placed was measured using a Gaussmeter with the Hall probe positioned using a micromanipulator. The field strength is shown to be in good agreement with those of the calculated profiles (figure 3.8). However, there was an approximately linear increase

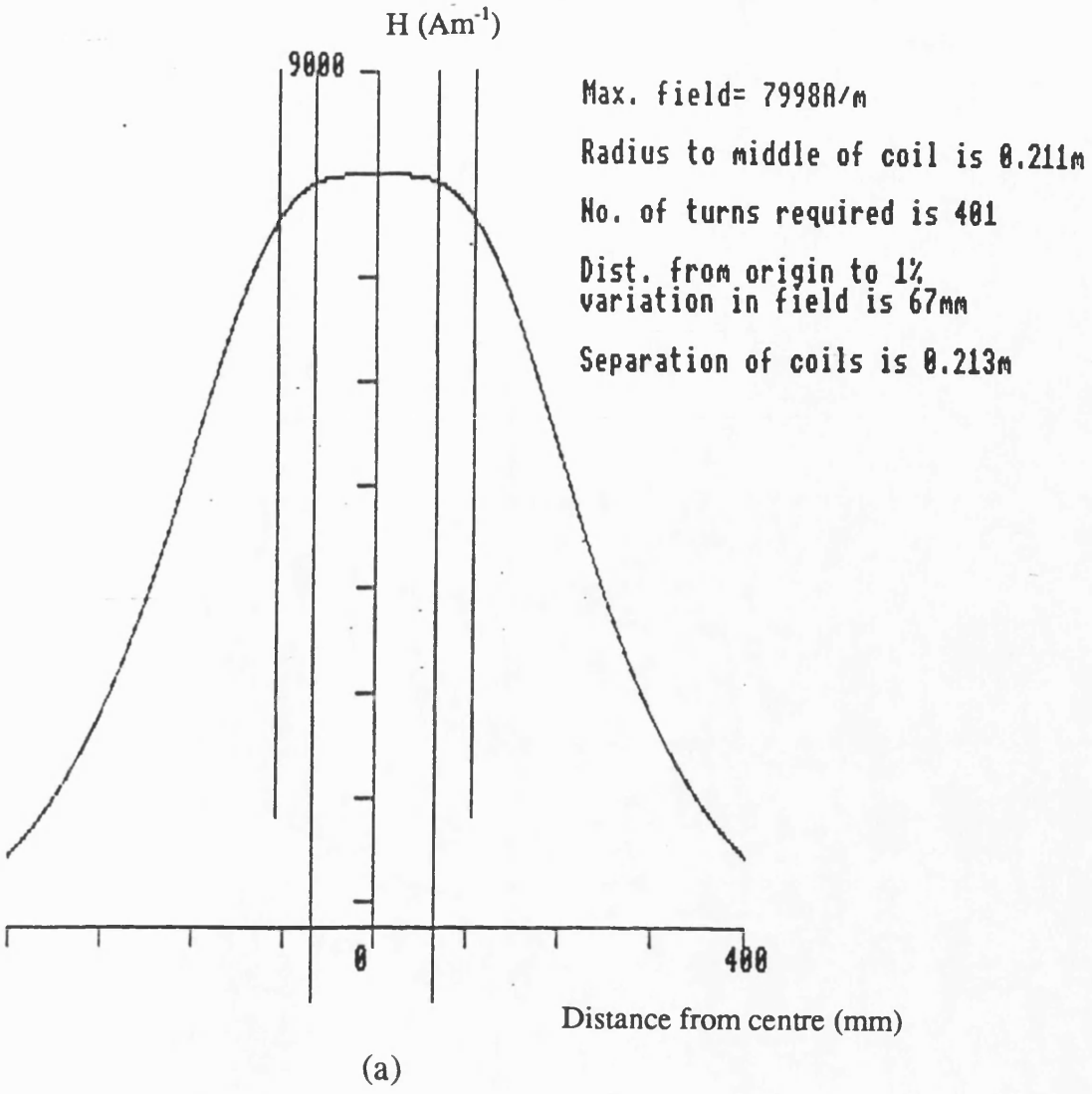

(a)

Figure 3.7: Calculated field profiles of the Helmholtz coils on the dilatometer apparatus using a) Ampères law and b) Ziljstra's method [J. Freestone, private communication] with coil current of 11.8 Amps (which was the maximum attainable in practice). The outer vertical lines represent the positions of the centres of the coils and the inner lines represent the region over which the field variation is less than 1%. Both methods predicted this range to be a total of 134mm. This compares with a maximum sample length of 70mm in this study.

The actual number of turns per coil was 400. The calculation of the values of maximum field strength were more sensitive to error than the shape of the field profile, but were in fairly good agreement with the measured value of $7894 Am^{-1}$.

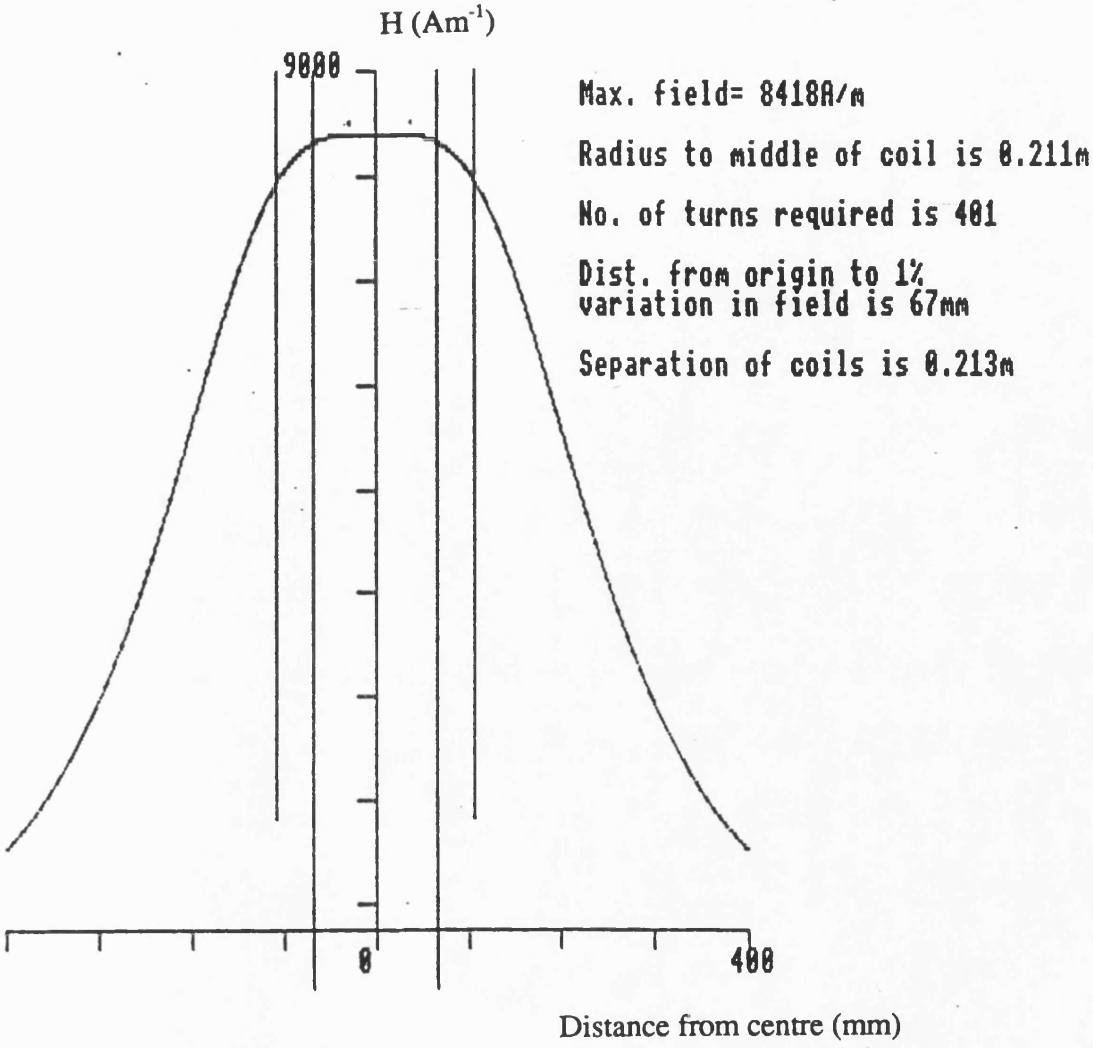
H (Am-1)
9000
Max. field= 8418A/m
Radius to middle of coil is 0.211m
No. of turns required is 401
Dist. from origin to 1% variation in field is 67mm
Separation of coils is 0.213m
0
400
Distance from centre (mm)

(b)

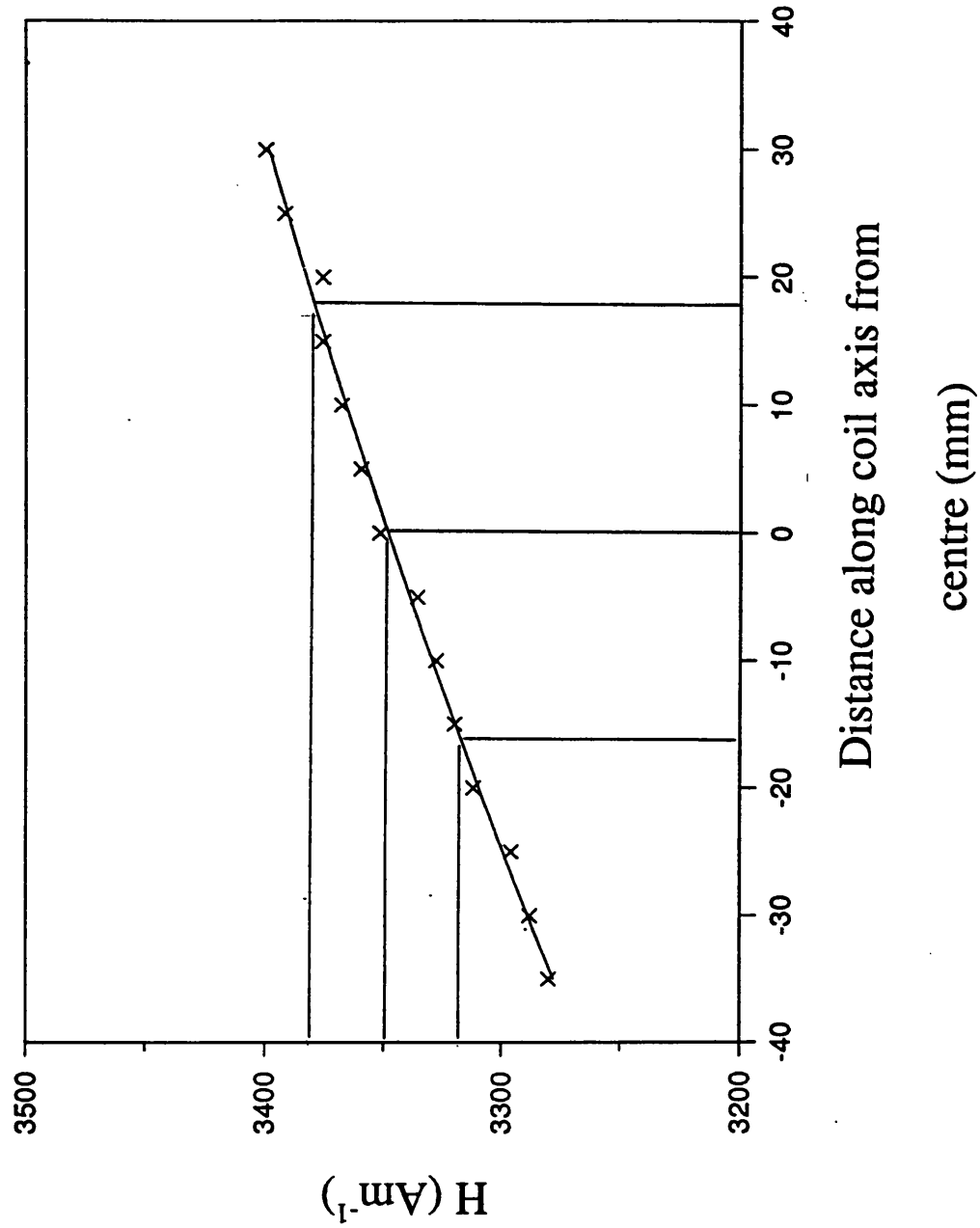

Figure 3.8: Measured field profile of the Helmholtz coils on the dilatometer apparatus with coil current of 5 Amps (low enough to avoid current heating of the coils and so ensure a steady field). There is a monotonic increase in H towards one of the coils due to slight differences in them. The length of sample free from the Tico pad clamp was generally 45mm. The field variation over this distance was approximately 3%.

in field with respect to position along the axis away from the end with the optical fibre assembly at the rate of ~1.84(Am^{-1})mm^{-1}. This measured variation amounted to 3% of the total field over the length of a typical sample (60mm), which was thought to occur due to slight differences in the packing tightness of the wire and their resistances (measured to be 5.2 and 5.3Ω). The materials measured were all magnetically very soft and had high permeability. Thus the magnetic flux lines converged into such a sample in position inside the field, with the effect of making the flux density more uniform inside the sample. Hence the variation in magnetisation along the sample was far less than that in applied field over the same region (although this would be difficult to quantify considering also the effect of shape demagnetisation).

As pointed out in Squire & Gibbs [1987], the coefficient of linear thermal expansion of most materials used in this study is of the order of $10^{-5}K^{-1}$. Thus a temperature change of 0.1K would cause a strain of 1 part per million - a significant proportion of the saturation magnetostriction of the samples measured. Therefore it was important that the sample was kept at constant temperature, with variations less than approximately 0.1K. To aid this the thermal mass of the aluminium block mounted on the x-table and the aluminium optical fibre housing were large, and the whole was situated in an insulated box. Nevertheless, over the period of an applied field cycle, typically one minute, some strain due to thermal fluctuations always occurred. As with the magnetisation rig, this drift was assumed to be linear and was corrected accordingly, so that the value of strain at saturation, i.e. the first, n/2th, and nth points in a file of n points were the same. Temperature variation was thought to be generally in the form of Brownian fluctuations, so the assumption of linear drift was only a good approximation when the drift was relatively small, i.e. approximately <10% of λ_s. This assumption was justified by taking measurements with zero applied field (and so zero magnetostrictive strain). In these readings the (thermal drift corrected) λ-H plot was always close to zero over the period

of measurement.

A typical λ-H data file is plotted in figure 3.9 (of VAC0040). The value of λ_s quoted was calculated as the difference between the average strain at saturation and the average strain of the two branches of the cycle at zero applied field. This is a good approximation to the minimum strain which occurs at zero magnetisation due to the very low coercivities of the sample used. The values were given as a ratio between the change in length due to applied field and the length of the unclamped portion of the sample, and were generally given in terms of "parts per million" (ppm).

3.2.3.1 Sources of Error

The errors can be divided into two classes; error in time-dependent measurement of position without any movement of the sample, and in time-independent measurement of change in position as the sample strained. The former tend to be random noise while the latter tend to be systematic errors.

The former errors arise from effects which vary the light intensity of the beam and the output of the LIA with time. These include shot noise at the detector, mechanical noise at optical fibre junctions, Johnson noise in the load resistors of the detectors, and amplifier noise in the LIA. As mentioned, variations in beam intensity could largely be removed by combination with the reference beam. The remaining noise was effectively averaged out by the PSD. A time constant on the LIA of 100ms was used for most of the readings taken in this study, so that random error of single data points became insignificant

Of the sources of systematic error, factors such as thermal drift, mechanical vibration and variations in background light level were minimised by careful control of the surrounding conditions and by the use of the vibration dampers and polystyrene lined

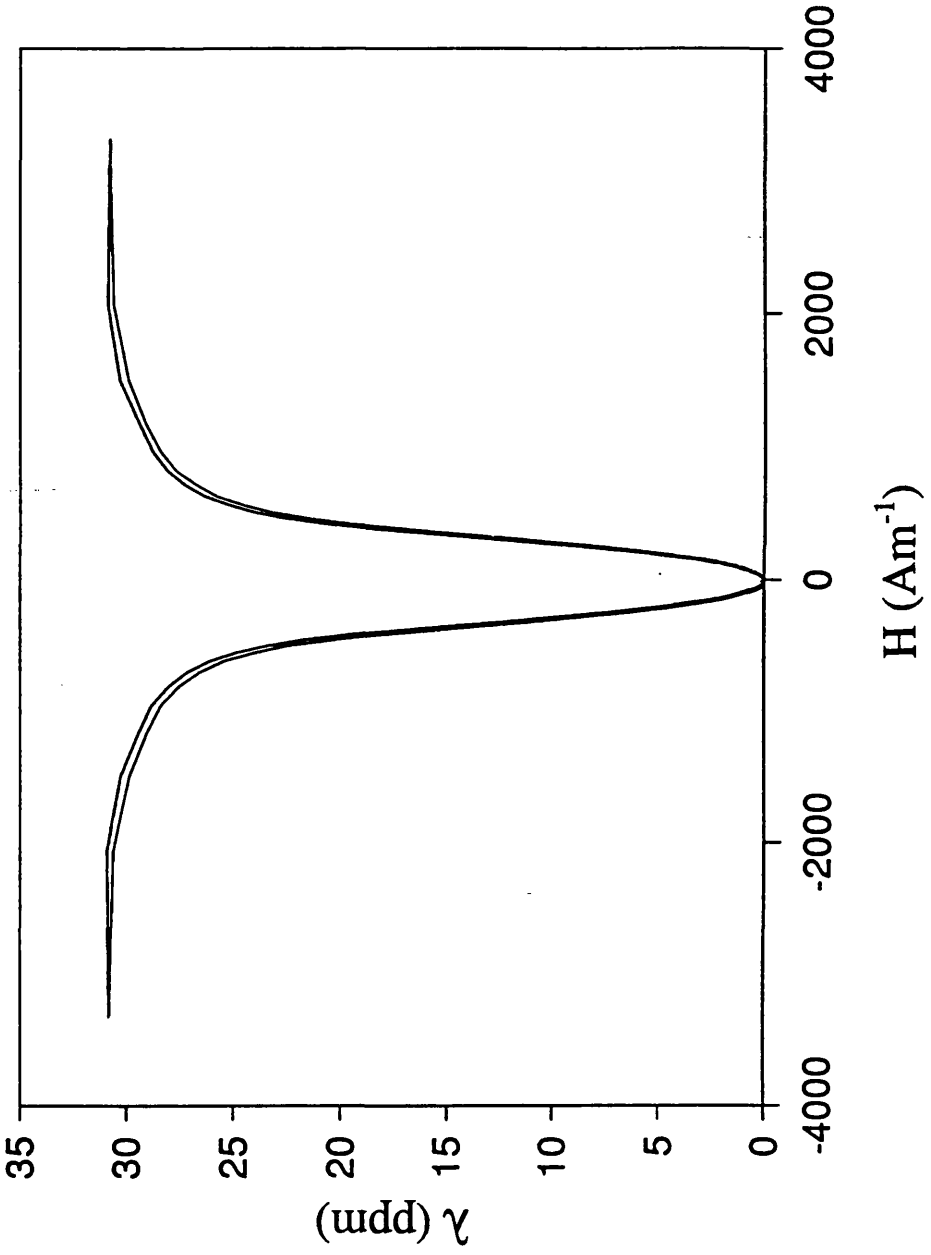

Figure 3.9: Typical measured λ-H loop. The loop shown here is of a transversely field annealed VAC0040 sample.

box. Also, all instrumentation was allowed to warm up before use.

Error in the linear regression calculation of the constant of proportionality between output and sample position, C, (equation 3.5) led to an error of approximately 2%. In most cases this constant had a value of approximately 5000mV/turn (where one turn of the x-table winder =12.5μm) while the error in its measurement was approximately 100mV/turn. However, there were noticeable differences in C for different sample holders due to differences in glass thickness, and any disturbance of the optical fibre junctions also had a significant effect. Therefore it was advisable to measure C at the beginning of a set of measurements and whenever sample holders were changed (ensuring that the glass was clean).

Non-proportionality between sample strain and output voltage and further error in C could arise due to non-uniformity of light intensity across the beam. This could be from the beam being out of focus at the detector, or from dirt and blemishes on the lens and sample holders. However calibration of output voltage to strain, C, always gave a very high degree of proportionality (figure 3.10), the linear regression being limited mainly by rounding errors of the data. Hence this error was judged to be small.

The largest errors were those that were not caused by the instrumentation or optical fibre assembly, but involved the sample itself. These include small errors in the measurement of the length of the sample protruding from the "Tico pad" clamp by lining it up with a ruler with 0.5mm gradings (estimated to be less than 0.2mm), the ends of the sample not being cut perfectly straight and square, the sample long axis not being positioned parallel with the field axis (the typical deviation estimated to be a few degrees), and the sample not being centred in the beam widthwise so that the sample did not completely cross the diameter of the beam. Finally, the spacing of the sample holder was important in keeping the sample flat without restricting it's movement. Too wide a spacing allowed vertical movement of the sample, having a small effect on C, but also

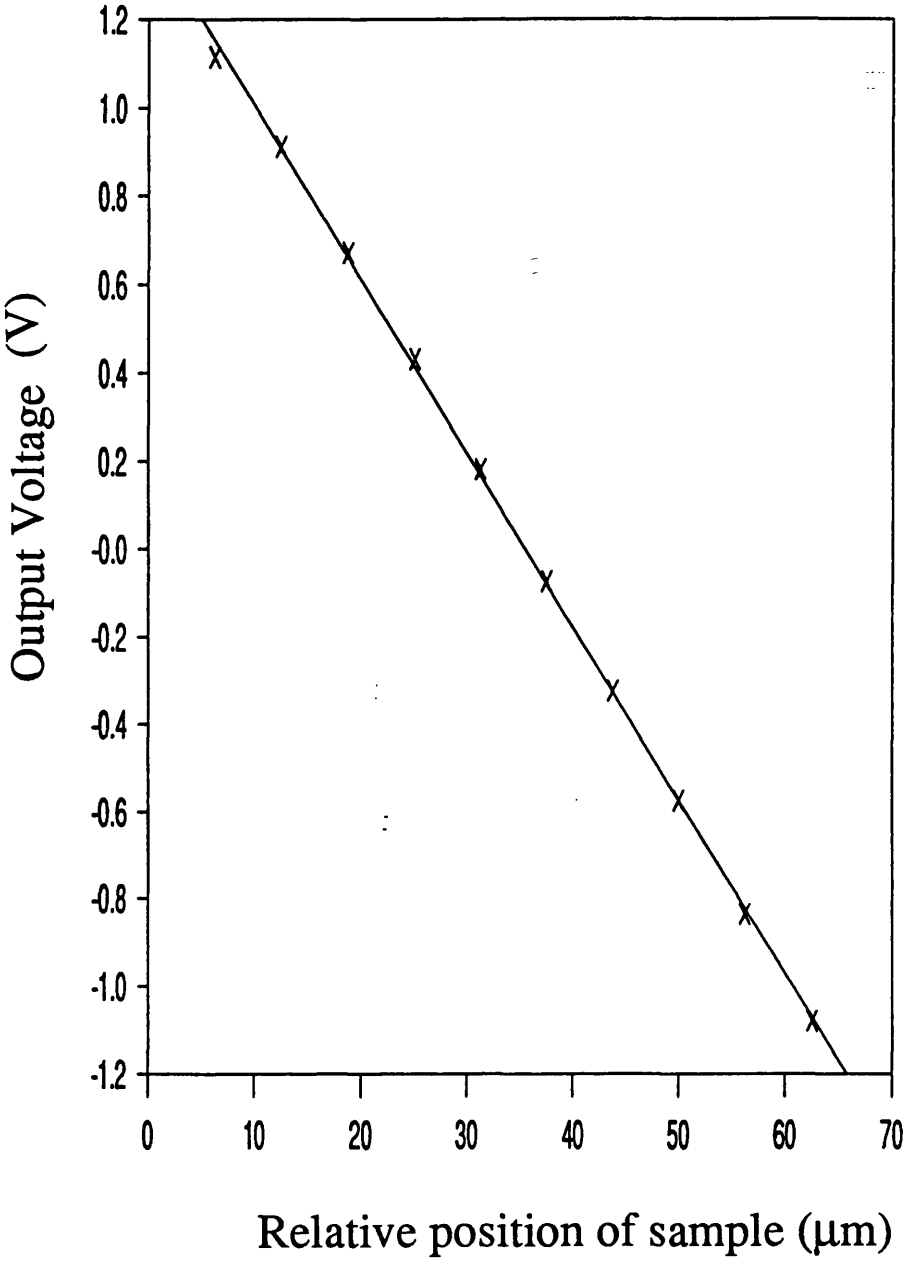

Figure 3.10: Typical LIA output to sample position calibration curve. The linear regression coefficient in this case is greater than 0.9997.

flapping as shown schematically in figure 3.11a, reducing the horizontal component of the strain, or even changing its sign. A typical λ-H plot of a flapping sample is shown in figure 3.11b. Too small a spacing introduces excessive friction between the holder and the sample. This not only has the effect of reducing the measured strain but also of increasing the apparent loss in the λ-H plot (figure 3.12). The error in λ_e due to flapping and sticking could not be corrected, only avoided. As mentioned, optimum spacing generally produced a smooth sliding fit between a sample and a holder. Beyond this it was necessary for the operator to recognise λ-H plots in which sticking or flapping occurred and reject the data.

A new rig was being designed and built at the time of writing which works on a closed loop system, the schematic of which is shown in figure 3.13. The sample and holder are placed on a piezoelectric translation stage whose drive voltage is derived from the output voltage from the LIA. As a magnetic field is applied and the sample strains, the change in output voltage is fed back to the piezoelectric shifter returning the sample edge to the null position, in the centre of the beam. This negates the need for the voltage-strain calibration constant, C. Also, the translation stage, with nanometre resolution, is mounted on an x-table with micrometre resolution and a range over several centimetres, while the optical fibre assembly is mounted on a similar y-table. The y-table allows fine transverse positioning of the sample edge within the beam reducing the error due to the sample not completely crossing the beam diameter, although this error is also removed in the new configuration if the position of the sample at zero field is set to the null position, regardless of the sample errors mentioned above (except the small reduction in λ_e due to some slight angle between sample axis and field axis).

The errors in the measurement of λ_e on the existing rig predominantly arose through the positioning of the sample squarely and centrally within the beam, and the movement of the sample within the holder. This is illustrated by the relatively low errors in the

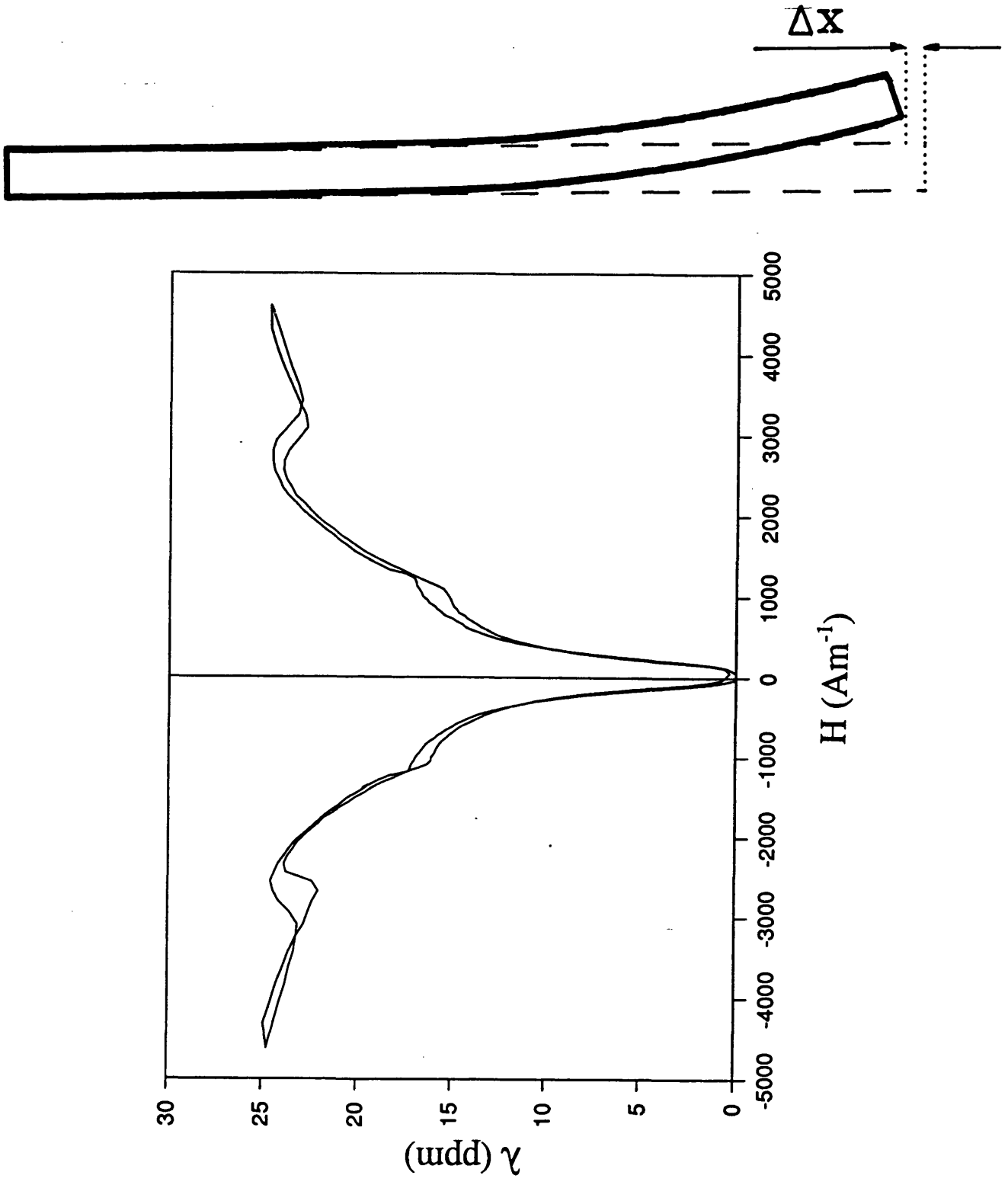

Figure 3.11: a) Schematic representation of sample flapping (exaggerated). The effect is an apparent reduction in strain by Δx. b) an example of a λ-H loop of a flapping sample. Note the reduction in strain at 1 and 3 kAm^{-1}, and the difference in the two halves of the loop at H=0.

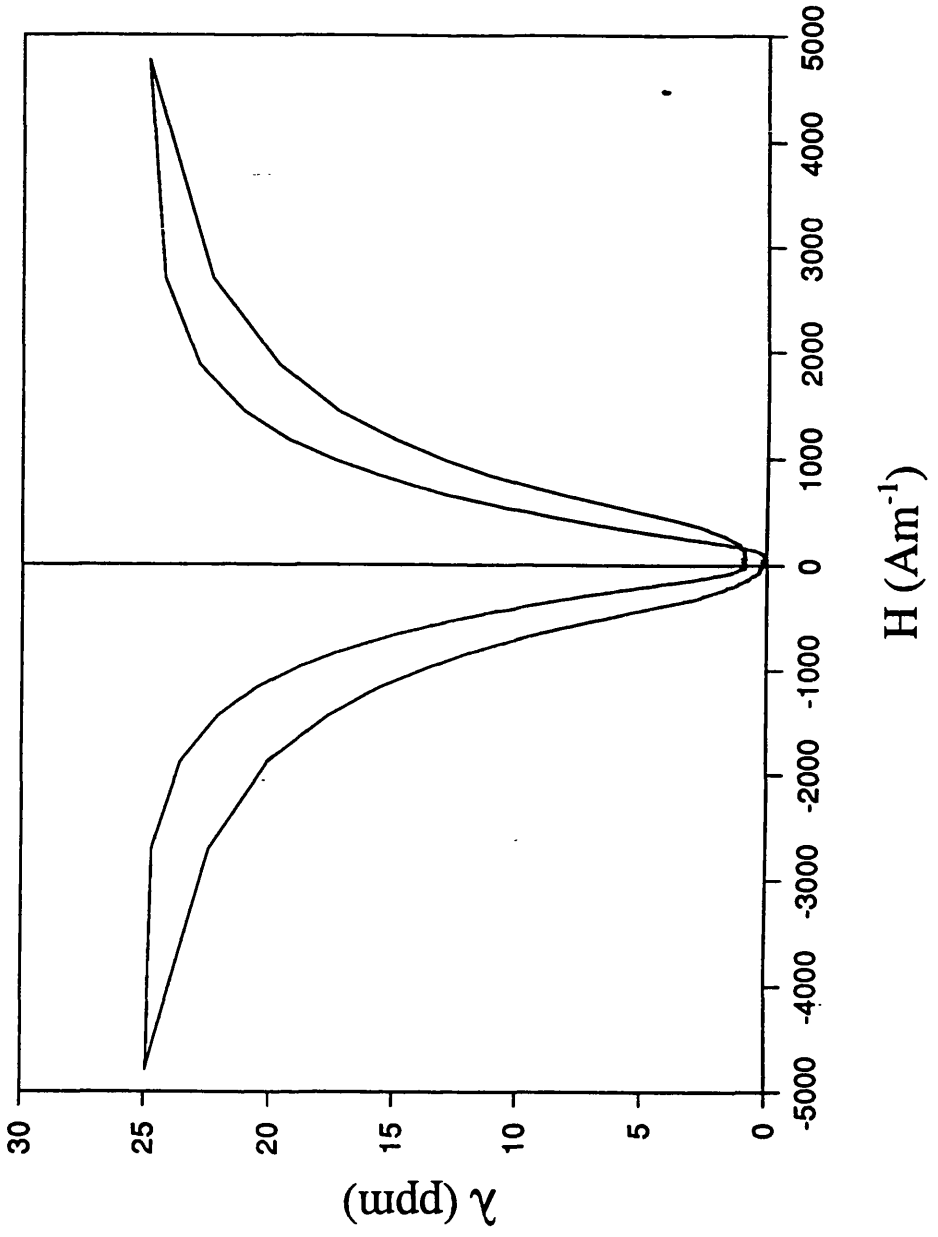

Figure 3.12: Example of a λ-H loop of a sample which was sticking against the glass slides of the sample holder. Note the large apparent loss and the difference in the two halves of the loop at H=0.

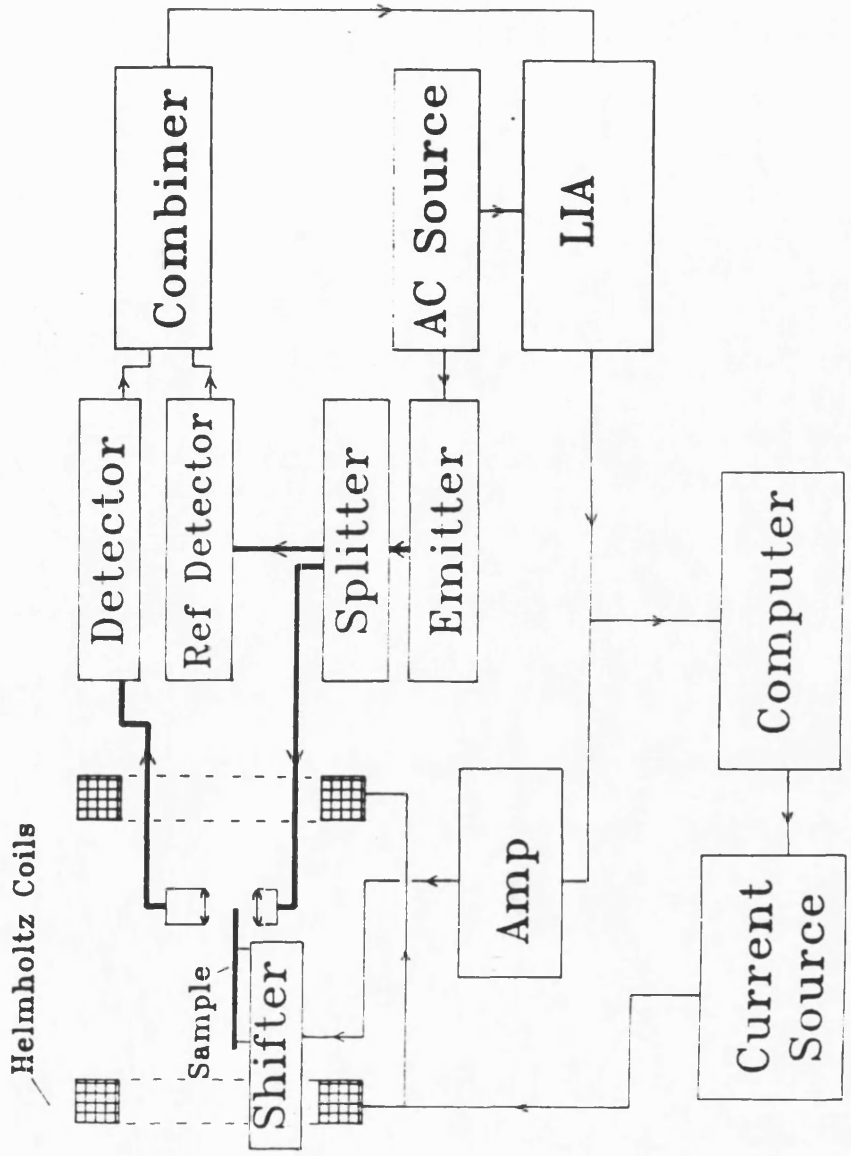

Figure 3.13: Block diagram of the new optical fibre dilatometer system. This incorporates a feedback configuration to the piezoelectric sample shifter, so that measurements are taken with the sample edge at a constant position within the beam [J. Freestone, private communication].

calculation of C, and also by the fact that, in the absence of any adjustments to the optical fibre assembly, the value of C for any given sample holder was repeatable to within it's error. Also, the repeatability of a λ_s reading for a sample was very high, approximately 0.1ppm, when the sample and holder were not disturbed between measurements (including measurements taken with different parameters such as shape factor and time of cycle). The most significant errors arose when the holder was removed from the rig and the sample removed and replaced in the holder. This effected changes in the sample to holder interaction and the positioning of the sample edge within the beam. As with the procedure in the measurement of M-H, the sample was measured in each of four orientations and the error quoted was the standard deviation of the mean of the property concerned.

3.2.4 ΔE Measurement

Young's modulus, E, of the samples was measured with respect to applied field using a vibrating reed method based on that from Berry and Pritchet [1975] as used by Squire and Gibbs [1989]. ΔE is the change in the value of E of a material from that at saturation. A sample was clamped 25mm from one end so that the plane of the sample was vertical. The clamp was connected to a mechanical oscillator driven by a variable frequency signal generator with a sinusoidal voltage output. The frequency of this output was measured with a counter timer. The vibration of the clamp caused the free end of the sample to vibrate. The amplitude of this vibration was at a maximum when the sample was driven at the resonance frequency of one of the modes of vibration. At the free end an optical fibre directed a beam from a tungsten light source onto the reflective side of the sample (i.e. the air side of the melt-spun ribbon) at an angle of 45°. This was reflected onto a photodetector directed into the reflected beam, also at 45° to the ribbon plane, 90°

from the incident beam. The output of the photodetector was fed into a pre-amplifier and then to a PSD (the most suitable amplification setting of which also depended on the mode of vibration - the lower the mode, the larger the amplitude of vibration), with the signal generator providing the reference. The PSD output was zeroed when the sample was not being driven. The amplitude of vibration was then directly related to the PSD output. The first mode of vibration or fundamental resonance generally occurred at a frequency between 10 and 50Hz. The ratios of the frequencies of the higher modes to the fundamental are a constant in ideal conditions (see Berry and Pritchet [1975]), although these are affected by the pole effect, especially in the lower modes. These ratios are shown in table 3.2 for the first six modes.

Mode of Vibration	Ratio of frequency to first mode
1	1
2	6.27
3	17.55
4	34.4
5	56.8
6	84.9

Table 3.2: Ratio of modes of vibration of sample in vibrating reed configuration, clamped at one end (from Nowick and Berry [1972], Appendix F).

However, as stated in Squire and Gibbs [1989], the applied field was not large enough for the pole effect to become significant (the pole-effect is fully discussed in the context of the vibrating reed method in Berry and Pritchet [1979]). Hence, once the fundamental was found, the frequencies of the higher modes could be estimated to a high degree, facilitating the process of finding them. The field was applied with a pair of Helmholtz coils connected to a dc power supply. The field was calibrated with respect to coil current using a Gaussmeter. The field from the coils was $2.83 \times 10^3 (Am^{-1})A^{-1}$ and the maximum current used was 2A. This was sufficient to saturate all the samples. The sample was positioned with its long axis along the coil's axis, halfway between them. With the sample saturated the frequency of one of the modes was measured (the readings

were always taken starting from the saturated state). In this study the fifth mode was used, along with the fourth mode in some instances to act as confirmatory data. These modes were chosen as they are not at a frequency close to that of any mains noise sources (the typical frequency of vibration of the fifth mode of vibration of the samples were ~1700Hz) and their amplitudes were large enough to allow accurate readings. As stated in Squire and Gibbs [1989], the absolute value of E obtained from this frequency value had perhaps 20% error due to the non-uniform thickness of the ribbon. However, the ratio of the squares of the resonant frequencies was equal to the ratio of the moduli at the different applied field:

$$\left(\frac{f(H)}{f_s}\right)^2 = \frac{E(H)}{E_s}, \qquad 3.7$$

where f(H) and f_s are the resonant frequencies at an applied field, H, and in the saturated state, respectively. The above expression was derived from the appendix in Berry and Pritchet [1975]. Hence the relative ΔE was obtained with respect to H. When f_s was found, the field was changed and the resonant frequency was measured for a series of values of H as it was cycled from maximum in one direction to maximum in the opposite direction. The data was presented in the form of E/E_s versus H, a typical example of which is shown in figure 3.14 for obliquely field annealed VAC0040, measured using both the fourth and fifth modes. The error in setting the current through the coils and the frequency of vibration at the signal generator were both very small, the former was less than $\pm 2 Am^{-1}$ while the latter was approximately ± 1Hz which corresponded to less than 0.1% error in E/E_s. Hence error bars are not shown.

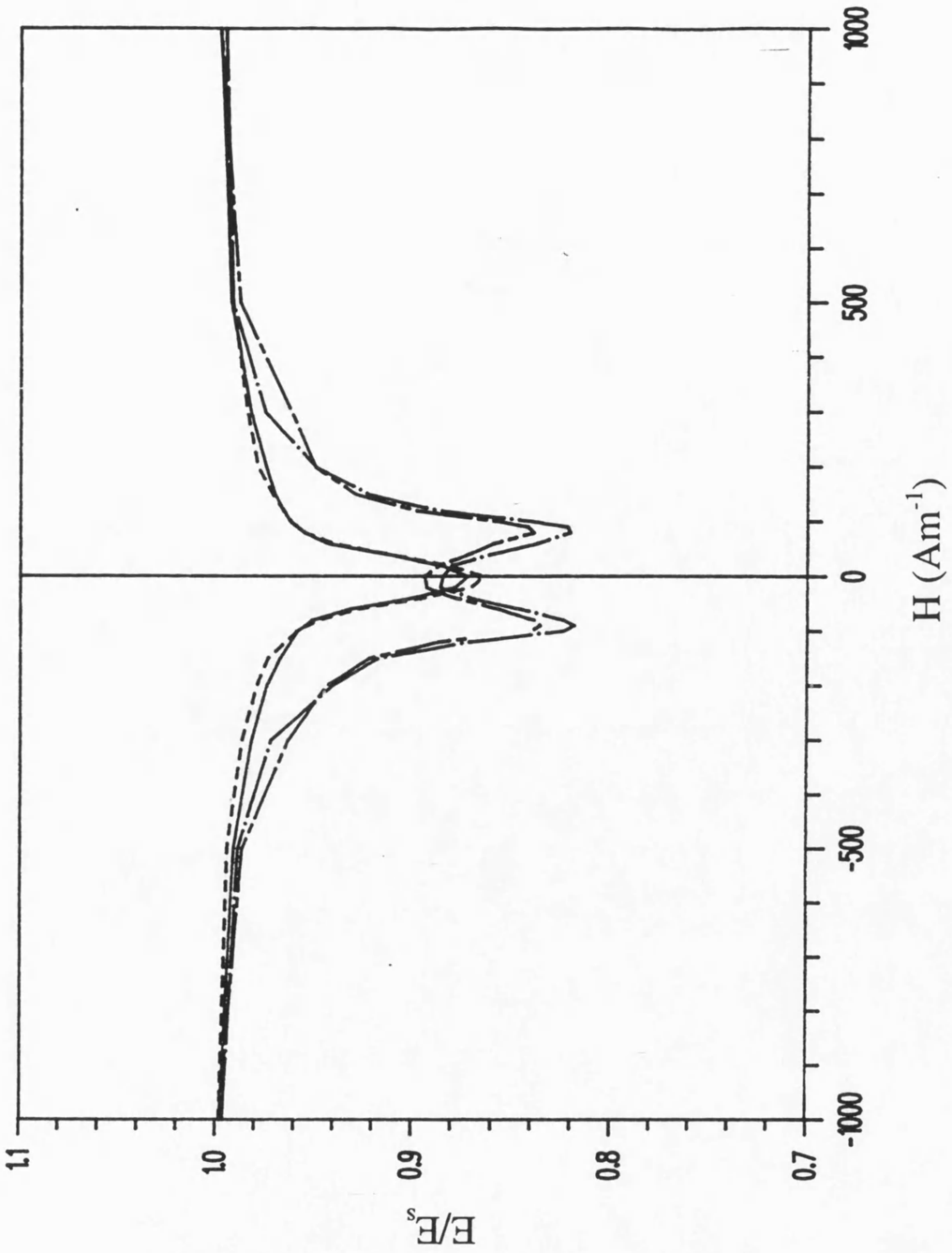

Figure 3.14: E/E_s vs. applied field for obliquely field annealed VAC0040, θ=30° and 60°, using both 4th and 5th modes of reed vibration. θ=30°: 4th mode (- - -), 5th mode (——). θ=60°: 4th mode (— · —), 5th mode (— — —). The plots are symmetrical within measurement error. The agreement between the two modes is good but some difference can be seen. Therefore all E/E_s measurements were taken using the same mode of vibration (5th).

3.2.5 Domain Examination System

The technique used to study the domain structure was the well established Bitter method. A colloidal suspension of fine ferromagnetic (generally a ferrite) particles is spread thinly over a polished or very smooth surface. The particles tend to aggregate around areas on the surface of greatest flux density out of the surface. These stray fields are strongest where domain walls meet the surface due to the rotation of the magnetic moment direction across them. Hence the domain walls show up as dark lines. Typical domain patterns in as-cast and field annealed Fe-Ni based amorphous ribbons are shown in figure 3.15. The application of this technique to amorphous metal ribbons is discussed and compared with other methods by Livingston [1979], Livingston *et al* [1982], and Livingston and Morris [1985]. Maze patterns are commonly seen on the surface of as-cast ribbons. These are surface closure domains, which indicate regions with domain structures with a significant perpendicular component, where the underlying magnetisation points out of the plane of the ribbon. This is invariably due to stresses caused by non-uniform cooling during the melt-spinning. Also, radial domain patterns appear around regions of the ribbon which were slower than the surroundings to solidify during this process. These regions contracted on solidification after its surroundings had already solidified, so forming radial stress fields. These were annealed out during subsequent heat treatments.

The surface was smooth enough on the air-cooled side of the ribbon to allow observation of domains without further surface preparation, although the surface roughness on the wheel-cooled side was too great and was not used.

The surface was placed flat at the centre of a horizontal coil connected to a 4A dc power supply, which produced a field of approximately 1.1-1.5kA/m at its centre. The field strength was not critical, but was required to be great enough to produce a flux

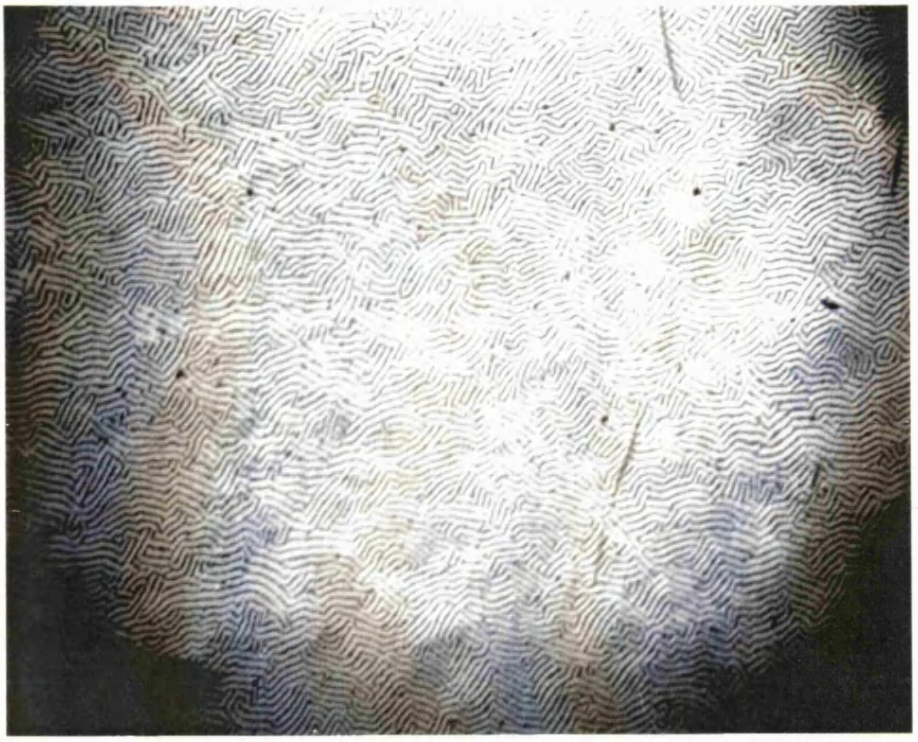

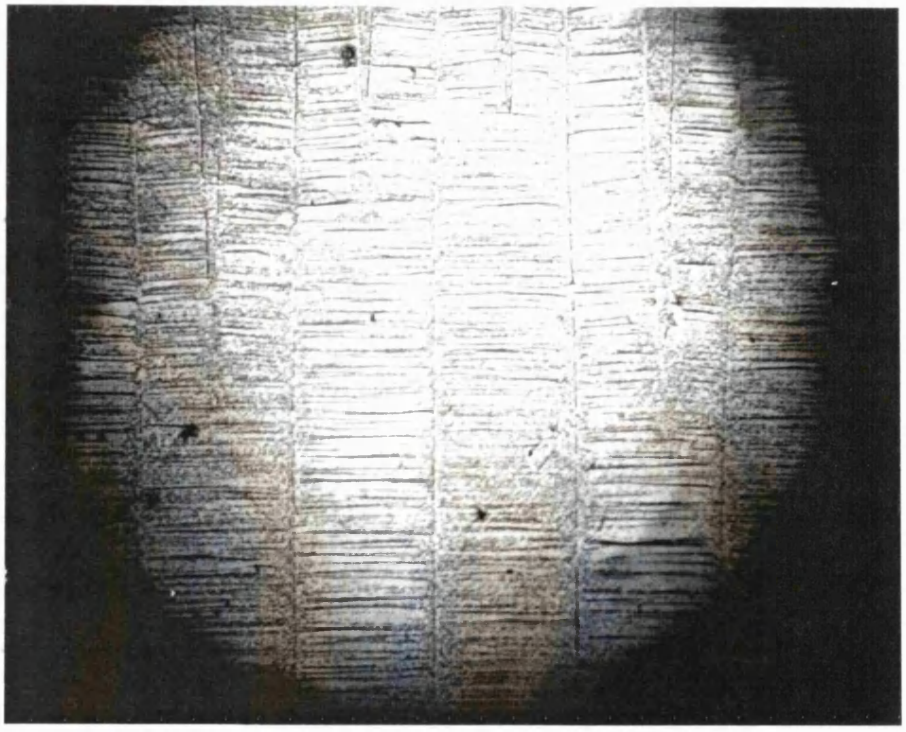

Figure 3.15: Photographs of domain pattern on typical as cast and transversely field annealed Fe-Ni based ribbon (METGLAS 2826MB)

gradient around the domain walls great enough to cause colloid aggregation. This field had the effect of increasing the flux density of the stray fields directed vertically out of the horizontal surface, causing more pronounced aggregation of the particles at the domain walls. The coil was mounted on an x-y table underneath a Carl-Zeiss optical microscope capable of x200 magnification (with a x2 converter lens). The microscope included its own through-the-lens lighting and a facility for mounting a 35mm SLR camera allowing examination through camera and eyepiece simultaneously, while allowing the eyepiece to be focussed independently from the camera.

A small amount of the colloid was placed onto the surface using a dropper. A microscope contact slide was placed over this, spreading the colloid out into a uniform film which was allowed to settle for one or two minutes to allow the image to develop. The vertical field was then applied and the domain structure observed and, if required, photographed. To avoid errors in the scaling of the image, it was necessary to ensure that each film taken included an image of a stage micrometer or graticule with 0.1 and 0.01mm line spacings. Thus, whenever a negative was enlarged and printed, the corresponding stage micrometer image was done under the same conditions, providing a graticule scale.

Where the domain structure was studied with respect to applied field, this field was provided by two coaxial pairs of Helmholtz coils, with the sample positioned at the centre. The larger pair had radii and spacing of 500mm. The field produced was measured to be $86(\pm 1)(Am^{-1})A^{-1}$ (see figure 3.16a), driven by a 5A power supply, giving a maximum field of approximately $440Am^{-1}$. As with the smaller coils, the current was monitored with a digital multimeter. The field profile was also measured, and was found to increase steadily towards one of the coils, with a 1% variation in field ~9mm either side of the centre of the microscope image. The area observed by the microscope was always less than 2mm in diameter, so a high degree of uniformity in magnetisation within

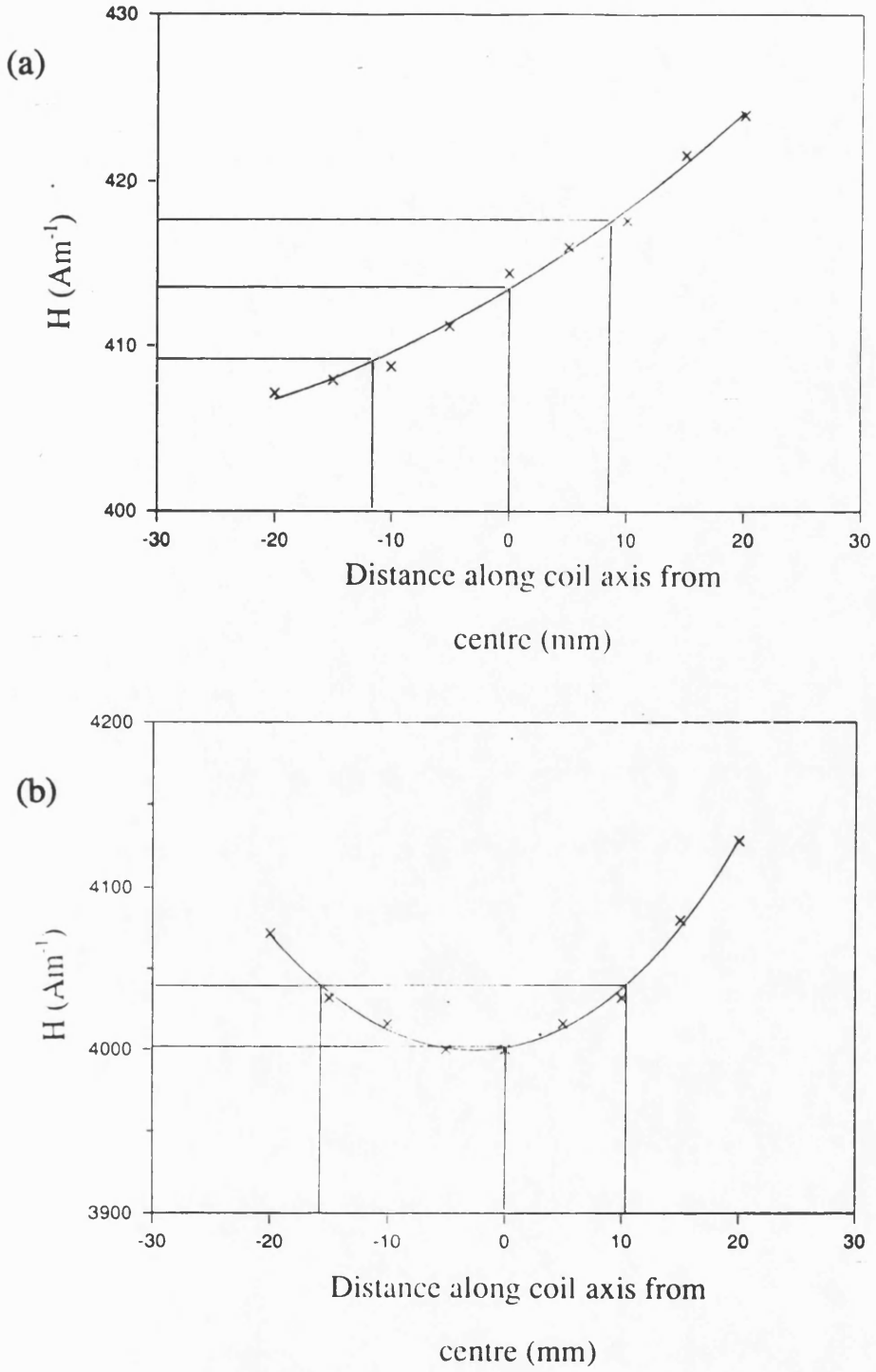

Figure 3.16: Measured field profiles at the centre of the Helmholtz coils surrounding the domain examination apparatus. a) Large coils, b) small coils, with coil current of 5 Amps in both cases. The distance over which the field variation was less than 1% was found to be approximately (a) 20mm and (b) 26mm. The region of ribbon visible under the microscope was approximately 3mm in diameter.

this region can be assumed. Similar measurements were made on the smaller coils, which were 90mm inner diameter (figure 3.16b). The field profile was less uniform since it was not possible for the coils to be spaced at 90mm due to the size of the horizontal coil beneath the microscope. The minimum convenient spacing was 180mm. The calculated field profile using the program discussed in section 3.2.3 is shown in figure 3.17 and predicts a 1% variation over 10mm either side of the centre. The measured profile was in good agreement with the prediction, with 1% variation over 10-12mm either side of the centre. The field was measured to be approximately 800(±30) $(Am^{-1})A^{-1}$, with a maximum field of over $4kAm^{-1}$. The larger pair of coils was used to apply smaller fields to the sample, with more sensitive adjustments, up to approximately $400Am^{-1}$. In most cases, this was sufficient to achieve close to saturation. The approach to saturation was covered in the field range $400\text{-}4000Am^{-1}$ by the smaller coils.

Various colloids were tested. Different colloids were available for a range of materials as the tendency to aggregate towards domain walls was related to the size and magnetisation of the colloid particle, as well as the domain wall width. This in turn depended on the saturation magnetisation and the exchange and anisotropy constants of the sample material. The colloid that gave the best results in this study was Ferrofluidics EMG805 (3-6% Magnetite by volume, $B_s \approx 0.02T$) diluted approximately 1:10 in distilled water. Oil and organic solvent based colloids were preferred to avoid corrosion of the material as far as possible. Unfortunately domain patterns could not be seen using those that were available.

It was found that the magnetic particles could not follow the domain walls unless they moved very slowly. As the applied field was stepped, the domain pattern was seen to disappear and the new pattern gradually reappeared a few seconds later. Care was needed to ensure that the process of photographing the domain pattern for each applied field was completed before the colloid began to dry out onto the sample, which tended

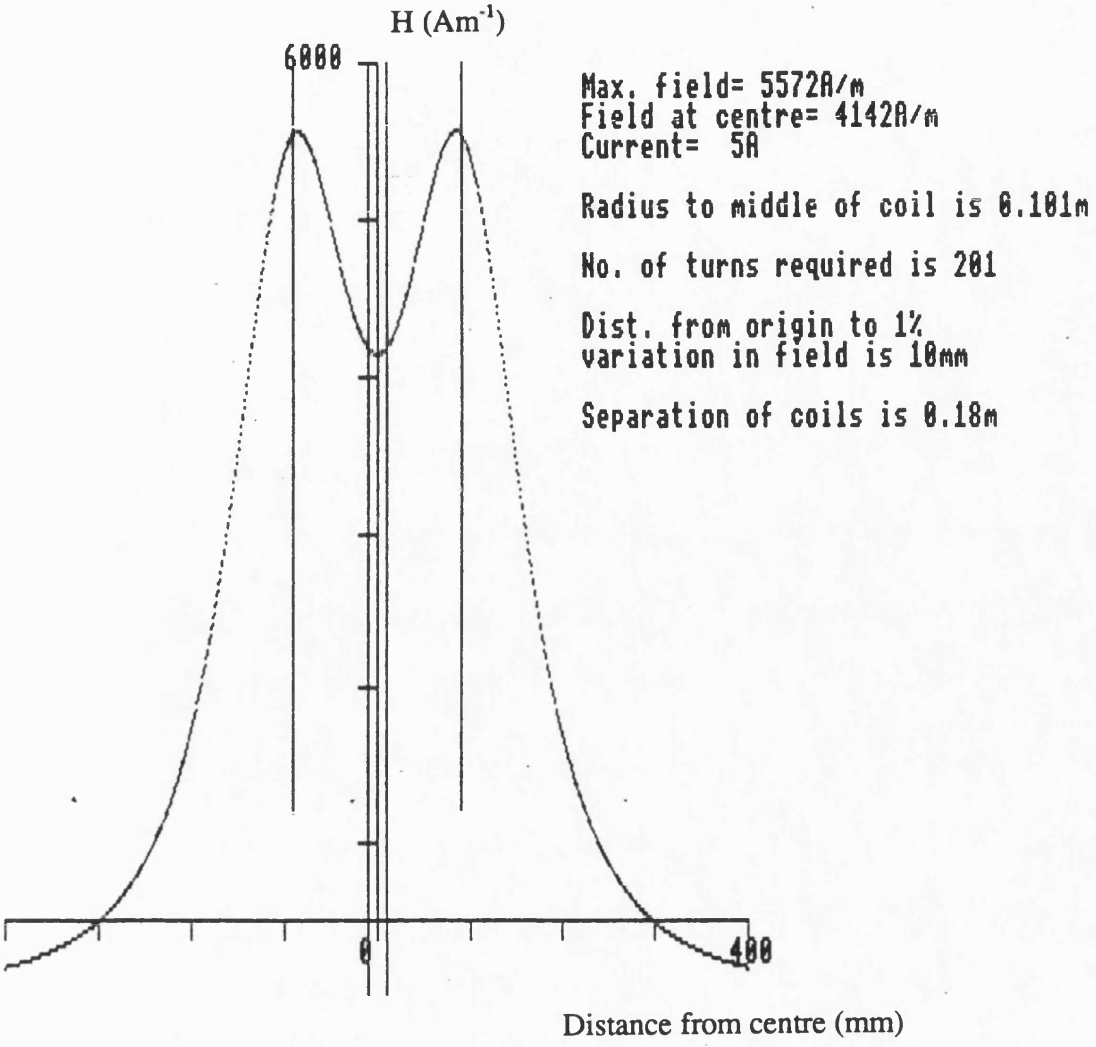

Figure 3.17: Calculated field profile of the small pair of Helmholtz coils on the domain examination apparatus [J. Freestone, private communication]. The outer vertical lines represent the positions of the centres of the coils. The inner lines represent the region over which the field variation is less than 1%. This was calculated to be approximately 20mm, compared with a measured value of 26mm.

to occur after a few minutes. The samples were then thoroughly cleaned with cotton wool buds soaked in acetone. This was found to be the best method of removing the dried colloid. The samples were placed in acetone in an ultrasonic bath. However, this did not appear effective at removing it.

3.2.5.1 Domain Area and Angle Measurement

During the investigation of the obliquely field annealed material, it was necessary to investigate the contribution of the domain wall movement to the magnetisation. This involved measuring the mean area and angle of magnetisation of two sets of domains: those with their magnetisations at an acute angle and those at an obtuse angle to the applied field direction. In the demagnetised state these domains have notionally equal areas and are magnetised along the field anneal induced easy axis direction at 180° from each other (see figure 2.5 [Squire 1990]). As the field is applied the domains whose magnetisation is at an acute angle to the field direction grow at the expense of the others. The angles of magnetisation of both sets of domains rotate towards this direction as the field is increased, and at some field strength the walls of the larger domains meet, making the material a single domain. This magnetisation process is the basis for the model used in Squire [1990]. The behaviour of the domain walls was shown to be critical in this model (see chapter 2 and 4).

Details of the domain pattern were quantified using a Cherry digitiser interfaced to a BBC Master computer. The x- and y-coordinates of the mouse were fed into it when one of its four buttons was depressed, together with a third variable denoting which button had been used. The data was then used to calculate domain areas and moment directions with two programs written by P.T. Squire. The photograph of the domain pattern was placed on the digitiser board at some arbitrary angle. The mean angle of the

domain magnetisation was measured by exploiting the fact that the secondary domain walls, which were seen within the main domains due to angular dispersion of magnetisation, as discussed in chapter 4, always lay perpendicular to this direction. Firstly the ribbon axis was determined with respect to the digitiser axes by defining two points along the axis. Generally this was done using the sample edge which was included in the photographs for this reason, but care was always taken to line the edge of the photograph frame up with the edges for the cases where these were not included in the pictures. A series of pairs of points defining the secondary walls within one of the sets of domains were input to the computer. The program then calculated the mean angle between these walls and the ribbon axis (and the corresponding standard deviation). The magnetisation direction was at right angles to this. The process was repeated for the other set of domains.

The accuracy of this method was limited by the finite spacing of coordinates on the digitiser grid (namely 0.1mm), and the ability of the operator to position the cursor precisely. Thus the accuracy was reduced in thin domains where the length of the secondary walls in the photograph was sometimes only a few millimetres. Also, there was some variation in the actual angle of these walls in the material, although this was small. Finally, the error in defining the direction of the ribbon axis was found to be ~0.1°. The combined errors in measuring the secondary wall angle was reflected in the standard deviation of the mean, taken from a sample of approximately 60-80 readings. This was generally of the order of 3-5°.

The mean relative areas of the two sets of domains was determined by measuring the area of a series of segments of the domains. A grid with line spacings of 10mm was laid over the photograph at right angles to the primary domain walls (in the field induced easy axis direction). This effectively split each domain into a number of rectangles (or, more precisely, parallelograms). The coordinates of the corners of each rectangle were

input to the computer and the area calculated. The mean and standard deviation for each set of domains could then be obtained, giving their relative areas. Errors arose from similar sources to those in the previous method, and were found to be of the order of 5-10%. By summing relative contributions of the longitudinal components of the magnetisations of the domains, the total magnetisation of the region within the photograph could be obtained. Thus, by repeating this for a range of applied fields, the M-H curve could be constructed and compared with the measured M-H plot of the whole sample.

3.2.6 X-ray Diffraction

The measurements were taken using the Philips X-ray diffraction system at Bath University. It included a 4kW X-ray generator with a 2kW copper target and a computer controlled diffractometer goniometer on which was mounted a proportional counter with graphite monochromator and automatic divergence slit assembly. The X-ray count was output to a dedicated chart recorder.

The trace was affected by statistical variations, and the frequency of the noise on the trace was dependent on the scan speed and chart recorder paper speed. A scan speed was selected so that the X-ray peaks were accurately resolved without being obscured by the noise. Generally, a scan speed of $0.03^{\circ}s^{-1}$ was used, and the measurements were taken over a range $2\theta=30\text{-}70^{\circ}$. The target potential and current determined the X-ray intensity incident on the sample and were generally set at 40kV and 30mA respectively. The wavelengths of the radiation emitted from the copper target, $K\alpha_1$ and $K\alpha_2$, are 0.15405 and 0.15443nm respectively, with a weighted mean of λ_{Cu}=0.15418nm. In the case of α-Fe, the lattice spacing, a, is 0.2866nm. From the Bragg equation,

$$\lambda_{Cu} = \frac{2a\sin(\theta)}{\sqrt{(h^2+k^2+l^2)}}, \qquad 3.8$$

the value of 2θ for the <110> and <200> peaks can be calculated to be 44.7° and 65.0°, respectively. Since the short range order of the amorphous phase is similar to the crystalline phase, its mean nearest neighbour spacing is similar. However, there is a wider distribution in the metallic glass due to the random nature of the structure. Therefore, the X-ray diffraction pattern of an Fe-based amorphous alloy has a broad peak around 2θ=45° (plus a smaller, broader one around 65°) as shown in figures 3.18 and 3.19. Crystallisation of the material has the effect of producing far sharper peaks at these angles on top of the amorphous "bumps", as illustrated figure 3.18 (from Sheard [1989]). The relative size of these peaks is dependent on the texture of crystallite growth on the surface. These can differ on the air-cooled and wheel-cooled sides of the ribbon [Herzer and Hilzinger 1986], and was shown to do so on the partially crystallised VAC7505 in this study, where the <200> peaks were significantly larger on the air-cooled side (figure 3.19). The heights and areas of these peaks were used as an approximate measure of the extent of crystallisation. The traces were inputted into a computer using the digitiser pad and the areas under the peaks (above the background level) were calculated in arbitrary units.

It should be noted that the region illuminated by the X-ray beam was approximately 13mm in diameter. Therefore the traces indicated the crystallisation over macroscopic scales, albeit within a small portion of the sample. Thus the assumption was made, as with the domain studies, that the region investigated was representative of the whole sample.

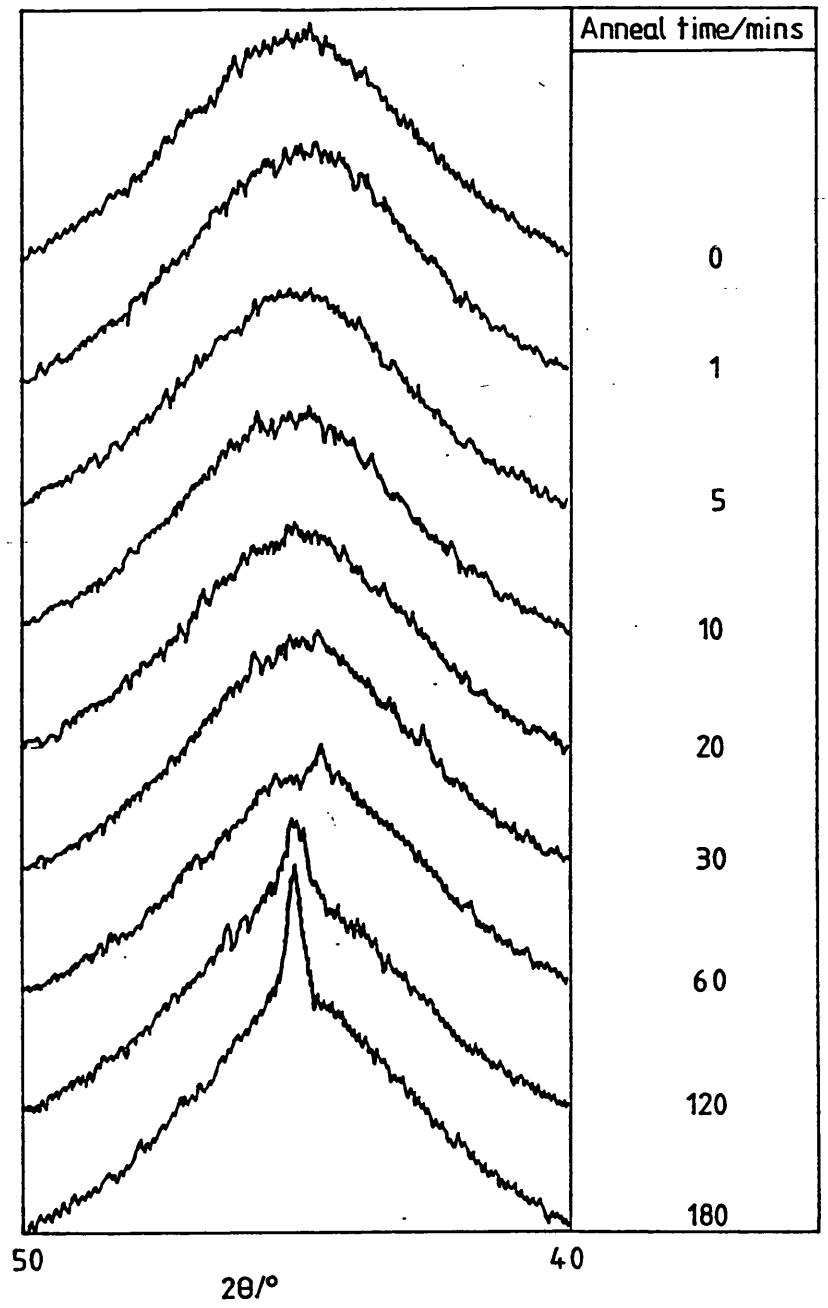

Figure 3.18: Variation of the <110> α-Fe X-ray diffraction peak of an Fe-based ribbon with respect to anneal time at a given temperature (reproduced from Sheard [1989]). As the anneal proceeds, crystallisation occurs, causing the sharp diffraction peak superposed over the amorphous "bump".

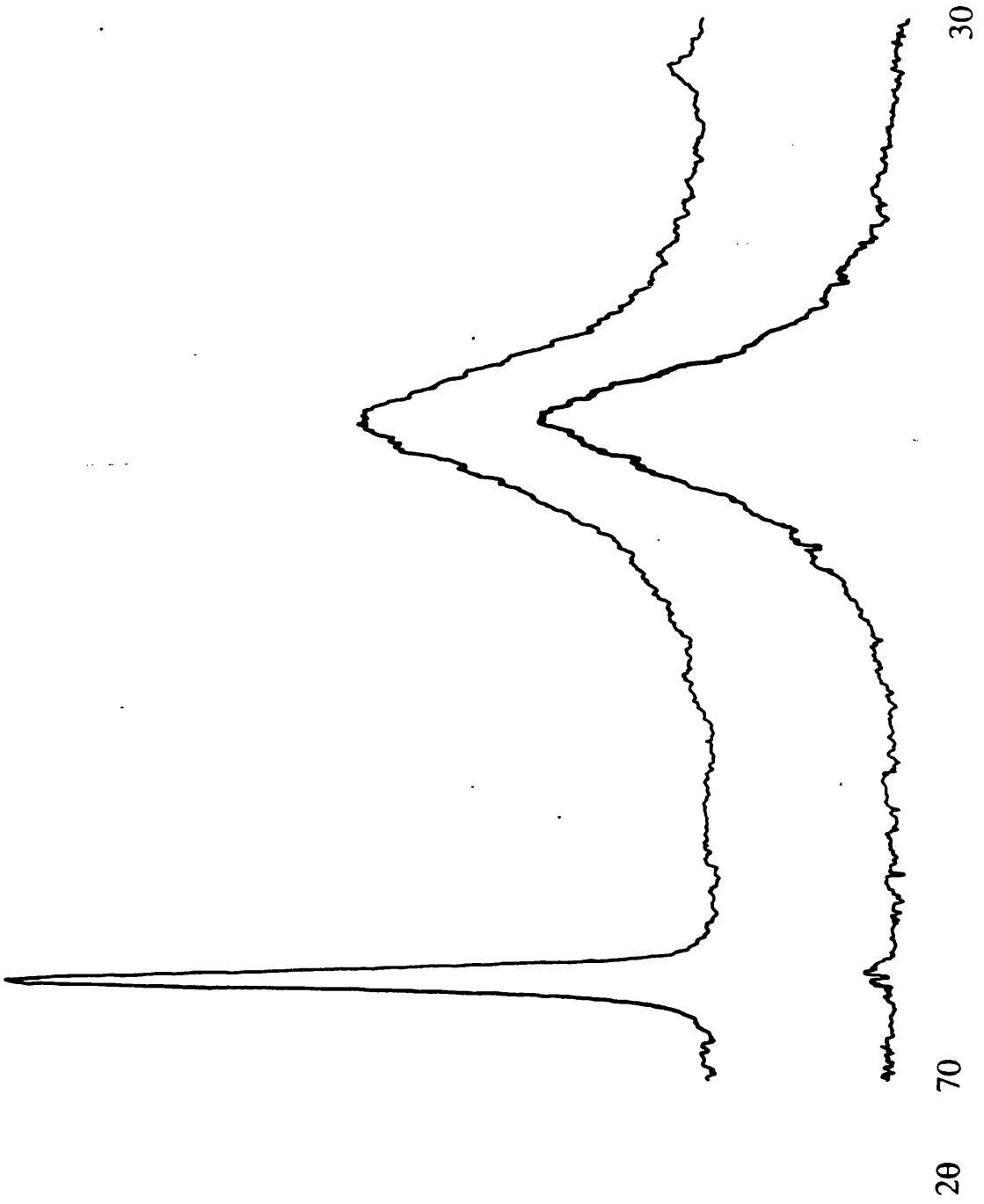

Figure 3.19: X-ray traces of typical partially crystallised sample of VAC7505, both air- and wheel-cooled sides of the ribbon. The <200> α-Fe peak at $2\theta \approx 62^{\circ}$ is far more pronounced on the air cooled side.

3.3 Calculation of Parameters

The measured data was in the form of magnetisation, M, and magnetostrictive strain, λ, as functions of applied field. The parameters of interest were extracted from this data by determining the best fit of linear or polynomial functions. The various parameters corresponded to coefficients of these functions.

3.3.1 Magnetisation Parameters

The parameters of prime interest obtained from the M-H data included the coercivity, H_c, the initial susceptibility, χ_0 (i.e. that at zero magnetisation), and the anisotropy constant, K_u.

3.3.1.1 Coercivity

The M-H measurement program included a procedure for calculating a good approximation to H_c. It selected the first three points in the M-H data set about zero magnetisation for each branch of the loop, and performed a straight line regression calculation on them. It then used this line to calculate the H-coordinates of the zero crossings, and took H_c as half of the difference between these values. It then repeated this process for the nearest five points about M=0. The two values of H_c were compared. If these values did not agree within a specified tolerance (in this study, 0.01% of the maximum applied field) then the process was repeated with two more points in each regression line, up to a maximum of 11 points. If the difference in H_c values lay outside the tolerance for nine and eleven point line regressions, then the whole process was repeated with successively larger tolerances until agreement between values was

achieved. The M-H loops of the samples measured in this study were generally very linear at low M, such that an increase in the tolerance was not required. As stated in Sheard [1989] this method gave H_c results with high reproducibility even on samples with low coercivities (i.e. less than $0.5Am^{-1}$). It was this method that was used to monitor the coercivity of the field annealed samples to ensure that they had not undergone appreciable crystallisation.

A more accurate method of determining H_c was to find the H-coordinates of the zero crossings of the best fit third-order polynomial described in the next section. There was very good agreement between the values obtained with this and the previous method in M-H loops with linear regions at low M, as was the case for the field annealed samples. However, this was not the case for the partially crystallised samples where the first method gave H_c values up to 10% higher than the second. The values of H_c of these samples, where quoted, were calculated using the polynomial fit.

3.3.1.2 Initial Susceptibility

The coefficients of the best fit third order polynomial to a pre-selected section of the M-H data was calculated using an iterative process. The polynomial was of the form:

$$M = B_0 + B_1H + B_2H^2 + B_3H^3 \qquad 3.9$$

The constant B_0 corresponded to the remanent magnetisation. The coefficient of the linear term, B_1, corresponded to the effective initial susceptibility, χ_{eff}. The higher order coefficients reflected the degree of deviation of the data from a linear relationship. For M-H loops where the selected region around M=0 was very linear, the quadratic and cubic terms were much smaller than the linear term.

The calculation was done by a pair of programs written by P.T.Squire. The first one read in the data from the initial magnetisation data file, plotted the data on screen,

prompted the user to specify the region of the M-H loop to be investigated and sent the data to a file in a format consistent with the second program (i.e. M- and H-coordinates). The second program then fit the user specified function to the data varying the coefficients in an iterative process. The program returned values for these coefficients and the corresponding standard errors, along with the root mean square deviation between the function and the data.

There were several M-H loops investigated with low χ_{eff} where the coefficients obtained were obviously unrealistic. It was found that simply changing the form of the polynomial so that the constant B_0 corresponded to an intercept in the H-axis rather than the M-axis yielded accurate results. It is thought that this was because the changes in B_0 during the iterative process were too large for data sets with low χ_{eff}, and the iterations did not converge. This modified polynomial was introduced initially because the difference between the two values of B_0 led directly to H_c. The exact form of the function was:

$$M = B_1(H+B_0) + B_2(H+B_0)^2 + B_3(H+B_0)^3 \qquad 3.10$$

3.3.1.2.1 Correction for Demagnetisation Effect

The internal field, H_i, experienced by a sample is always less than the applied field, H_a, within which it is positioned. This is due to the demagnetisation effect where poles are induced at the ends (and at any edges with a perpendicular magnetisation component to the field direction) causing an internal field anti-parallel to the applied field [Appendix 3, Chen 1986] (see chapter 1). Consequently, all the field dependent parameters needed to be corrected for this effect. The internal field was reduced by the demagnetising field, H_d:

$$H_i = H_a - H_d, \qquad 3.11$$

where H_d is the product of the magnetisation and the demagnetisation factor, D. This factor was calculated for each sample using the general ellipsoid method [Osborn 1945]. As given in chapter 1, the expression for the internal field becomes

$$H_i = \frac{H_a}{1 + D\chi}. \qquad 3.12$$

The true initial susceptibility is therefore given by

$$\chi_0 = \frac{\chi_{eff}}{1 - D\chi_{eff}}. \qquad 3.13$$

The reciprocal of D, given by $M/(H_a-H_i)$ or M/H_d, is the susceptibility of a sample with infinite true susceptibility and a demagnetising factor, D. It is termed the demagnetisation susceptibility, χ_d. The true susceptibility is given in terms of this by the expression:

$$\frac{1}{\chi_0} = \frac{1}{\chi_{eff}} - \frac{1}{\chi_d}. \qquad 3.14$$

3.3.1.3 Anisotropy Constant

As discussed in chapter 1, the anisotropy energy E_k (per unit volume of the material) can be determined by measurement of the area between the M-H plot and the M-axis (see figure 1.1). The M-H measurement program included a procedure to do this by the trapezium method. The trapezia were defined by successive pairs of points in the M-H data set together with the corresponding points of the same M-coordinate on the M-axis. Hence the calculated area was an approximation to

$$E_k = \int_0^{M_s} \mu_0 H \, dM. \qquad 3.15$$

This can also be given by the integral

$$E_k = \int_0^{H(M=M_s)} \mu_0(M_s - M)dH. \qquad 3.16$$

This method of measurement of anisotropy is generally not the most accurate. The most common method of direct measurement is the torque magnetometer, which measures the torque applied on a wire supporting a sample as the sample rotates to orientate its easy axis into the applied field direction. The principle of this kind of magnetometer is discussed in Cullity [1972], together with a working design.

The method of calculation of K_u used in this study was that outlined in Livingston [1982]. If it is assumed that magnetisation occurs by moment rotation only (no domain wall movement) as is the case in transverse field annealed amorphous alloys, then the magnetisation is proportional to the applied field until saturation is achieved at $H=H_k$. The M-H plots of typical transversely field annealed samples of VAC0040 and METGLAS 2605S2 are shown in figure 5.1. The high degree of linearity between saturated states illustrates the extent to which this assumption holds in practice. The susceptibility is then simply

$$\chi_0 = \frac{H_k}{M_s} \qquad 3.17$$

over the range $H<H_k$. The anisotropy energy, E_k, is given by

$$E_k = \frac{\mu_0 H_k M_s}{2}. \qquad 3.18$$

The anisotropy energy is given in terms of the anisotropy constant,

$$E_k = -K_u \cos^2\theta, \qquad 3.19$$

where θ is the angle between magnetisation and applied field, which is 90° in TFA material. Therefore the anisotropy constant,

$$K_u = \frac{\mu_0 M_s^2}{2\chi_0} = \frac{B_s^2}{2\mu_0\chi_0}. \qquad 3.20$$

Consequently, K_u could be calculated once the susceptibility was known. The value of B_s was obtained from manufacturers' data.

This method is only valid where the magnetisation is transverse to the field direction, with well defined transverse domains, as described in Livingston's model. In the case of well defined domains at an oblique angle, the M-H plots are not purely linear, as described in Squire [1990] (see chapter 2), and examples are shown for a series of angle in figure 2a of that paper. Therefore this method was not used to calculate the value of K_u for the obliquely field annealed samples.

3.3.2 Magnetostriction Parameters

The important parameters measured included the engineering magnetostriction, λ_e, from which the saturation magnetostriction, λ_s, could be derived, the maximum variation in magnetostriction with respect to field, $d\lambda/dH$, and the quadratic coefficients of the best fit fourth order polynomial of the λ-H and λ-M plots.

3.3.2.1 Engineering Magnetostriction

As stated in chapter 1, the engineering magnetostriction, λ_e, in this study is given by the strain induced by a saturating applied field, from the demagnetised state. Since the demagnetised state is not at zero applied field, it is best obtained by cycling the field from saturation in one direction to saturation in the opposite direction. The λ-H measurement program, however, returned an approximation to λ_e simply by calculating the difference between the mean of the strain data at saturation (i.e. the 1st, n/2th and nth points of a file of n points) and the mean of two points at minimum field (i.e. n/4th and 3n/4th points). This was a quick method which ignored the remanence and the

ambient field. However, it gave a very good indication of the more accurate value since the horizontal component of the earths field along the coil axis was small (of the order of $10Am^{-1}$) and the remanence was small due to the very low loss of the materials.

The more accurate value of λ_e was obtained using a pair of programs which found the components of the best fit 4th order polynomial to the data, similar to those used with the M-H data described earlier, also written by P.T.Squire. These programs also gave values for the effective (measured) quadratic coefficient, C_{eff}. The first program read the initial λ data file in and plotted one half of the λ-H loop on the screen. It then prompted the user to select a portion of the data around the low strain, low magnetisation region by means of a cursor. This portion was saved in a file in a format which could be read by the second program (λ- and H-coordinates). The next program then used the same iterative process to obtain the components of the best fit polynomial. The λ-H variation is symmetrical about λ(M=0), and as such should be approximated using an even function such as an even-powered polynomial, unlike the M-H plot which is close to an odd function. The function used here comprised zeroth, second and fourth orders:

$$\lambda = B_0 + B_1(H - B_3)^2 + B_2(H - B_3)^4 . \qquad 3.21$$

As before, the program also returned the standard errors of each coefficient and the root mean square deviation of the fit. The differences between the values of B_3 of the two halves of a data set corresponded, in principal, to twice the coercivity. Most importantly, B_0 corresponded to the maximum strain, λ_e. Generally the standard error in B_0 due to the fit was less than the variation from different measurements. Therefore the quoted values of λ_e and error in this study were obtained by taking the mean and standard deviation of the eight values of B_0 from the four data sets taken on each sample. The repeatibility of the readings was tested by taking a series of measurements on one particular (VAC0040) sample after removing it from the holder and replacing it each time. Six measurements were taken. The resulting mean and standard deviation of λ_e

were 30.6 and 0.8ppm respectively, i.e. 2-3% error.

3.3.2.2 Quadratic coefficients of λ-H and λ-M

If magnetisation proceeds by moment rotation alone in material with transverse easy axis, then the λ-H and λ-M plots are purely quadratic [Livingston 1982]. This is an ideal case and the fourth order (quartic) term was included to account for any deviation from this. Since λ tended to level off at the approach to saturation (see figure 3.9) this term was almost always of the opposite sign to the quadratic. However, the portion of the λ-H plot selected was always at fields well below the approach to saturation and as a result the quartic term was far smaller than the quadratic and had a second order correcting effect. The measured quadratic coefficient (without correction for the demagnetisation effect), C_{eff}, thus corresponded to the B_1 coefficient from equation 3.21. The program allowed comparison between the data and the best fit line in graphical form and the fit appeared very close on typical traces. As with λ_e, the standard error from the fit was less than the variation from different measurements and the quoted quadratic coefficients and errors were the mean and standard deviations of the set of eight values from each sample. The variation in the coefficients as the selected portion of the λ-H plot was increased was illustrated by fitting the quartic to sections of different sizes from the same oblique annealed METGLAS 2605S2 data file (table 3.3).

It was found that the best fit quadratic coefficient increased by about 7% as the selected portion of the plot was increased to approximately cover the range between the inflections on either side. Also the quartic coefficient decreased, giving more confidence in the value of C_{eff}. Similar readings on a transversely field annealed METGLAS 2605S2 sample indicated that C_{eff} approached a maximum over a range of λ-H which covered 5-10% of the total length change, and that it decreased by approximately 5% as the

H (Am^{-1}): 1st Half	No. points	λ_e	C_{eff}	B_4
±25	~20	52.33	$3.53x10^{-3}$ ($7.6x10^{-5}$)	$-2.78x10^{-7}$ ($1.0x10^{-7}$)
±50	~30	52.33	$3.78x10^{-3}$ ($6.2x10^{-5}$)	$-1.30x10^{-8}$ ($2.9x10^{-8}$)
±70	~50	52.35	$3.78x10^{-3}$ ($6.3x10^{-5}$)	$-1.25x10^{-8}$ ($1.5x10^{-8}$)
2nd Half				
±25	~20	52.18	$3.50x10^{-3}$ ($9.5x10^{-5}$)	$-4.42x10^{-7}$ ($1.6x10^{-7}$)
±50	~30	52.18	$3.66x10^{-3}$ ($5.3x10^{-5}$)	$-8.38x10^{-8}$ ($2.7x10^{-8}$)
±70	~50	52.19	$3.75x10^{-3}$ ($6.9x10^{-5}$)	$-1.08x10^{-8}$ ($1.2x10^{-8}$)

Table 3.3: Variation of best fit polynomial coefficients with extent of data selected from a typical obliquely annealed METGLAS 2605S2 λ-H 256-point data set.

section was increased to cover about half the strain, around the inflections. In both cases, the effect on λ_e was notably less than the error in the measurement. Generally, the sections selected from the λ-H loops in this study covered about 5% of the total strain.

The intrinsic λ-H quadratic coefficient, C_q, i.e. the quadratic coefficient of λ with respect to the internal applied field, H_i, was obtained by the expression:

$$C_q = C_{eff}\left(\frac{H_{eff}}{H_i}\right)^2 = C_{eff}\left(\frac{\chi_0}{\chi_{eff}}\right)^2 \qquad 3.22$$

$$= \frac{C_{eff}}{(1 - D\chi_{eff})^2},$$

and the error was calculated from the combination of errors of the component parameters (see Appendix).

The λ-M quadratic coefficient, C_Q, was similarly obtained from the expression:

$$C_Q = \frac{C_{eff}}{\chi^2_{eff}}. \qquad 3.23$$

An alternative method of determining C_Q was to measure the quadratic coefficient of a λ-M plot directly, as described below.

3.3.2.3 λ-M plots

These plots were produced from the λ-H and M-H plots. The M-H data was read into a program which then fitted a spline to each half of the loop (spline parameters could be adjusted within the program). The λ-H data was then read in and the interpolated value of M for each H value in this data set was found from the spline. Since the magnetisation data were always normalised to the manufacturers' values of B_s, the plots are more precisely λ-B, which can be considered as λ-μ_0M.

The quadratic coefficients were then found in the same way as for the λ-H data, described above. The values of the coefficients were calculated for the best fits of the two halves of a typical TFA VAC0040 λ-M loop, both with and without the quartic term in the polynomial, together with the root mean square deviations (RMSD). The results are given in table 3.4, where

$$\lambda = B_0 + B_1(\mu_0 M + B_3)^2 + B_2(\mu_0 M + B_3)^4. \qquad 3.24$$

It can be seen that the quartic term had very little effect on the values of λ_e and the offset. In the case where the quartic coefficient was large, the effect was to reduce the quadratic coefficient by about 12%, while the lower term reduced it by 3%. Also, the RMSDs were comparable in both cases implying that the quality of the fit was not significantly affected by the removal of the quartic term. Similar comparisons on VAC0040 oblique annealed sample λ-B data gave better agreements, with maximum

		B_0	B_1	B_2	B_3	RMSD
With quartic component:	1st Half	29.74	-37.68 (0.68)	-17.57 (10.8)	0.0616	0.0359
	2nd Half	29.62	-34.03 (0.78)	-56.69 (9.8)	0.0551	0.0544
Without quartic component:	1st Half	29.74	-38.74 (0.21)	0	0.0615	0.0364
	2nd Half	29.66	-38.32 (0.30)	0	0.0546	0.0660

Table 3.4: Comparison of best fit polynomial coefficients to typical TFA VAC0040 data, with and without fourth order terms.

correction on B_2 of approximately 7%. This confirmed that this quartic term only had a second order correcting effect and that the assumption of a quadratic λ-M relationship (and λ-H) holds well.

The values of C_Q obtained from C_{eff} and χ_{eff} (equation 3.23) and from direct measurement from the derived λ-B plots for the five $\theta = 90^\circ$ oblique annealed samples were compared and the agreement was found to be within 3% of each other for all alloys except the METGLAS 2605S2, which was approximately 10% different. Apart from the METGLAS 2605S2 these were all within error of each other, giving very good agreement between the two methods (the details are given in chapter 4). The values of C_Q quoted in this study were calculated using equation 3.23.

3.3.2.4 $d\lambda/dH(maximum)$

There were two basic methods of calculating $\left|\frac{d\lambda}{dH}\right|_{max}$ at the inflections of the λ-H plots. The first was to fit a cubic to the data around the inflection, such that:

$$M = B_0 + B_1H + B_2H^2 + B_3H^3 . \qquad 3.25$$

The maximum gradient then corresponded to the linear coefficient, B_1. Although this gave a good degree of accuracy, it was not normally used in this study merely because of the time involved in processing the data. An exception to this was the obliquely field annealed material, where this method was used.

The second method was to do a simple straight line regression. A program performed a regression on a pre-specified number of points (typically 6-12) for all successive sets of points in the data file, and returned the maximum gradient and its standard error. The mean and standard deviation were then found for the four quarters of the four data sets of each sample. An alternative program, written by P.T.Squire, did a straight line regression on three points around the point marked by a cursor, with the error and the H-coordinate. Although the regressed straight line gradient approached that of the tangent of the plot as the number of points in the regression was decreased, the associated error increased. The variation of the mean gradient measured on all four branches of a typical transversely field annealed VAC0040 λ-H plot is shown with respect to number of points in figure 3.20, and was seen to increase appreciably only where the regression was over two points and so was very sensitive to the effect of noise. If the approximately linear increase in gradient with decrease in number of points were extrapolated to zero points, indicating the gradient at a single point, then the measured values from six and twelve points were roughly 2.5% and 5% lower. This difference was found to be greater in samples with appreciable crystallisation. The difference in 6-point and 12-point regression was measured in 256-point partially crystallised VAC7505 data files to be about 1-2% for the lowest coercivity samples, increasing to about 7% where H_c was close to $100Am^{-1}$, although this decreased to only 2% when the data file was increased to 512 points. Also, the values obtained from 12 point regression and the cubic fitting method described above were compared for the METGLAS 2826MB

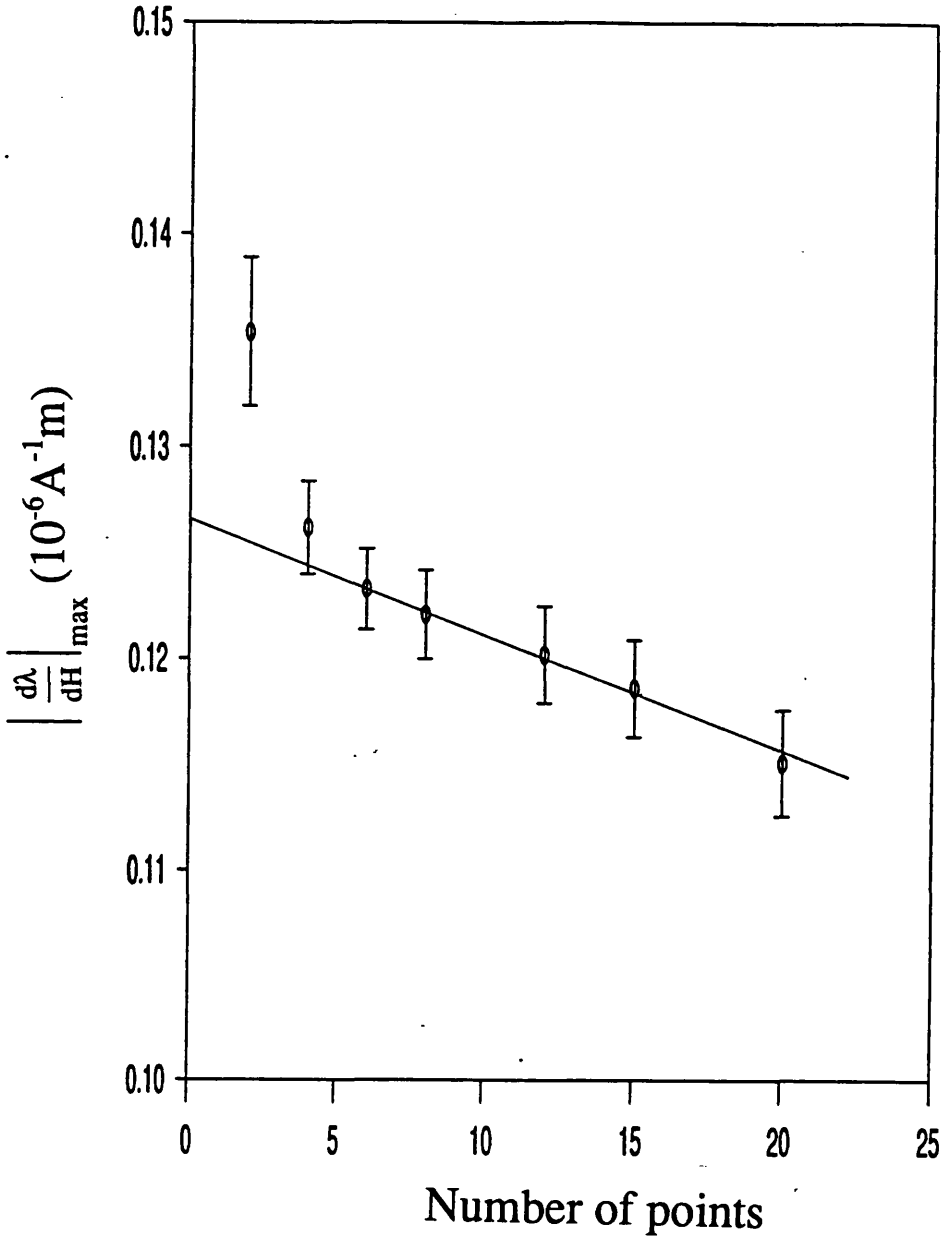

Figure 3.20: $d\lambda/dH$ as a function of number of points used in the straight line fit used.

Not surprisingly, the maximum gradient decreases as more points are used in the line fitting, this decrease being approximately linear for fits with relatively few points. Line fits with fewer than five or six points are appreciably affected by the noise of the λ-H data. The maximum gradients of line fits of six points were found to be about 2.5% below that extrapolated to the ordinate (which represents infinitely small straight line fit with noise removed).

oblique annealed samples (256 point data files), and gradients from the regressions were found to be 5-7% lower for the TFA samples, which is roughly consistent if the value from the cubic fit is also considered to be the gradient at a single point on the plot. Therefore, it can be assumed that the maximum gradient values obtained from the regressions used in this study are a few percent below the actual values, and the values obtained from the cubic fits are accurate to within their errors.

The intrinsic gradients were corrected for the demagnetisation effect using the expression:

$$\frac{d\lambda}{dH} = \left(\frac{d\lambda}{dH}\right)_{eff} \frac{H_a}{H_i} \qquad 3.26$$

$$= \left(\frac{d\lambda}{dH}\right)_{eff} \frac{\chi_0}{\chi_{eff}}.$$

4 Oblique Field Annealing

4.1 Introduction

The first part of the study involved the measurement of four Fe and Fe-Ni based alloys, namely METGLAS 2605SC (standard and super-smooth surface), METGLAS 2605S2, METGLAS 2826MB and VAC0040. Samples were field annealed at a series of oblique angles, θ, where θ is the angle between the anneal field and the sample long axis, to induce a uniaxial magnetic anisotropy in the anneal field direction. The magnetisation was always measured parallel to this axis. This was the basis of the phenomenological model of Squire [1990]. This enabled the data and model to be compared, the assumptions in the model tested, and the relevant parameters in the model to be measured. Much of this work was done in conjunction with P.T. Squire.

Each anneal was performed on a different sample cut from the same sections of ribbon and, where applicable, all samples of the same alloy had been stress relieved simultaneously. In this way, the initial state of the samples of each alloy were as similar as possible, as confirmed by measurement of H_c.

Even with careful precautions, there were found to be notable sample to sample variations. The intrinsic scatter between as received specimens from the same reel may not be negligible [Jagielinski 1982]. This variation is mainly due to quenched in stresses which are annealed out in this study. However, variations also occur due to differences in the anneal conditions, such as anneal temperature. The variation in anneal field for different anneals was insignificant. The anneal temperature was constant to within ~1°C, and the error in the anneal time was of the order of seconds. Another factor was differences in the positioning of the samples within the aluminium plates, and the positioning of the plates within the annealing magnet, which would be more difficult to quantify, but were thought to be insignificant. Pairs of samples were field annealed simultaneously in the

anneal time and temperature part of the study in chapter 5, and in that study the parameters measured on the different samples of the same anneal were generally found to agree within the errors for each sample. Consequently these errors were considered to be large enough to incorporate the sample to sample variation.

The second part of the study was similar to the first, but involved a single VAC0040 sample which was field annealed at a series of angles, θ, beginning with 90°. The 90° anneal was repeated at the end to ascertain the progressive change in properties as a result of repeated anneals, likely to result from partial crystallisation or incomplete stress relief. In this way the sample to sample variation was eliminated.

The magnetostrictive strain of the samples, λ_e, was measured with respect to θ. The expression for $\lambda_e(\theta)$ is given by equation 1.6, where $\theta=\theta_i$. In this study, the applied field was always enough to saturate the samples, so that $\theta_f=0$. Equation 1.6 then reduces to

$$\lambda_e(\theta)=\frac{3}{2}\lambda_s\sin^2\theta\,. \qquad 4.1$$

The spread in moment direction is discussed in chapter 2. This spread can be described by a Gaussian distribution, so that the probability of the deviation of the local moment by an amount ψ from the induced direction, θ, is given by

$$P(\psi)=\frac{1}{\delta\sqrt{2\pi}}\exp\left(\frac{-\psi^2}{2\delta^2}\right), \qquad 4.2$$

where δ is the standard deviation of the direction distribution. Equation 4.1 can then be expressed with the above distribution in moment direction about the induced direction, at angle θ (with cut-off at $\psi=\pm3\delta$) rather than for pure moment collinearity along it. The resulting expression for λ_e becomes

$$\lambda_e(\theta)=\frac{3\lambda_s}{2\delta\sqrt{2\pi}}\int_{-3\delta}^{3\delta}\sin^2(\theta+\psi)\exp\left(\frac{-\psi^2}{2\delta^2}\right)d\psi, \qquad 4.3$$

where ψ is the angle between the initial local moment direction and easy axis. Barandiarán *et al* [1989] showed that the combined local easy axis magnitude and direction distributions were close to Gaussian, implying a similar distribution in moment direction. The choice of type of distribution, however, is arbitrary and the relevant parameters of the Squire model are not sensitive to this. The (normalised) effect of moment spread, δ, on $\lambda_e(\theta)$ for different δ, and on $\lambda_e(90°)$ were found by calculating the integral above, and are shown in figure 4.1. $\lambda(\theta)$ is suppressed for $\theta>45°$ and is increased for $\theta<45°$. It can be seen that there is notable suppression of $\lambda_e(90°)$ arising from moment spread. For instance a spread of $\delta\approx20°$, which is a realistic figure in some as cast materials, results in a reduction in λ_e by approximately 10%. Hence moment spread can have a notable effect.

The variation of normalised $\chi_0(\theta=0$ and $90°)$ with δ is shown in figure 4.2a assuming a ratio, *c*, of 20. This was derived by averaging the expression for χ_0 from Squire [1990] (equation 28, $\chi_0 \propto \sin^2(\theta)+c\cos^2(\theta)$) over a Gaussian distribution of the deviation of the magnetisation from the induced angle, ψ, between the limits of $\pm3\delta$, i.e.

$$\chi_0 = \frac{\mu_0 M^2}{2K_u\delta\sqrt{2\pi}}\int_{-3\delta}^{3\delta}[\sin^2(\theta+\psi)+c\cos^2(\theta+\psi)]\exp\left(\frac{-\psi^2}{2\delta^2}\right)d\psi. \qquad 4.4$$

Figure 4.2b shows the variation of normalised $\Delta E/E$ at zero applied field (and zero stress) with respect to δ, obtained by a similar averaging of the expression for $\Delta E/E$ from Squire [1990] (equations 46 and 47 from that paper, where h=0, γ=0, ϕ_1=0), i.e.

$$\frac{\Delta E}{E} = \frac{9\lambda_s^2 E_s}{8K_u\delta\sqrt{2\pi}}\int_{-3\delta}^{3\delta}\sin^2 2(\theta+\psi)\exp\left(\frac{-\psi^2}{2\delta^2}\right)d\psi. \qquad 4.5$$

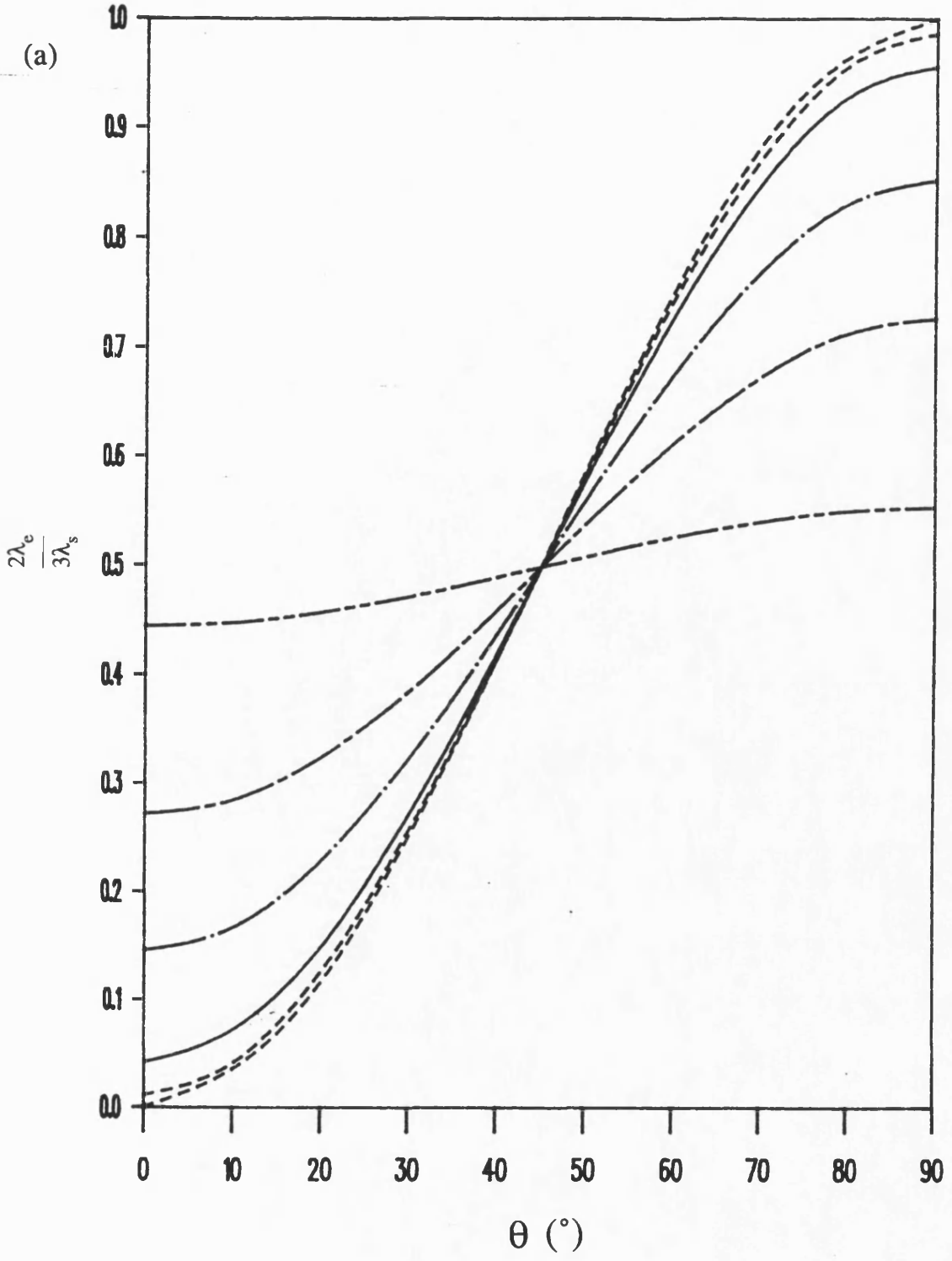

Figure 4.1: a) Normalised λ_e-θ assuming pure rotation of magnetisations with a Gaussian angular distribution for a series of moment spreads, δ. (δ=0 - - - -, 6 - - - -, 12° ———, 24°— · —, 36°— - —, 60°— - - –), b) Normalised $\lambda_e(90°)$ as a function of angular spread of magnetisation, δ.

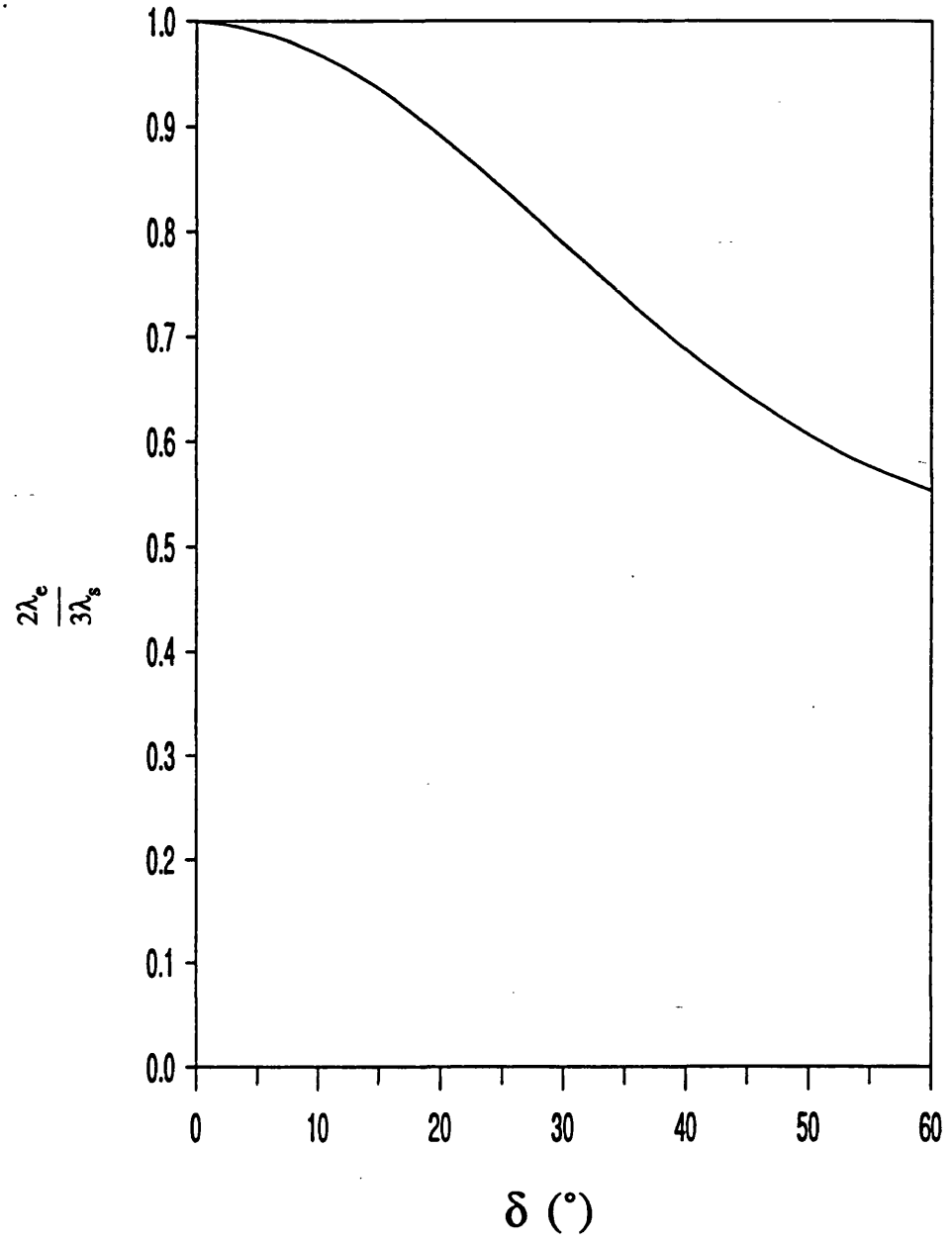
1.0
0.9
0.8
0.7
0.6
0.5
0.4
0.3
0.2
0.1
0.0
$\frac{2\lambda_e}{3\lambda_s}$
0
10
20
30
40
50
60
δ (°)

(b)

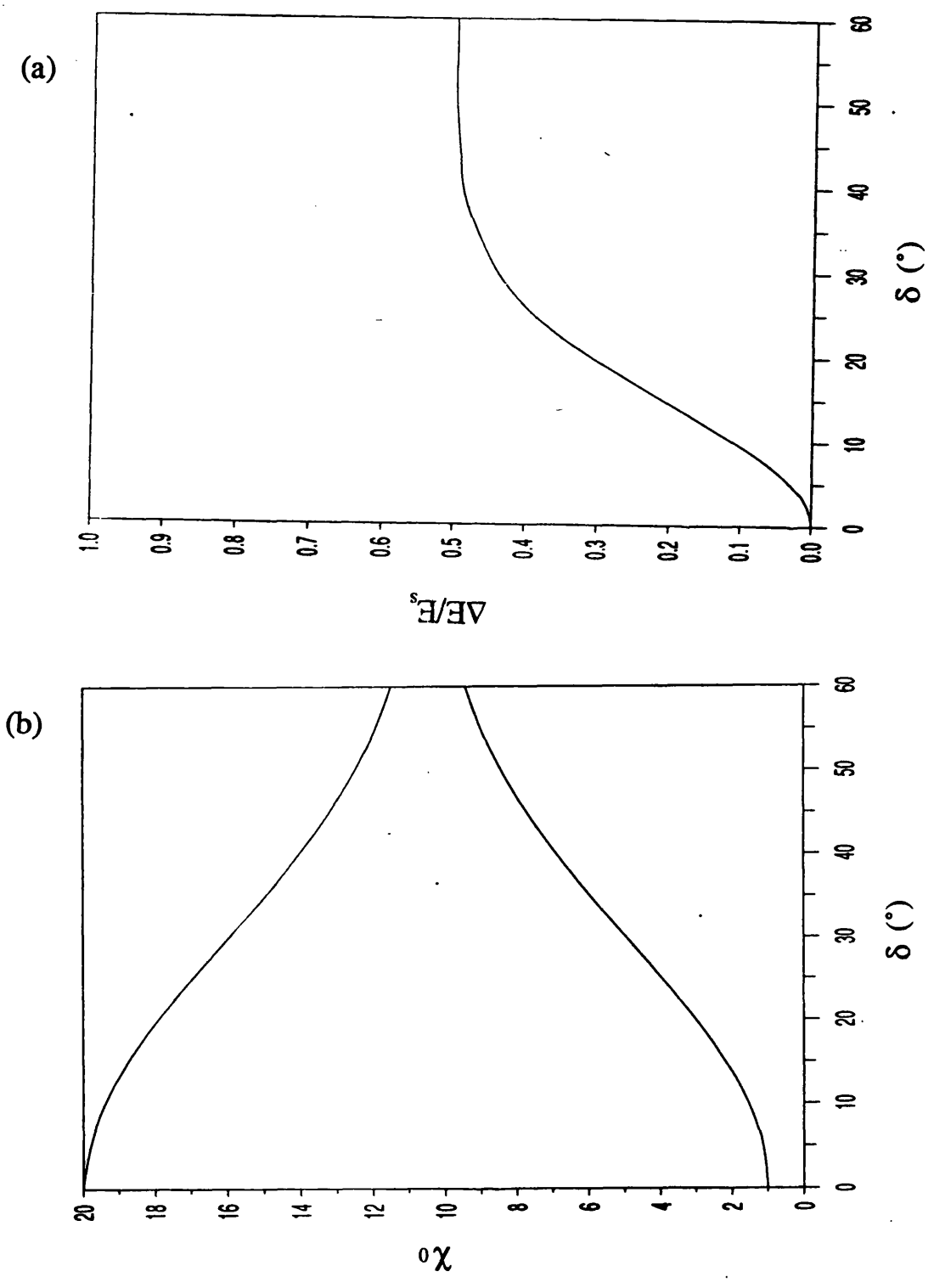

Figure 4.2: a) Initial susceptibility for $\theta=0$ and 90° as a function of δ, normalised to $\chi_0(90°)=1$ and assuming a ratio c of 20. b) $\Delta E/E_s$ (H=0, $\sigma=0$) for $\theta=90°$ versus δ.

The assumption was made that the moment spread was notionally the same for all θ for each alloy for two main reasons. Firstly, care was taken to keep the heat treatments as consistent as possible, i.e. variables such as anneal temperature, and rate of heating and cooling (as stated, judging from the difference in parameters of different samples with the same anneals, the error due to variation in anneal conditions was generally less than the errors due to measurement for each sample). Secondly, although the shape factor meant that the internal applied field, H_i, was higher during the lower θ anneals, in the case of the transverse field anneal, M_s was $1.25\times10^6 Am^{-1}$ and the demagnetisation factor across the sample was 4.9×10^{-3}, so the demagnetising field was approximately $6\times10^3 Am^{-1}$, less than 2% of the external applied field of $3.2\times10^5 Am^{-1}$. Hence it could be assumed, since H_k was of the order of 10^2-$10^3 Am^{-1}$ along the easy axis (measured at room temperature), that the samples were fully saturated during the anneals for all θ.

4.2 Comparison of Different Compositions

This section is split into three parts. Firstly the engineering magnetostriction was measured for each alloy for a series of oblique annealing angles. From this the moment spread and λ_s were estimated. Secondly, the variation of the susceptibility and parameters involving the magnetostrictive response were obtained and compared with the predictions of the Squire model. Thirdly, results of domain studies are presented and discussed.

The annealing conditions are shown in table 4.1. Two of the alloys were subjected to a pre-anneal stress relief, the conditions of which were chosen to decrease H_c to close to its minimum. The field anneals on the METGLAS 2605SC and VAC0040 (370°C) were found to reduce H_c to close to the mimimum, so an additional stress relief was not deemed necessary. The METGLAS 2605S2 ribbon was found to be well stress relieved

in the as-received state, possibly because this particular batch had been manufactured with a relatively slow quench rate. This was reflected in the relative brittleness of the ribbon.

Alloy	Stress Relief		Field Anneal	
	T_a	t_a	T_a	t_a
	(°C)	(min.)	(°C)	(min.)
METGLAS 2605S2			420	10
			400	180
METGLAS 2605SC			390	10
METGLAS 2826MB	360	10	345	30
VAC0040			370	30
	370	30	250	20

Table 4.1: Anneal conditions

4.2.1 λ_s and Moment Spread

The λ_e data is presented with respect to θ (measured from domain photographs) for the alloys listed in table 4.1 in figure 4.3. Also shown is the theoretical variation as given by equation 4.3 for different δ (δ=0°,10°,20°). In figure 4.4 a series of λ-H plots are shown for a series of θ measured on METGLAS 2605S2 and VAC0040 samples to illustrate the λ_e-θ variation. Since $3\lambda_s/2$ was unknown, it was not possible to accurately normalise the theoretical plots for each alloy. Considering that it is symmetrical about θ=45° so that

$$\lambda_e(\theta) = \frac{3\lambda_s}{2} - \lambda_e(90-\theta) \qquad 4.6$$

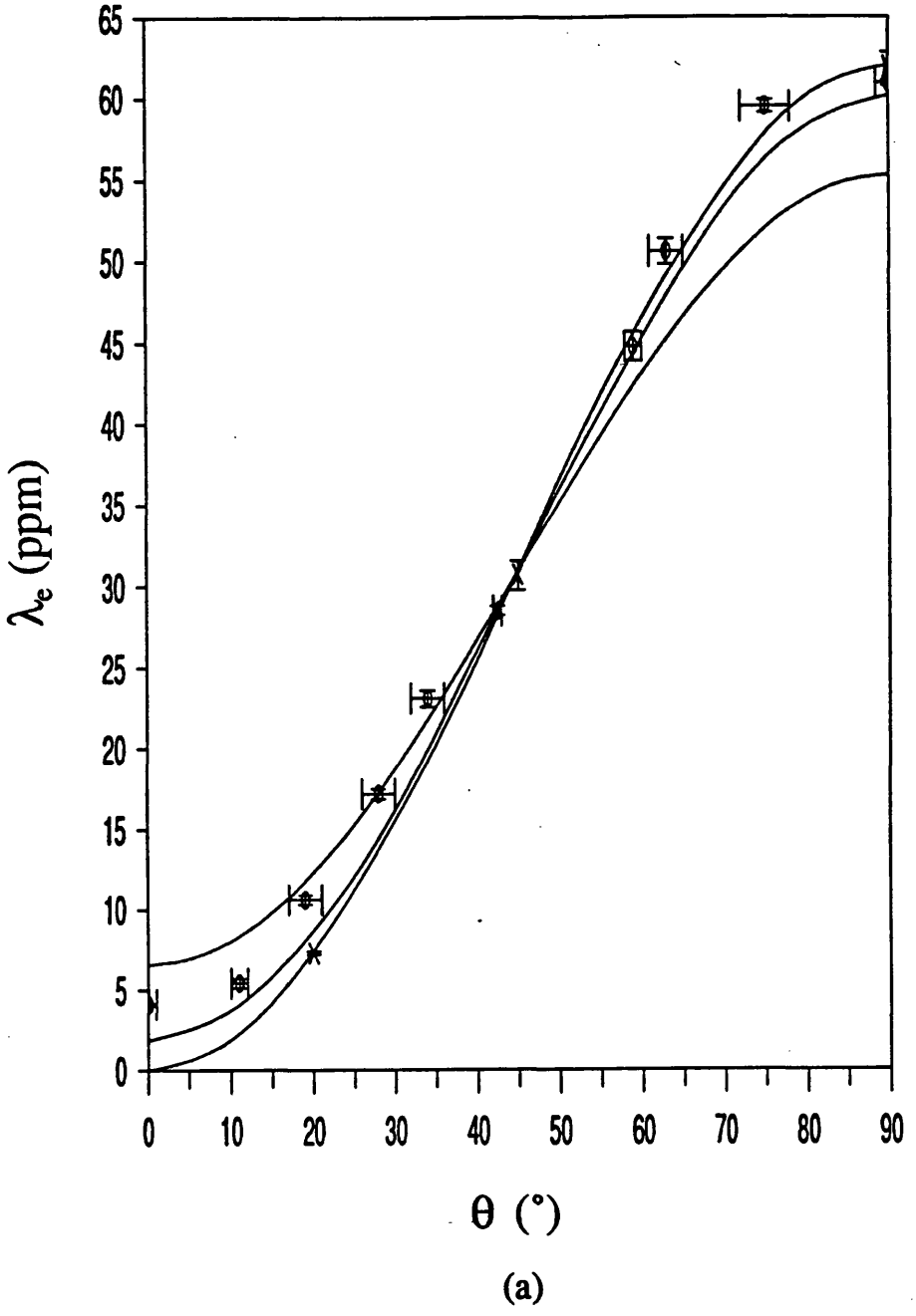

(a)

Figure 4.3a-d: λ_e-θ for each alloy. Also plotted are calculated λ_e-θ variations for δ=0, 10° and 20°, normalised to give a good agreement with the data.

a) METGLAS 2605S2 (o - 10 minutes at 420°C, × - 180 minutes at 400°C), b) METGLAS 2605SC (o - standard ribbon, × - super-smooth surface), c) METGLAS 2826MB, d) VAC0040 (o - 30 minutes at 370°C, × - 20 minutes at 250°C).

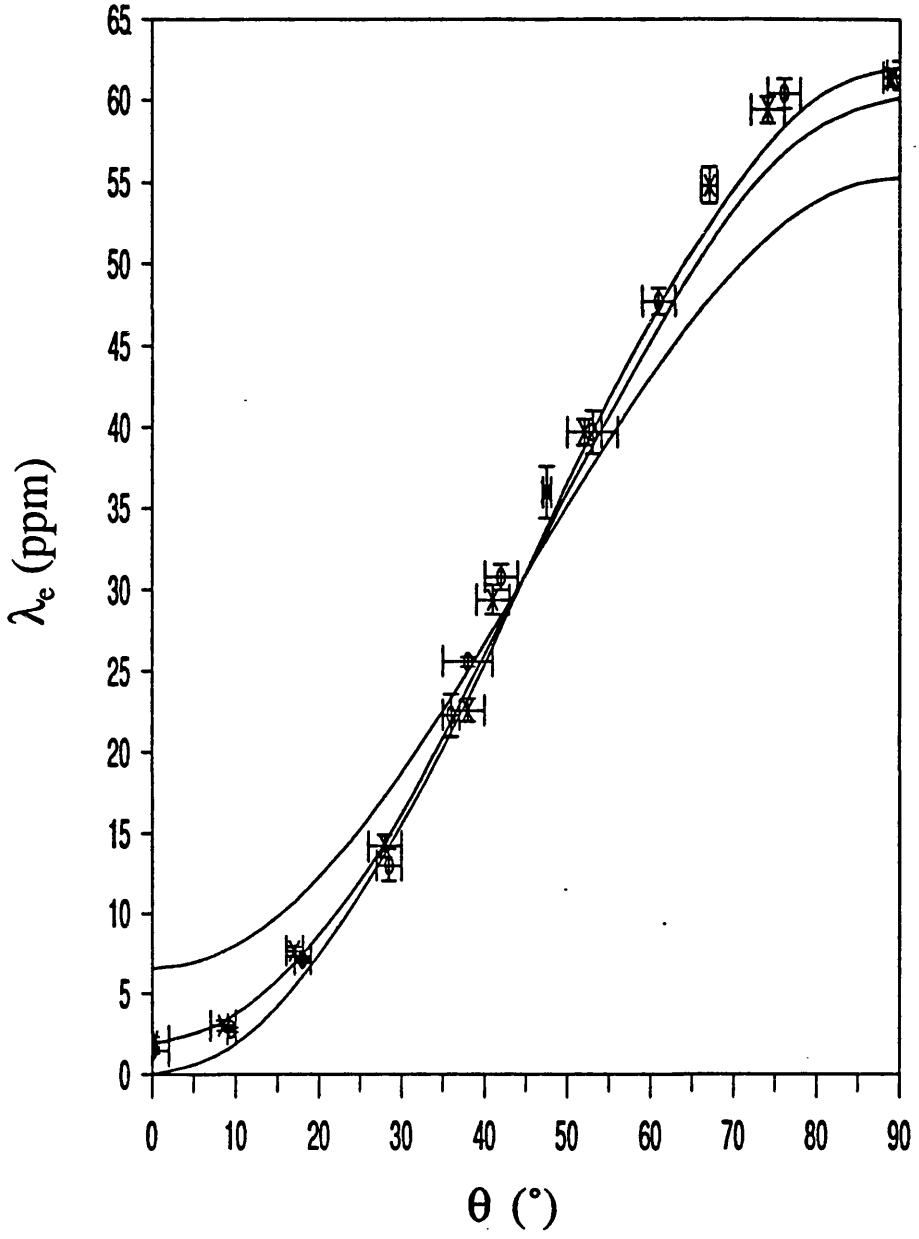
65
60
55
50
45
40
35
30
25
20
15
10
5
0
λ_e (ppm)
0
10
20
30
40
50
60
70
80
90
θ (°)

(b)

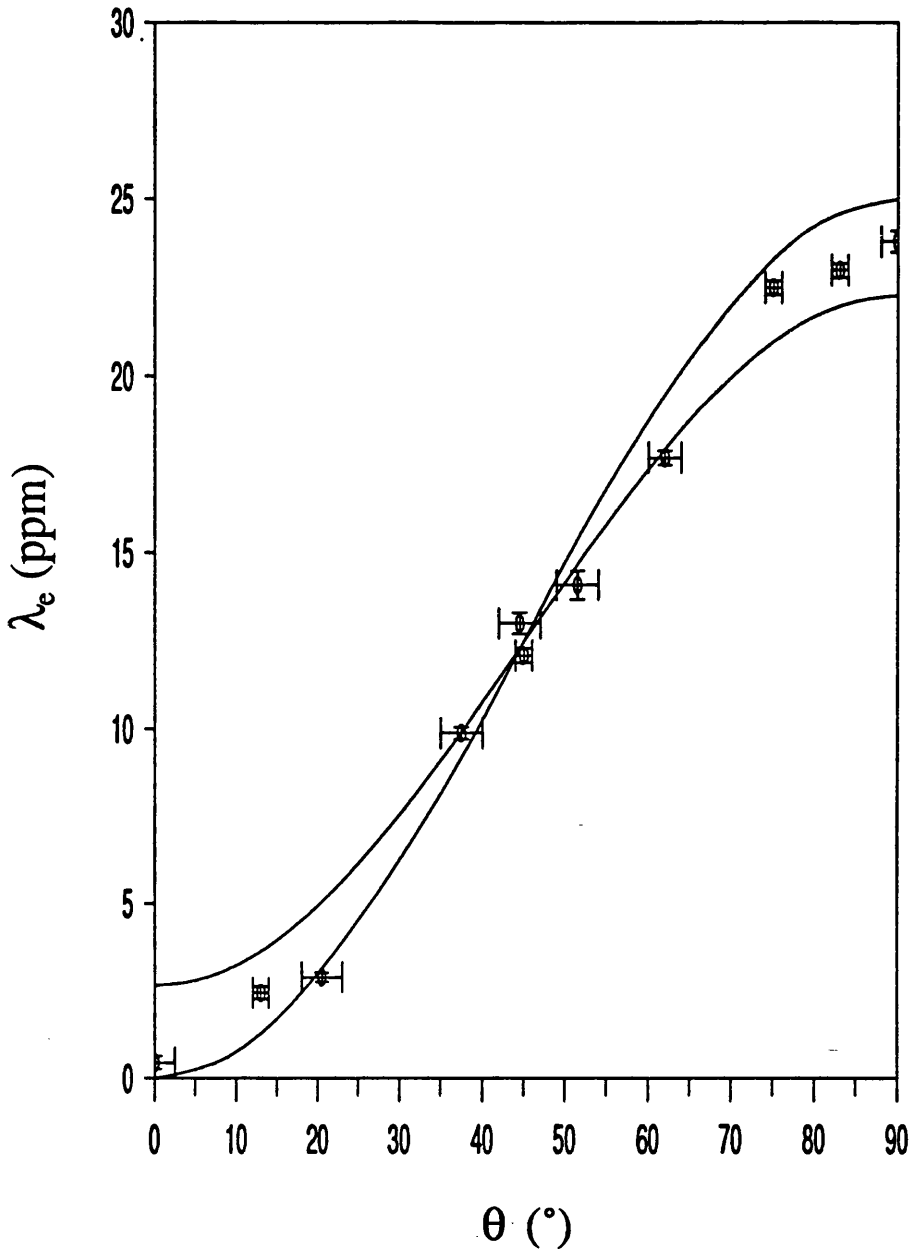

(c)

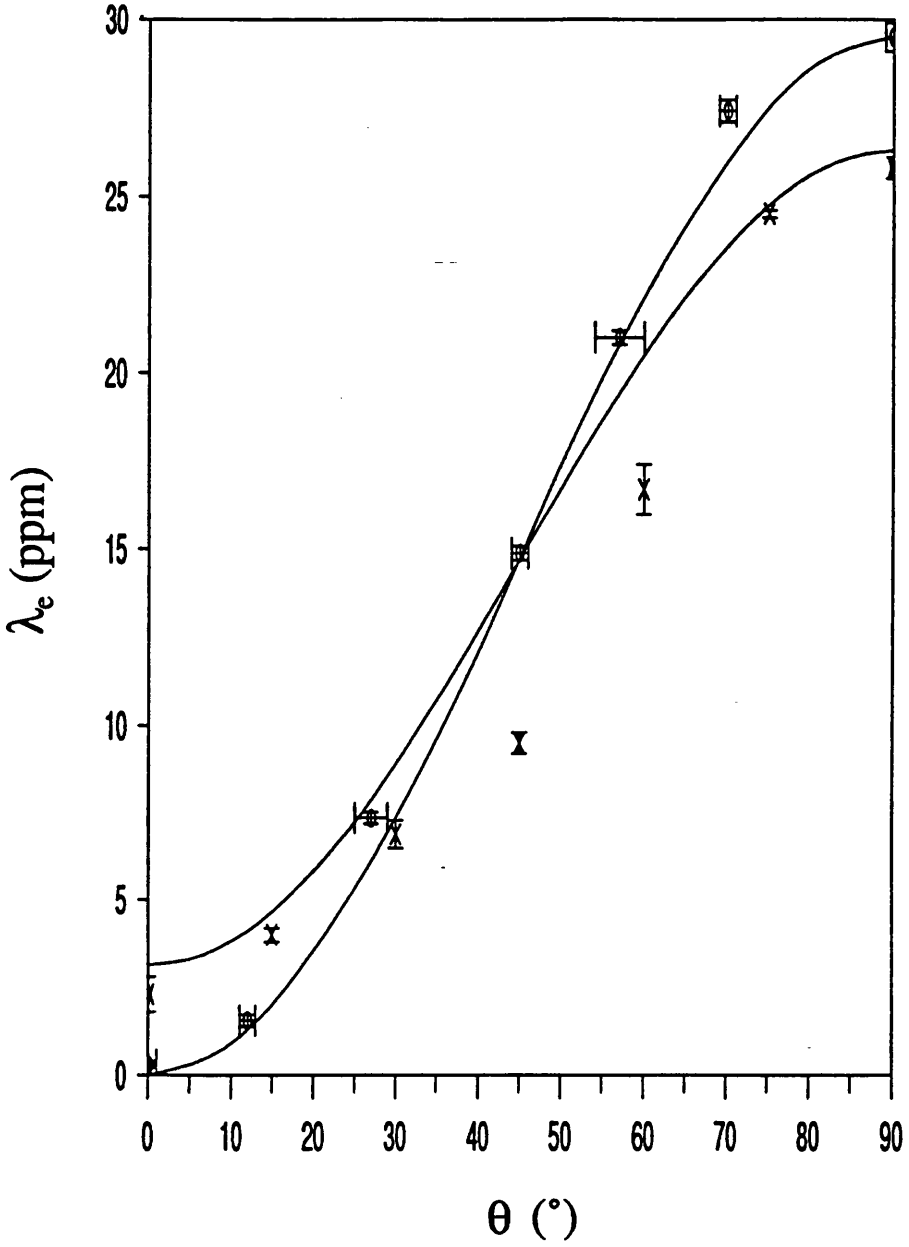

(d)

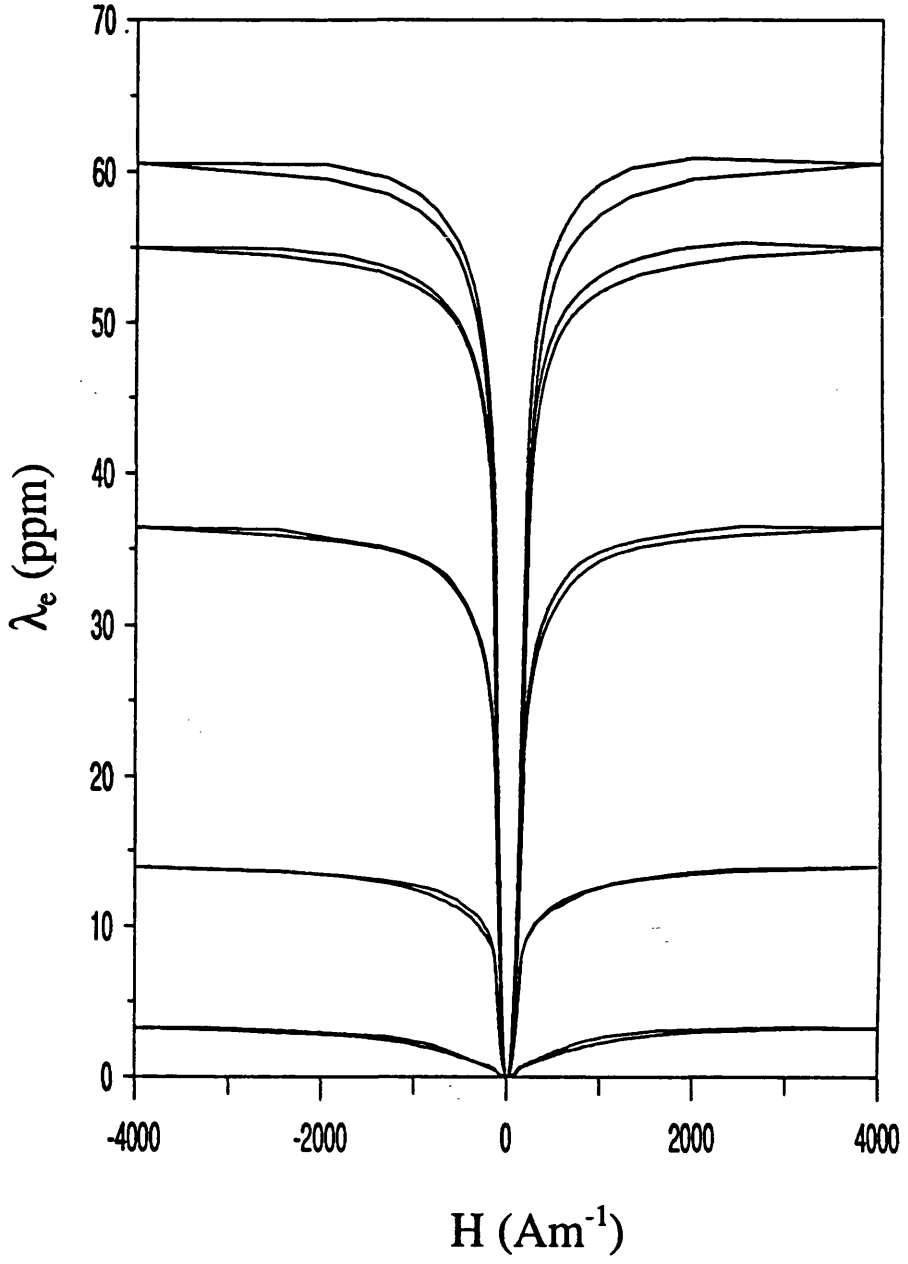

(a)

Figure 4.4: λ-H for different values of θ. a) METGLAS 2605S2 (θ=10°, 30°, 50°, 70°, 90°), b) VAC0040 (θ=0°, 15°, 30°, 45°, 60°, 75°, 90°).

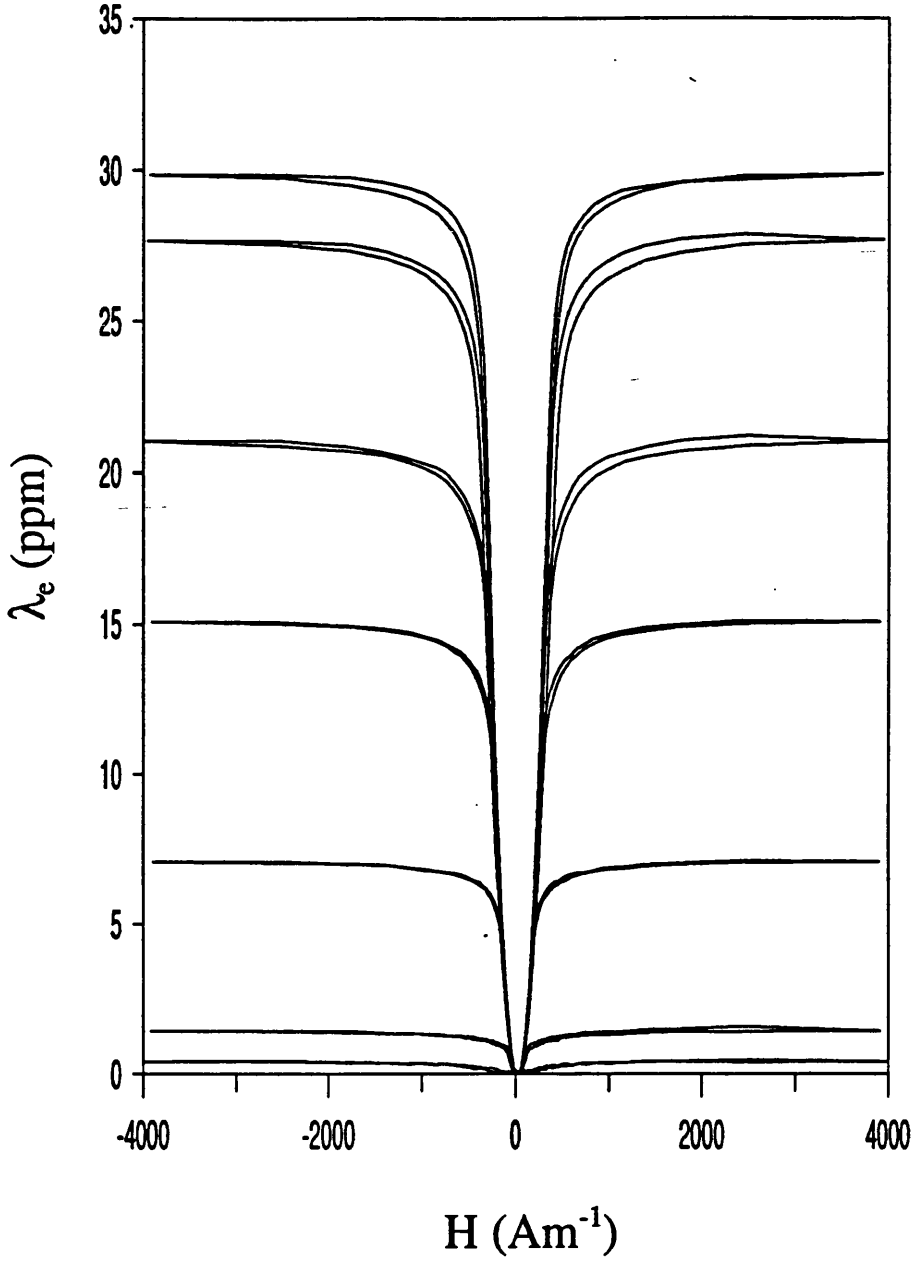

(b)

(and as a result $\lambda_e(\theta=45^\circ)=3\lambda_s/4$, regardless of δ), the normalisation factors for these curves, therefore, were estimated so as to give the best fit to the data. It was found that the spread was 0-20° in all of the alloys. The normalisation factors, $\lambda_e(90^\circ,\delta=0)$, which were used in the figures, and the estimated spreads are given in table 4.2.

Alloy	$3\lambda_s/2$ (ppm)	δ (°)
METGLAS 2605SC	61.5 (0.6)	~5
METGLAS 2605S2	61.5 (0.9)	~5
METGLAS 2826MB	25 (1)	~10
VAC0040	29.0 (1.0)	~0-3

Table 4.2: Estimated values for $\lambda_e(90^\circ)=3\lambda_s/2$ for $\delta=0$, and for measured spread, δ (errors in brackets).

The anneals were not originally chosen strictly to obtain minimum moment spread, but rather for good magnetomechanical coupling [Squire *et al* 1990], following the method of Modzelewski *et al* [1981] of annealing slightly above T_c for 10 minutes followed by a slow cool. It was therefore expected that these anneals would fully induce uniaxial anisotropy. It was found (see chapter 5) that this was the case for VAC0040. However, maximum K_u had not been attained in the METGLAS 2605S2 material (K_u was measured to be ~34Jm^{-3}, compared with a maximum value of approximately 80Jm^{-3}),

implying that a uniaxial anisotropy may not have been fully induced. Some readings on this alloy were repeated on a set of samples that had been field annealed for 3 hours at 400°C, which had been shown to induce maximum K_u [Bucholtz *et al* 1986]. After this more extensive anneal the spread was found to be slightly smaller and was estimated to be very close to zero. Readings were also repeated on a set of VAC0040 samples annealed at 250°C for 20 minutes, which was shown to induce a suppressed value of K_u (see chapter 5) and non-uniaxial anisotropy from domain studies (section 4.2.3). As expected, the data from this set pointed to a larger moment spread than the 370°C anneals.

There was no remarkable difference between the data for the standard and the "super-smooth" METGLAS 2605SC samples within measurement error, so it was concluded that the surface roughness was not a cause of significant additional moment spread.

It was concluded that when the moment spread was accounted for, the data agreed well with the theoretical $\lambda_e \propto \sin^2(\theta)$ relationship.

4.2.2 Variation of Magnetostriction Parameters with θ

The χ_0-θ data are shown in figure 4.5. Also shown is the theoretical relationship from Squire [1990], with c (defined in equation 2.18) normalised to the data at θ=0° and 90°, where this was of the order of 20 in all of the alloys measured. There was a definite discrepancy between the data and the model, the former decreasing more rapidly with increasing θ than the latter at low θ. This was thought to arise partly from the moment spread, but mainly from the fact that the model had assumed a constant domain wall movement parameter, β. Variation in β directly affects the χ_0-θ relationship, and hence also that for C_Q, as described in the Squire model. From this data it was seen that domain walls move more readily than predicted at low θ resulting in a more pronounced increase

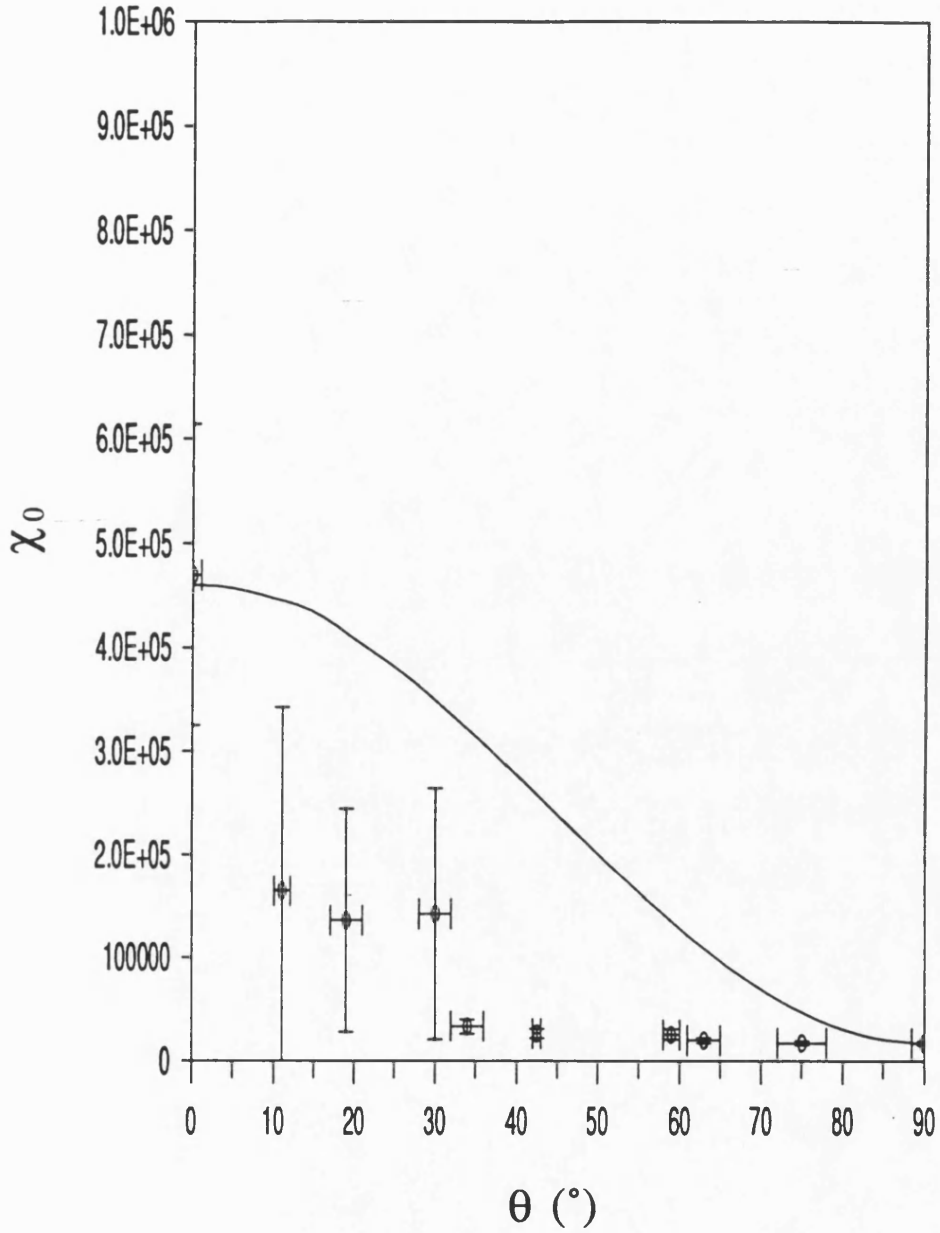

(a)

Figure 4.5a-d: χ_0-θ for each alloy. Also shown is the theoretical variation (from Squire [1990]) normalised to both $\chi_0(0)$ and $\chi_0(90°)$.

a) METGLAS 2605S2, b) METGLAS 2605SC (o - standard ribbon, × - super-smooth surface), c) METGLAS 2826MB, d) VAC0040.

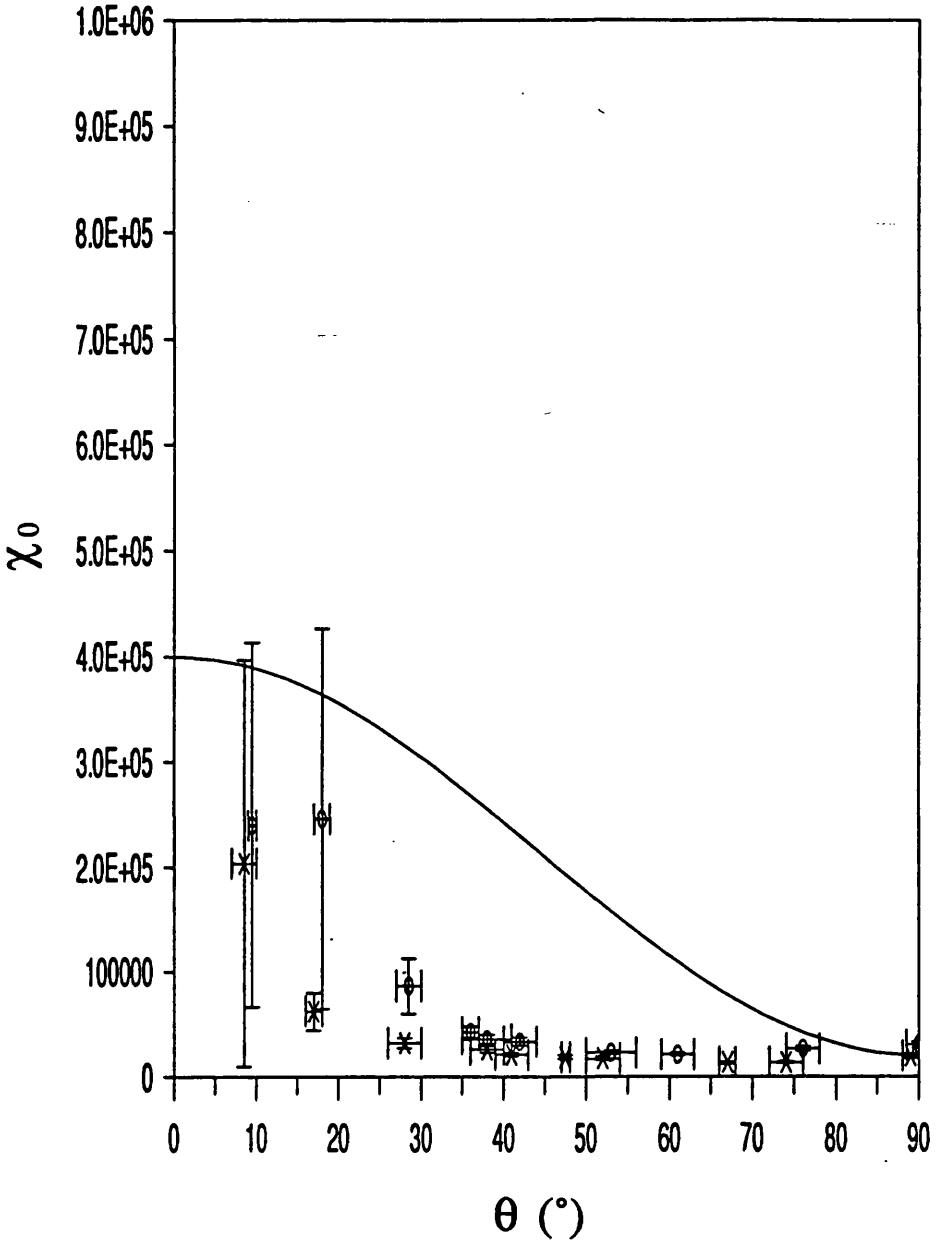
1.0E+06
9.0E+05
8.0E+05
7.0E+05
6.0E+05
5.0E+05
4.0E+05
3.0E+05
2.0E+05
100000
0
χ0
0
10
20
30
40
50
60
70
80
90
θ (°)

(b)

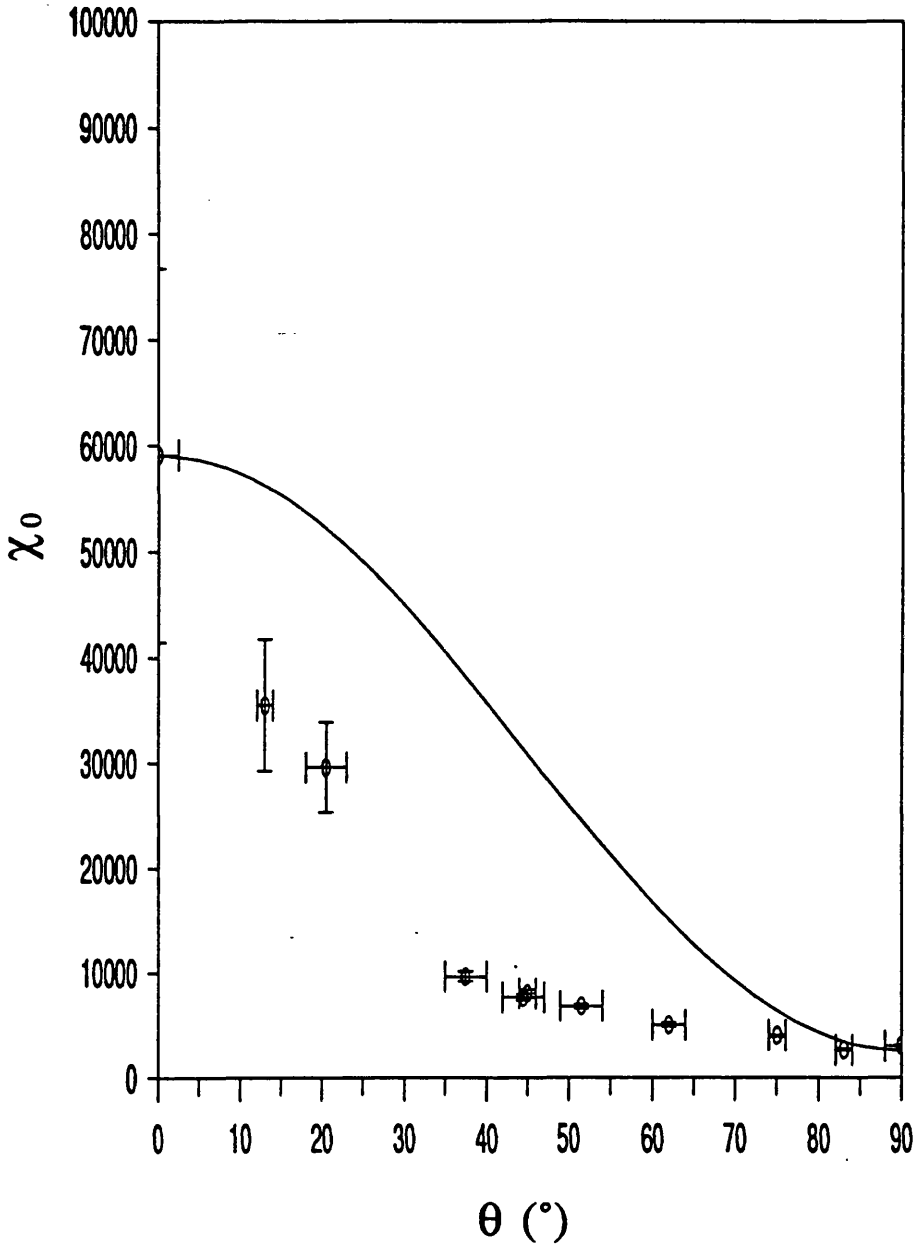
100000
90000
80000
70000
60000
50000
40000
30000
20000
10000
0
χ_0
0
10
20
30
40
50
60
70
80
90
θ (°)

(c)

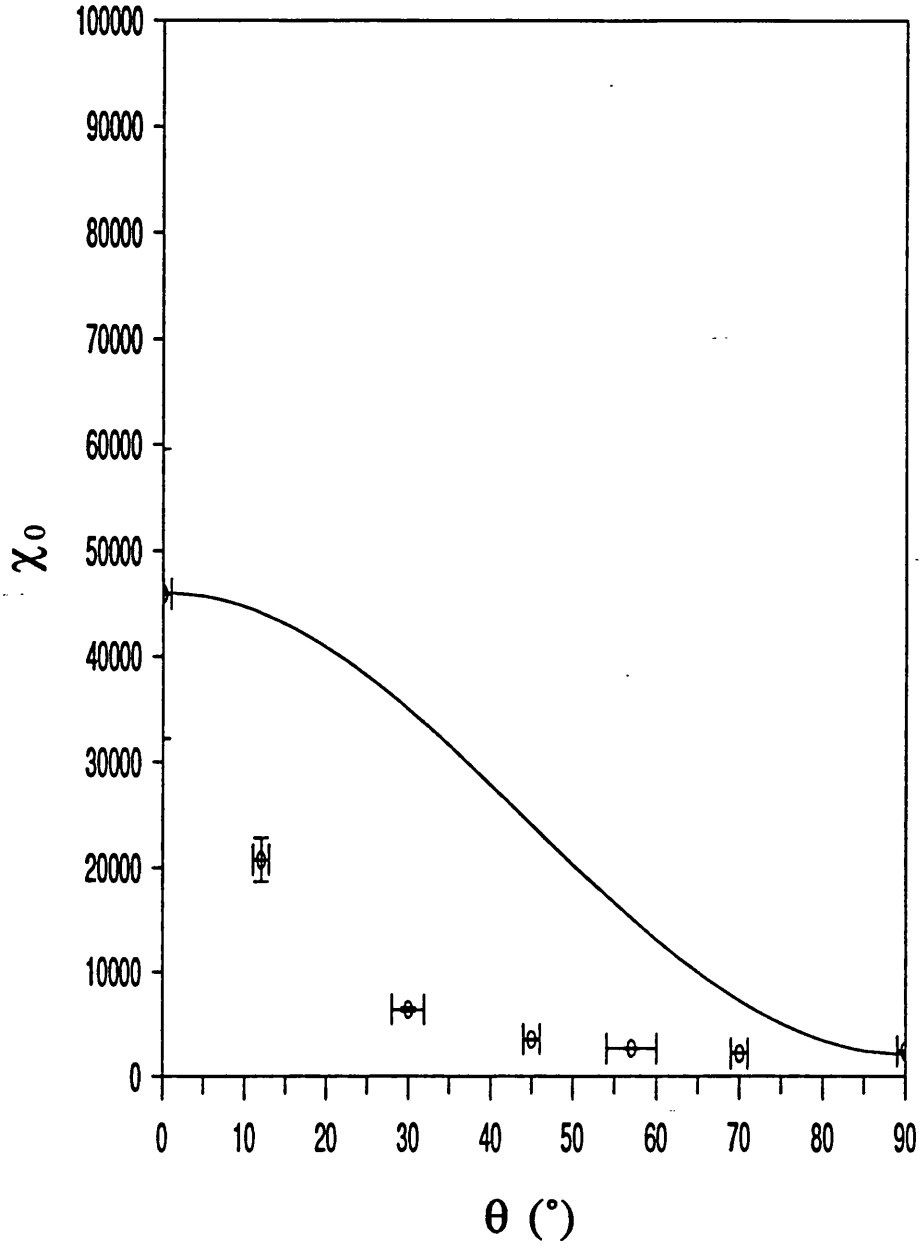
100000
90000
80000
70000
60000
50000
40000
30000
20000
10000
0
χ_0
0
10
20
30
40
50
60
70
80
90
θ (°)

(d)

in χ_0 with decreasing θ (the data appears lower than the predicted curve since this was normalised to the data at θ=0 and 90°). Development of the model to take account of variation in the domain wall parameter is discussed in the second part of this study.

The quadratic coefficients of the best fit even ordered polynomials on the λ-M data at low M are shown in figures 4.6. The measured coefficients are presented together with the corresponding predicted variations from the Squire model. These relationships are not theoretically purely quadratic except at θ=90°. The fit to a quadratic degraded at low θ, as predicted in the model. However, the λ-M data was still a good approximation to a quadratic judging from the agreement between the data and the theoretical relationship. These theoretical curves in the figures were obtained from equations 38 and 39 from Squire [1990], using the measured values for $3\lambda_s/2$ and c for each alloy. The C_Q data increase monotonically with θ due to the resulting increase in λ_e with no change in M_s. They follow a similar trend to the predicted variations. However, the data was consistently high in all the alloys measured. This discrepancy was examined by considering the shapes of the λ-M curves.

The λ-M plots, obtained from λ-H and M-H data sets, were obtained for the θ=90° samples for all alloys. Since in this case magnetisation notionally proceeds by moment rotation alone, these were all expected to appear close to quadratics. Figure 4.7 shows these data sets with normalised λ and M scales. All the data sets lie close to quadratics at low M (i.e. the contribution to λ from the quartic component of M was small), though they all showed some levelling off from this quadratic at the approach to saturation. This arose mainly from the levelling off of the λ-H data towards saturation more gradually than the M-H data, possibly due to sample-holder interaction (friction), and so is likely to be an attribute of the measurement procedure. As a result the quadratic coefficient, C_Q, measured on these curves was always greater than that predicted from equation 2.21 using the measured value of λ_e to obtain the λ normalising factor, where $\lambda_e(90°)=3\lambda_s/2$.

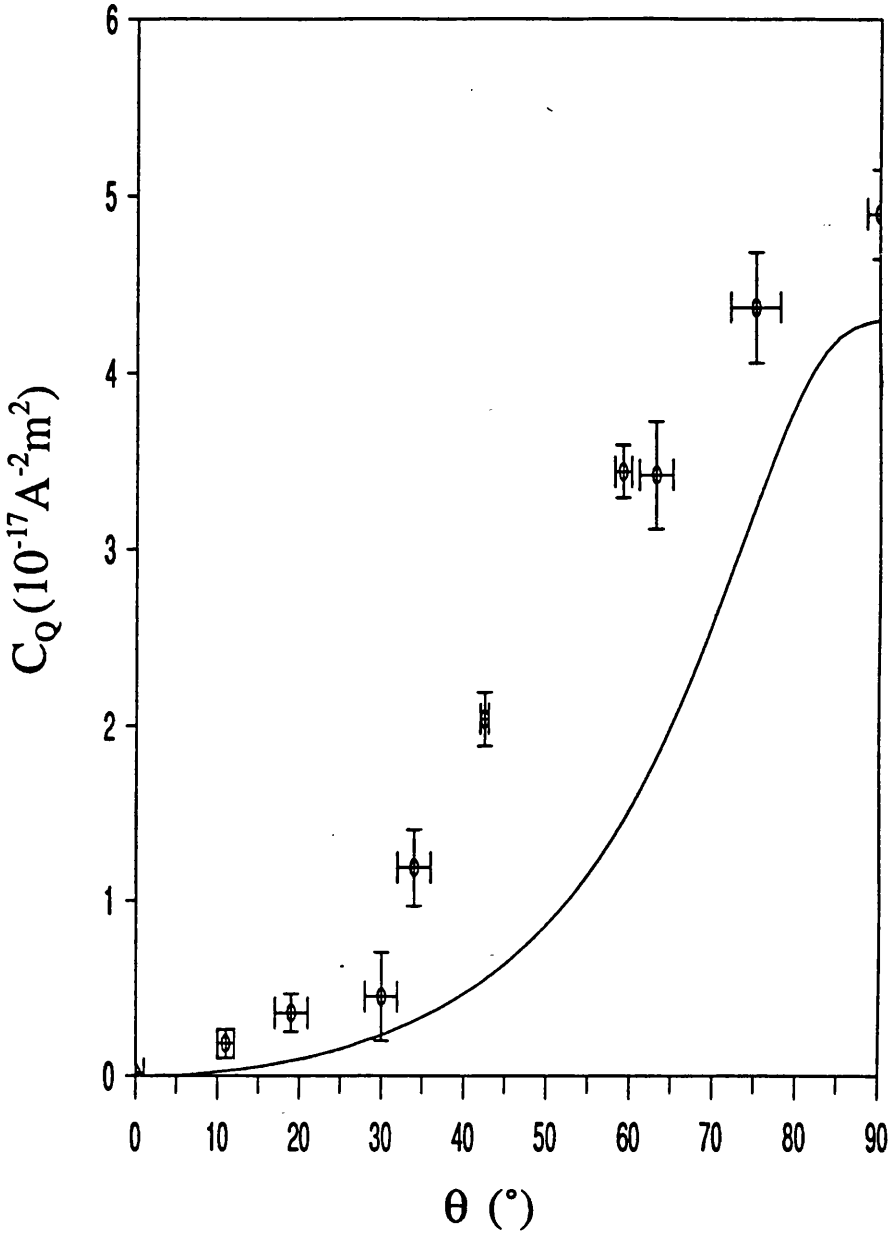

(a)

Figure 4.6a-d: C_Q-θ for each alloy. Also shown is the theoretical variation (from Squire [1990]) normalised to $\lambda_e(90°)/M_s^2$. Key as figure 4.5.

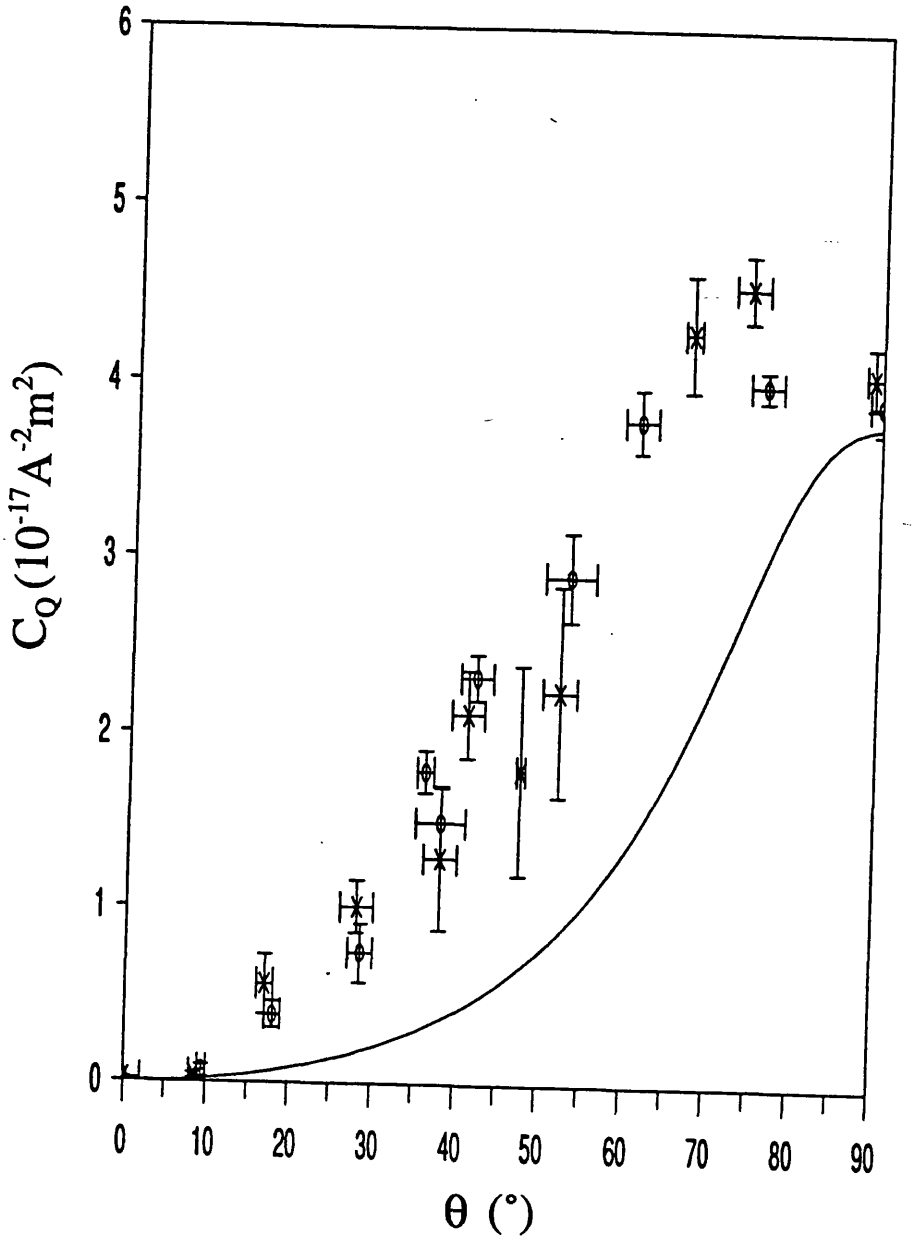

(b)

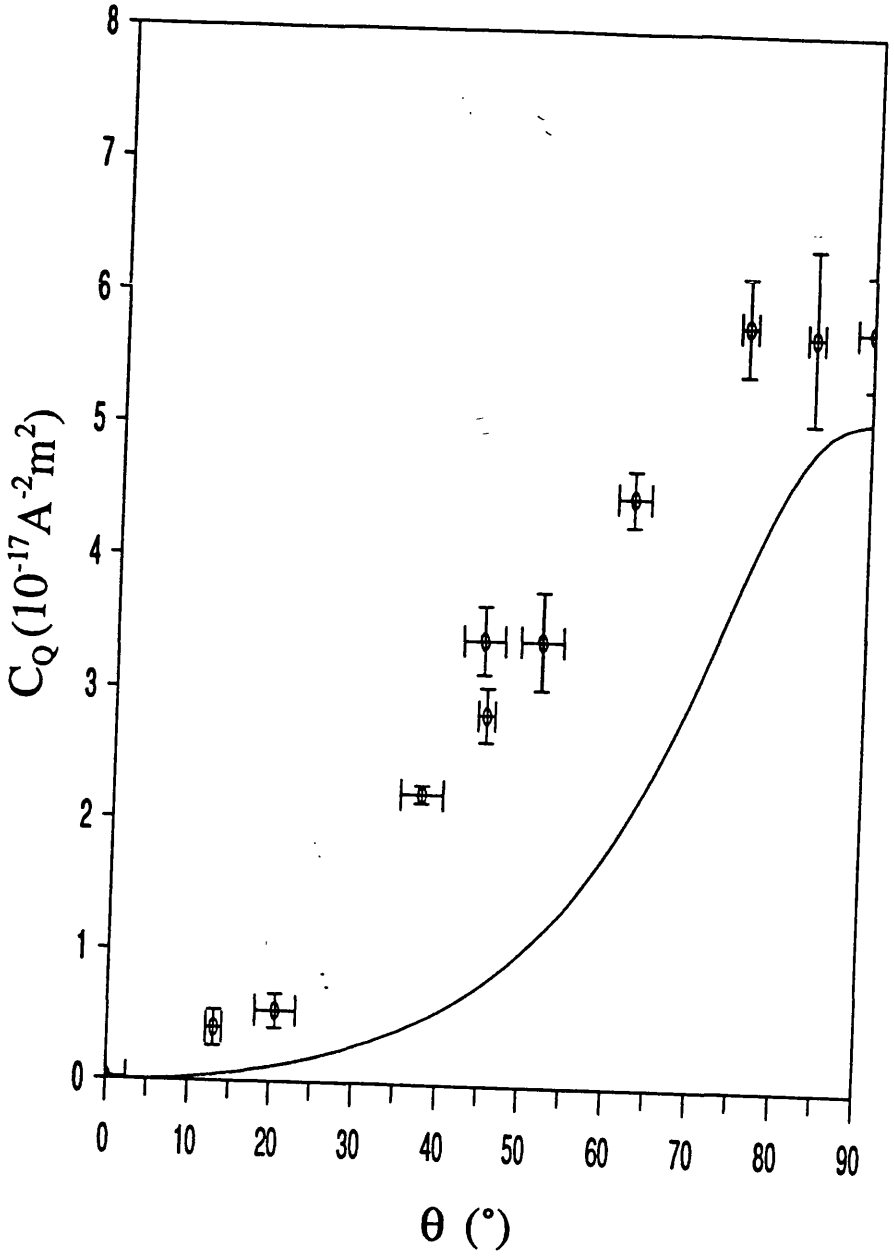

(c)

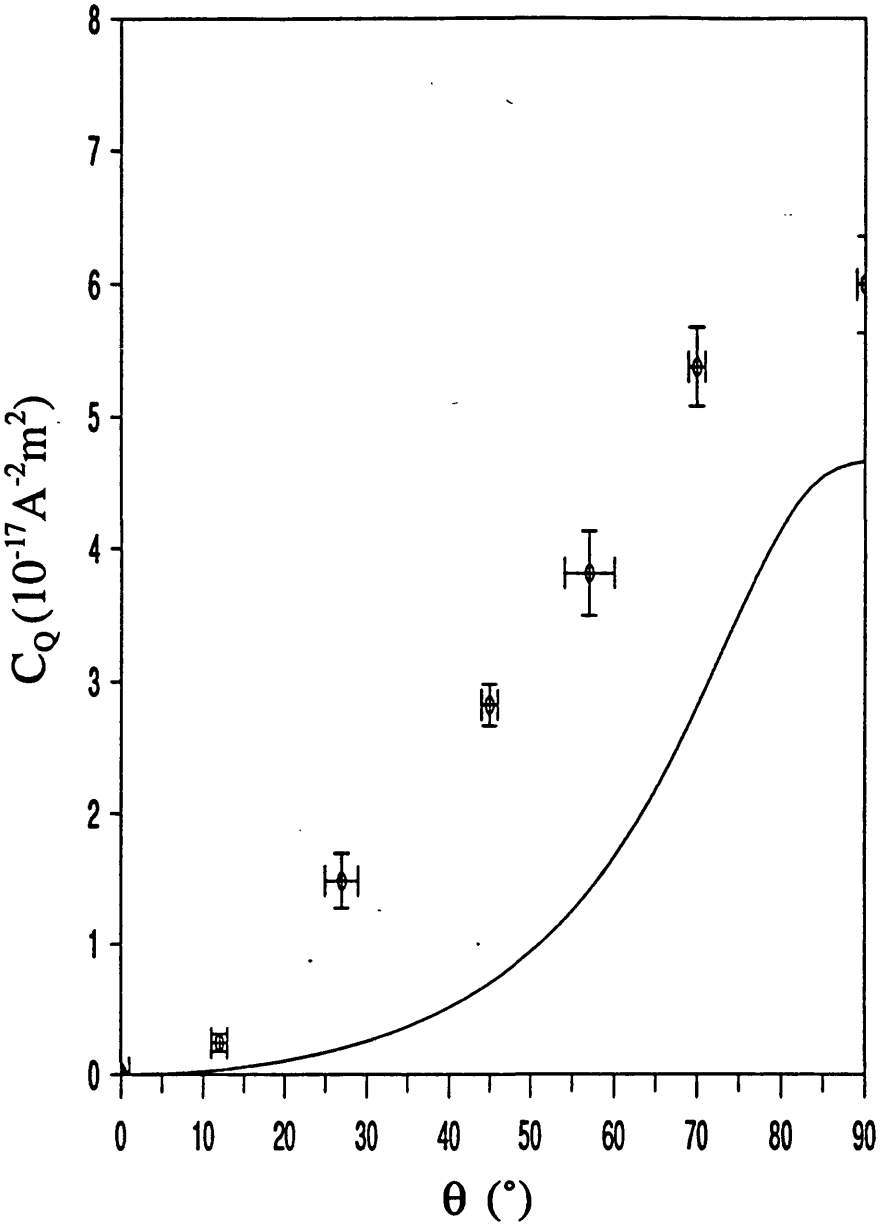

(d)

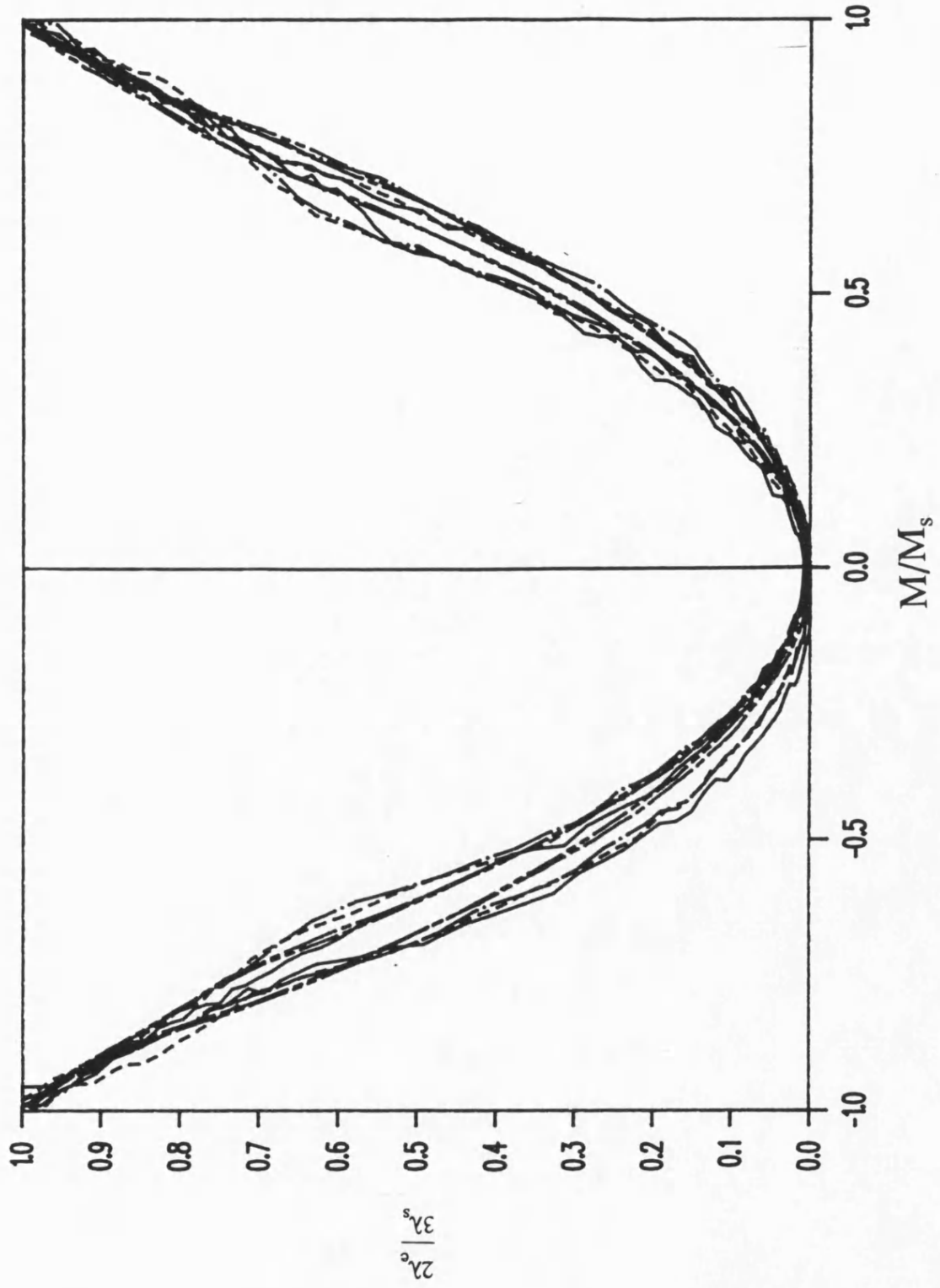

Figure 4.7: Typical λ-M plots of transversely field annealed samples of each alloy, normalised in the λ and M axes. All plots are of a similar form; they are close to quadratic for low M, and level out slightly at the approach to saturation. (METGLAS 2605S2 - - - , METGLAS 2605SC ———, METGLAS 2605SC (super-smooth)— · —, METGLAS 2826MB — - —, VAC0040— - - —).

The quadratic coefficient of the λ-M plots were calculated (in the same way as λ-H plots). These are presented in table 4.3, together with the predicted values, and those measured via C_q, from the λ-H plots (see equation 3.23).

Alloy	B_s	$\lambda_c(90°) = 3\lambda_s/2$	C_Q(calculated)	C_Q(measured via λ-H)	C_Q(measured via λ-M)
	(T)	(ppm)	$10^{-17}(A^{-2}m^2)$	$10^{-17}(A^{-2}m^2)$	$10^{-17}(A^{-2}m^2)$
METGLAS 2605SC (standard)	1.61	61.5 (0.9)	3.75 (0.05)	3.90 (0.16)	4.01 (0.05)
METGLAS 2605SC (super-smooth)	1.61	61.4 (0.6)	3.74 (0.04)	4.06 (0.17)	4.12 (0.05)
METGLAS 2605S2	1.58	60.9 (0.2)	3.85 (0.01)	4.90 (0.25)	4.01 (0.05)
METGLAS 2826MB	0.88	23.8 (0.3)	4.85 (0.06)	5.78 (0.43)	5.86 (0.04)
VAC0040	1.0	29.5 (0.4)	4.66 (0.06)	5.99 (0.36)	5.81 (0.09)

Table 4.3: Comparison of λ-M quadratic coefficients a) calculated from $\lambda_c(90°)$ b) measured from C_q/χ_0^2 c) measured from λ-M plots (errors in brackets)

The two sets of measured C_Q agree within experimental error, except METGLAS 2605S2, and as mentioned above, they are consistently higher than the calculated values.

The normalised plots all appear similar regardless of alloy composition, implying that magnetisation was due to the same processes, i.e. predominantly moment rotation. The hysteresis shown by these curves was thought to be more a consequence of the

measurement procedures than a real effect (it may have arisen from small amounts of sticking of the sample within the holder in the magnetostriction measurement rig, and the effect would have been made more apparent when plotted with respect to M rather than H). Typical λ-M plots for a series of θ measured on the VAC0040 samples are shown in figure 4.8 to illustrate that the general shape of the curves does not alter radically, and can be approximated by a quadratic over almost the whole range of θ.

The variation of the gradient of the inflections of the λ-H data sets are shown in figure 4.9 (again, after accounting for the shape demagnetisation). It was seen to vary monotonically from (notionally) zero at $\theta=0$ to maximum at $\theta=90°$. This was approximately $1.2\text{-}1.6\times10^{-6}A^{-1}m$ in the case of the Fe based alloys and was approximately an order of magnitude less for the Fe-Ni alloys, due to lower λ_s and higher anisotropy energies, requiring larger applied fields to achieve saturation. The large errors in the METGLAS 2605S2 data are due partly to the relatively large errors in χ_0, which can have a profound effect on the data by way of the correction for demagnetisation, particularly when χ_0 is so high that $\chi_{eff}\approx\chi_d$ (see appendix). The scatter in the METGLAS 2826MB data results from scatter in both the λ_s and χ_0 data, possibly because of inhomogeneities in the samples due to the field anneals not fully inducing uniaxial anisotropy.

4.2.3 Domain Studies

Examples of photographs of the domain structures are shown in figure 4.10. They show main domains whose walls lay in the annealing field direction implying 180° walls with magnetisation along the induced easy axis at an angle θ to the sample long axis. The domain width was dependent on the shape factor of the sample in the magnetisation direction [Livingston *et al* 1982]. Thus transverse domains were finer than longitudinal

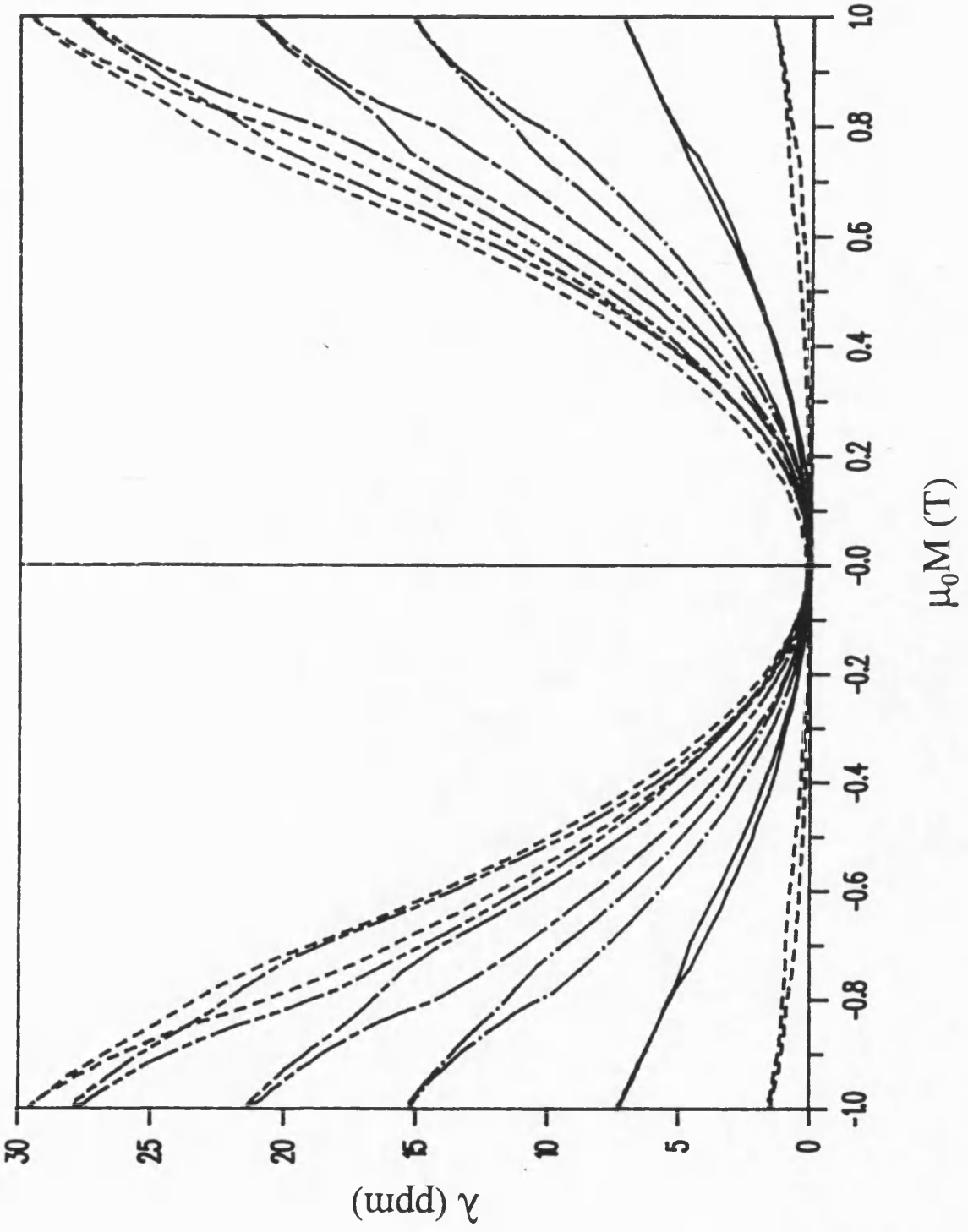

Figure 4.8: Typical λ-M plots of obliquely field annealed VAC0040 for a series of θ. The plots can be closely approximated to quadratic for all θ measured. (θ=90°– – – –, 75°— - - —, 60°— - - — , 45° — · —, 30° ——— , 15° - - - -)

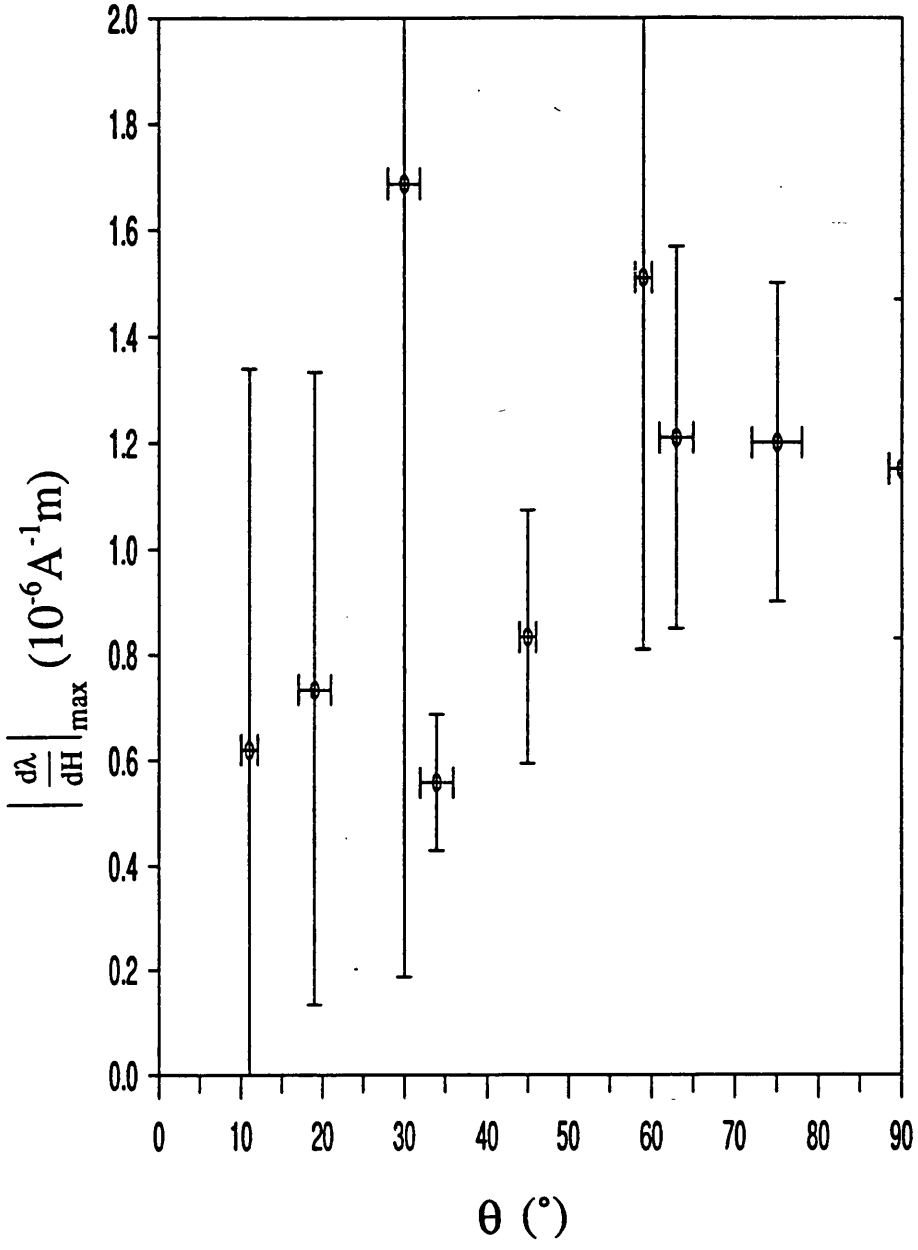

(a)

Figure 4.9a-d: dλ/dH(max)-θ for each alloy. Key as figure 4.5.

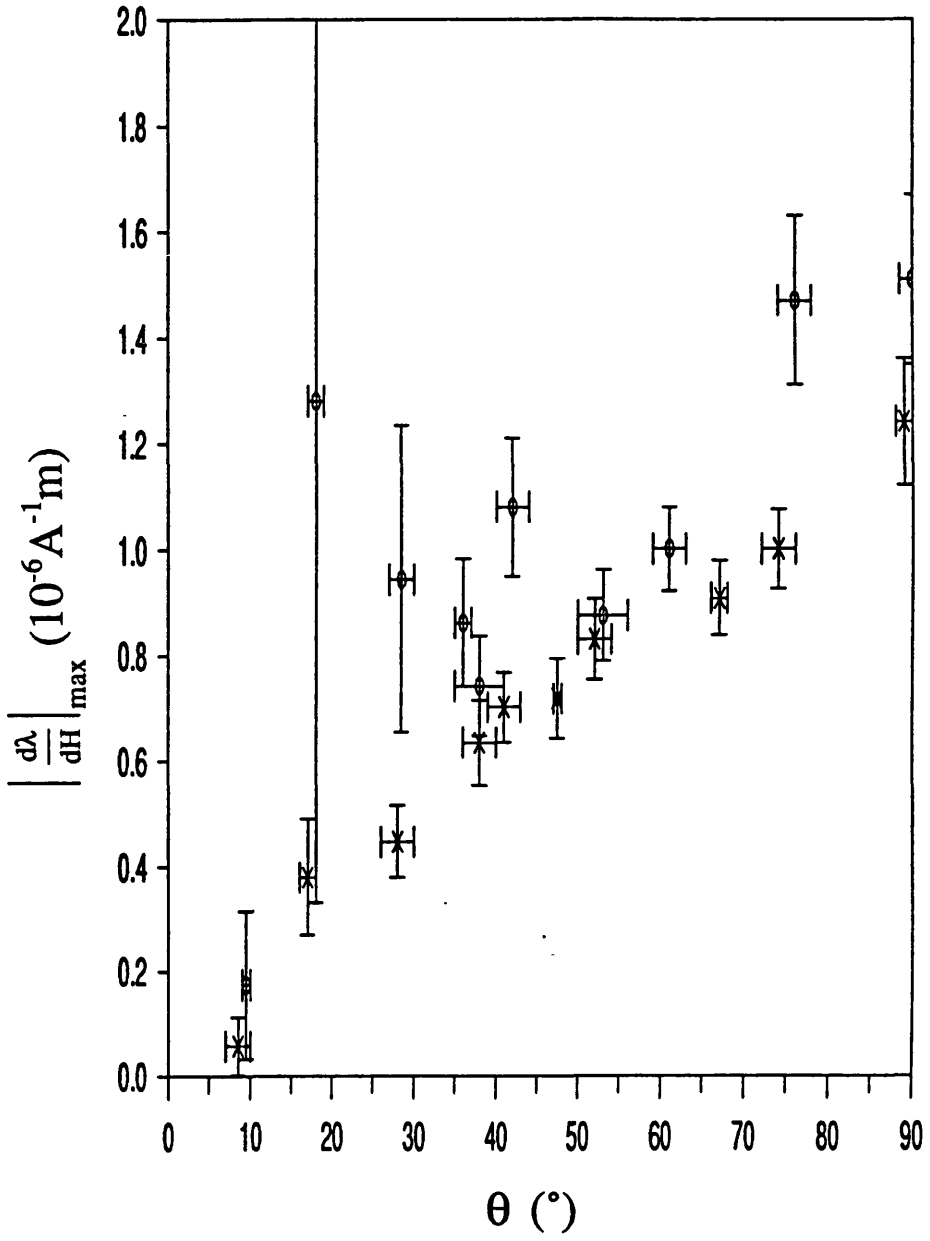
2.0
1.8
1.6
1.4
1.2
1.0
0.8
0.6
0.4
0.2
0.0
0
10
20
30
40
50
60
70
80
90
θ (°)
$\left|\frac{d\lambda}{dH}\right|_{max}$ ($10^{-6}A^{-1}m$)

(b)

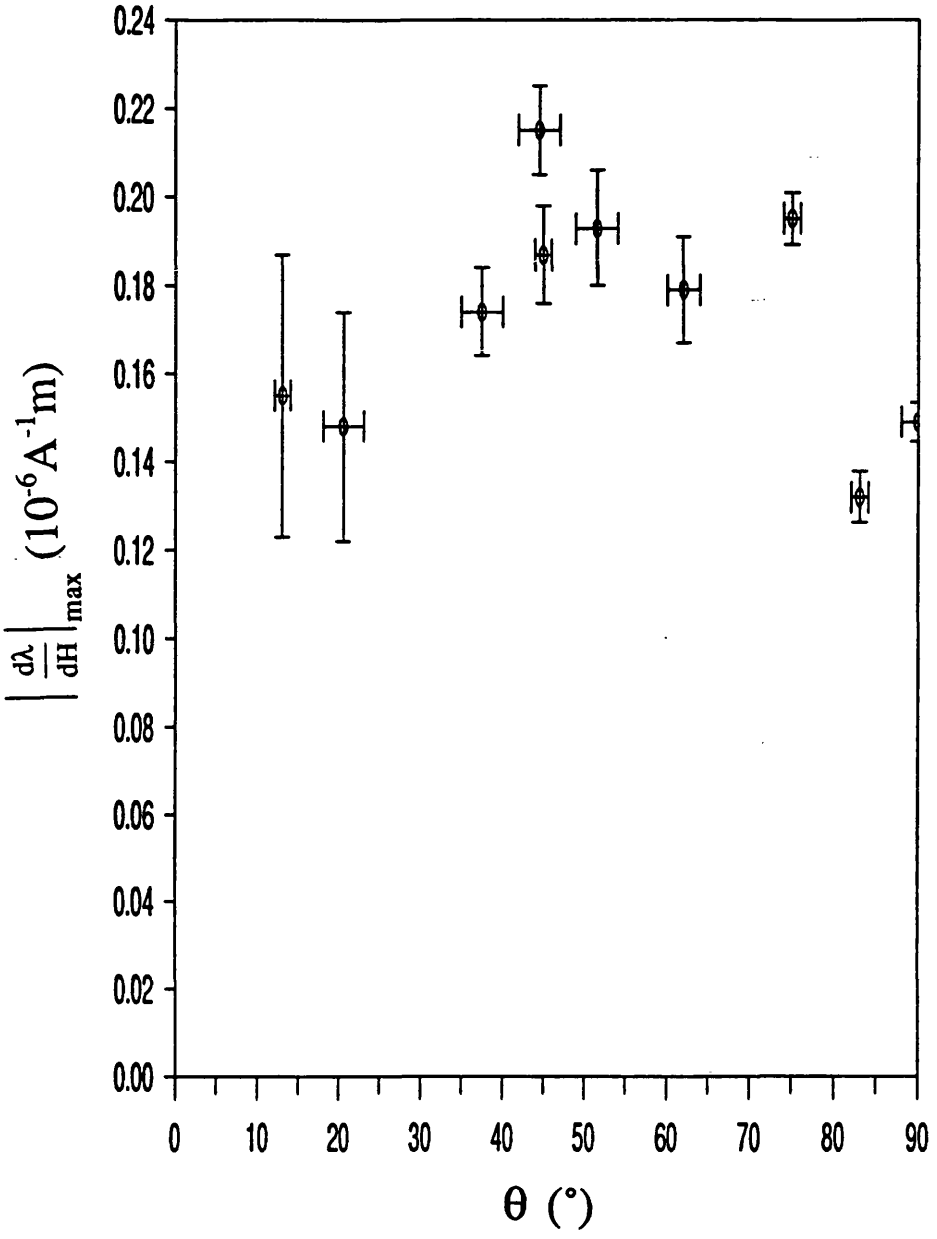
0.24
0.22
0.20
0.18
0.16
0.14
0.12
0.10
0.08
0.06
0.04
0.02
0.00
$\left|\frac{d\lambda}{dH}\right|_{max}$ ($10^{-6}A^{-1}m$)
0
10
20
30
40
50
60
70
80
90
θ (°)

(c)

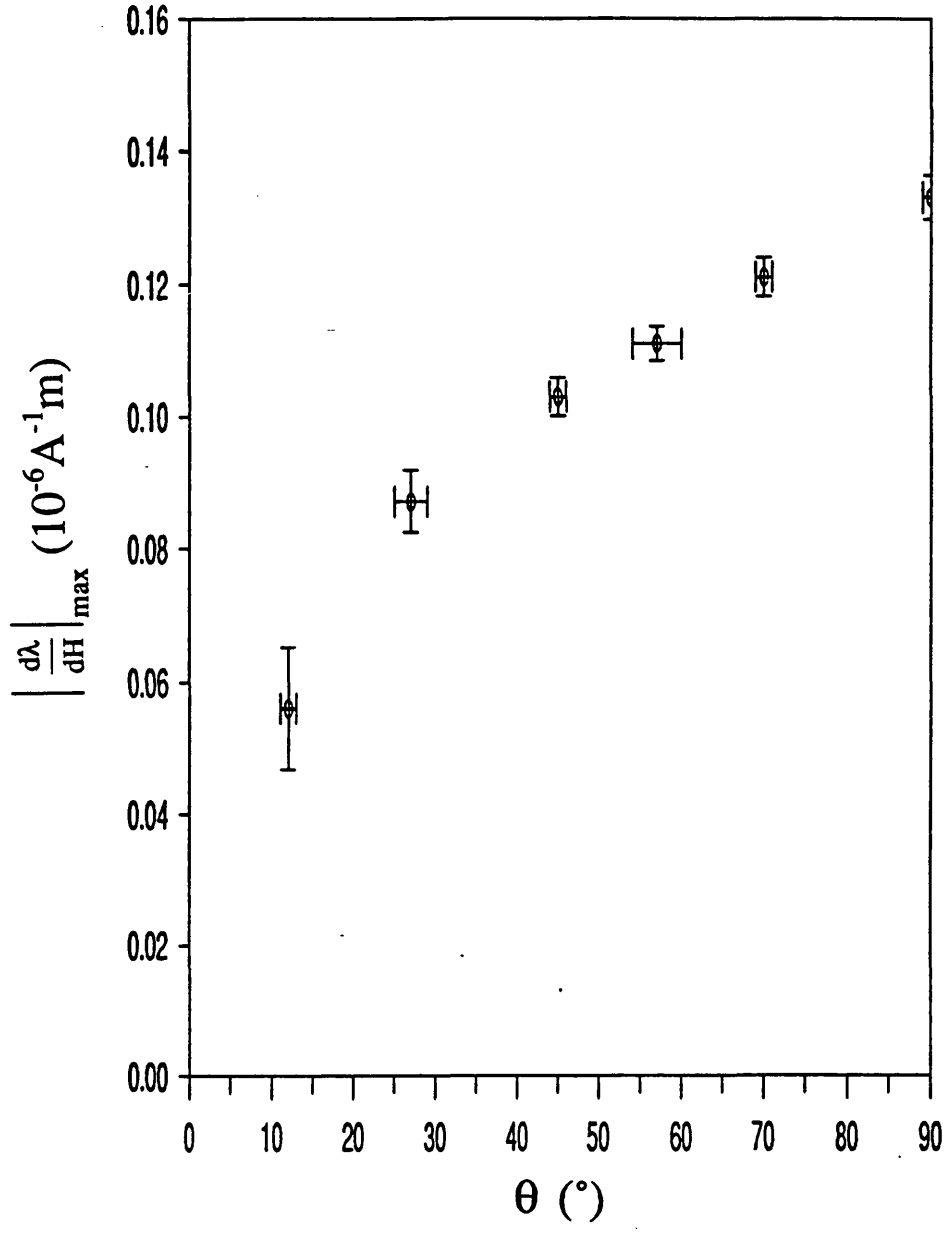
0.16
0.14
0.12
0.10
0.08
0.06
0.04
0.02
0.00
0
10
20
30
40
50
60
70
80
90
θ (°)
$\left|\frac{d\lambda}{dH}\right|_{max}$ ($10^{-6}A^{-1}m$)

(d)

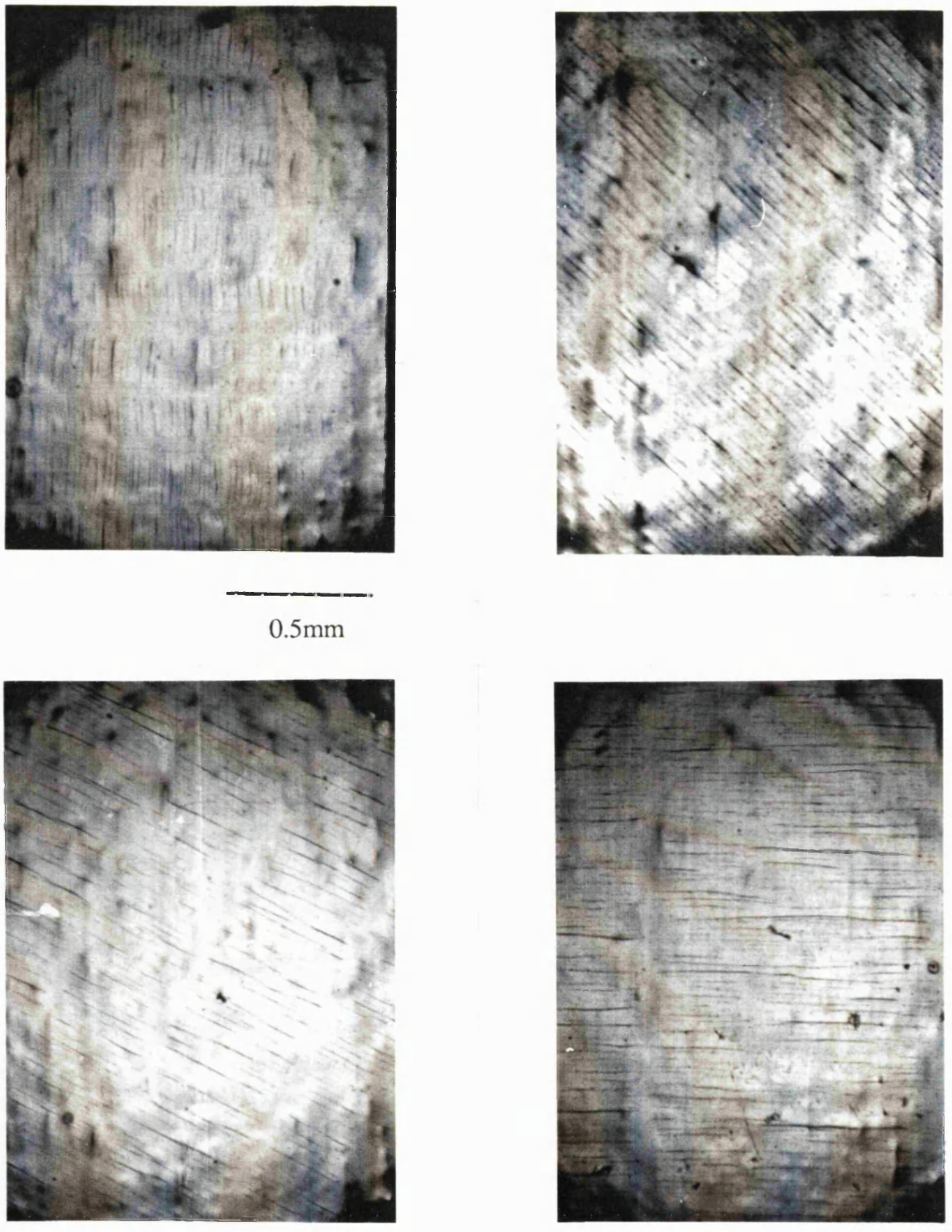

Figure 4.10: Typical domain photographs of obliquely field annealed VAC0040.

ones. For instance, in the photographs shown of VAC0040, the width of the longitudinal and transverse domains were ~1mm and ~0.2mm respectively. The corresponding dimensions were similar for the other alloys. Within each main domain a series of striations could be seen which were perpendicular to the main walls in the absence of an applied field. Initially it was thought that these might have arisen from the aggregation at surface features such as fine cracks [Tebble 1969] due to stray fields from the poles set up around them (figure 4.11). In this case the striations would be maximum at cracks which were perpendicular to the magnetisation.

However, Smith *et al* [1988] suggested that they were secondary walls within the main domains. The secondary domains existed due to some dispersion in the magnetisation direction within the larger ones. Hence the walls became more spread as the magnetisation within a primary domain increased and were orientated perpendicular to its direction. They stated that the wavelength of the dispersion was of the order of 70μm and that the extent of this deviation from the mean direction could not be determined from the structure of the secondary walls. The herring bone pattern seen in their samples of transverse field annealed $Fe_{67}Co_{18}B_{14}Si_1$ indicated a 15° deviation from the macroscopic magnetisation direction in the primary domains (although this deviation is anneal dependent) [Smith *et al* 1988]. A schematic diagram of this domain structure and the effect of applied field on it is shown in figure 4.12.

The dispersion in moment direction was greatest in samples in which a uniaxial anisotropy had not been fully induced by the field anneal. From domain photographs it was seen that the moment spread was often in the form of deviations of the magnetisation directions within the domains from the anneal field direction. This resulted in the herring bone domain pattern (as discussed above). This spread was easily quantified, but tended to be small and not widespread over the sample. Regions where these deviations were as high as 5° were rare and localised (generally less than a millimetre across). There was

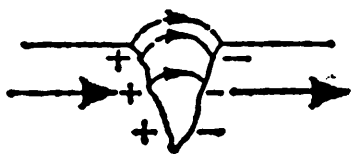

Figure 4.11: Stray field around a surface crack, causing aggregation of colloid around it (reproduced from Tebble [1969]).

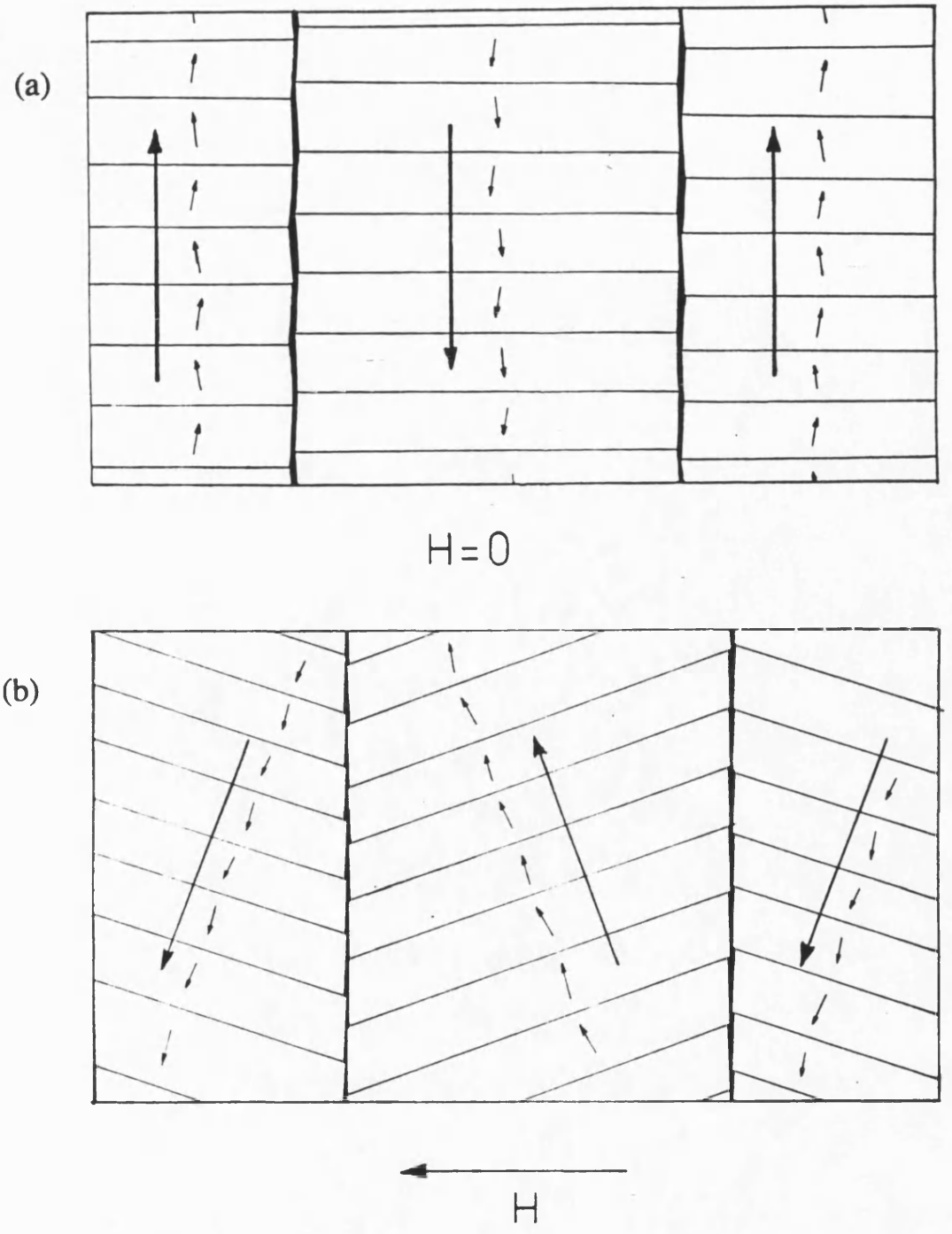

Figure 4.12: Schematic representation of the domain structure of material with uniaxial macroscopic anisotropy (after Smith *et al* [1988]). The main domains are separated by 180° walls. Within these domains are secondary domains with walls normal to the overall direction of magnetisation of the main domains, and with spatially fluctuating magnetisation directions. a) In zero applied field, b) with applied field, H.

some variation in the angle of the main domain walls from region to region, particularly at the edges where the non-uniformity of the applied field and the stresses due to cutting were at their greatest. An estimate of this variation is illustrated by the error bars on the θ values. In the Fe-based alloys, where K_u is markedly smaller than the Fe-Ni alloys as discussed in chapter 2, the low anisotropy in some cases resulted in the main domain walls becoming too wide for the perpendicular flux density to cause aggregation of the colloid, and consequently the walls were very difficult to pick out using the Bitter method.

Overall, however, the main domain structures, where seen, were of distinct striped patterns. Only rarely were stress induced maze domain patterns seen. This was confirmed by photographs of the domain structure on the samples taken using the Kerr effect, by M. Kuzminski of the Polish Academy of Science, Warsaw. The images were photographed using a CCD camera and were input to an image processing software package on a PC, where the contrast was enhanced. Figure 4.13 shows typical domain photographs of obliquely annealed VAC0040 (the ambient field was approximately $35Am^{-1}$ along the sample long axis, with an applied offset field in the opposite direction of $40Am^{-1}$). These photographs show clear stripe domain patterns. However, the changes in contrast due to secondary domain structure within the main domains was too low to be seen. As with the Bitter pattern photographs, there was evidence of domains nucleating or joining near the sample edges.

4.3 Oblique Annealing of Single VAC0040 Sample

VAC0040 was chosen for this part of the study because the data obtained from the previous section were of a high quality (i.e. low errors and scatter). The main reason for

(a)

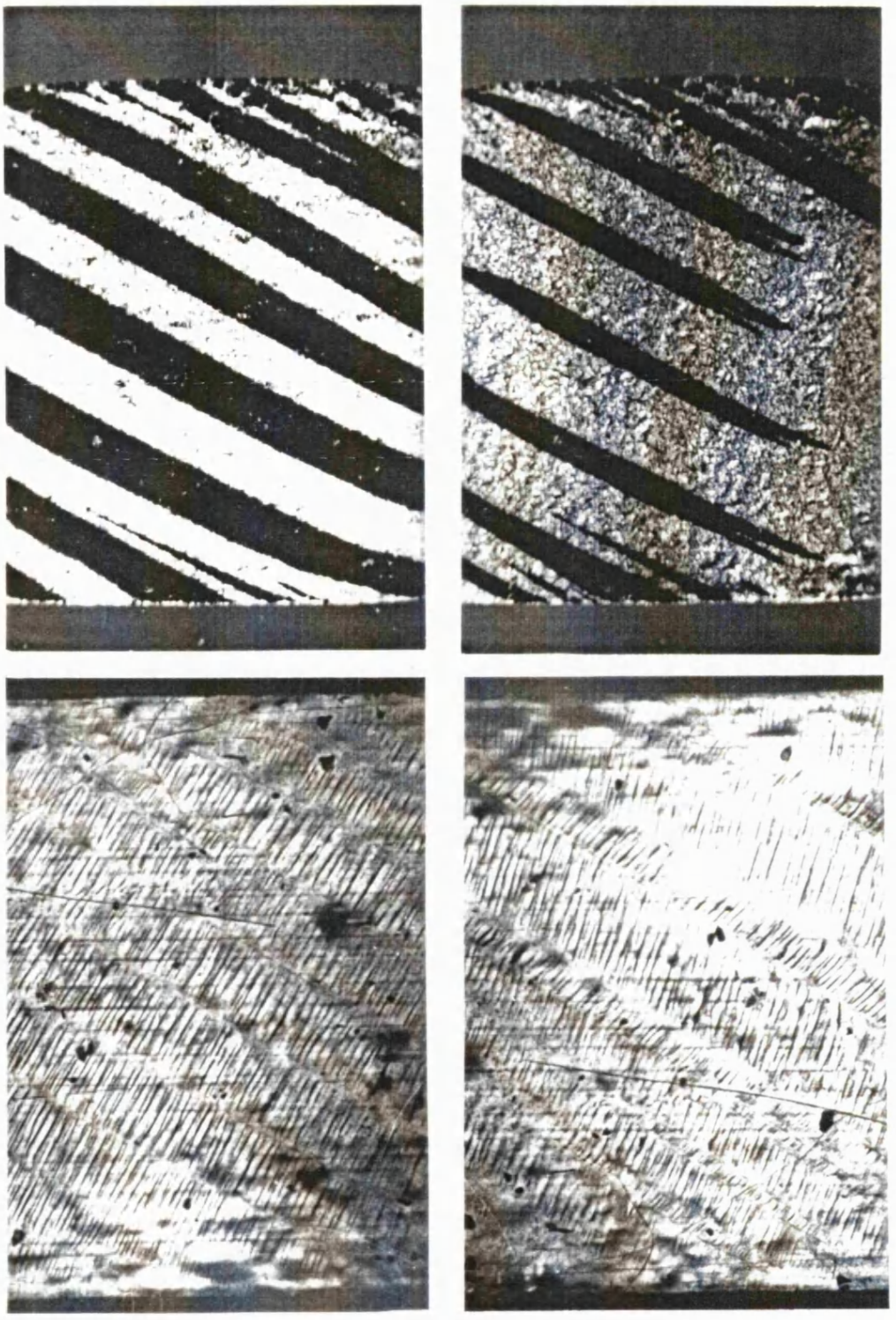

Figure 4.13: Comparison of photographs of domain patterns on obliquely field annealed VAC0040 using Kerr and Bitter methods. (a) $\theta=30^{\circ}$ and (b) $\theta=60^{\circ}$. There is slight aberration on the Kerr photographs because the photographs were taken of the image on a VDU screen. It should be noted that the ambient field was different in the two sets of apparatus, reflected by slight differences in the domain structures.

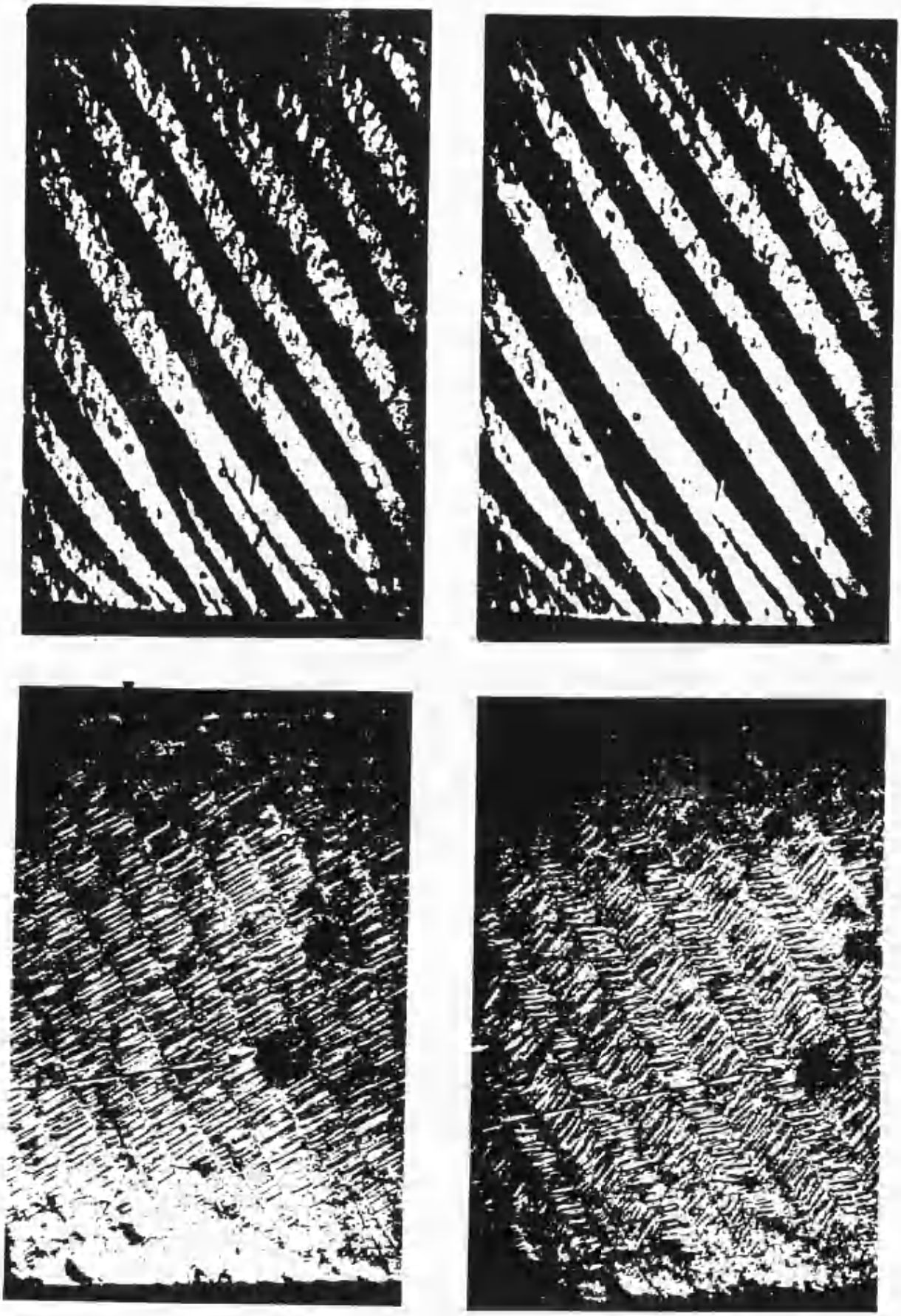

(b)

this is that the Curie temperature is approximately the same as the crystallisation temperature so that field anneals could be performed below T_c, but close enough to T_x for the kinetics of structural rearrangement to be fast enough to allow full development of K_u within relatively short times, without inducing significant crystallisation. Also M_s was high enough and the ribbon surface roughness was low enough to produce clear Bitter domain patterns. To reduce the shape demagnetising effect, the sample was cut with dimensions 70×3mm from the notionally 25μm thick ribbon. Also, it was wedged at the ends so that they were wide enough (≈5mm) to cut across the whole light beam in the optical fibre dilatometer (figure 4.14). The mean thickness of the sample was measured by weighing it and dividing the mass by (length × width × density), where density was measured by the manufacturer to be 7750kgm^{-3}. It was found to be 28.8μm (measurement error ±0.5μm).

The sample was subjected to a series of field anneals at 350°C for 10 minutes at θ=90°,0°,45°,75°,15°,60°,30°, and again at 90°, in that order. After each anneal, M-H, λ-H and ΔE measurements were taken. Also typical regions of the domain pattern were photographed for different applied fields along the sample axis.

The λ_e-θ and χ_0-θ variations are shown in figure 4.15 and 4.16, and the quadratic coefficients in figures 4.17 and 4.18. The parameters of the initial and final transverse anneals were within error of each other, implying that there was no significant progressive degradation due to crystallisation. This was borne out by the values of H_c. The values after the first and last anneals were 3.6 and 1.5(±1.1)Am^{-1}, reflecting a small degree of stress relief, most of which occurred during the second anneal. The moment spread was estimated from the $\lambda_e(\theta=0)$ data to be approximately 8-10° (from equation 4.3), although the strain was so low that there was difficulty in its measurement. The variation of λ_e with θ indicated very low spread, probably less than 5°. The λ_e data was comparable with the corresponding VAC0040 data from the first part of the study, although were

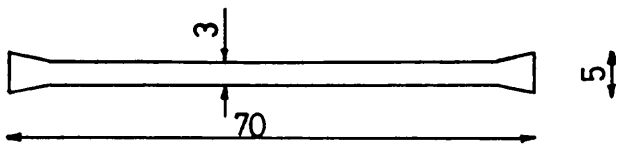

Figure 4.14: Shape of the VAC0040 sample. The ends were wedged so that the ends were wide enough to fully cut across the dilatometer beam, while reducing the sample shape factor.

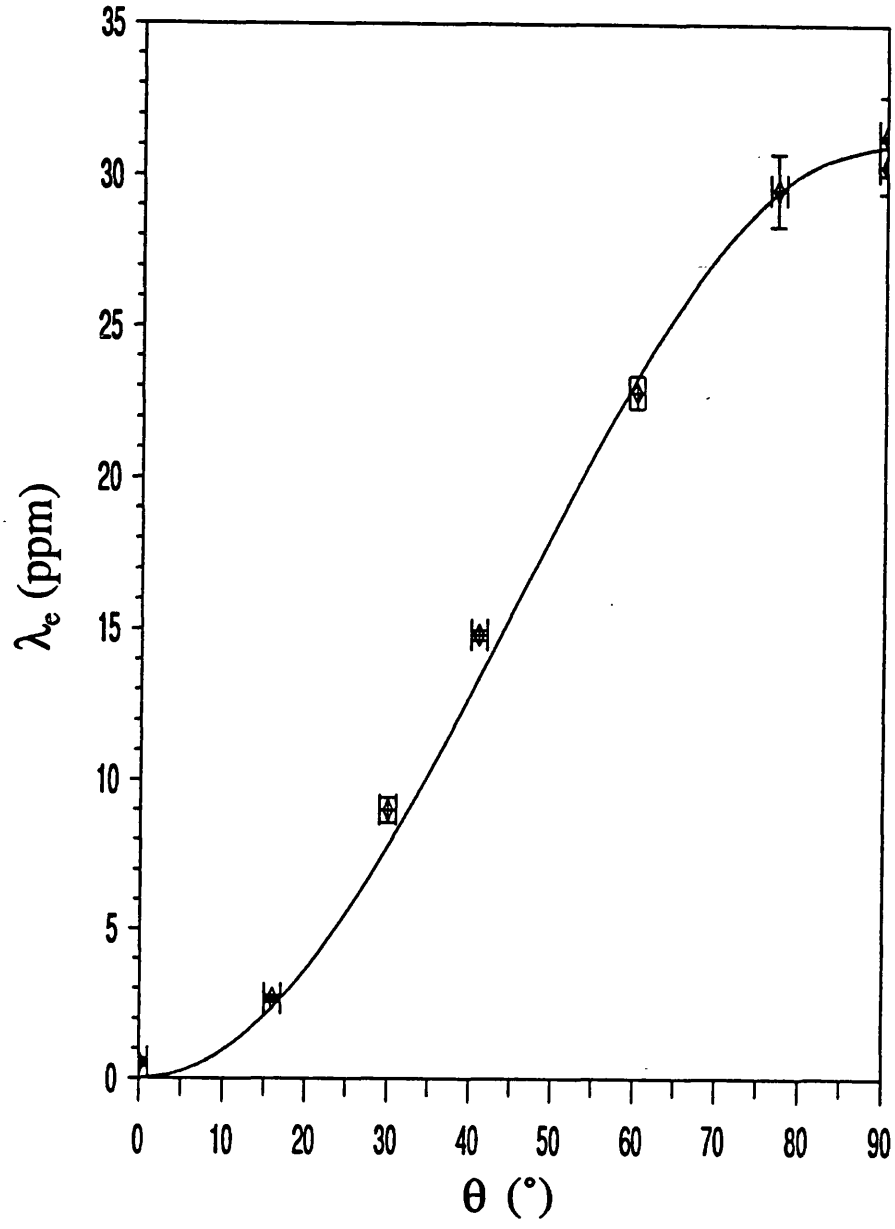

Figure 4.15: λ_e-θ of the VAC0040 sample. The first and last readings, at θ=90°, are well within error of each other. The data is close to the theoretical variation for δ=0, hence the spread is small.

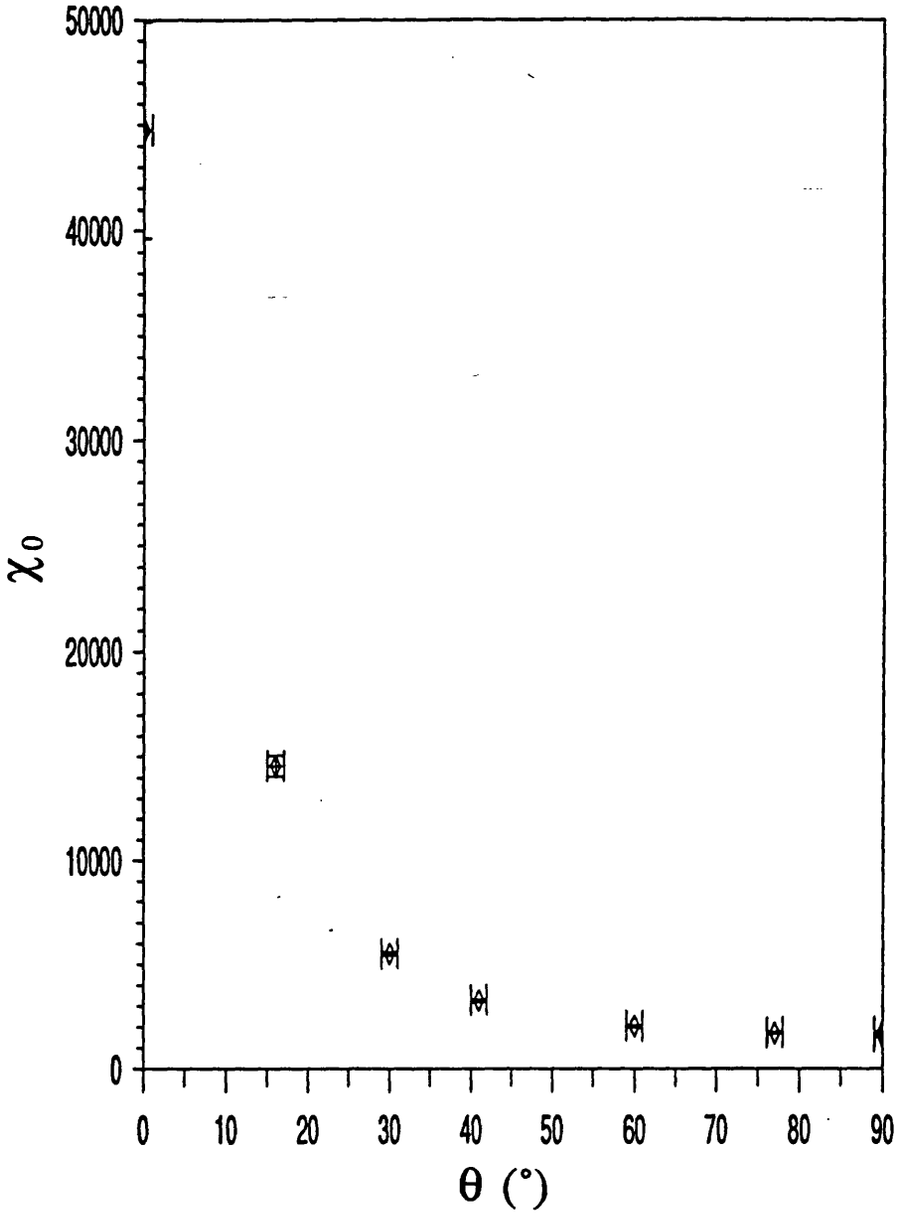

Figure 4.16: χ_0-θ for the VAC0040 sample. This data is similar to that in the previous section.

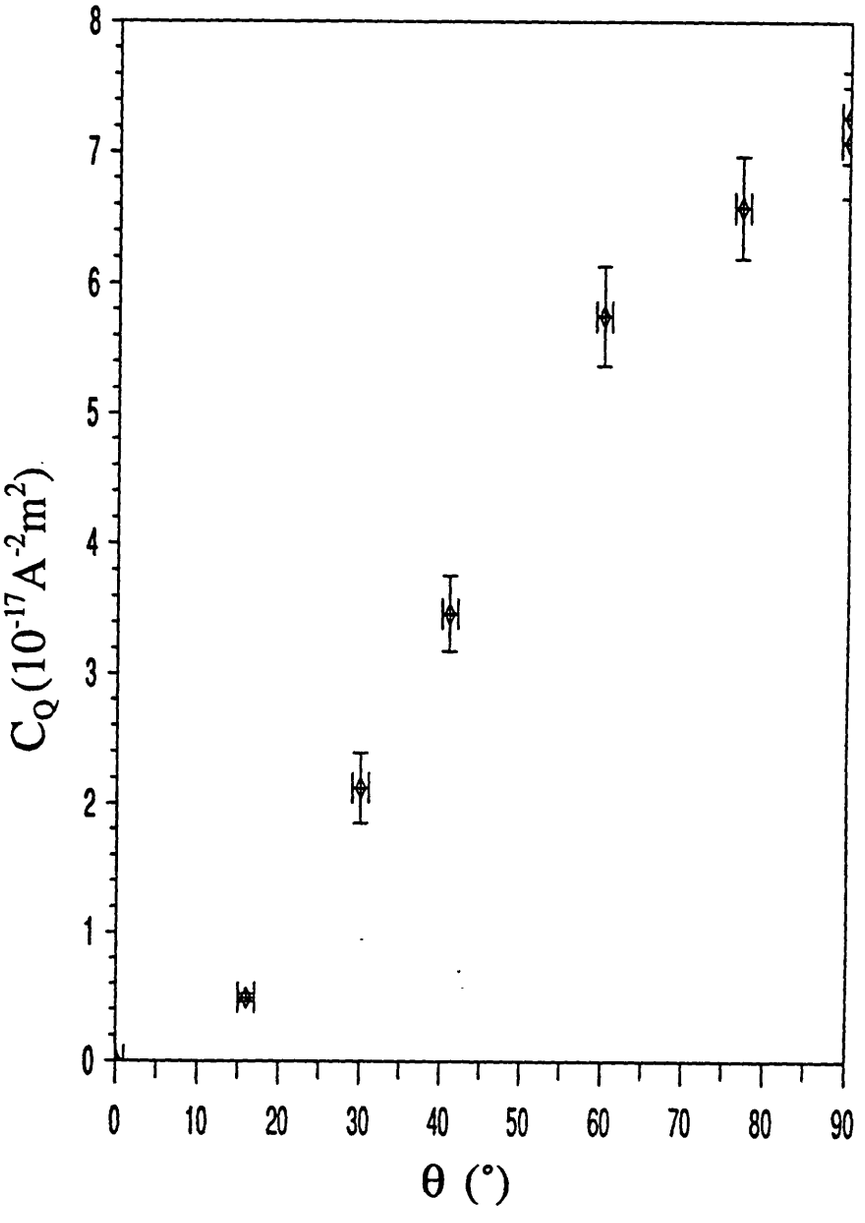

Figure 4.17: C_Q-θ for the VAC0040 sample. Again, the data is similar to that in the previous section and the agreement between the first and last data points are very good.

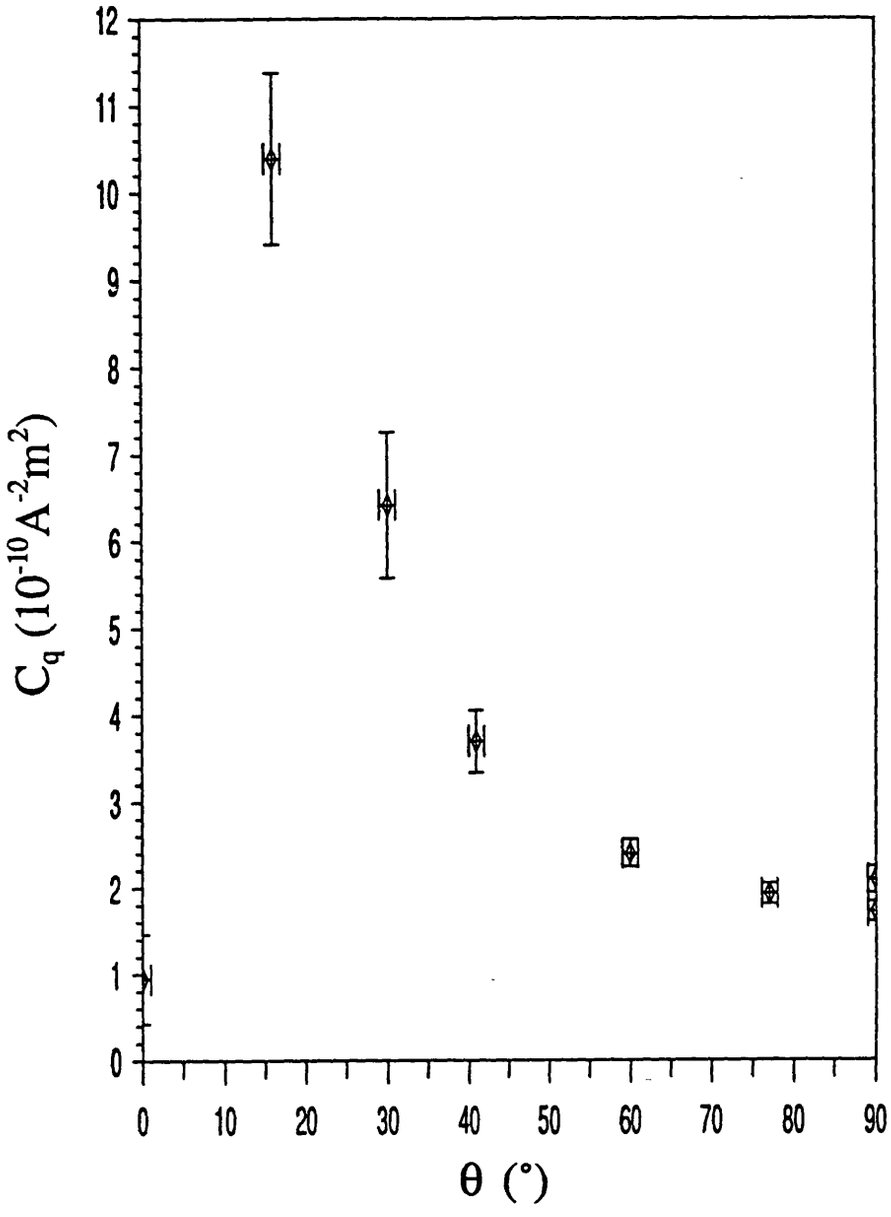

Figure 4.18: C_q-θ for the VAC0040 sample. Note that the maximum value lies between θ=0 and 15°. Again, the agreement between the first and last data points are very good.

slightly higher, possibly due to small differences in the calibration of the different sample holders. There was very good agreement between the χ_0-θ corresponding data sets.

The variations of the λ-M quadratic coefficients agree well with the corresponding data in the previous section, conveying greater confidence in the readings.

As θ increased, λ_e increased by the $\sin^2(\theta)$ relationship, while χ_0 decreased simultaneously as shown in figure 4.5. As a result, C_q was seen to increase initially with increase in θ, reach a maximum and then decrease. The maximum was found to occur at low θ. At this stage the samples exhibited appreciable λ_e, and at the same time very high susceptibility. The maximum value of C_q was found to be approximately $1\times10^{-5}A^{-1}m$.

$\Delta E/E$ measurements are shown for the fifth mode of sample vibration for a series of θ in figure 4.19. The maximum $\Delta E/E$ was found to be approximately 0.3, at $\theta=90°$. The predicted $\Delta E/E$ is given by equations 46 and 47 in Squire [1990], illustrated in figures 10 and 12 in that paper. The large discontinuities seen in the calculated curves at high θ were due to the magnetisation of one of the sets of domains flipping, causing a sudden increase in sample magnetisation. However, as mentioned in section 2.2.2.3, it was proposed that the magnetisation vectors of the domains were coupled together, so that the rates of magnetisation rotation were inter-related, so prohibiting moment flipping. Measurements were made of domain magnetisation directions using photographs of secondary domain walls within a series of applied fields, as discussed below, on the sample where $\theta=30°$ and 60°. Figure 4.20 shows the variation of the angle of rotation, from the induced easy axis, of the magnetisations of both sets of domains, ϕ_1 and ϕ_2. The rates of rotation, $d\phi_1/dH$ and $d\phi_2/dH$, were constant of the whole range of H and, as predicted, the gradients were approximately equal [Squire *et al* 1991]. This constraint on moment flipping has little apparent effect on the M-H and λ-H variations in the model. However, the $\Delta E/E$ variation is significantly altered, quashing the discontinuities. Consequent modifications to the model will be published by Squire at a later date.

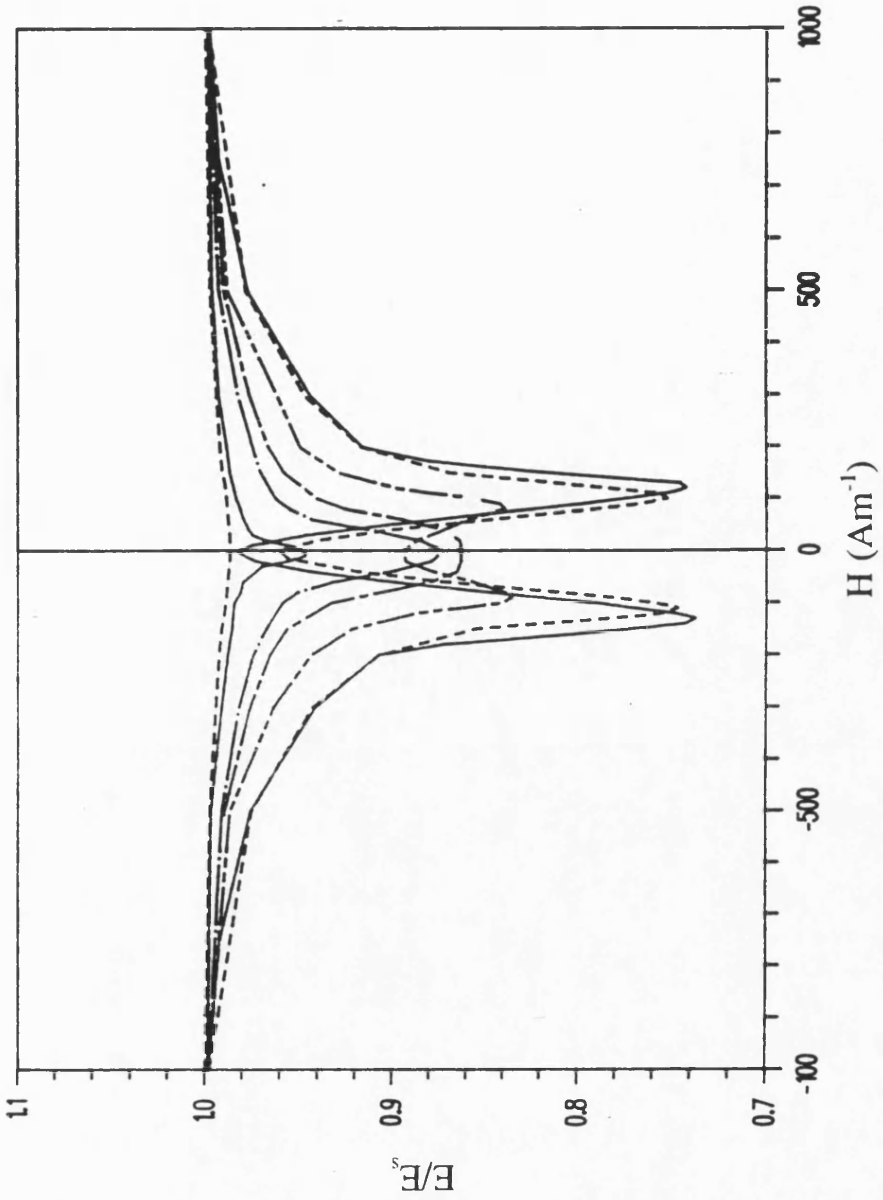

Figure 4.19: E/E_s for the VAC0040 sample, for a series of θ. The data follow the trends shown in the theoretical variations in the Squire model, that is, ΔE is greatest at $\theta = 90°$. The field at which the minimum occurs approaches zero as θ approaches 45°. For $\theta < 45°$, the minimum is at H=0, and ΔE at this point decreases to zero as θ also approaches zero. The maximum $\Delta E/E_s$ was approximately 0.25. The small deviation of the $\theta = 90°$ and 0° data from $E/E_s = 1$ at H=0 points to a spread in the magnetisation.

($\theta = 90°$ ——— , 75° - - - - , 60° — - - — , 45° — - — , 30° — · — , 15° ——— , 0° - - - -).

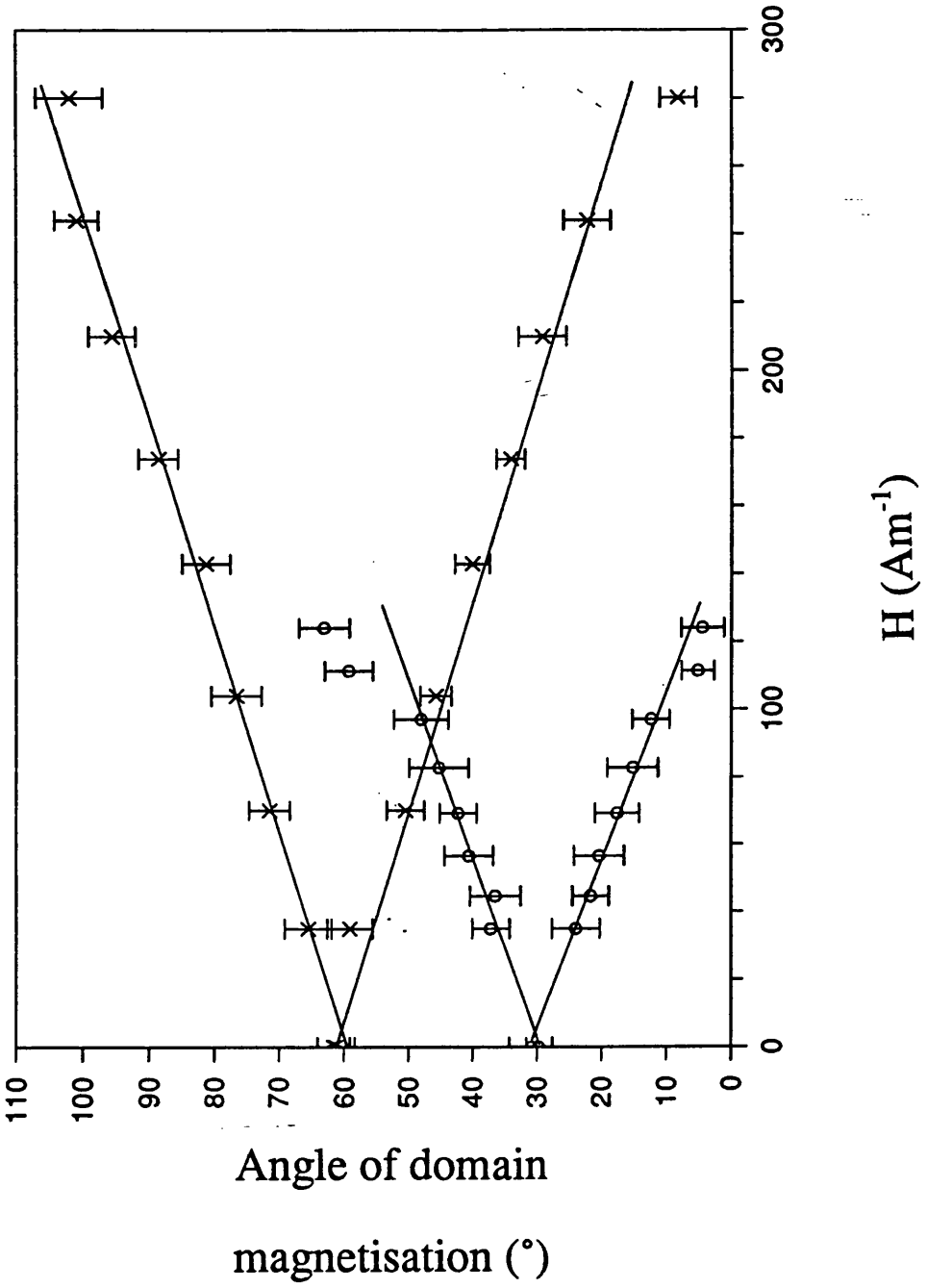

Figure 4.20: Angle of domain magnetisation of each of the two sets of domains on oblique field annealed VAC0040 (θ=30° and 60°) as a function of applied field. For each angle the rate of rotation with respect to field, $d\phi/dH$, was constant within measurement errors, and was equal for both sets of domains. $\theta = d\phi/dH$=0.20 (a.u.)$A^{-1}m$ and 0.16 (a.u.)$A^{-1}m$ for θ=30° and 60° respectively. (o - θ=30°, × - θ=60°)

Whereas the effect of moment spread on λ_e is most evident at $\theta=0$, where it results in non-zero strain, for ΔE it is most evident at $\theta=90^\circ$ where $\Delta E(H=0)$ becomes non-zero. This particular measurement on this sample yielded a value of $\Delta E/E$ at H=0 of 0.013(±0.002). This is very close to zero and indicates a low moment spread. By calculating this variation of $\Delta E/E$ with respect to the spread in the normal distribution of θ, as given by equation 4.4, it was possible to determine the spread sufficient to yield the value measured. This spread was found to be ~3°. This result, however is subject to large relative errors. This is because the measured parameter (in this case, frequency of vibration, f) was proportional to $E^{1/2}$, and so the associated error in this, while small relative to E, becomes large relative to ΔE where $E \approx E_s$, as is the case where H=0 and $\theta=0$ with very low moment spread. Also, although the pole effect was small in these samples, the correction on $\Delta E/E$ may also become significant where ΔE is very close to zero. The correction in f_s can be made by fitting a straight line through the f/f_s data at (notionally) saturation. At saturation, the pole effect results in a non-zero gradient in f with respect to H. The intercept of this line at H=0 yields the actual value of f_s, and the f/f_s data can be corrected for this. It was not possible to make this correction in this instance since there was not enough data at saturation to obtain a straight line fit with sufficient accuracy to calculate the gradient. The measurement error in ΔE, which can therefore be significant in these materials, has a corresponding effect on the error in the value of the moment spread, δ.

The domain photographs all showed good coherent stripe domain patterns. There was little or no herring bone pattern by the secondary walls implying almost zero spread due to deviation in domain magnetisation direction. When the sample was subjected to an applied field along its long axis, the moment directions, illustrated by the orientation of the secondary walls, were seen to rotate to align with the field, and the domain walls were seen to move so that the domains with their moments at an acute angle to the field

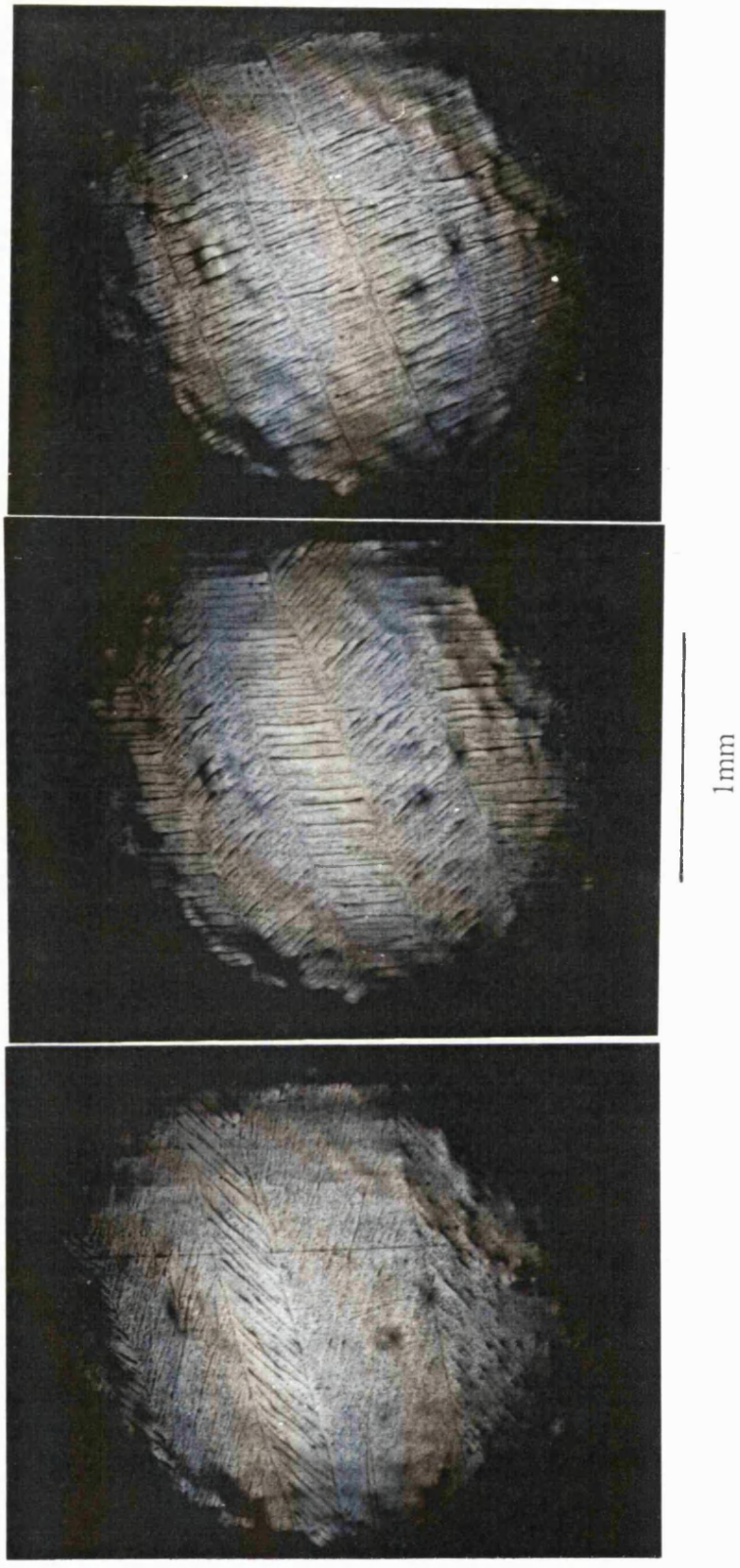

Figure 4.21: Photographs of the domain structure of obliquely field annealed METGLAS 2605SC (super-smooth surface) for a series of applied fields. Note that the secondary walls rotate, remaining normal to the domain magnetisation directions. The domain walls shift with increasing field so that one set of domains grow at the expense of the others.

direction grew at the expense of the others. This is illustrated in figure 4.21 on a typical region of obliquely annealed METGLAS 2605SC (super-smooth surface). As discussed in chapter 3, the secondary walls on average lie at right angles to the magnetisation direction, so enabling the angle between magnetisation and sample axis to be determined. Photographs were taken of particular regions on all the samples for a series of applied fields, H, up to the approach to saturation. A typical series of such photographs showing the development of magnetisation with increasing H for a particular value of θ is shown in figure 4.22. Using a digitiser pad, the relative areas of the two sets of domains were measured with respect to H, as well as the angles between their magnetisation and the field direction, ($\theta-\phi_1$ and $\theta+\phi_2$, see figure 2.5). From this information the sample magnetisation could be obtained. In this way, the M-H curves could be constructed. Those obtained from the VAC0040 sample at different θ were very linear, which acted as confirmation of the domain measurements. Figure 4.23 shows the comparisons between the constructed M-H data and that from the M-H rig for $\theta=30^\circ$ and 60°. The susceptibilities were calculated by determining the gradient of the best fit straight lines through the data. These were consistently higher than that obtained from the measured M-H plots, the greatest difference being approximately 20%, although the discrepancy was only a few percent in some samples. One possible reason for this was the variation in the magnitude of the internal field, H_i, within the ribbon. As discussed in Cullity [1972], the demagnetising effect is greater near the ends of rectangular samples, with correspondingly greater demagnetising fields. This results in a reduction of H_i at the sample ends. The regions of the surface from which the measurements were taken were of the order of a few square millimetres, so variations in the internal field over these (or longer) ranges would be reflected by differences between M-H loops derived from the domain measurement data and the M-H loop measured on the whole sample. Hence, regions where the domain measurements yielded higher susceptiblilty than that measured

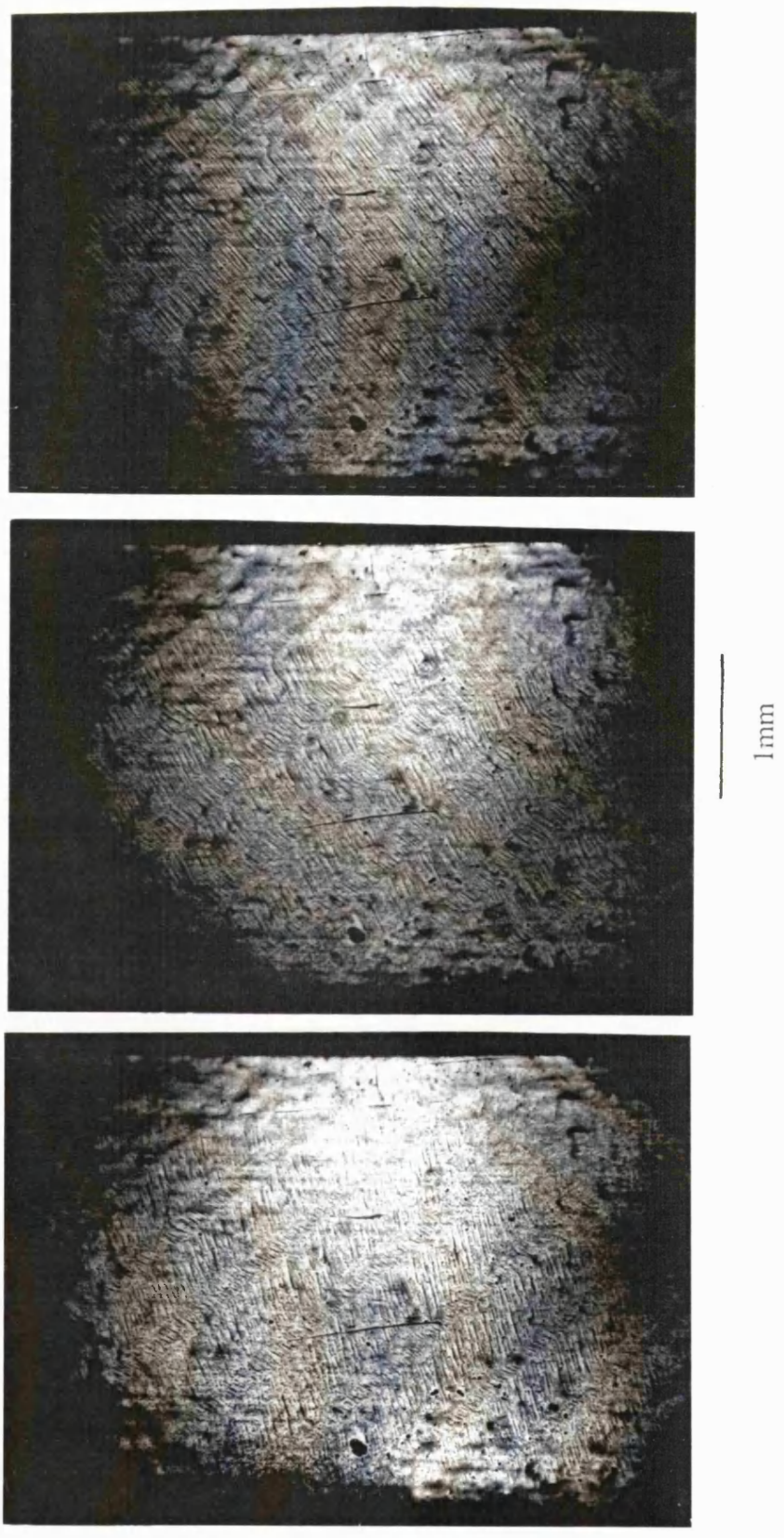

Figure 4.22: Photographs of the domain structure of obliquely field annealed VAC0040 for a series of applied fields.

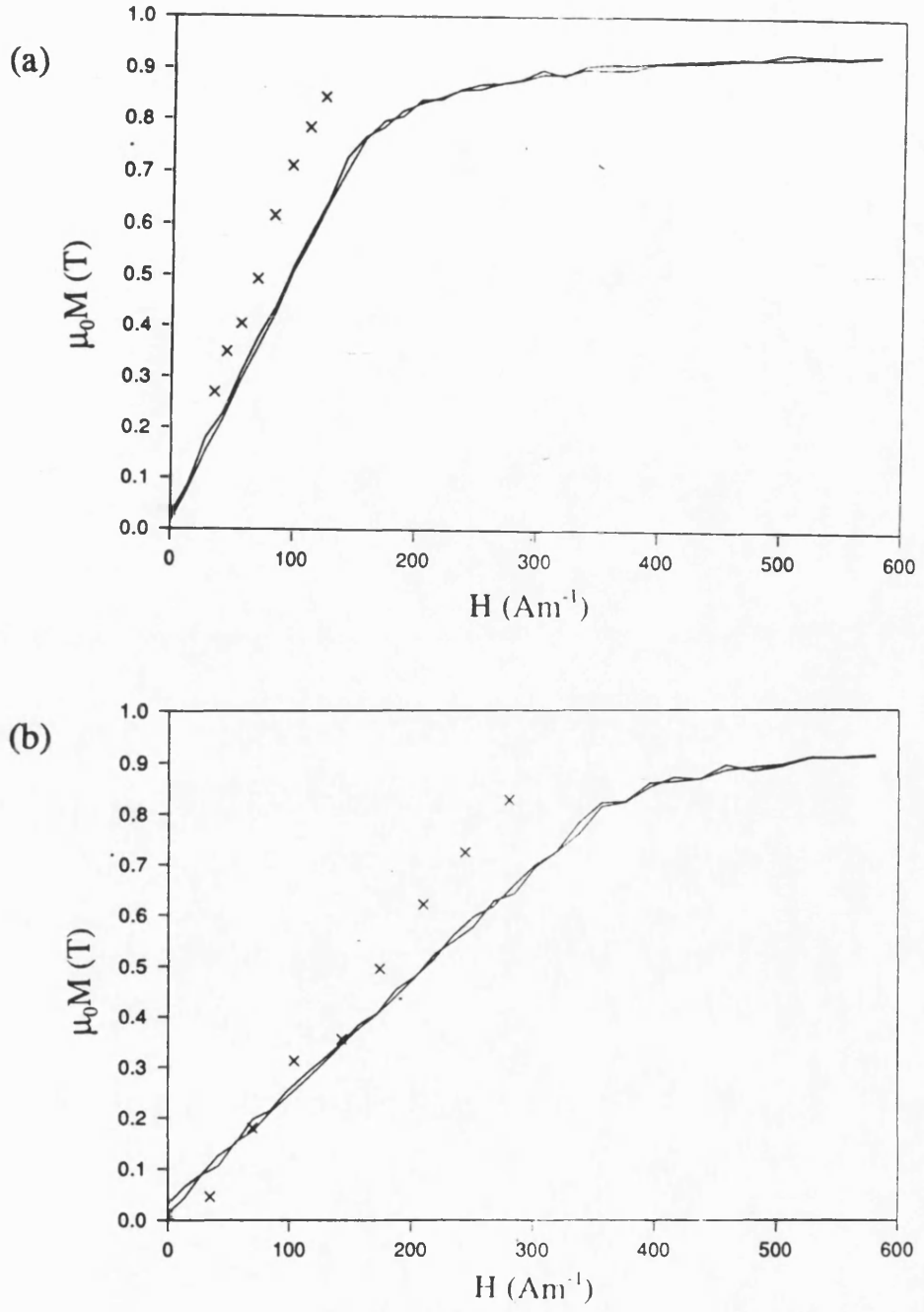

Figure 4.23: Comparison of M-H data of obliquely annealed VAC0040 sample, from direct measurement and reconstruction from domain studies, a) $\theta = 30^{\circ}$, b) $\theta = 60^{\circ}$. Solid line - measured data, × - obtained from domain photographs.

The data constructed from the domain photographs lie close to a straight line. However, the susceptibility obtained from this data was systematically higher than that of the measured data by as much as 20%.

over the sample as a whole were likely to have been towards the centre where the demagnetising field had less of an effect. A second reason was thought to be differences in the calibration of the applied field, described in chapter 3. The field from the coils on the domain examination rig were measured using a Gaussmeter, while that from the solenoid on the magnetisation measurement rig was determined from the turns per unit length. Ideally, the same method of calibration would have been used, but the Hall probe was not used in the solenoid because of the difficulty of access. If the difference in susceptibility is accounted for, the M-H plots obtained from the data from the domain studies are in good agreement with those measured using the magnetisation rig.

Measurements on the variation in fractional area of the two sets of domains were taken on the single VAC0040 sample using the Bitter domain patterns. Similar measurements were done on the set of VAC0040 obliquely field annealed samples considered in section 4.2, using the Kerr domain photographs provided by Kuzminski. After accounting for differences in ambient fields and image magnifications, it was found that they appeared to move more readily with field in the Bitter photographs, as shown in figure 4.24. Specifically the rate of change of domain area was measured to be 6.9 and 5.1a.u.$(Am^{-1})^{-1}$ for the Bitter and Kerr domain data. This was found to be due to the difference in the demagnetisation factors, and the relative rate of growth of the domains with respect to internal applied field was approximately equal for both sets of measurements, i.e. 9.5 and 9.3a.u.$(Am^{-1})^{-1}$ respectively.

Consequently, the agreement (after accounting for variations in susceptibility) between the M-H data constructed from the domain photographs, using both Bitter and Kerr methods, and the measured M-H loops using the magnetisation rig gives confidence to the domain pattern data. It indicates that the data represents macroscopic regions of the samples very well. Also, the domain patterns seen on the surfaces clearly represented the bulk domain structures.

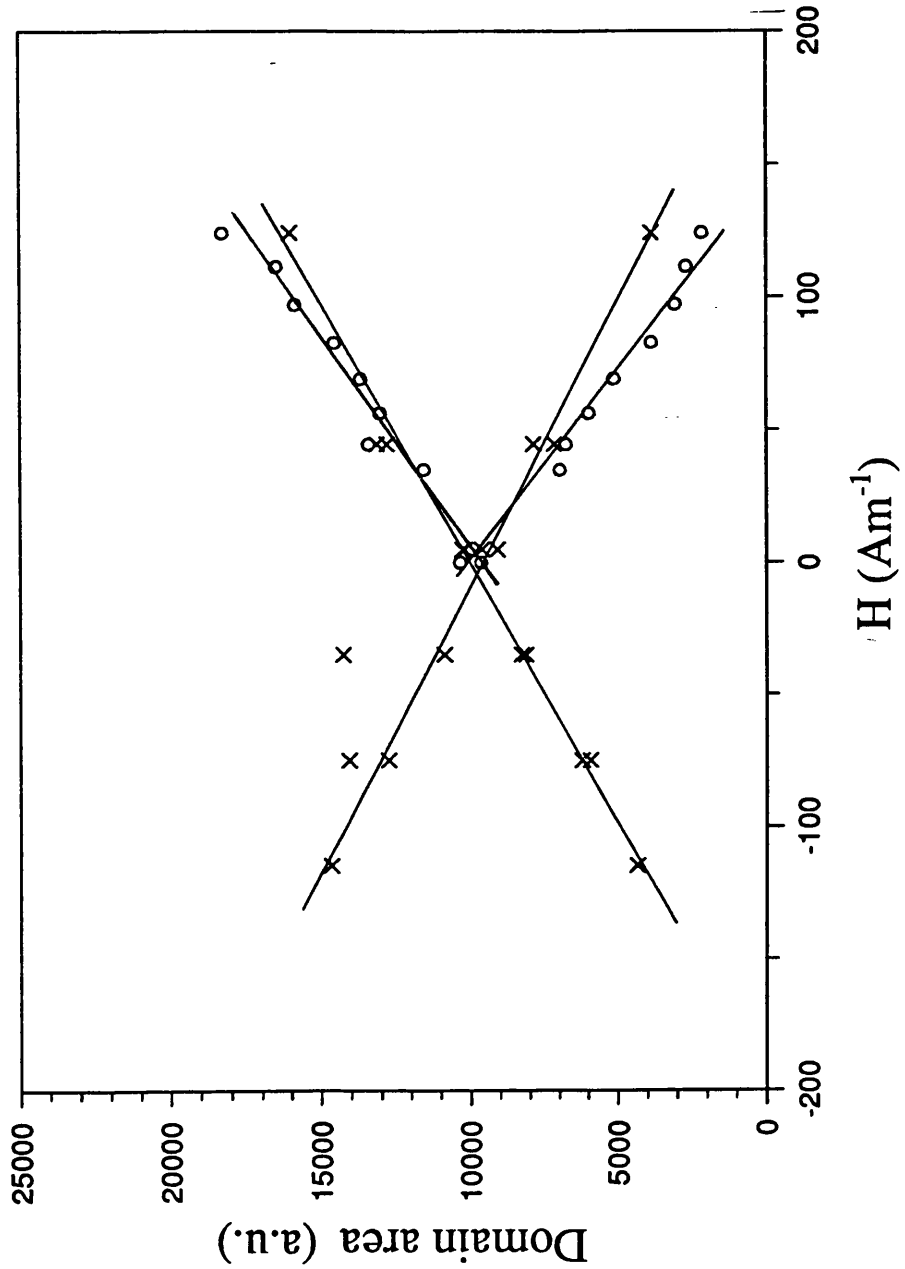

Figure 4.24: Areas of each of the two sets of domains on the obliquely field annealed VAC0040 (θ=30°) from both Bitter and Kerr photographs. (o - Bitter method, × - Kerr method). The data was normalised to 1000 a.u. at H=0 and the Kerr data was corrected for the ambient field. In both cases, the rate of change of area with respect to field was constant (within the scatter of the data). d(Area)/dH=6.9 (a.u.)A^{-1}m and 5.1 (a.u.)A^{-1}m for the Bitter and Kerr data respectively. The difference in these rates was because of the different shape factors of the samples examined. In both cases d(Area)/dH_i≈9.4(±0.2) (a.u.)A^{-1}m.

From the measurement of magnetisation and domain wall movement with respect to applied field, the domain wall parameter, β, and the magnetic anisotropy energy density within the domains, K_u, were determined using equations from the Squire model [Squire 1990, section 2]. In this way their variation with θ were analysed. The wall parameter was given by

$$\beta = \frac{A}{w} \qquad 4.7$$

where A and w are the wall area per unit volume and the mean wall stiffness. The wall energy, U_w, was dictated by the product of A and the wall potential which was parabolic with a coefficient w, i.e.

$$U_w = w x^2 A \sin^2\theta . \qquad 4.8$$

The model assumed a constant mean wall stiffness, and so a constant wall potential for all θ. From the measurements, however, it was found that the wall parameter (and so w) varied with θ, as shown in table 4.4.

θ (°)	$\theta_{measured}$ (°) (±2°)	β ($J^{-1}m^3$)
0	0	(2.8×10^{-2})
15	13.6	(1.9×10^{-2})
30	31.9	$4.4(\pm0.7)\times10^{-3}$
45	39.4	$2.2(\pm0.3)\times10^{-3}$
60	60.3	$1.8(\pm0.5)\times10^{-3}$
75	79	$5.3(\pm8)\times10^{-4}$
90	90	

Table 4.4: Variation of domain wall parameter with respect to θ in obliquely field annealed VAC0040 (Squire, private communication)

Modifications in the model are currently being included to allow for these variations, and also to account for coupling magnetisation direction between domains, and finally to allow for averaging over distributions in parameters such as moment direction, domain wall potential and anisotropy constant, rather than single values. These should produce an improvement in the agreement with experimental measurement.

5 Anneal Time and Temperature Study

5.1 Introduction

A series of transverse (θ=90°) field anneals were performed on samples of two alloys. The alloys chosen were METGLAS 2605S2 and VAC0040. The Fe-Ni alloy was chosen because of the significant temperature variation in K_u, which is due to the dependence of the directional pair ordering on the topological disorder arising from the effects of entropy. Also, this alloy has a relatively high value of λ_s (≈20ppm from chapter 4). The Fe-based alloy was chosen because of its high λ_s and low K_u (approximately 40ppm and 80Jm^{-3} respectively), and to contrast with the binary alloy. The relevant parameters such as λ_s, M_s and K_u are similar for METGLAS 2605S2 and METGLAS 2605SC. The former was chosen in preference to the latter mainly because it allowed the λ_e results to be directly compared with similar readings by Bucholtz *et al* [1986]. Anneal conditions are shown in table 5.1.

Alloy	Stress Relief		Field Anneal	
	T_a	t_a	T_a	t_a
	(°C)	(min.)	(°C)	(min.)
METGLAS 2605S2	405-410	30	250, 300, 400, 420	10-180
VAC0040	370	30	250, 300, 350	10-720

Table 5.1: Transverse field anneal conditions

5.2 K_u and λ_s

As described in chapter 3, the macroscopic anisotropy constant, K_u, was calculated directly from the initial susceptibility, χ_0. This assumed that the M-H relationship was linear where $M<M_s$, as occurs when magnetisation proceeds by way of moment rotation alone. Figure 5.1 shows typical M-H plots from each alloy. They show a high degree of linearity with fairly sharp knees at the approach to saturation.

The induced macroscopic anisotropy, K_u, is shown with respect to anneal time, t_a, for a series of anneal temperatures, T_a, in figure 5.2. The VAC0040 data is similar to that of ribbon of the same composition measured by Becker [1978]. The temperature dependence of the fully developed K_u at long t_a, i.e. the asymptotic limits in the figures, is plotted in figure 5.3, together with those of Becker. This confirmed that K_u measured in these samples was due to ordering of Fe-Ni pairs. The values of K_u of the METGLAS 2605S2 did not approach an asymptote within the anneal times used in this study. The difference between T_x and T_c in this alloy is so great that the kinetics of the development of uniaxial anisotropy due to annealing at temperatures below T_c were too slow to fully develop K_u within these anneal times, so it was not possible to quantify the temperature dependence of K_u, which was expected to be insensitive to T_a. The maximum K_u induced was, however, approximately of the order of a quarter of that of the binary alloy, as found by Luborsky and Walter [1977a and b], although any difference between this data and that of Luborsky and Walter, and of Becker is probably due to slight differences in composition. It should be noted that there was little difference between the 400°C and 420°C data. This implies that T_c, which was given to be 415°C for the as cast material by the manufacturer, was above this value, otherwise a uniaxial anisotropy would not have been induced. This was thought to be due to an increase in T_c as a result of the heat treatment.

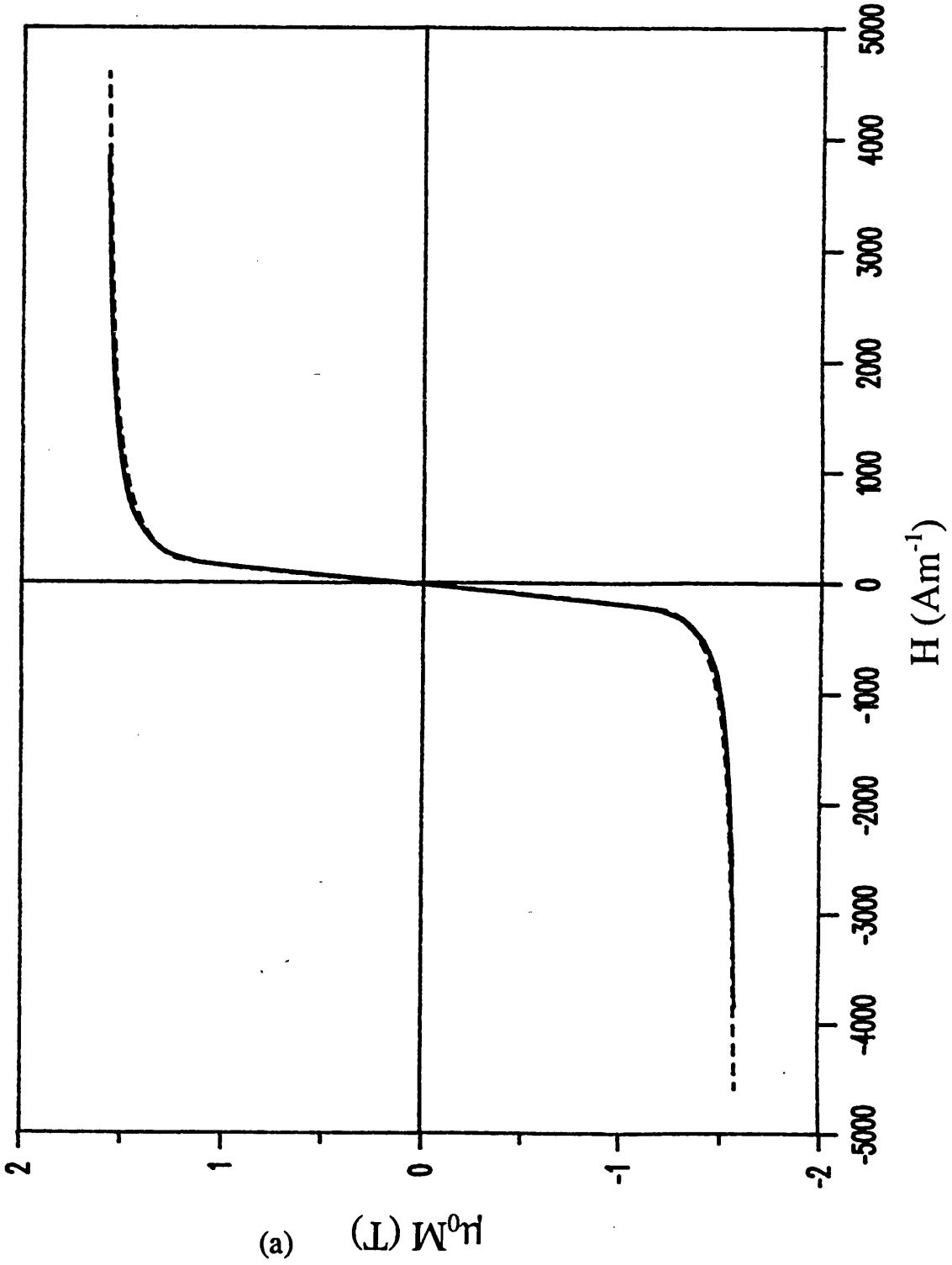

(a)

Figure 5.1: Typical measured M-H loops of transversely field annealed METGLAS 2605S2 and VAC0040 samples. Note that the curves are linear over a large range of magnetisation. They exhibit some rounding off at the approach to saturation.

a) METGLAS 2605S2, T_a=400°C dotted line - t_a=10 mins, solid line - t_a=180 mins.

b) VAC0040, T_a=350°C dotted line - t_a=10 mins, solid line - t_a=120 mins.

(b)

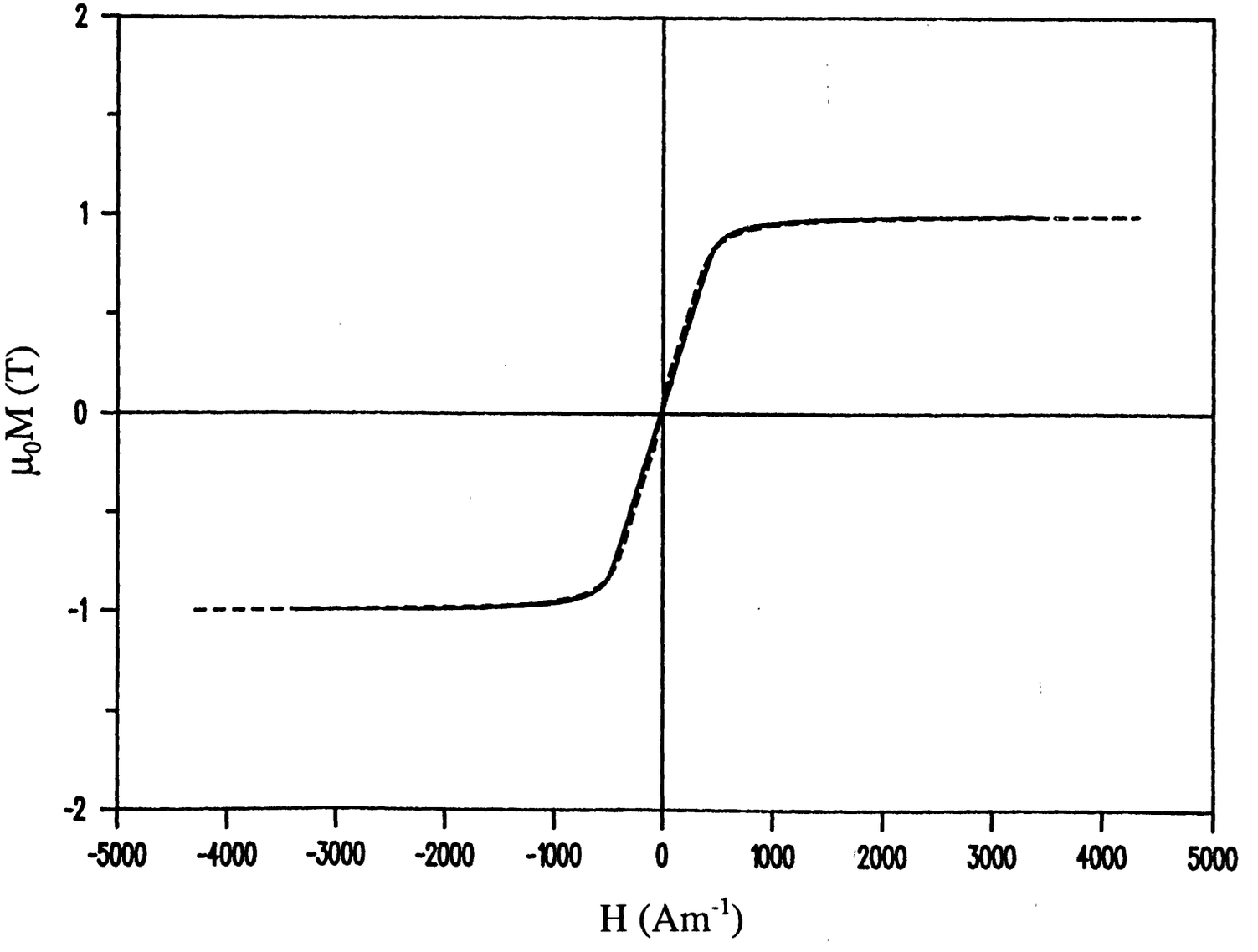
2
1
0
-1
-2
$\mu_0 M_0 \mu$ (T)
-5000
-4000
-3000
-2000
-1000
0
1000
2000
3000
4000
5000
H (Am^{-1})

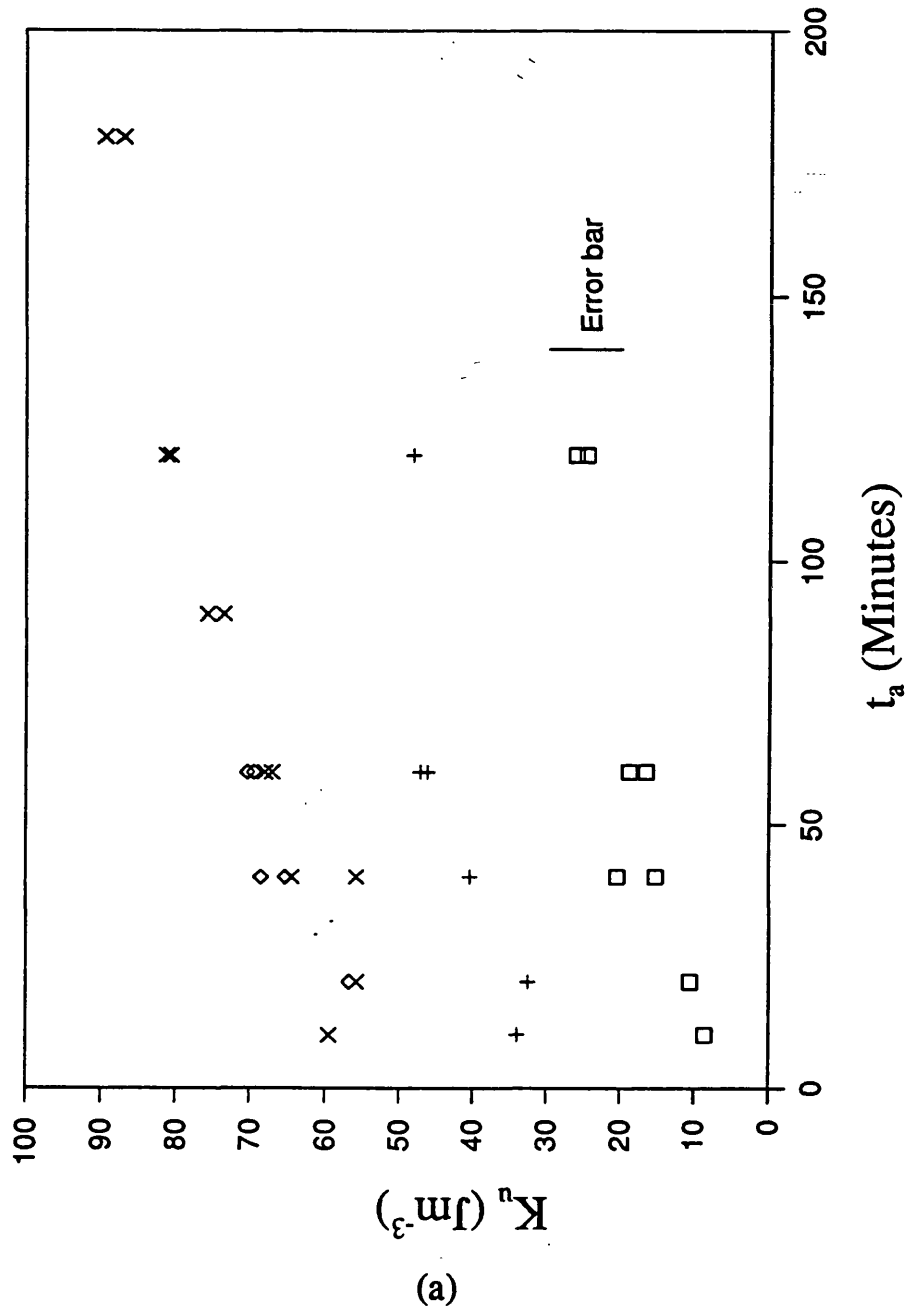

Figure 5.2: Anisotropy constant of transversely field annealed samples versus anneal time for different anneal temperatures.

a) METGLAS 2605S2, T_a=250°C - □ , 300°C - + , 400°C - × , 420°C - ◇), b) VAC0040, T_a=250°C - + , 300°C - □ , 350°C - × , 370°C - ✳), c) as (b) but with log-time scale on the abscissa.

(b)

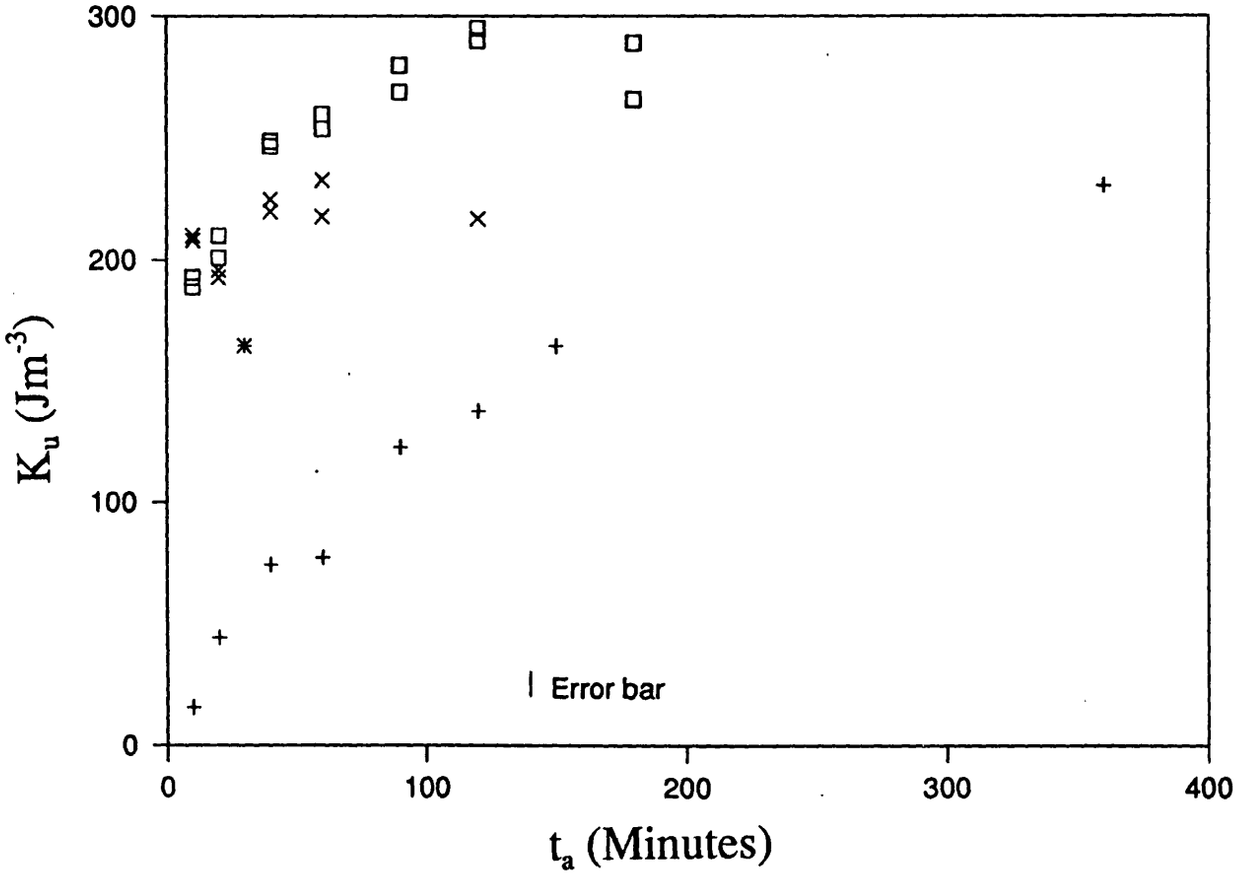

(c)

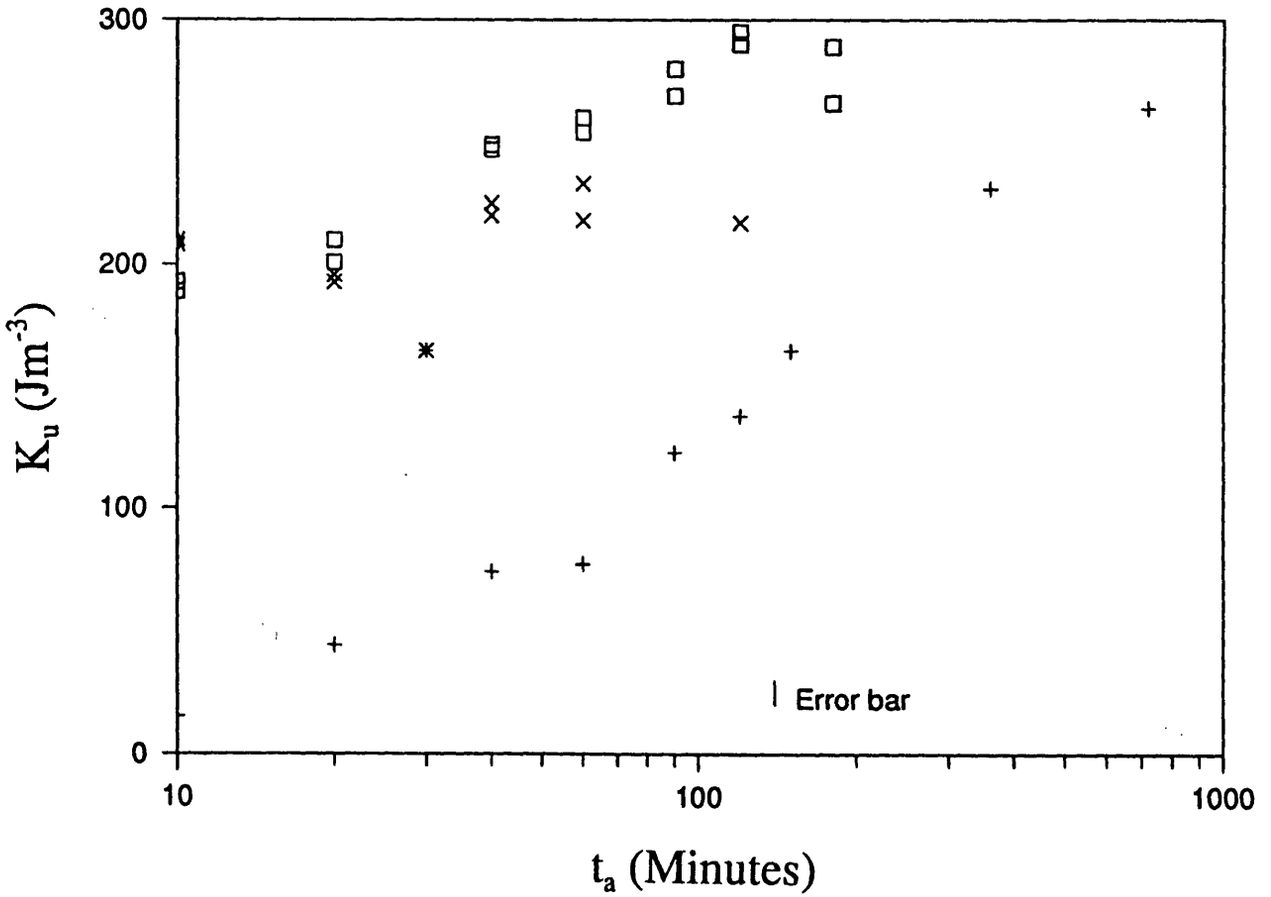

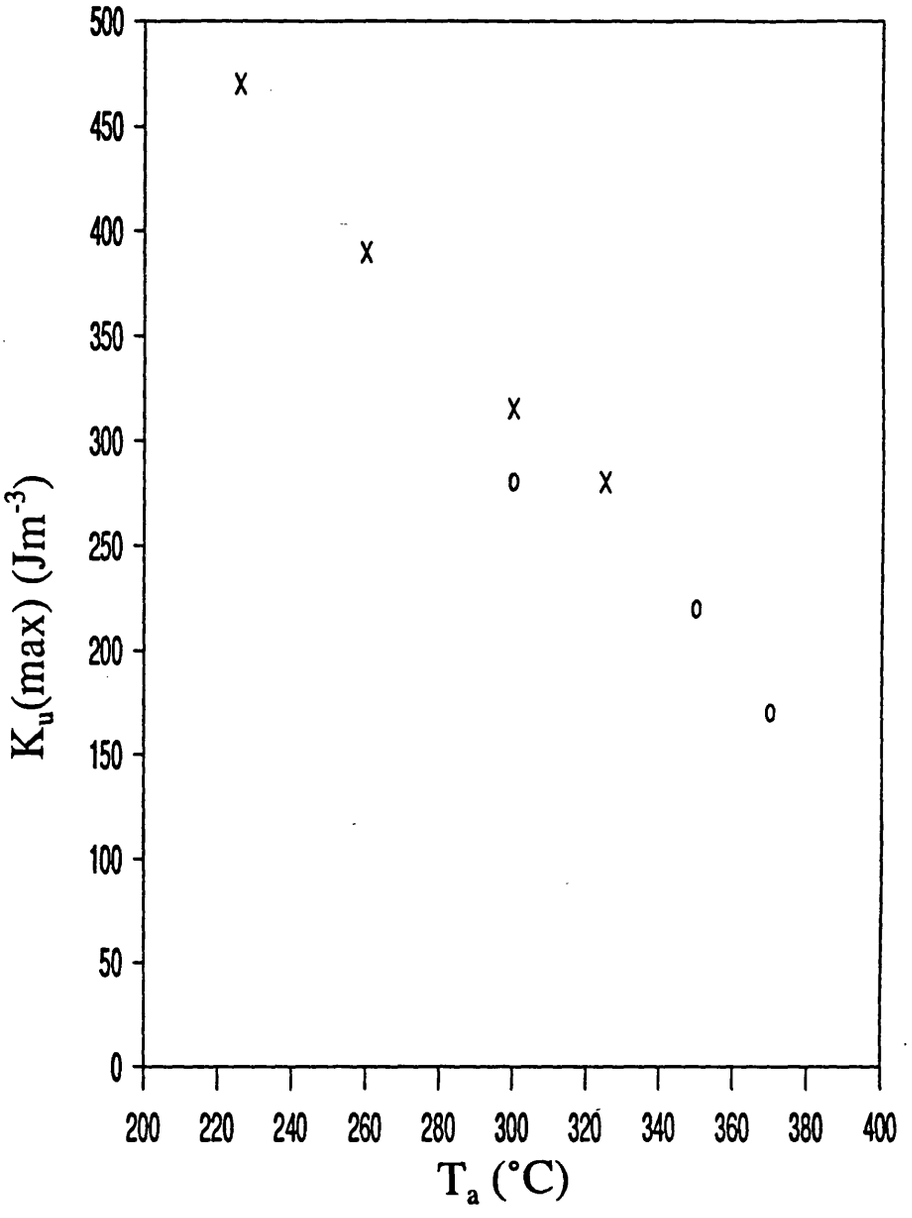

Figure 5.3: Maximum induced anisotropy constant induced by field annealing versus anneal temperature for $Fe_{40}Ni_{40}B_{20}$. (o - VAC0040 data, × - corresponding data from Luborsky and Walter [1977]).

The development of λ_e for each alloy with respect to t_a is shown in figure 5.4. There are two main points to note. Firstly, the fully developed (i.e. at $t_a=\infty$) λ_e(max) is not a function of T_a. The value of λ_e(max) is 30(±0.7)ppm for VAC0040 and 62(±1)ppm for METGLAS 2605S2. Therefore it can be inferred that since the value of λ_e(max) is not a function T_a, it is also independent of K_u(max). The magnetostriction is dependent on the degree of rotation of moments only. It is not dependent on the magnitude of the anisotropy dictating the initial moment directions, only the directions themselves. The only instance in which the magnetostrictive strain depends on K_u is where the final magnetised state is not at saturation. In this case the moment directions in the magnetised state, and therefore the degree of moment rotation, are dependent on the local anisotropy.

Secondly, the full development of λ_e was attained well before that of K_u. For instance, in the case of VAC0040 at 300°C the maximum value of λ_e was attained after approximately 10-20 minutes, while the K_u was not fully developed until after approximately 100 minutes. Similarly with the METGLAS 2605S2, the anisotropy had not reached a maximum value after 180 minutes, even at the highest anneal temperature used, while the maximum λ_e was achieved after 10-20 minutes at the same anneal temperature. Hence it can be inferred that at any given temperature the measurable moment spread has decreased as far as possible before the full development of the uniaxial anisotropy. This is an important result. It has been established that moment spread is predominantly a result of competition between local anisotropy and exchange, and that maximum λ_e is due to maximum moment rotation, i.e. maximum attainable moment alignment in the transverse direction. Since the local anisotropy is not negligible, the moment alignment can be attributed to alignment of local easy axes, which is reflected in an increase in K_u in the transverse direction. Further increase in K_u beyond the point of maximum attainable alignment points to other processes contributing to the development of K_u, with slower kinetics, and therefore an activation energy spectrum

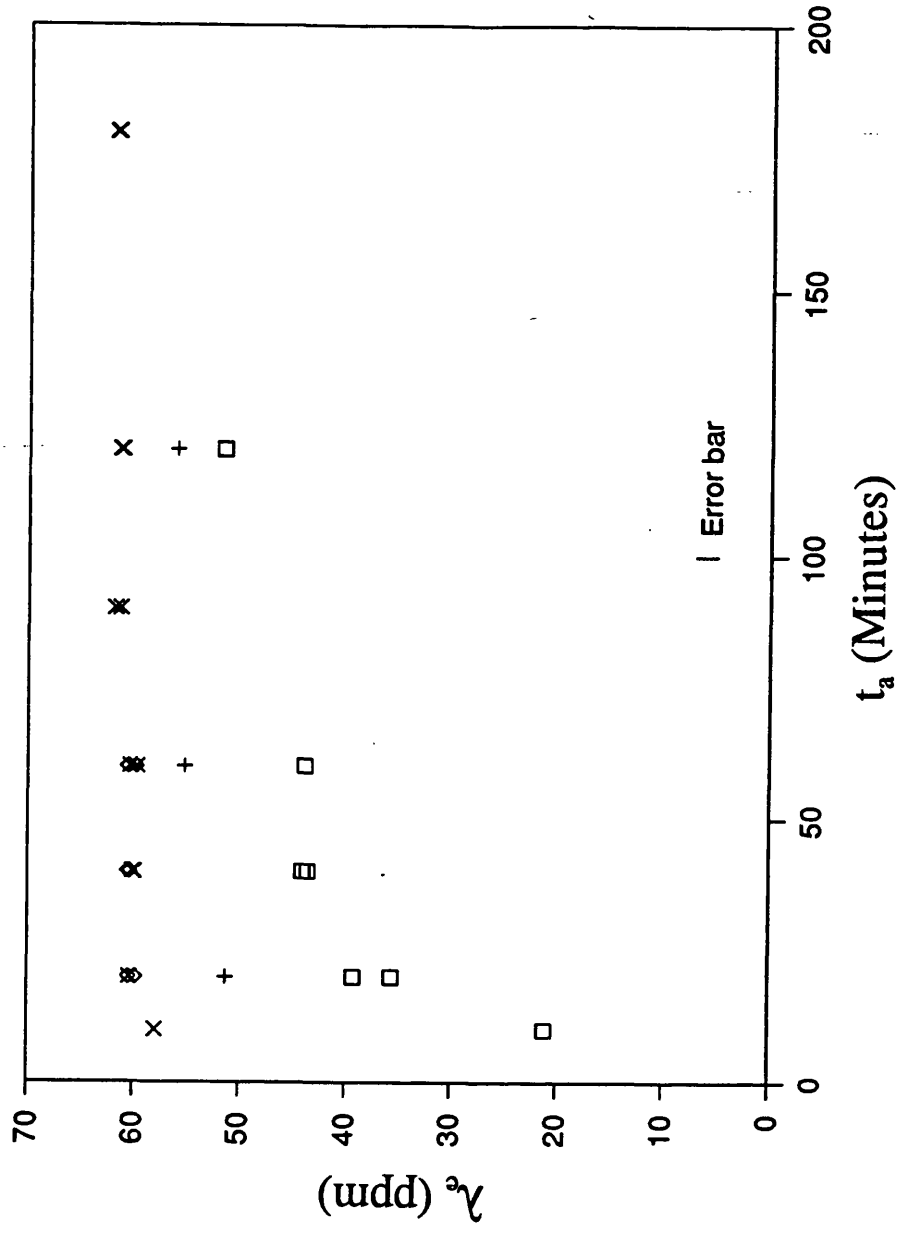

(a)

Figure 5.4: Engineering magnetostriction of transversely field annealed samples versus anneal time for different anneal temperatures. a) METGLAS 2605S2, b) VAC0040. Key as figure 5.2.

(q)

35
30
25
20
15
10
5
0
0
100
200
300
400
λ_e (ppm)
t_a (Minutes)
Error bar

comprising higher energies. Therefore development of K_u is due to different processes with different activation energy spectra, having different effects on the development of λ_e. The nature of these processes is considered in the final chapter.

The moment spread can, in principle, be predicted from calculations on the contributions of the exchange and anisotropy, given the distributions in the anisotropy direction and magnitude. However, the opposite does not hold, i.e. these distributions cannot be predicted from the moment spread alone. Barandiarán *et al* [1989] obtained the anisotropy magnitude distribution from the second derivative of the M-H plot, assuming a purely transverse induced easy axis (i.e. zero spread in easy axis direction). They stated that it is difficult to distinguish between distributions of transverse anisotropy magnitudes, and a single anisotropy which deviates from the transverse direction. The results presented above show that the effects of the two distributions (direction and magnitude) are separate. Changes to the former, for instance, are dictated by structural changes which induce the rotation of the easy axes of the local structural units, and which tend to have lower activation energy spectra, while changes to the latter are caused by pair ordering, and therefore by structural changes generally involving higher activation energy spectra.

Bucholtz *et al* [1986] showed reduction of moment spread along with the corresponding development of λ_e with respect to t_a. Given the value of moment spread from λ_e measurements, it would be possible to obtain the weighted contributions to the measured M-H plot from the theoretical M-H plots for each value of θ (the expressions for these theoretical plots as a function of θ are given in section 3 of Squire [1990]). The distribution in the magnitude of K_1 could then be determined for the $\theta=90°$ M-H curve using the method from Barandián *et al*. The same calculation for $\theta<90°$ becomes far more complex and includes factors involving domain wall movement. Thus there are too many variables to determine the distributions in local anisotropy direction and

magnitude from the information obtained from M-H and λ-H plots. If it were possible to calculate the distributions in this way, they would only reflect the local anisotropies seen by moments that contributed to λ_e. These moments would only do so by undergoing rotation. This calculation would therefore be unable to predict anything about the local anisotropies that were so great as to inhibit significant moment rotation, as discussed in chapter 2. Therefore the calculated distributions would give consistently low values of spread and K_L.

5.3 C_q, C_Q and $d\lambda/dH$

The quadratic coefficients of the best fit quartics to the λ-M data are plotted for each alloy with respect to t_a in figure 5.5. This property is independent of K_u (and so T_a) and shape factor. It was found to increase with increasing λ_e with maximum values of approximately 5.5×10^{-17} ($\pm5\times10^{-18}$) $A^{-2}m^2$ for METGLAS 2605S2 and 6.5×10^{-17} ($\pm5\times10^{-18}$) $A^{-2}m^2$ for VAC0040. Typical λ-M plots of transverse field annealed samples are shown in figure 4.7. When λ_e is fully developed, the λ-M plot is close to a quadratic with $C_Q \approx \lambda_e(max)/M_s^2$. The degree to which the measured plots can be described by a quadratic is discussed in chapter 3. Since the shape of the λ-M plot is of a definite, well classified form with its parameters, λ_e and M_s, insensitive to variations in anneal conditions and sample shape, this is potentially a useful parameter to exploit in transducers.

Parameters involving the applied field dependence of λ, such as $\left|\frac{d\lambda}{dH}\right|_{max}$ and C_q are directly dependent on both λ_e and K_u. $\left|\frac{d\lambda}{dH}\right|_{max}$ is shown for each alloy with respect to t_a in figure 5.6. It is determined by two competing processes. It increases with increasing λ_e, as moment collinearity is induced. At the same time it decreases with increasing transverse anisotropy constant, since larger fields are required to attain a given M and

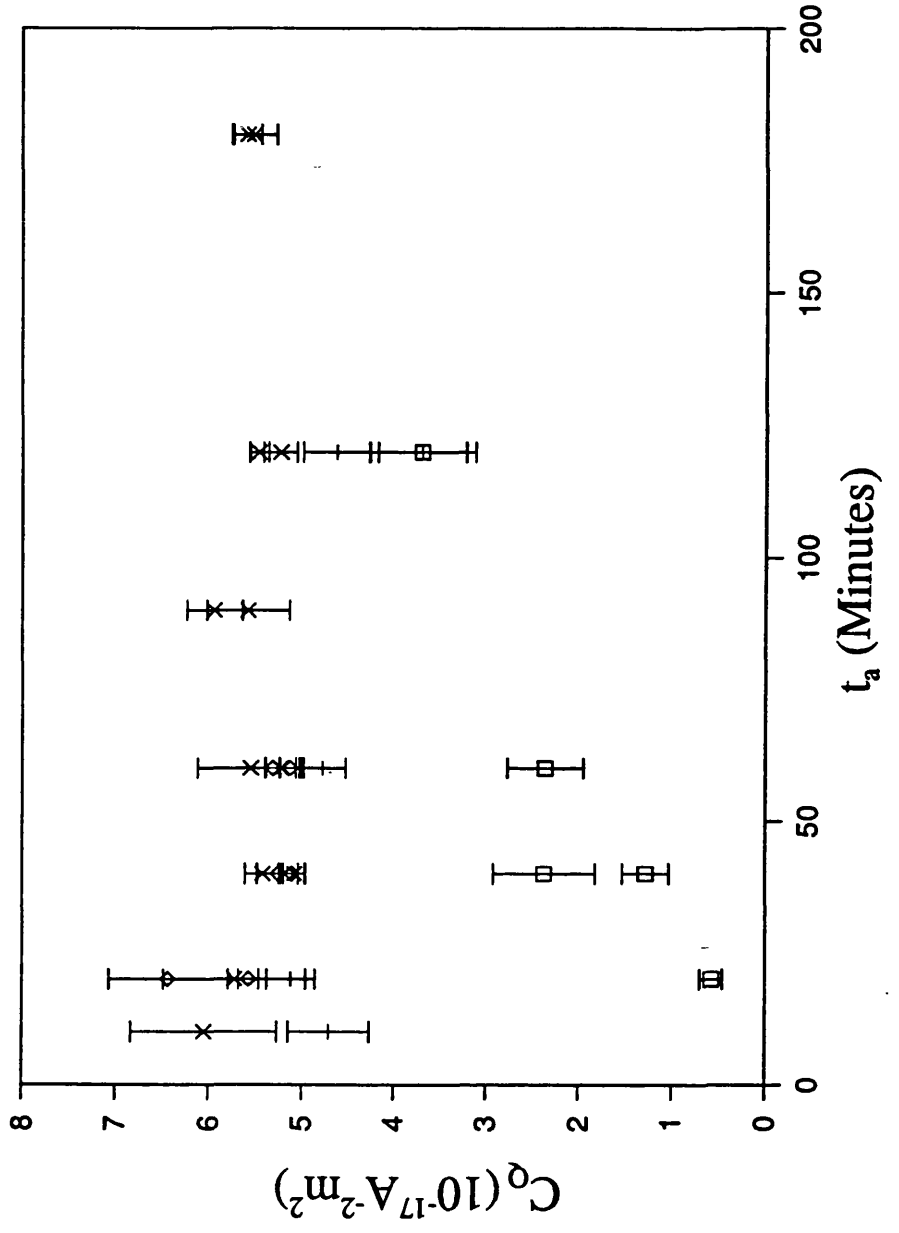

(a)

Figure 5.5: C_Q versus anneal time for different anneal temperatures. a) METGLAS 2605S2, b) VAC0040. Key as figure 5.2.

(q)

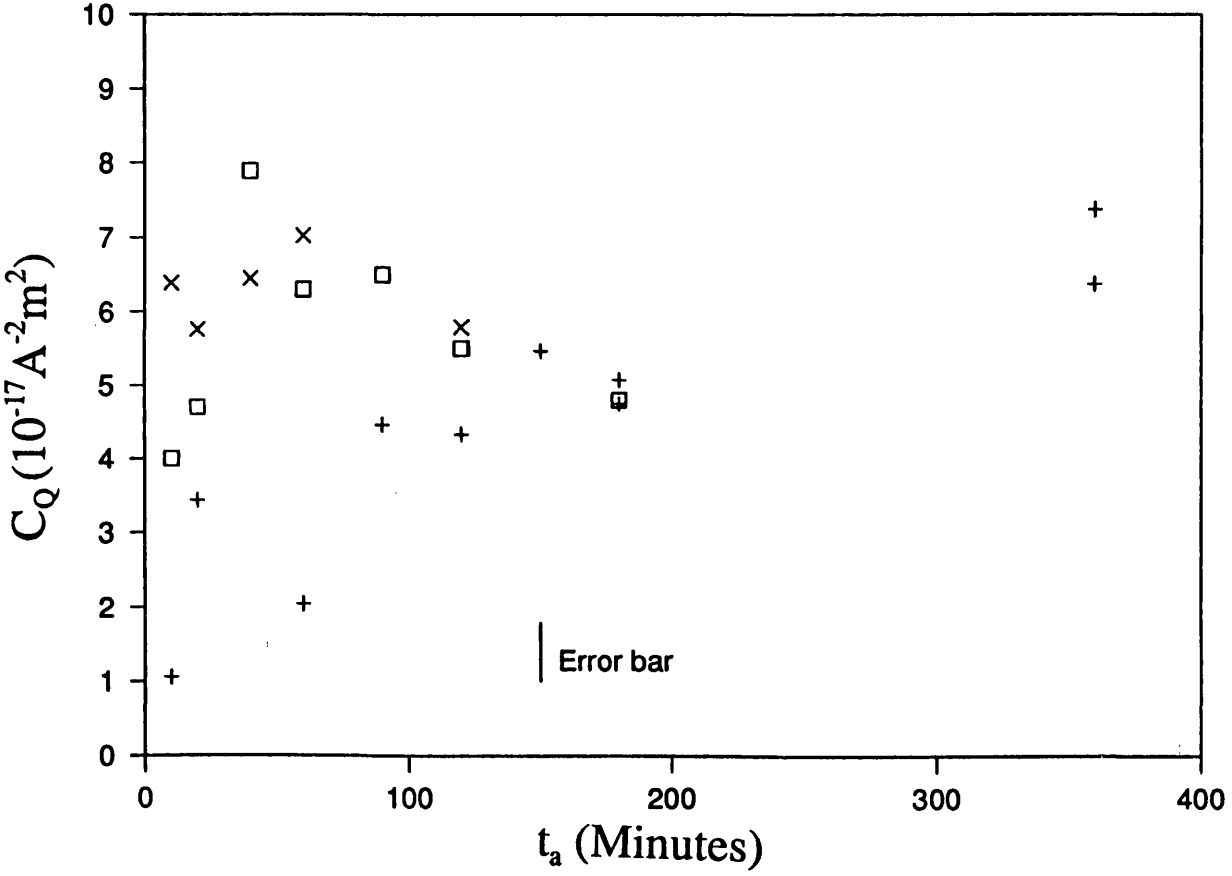
10
9
8
7
6
5
4
3
2
1
0
0
100
200
300
400
$C_Q(10^{-17}A^{-2}m^2)$
t_a (Minutes)
Error bar

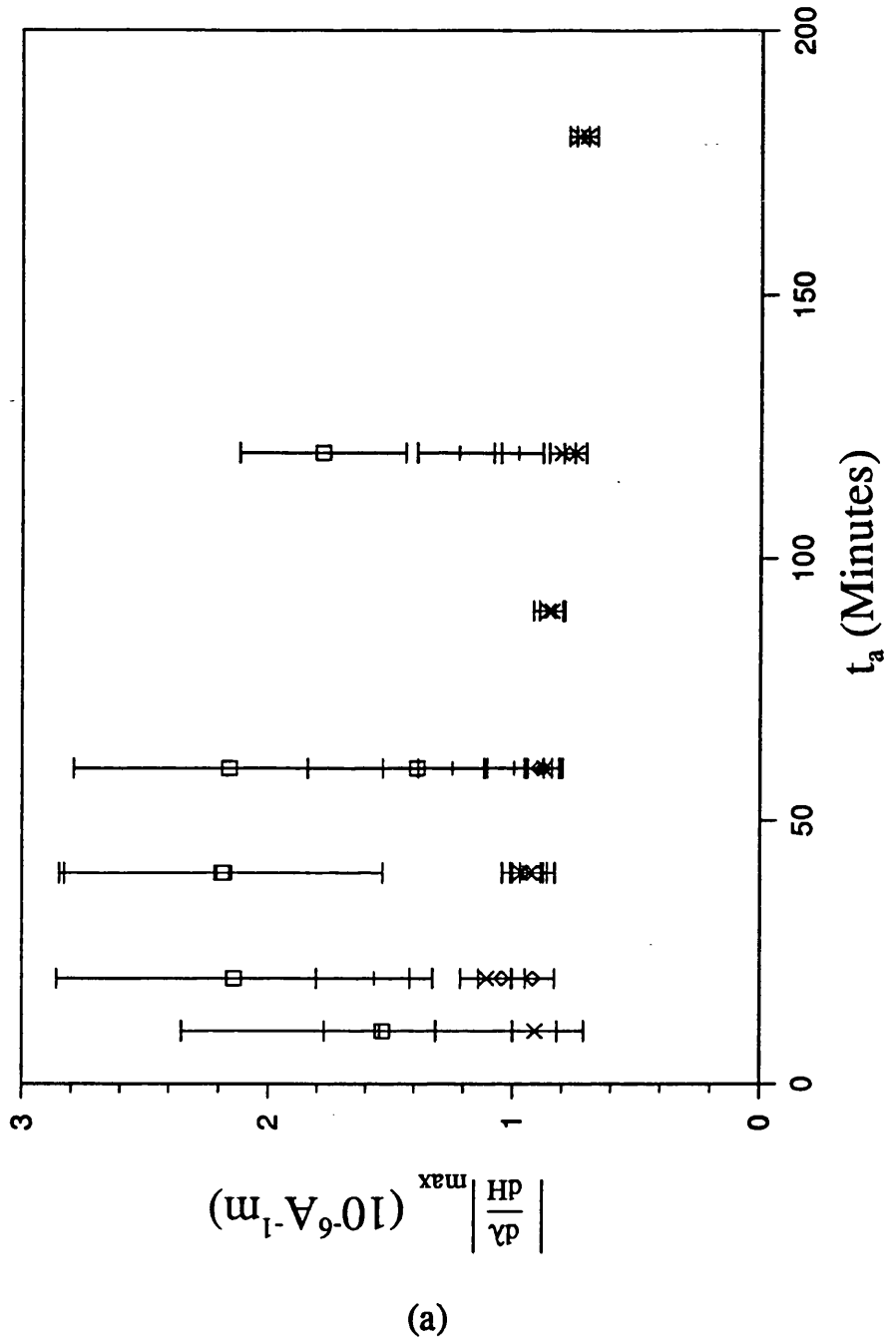

(a)

Figure 5.6: dλ/dH(max) versus anneal time for different anneal temperatures. a) METGLAS 2605S2, b) VAC0040. Key as figure 5.2.

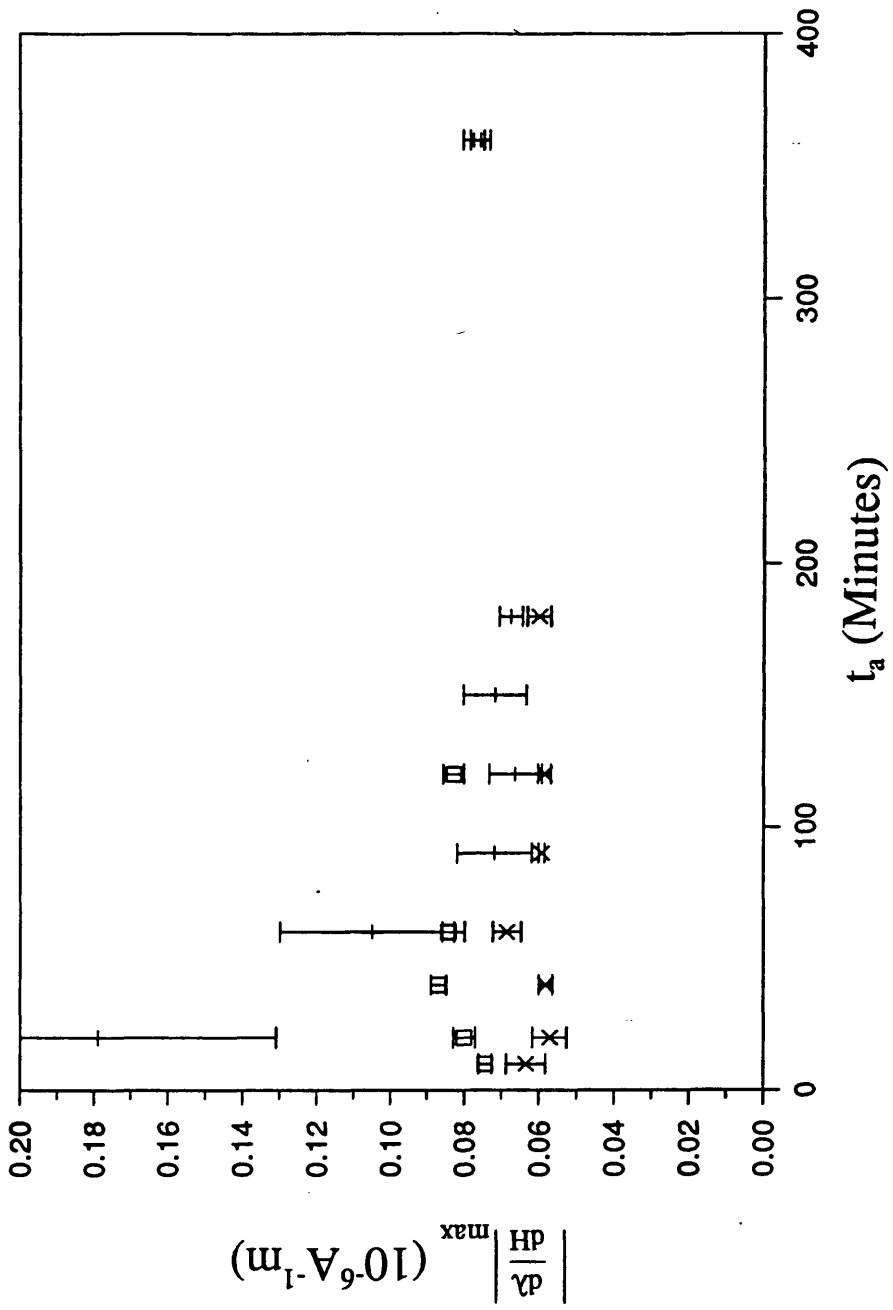
0.20
0.18
0.16
0.14
0.12
0.10
0.08
0.06
0.04
0.02
0.00
0
100
200
300
400
t_a (Minutes)
$\left|\frac{d\lambda}{dH}\right|_{max}$ ($10^{-6}A^{-1}m$)

(b)

hence λ_e. Consequently a maximum in $\left|\frac{d\lambda}{dH}\right|_{max}$ occurs with respect to t_a for a given T_a. In the alloys studied $\left|\frac{d\lambda}{dH}\right|_{max}$ increases due to development of λ_e faster than it decreases due to increase in K_u, up to the point where λ_e reaches its maximum. It then decreases until K_u also reaches its maximum. Thereafter it remains constant, where both λ_e and K_u are fully developed. These trends were seen in both alloys.

In METGLAS 2605S2 the maximum in $\left|\frac{d\lambda}{dH}\right|_{max}$ was found to occur after approximately 40-60 minutes at T_a=250°C, and after approximately 20 minutes at 300°C, while it seems to occur within 10 minutes at the higher temperatures. The full development of K_u was not achieved within the anneal times used, so direct observation of the variation of $\left|\frac{d\lambda}{dH}\right|_{max}$ with T_a could not be made. It was expected that $\left|\frac{d\lambda}{dH}\right|$ would be insensitive to T_a, reflecting the similar property in K_u. Judging from the T_a=400°C and 420°C data, it is expected that the asymptotic value was approximately $6\text{-}7\times10^{-7}A^{-1}m$ for a range of temperatures.

In VAC0040 the value was constant after 10 minutes at T_a=300°C and 350°C, and had reached a maximum at around 10 minutes at 250°C. The asymptotic value was more dependent on T_a because of the temperature dependence of K_u, so that as T_a increased, K_u decreased leading to a decrease in $\left|\frac{d\lambda}{dH}\right|_{max}$. These values were found to be approximately $8\times10^{-8}A^{-1}m$ and $6\times10^{-8}A^{-1}m$ at T_a=300°C and 350°C respectively.

The variation of C_q with t_a is shown for each alloy in figure 5.7. These show very similar trends to those of $\left|\frac{d\lambda}{dH}\right|_{max}$. The asymptote of the METGLAS 2605S2 data sets was approximately $5\times10^{-9}A^{-2}m^2$ (again judging from the T_a=400°C and 420°C data) while the corresponding values in VAC0040 were approximately $1\times10^{-10}A^{-2}m^2$ and $2\times10^{-10}A^{-2}m^2$ for T_a=300°C and 350°C respectively.

The maximum values of these parameters were significantly higher than the asymptotic ones. In METGLAS 2605S2 the maximum $\left|\frac{d\lambda}{dH}\right|_{max}$ and C_q were approximately $2.2(\pm0.6)\times10^{-6}Am^{-1}$ and $1.0(\pm0.2)\times10^{-7}A^{-2}m^2$. The corresponding maximum

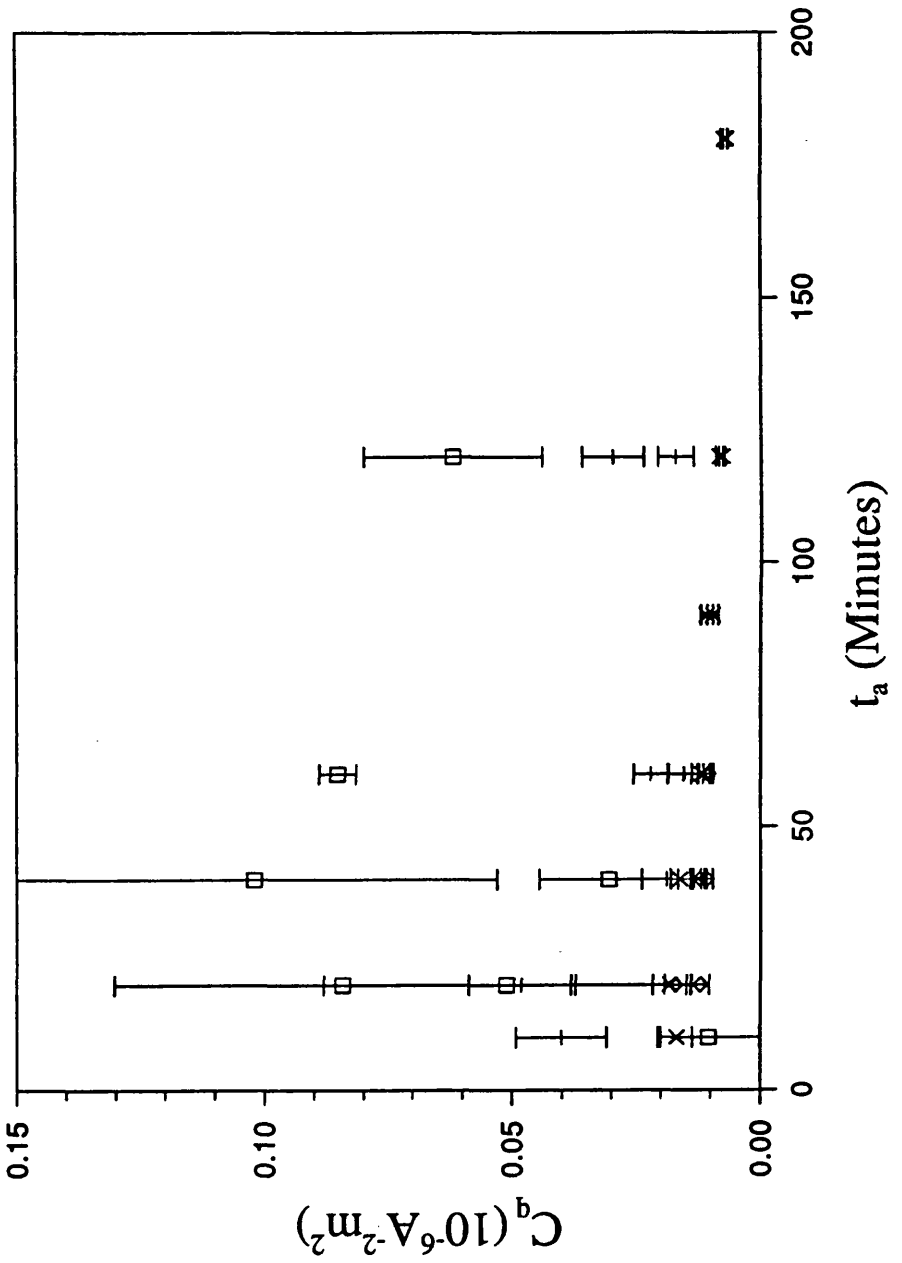

(a)

Figure 5.7: C_q versus anneal time for different anneal temperatures. a) METGLAS 2605S2, b) VAC0040, c) as (b) with expanded y-scale. Key as figure 5.2.

(q)

0.0020
0.0018
0.0016
0.0014
0.0012
0.0010
0.0008
0.0006
0.0004
0.0002
0.0000
C_q (10^{-6}A^{-2}m^2)
0
100
200
300
400
t_a (Minutes)

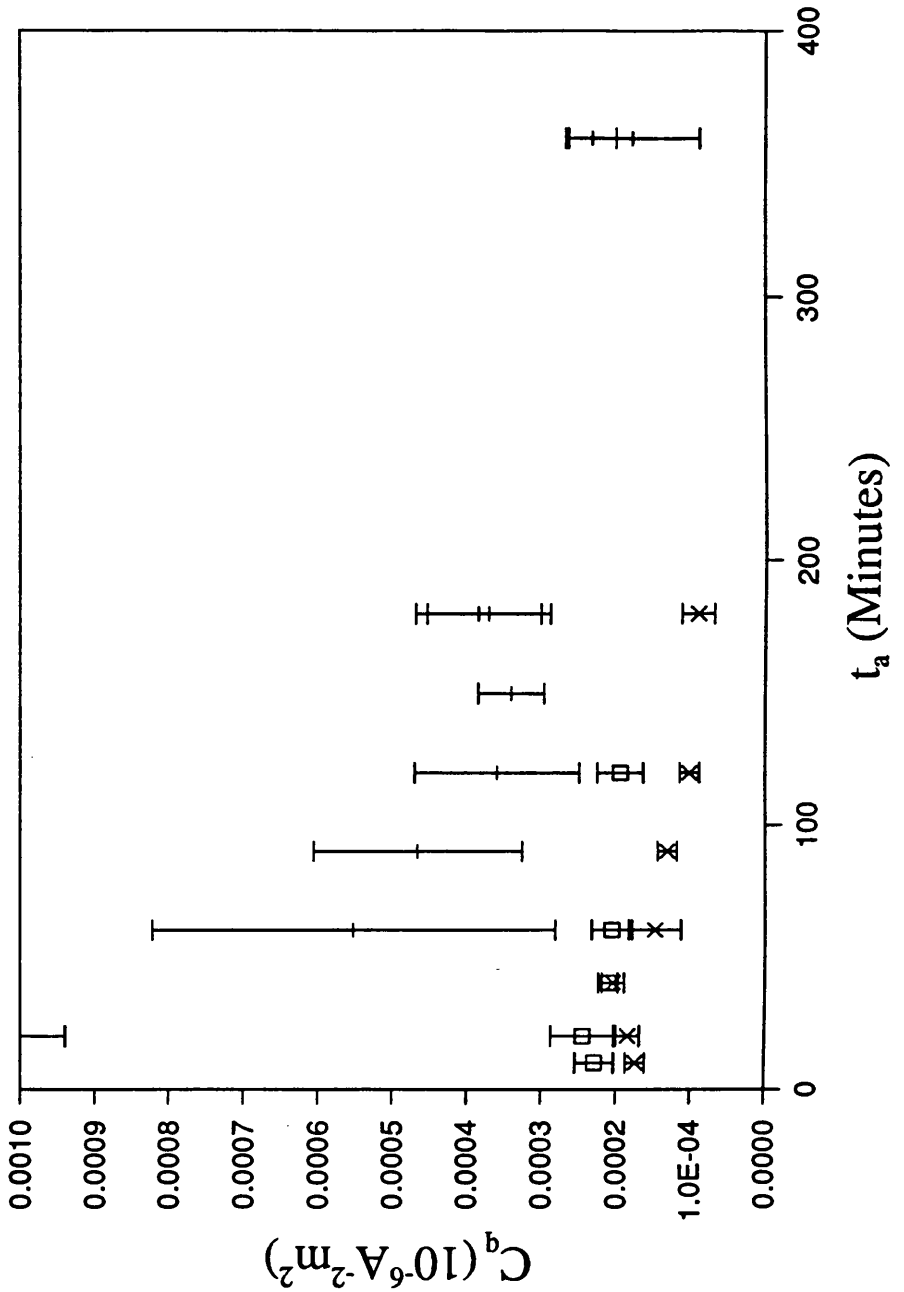
0.0010
0.0009
0.0008
0.0007
0.0006
0.0005
0.0004
0.0003
0.0002
1.0E-04
0.0000
C_q ($10^{-6}A^{-2}m^2$)
0
100
200
300
400
t_a (Minutes)

(c)

values in VAC0040 could not be determined exactly from the data, but was known to be at least $2.8(\pm 0.6)\times 10^{-7} Am^{-1}$ and $7(\pm 2)\times 10^{-9} A^{-2}m^2$. The large errors arise as a consequence of the combination of errors in λ_e, χ_{eff} and χ_0 (as covered in the appendix), and the trend in the data suggest that these errors might be overestimated, particularly near their maxima.

5.4 Domain Studies

The domain structure was investigated on VAC0040 samples annealed with T_a=250°C and 300°C. The samples with approximately fully developed K_u exhibited clear, coherent stripe domains with the main walls close to the transverse direction, as illustrated in figure 5.8, for typical regions of two such samples. This structure was less definite on samples where K_u was not fully induced, such as the VAC0040 samples annealed for less than approximately 720 and 100 minutes at 250°C and 300°C respectively. Where K_u was suppressed, the domain structure was less clear. The domain walls in many cases were too wide to cause colloid aggregation, so making them difficult to pick out. For the same reason the secondary walls were also obscure in many instances. Figure 5.9 shows typical domain structures of samples with suppressed K_u. The edges showed regions of transverse domains. The walls curved away from the transverse direction at approximately 1mm from the edges and became less distinct towards the middle. In some cases these walls became zigzagged towards one side of the sample, although judging from the secondary walls the magnetisation was in a more transverse direction than the main walls in the region. A schematic diagram of this structure is given in figure 5.10. It was thought that this domain structure was caused by the following circumstances. The sample was twisted in its initial condition when it was cut from the ribbon. The internal stresses causing the twist were not fully annealed out during the

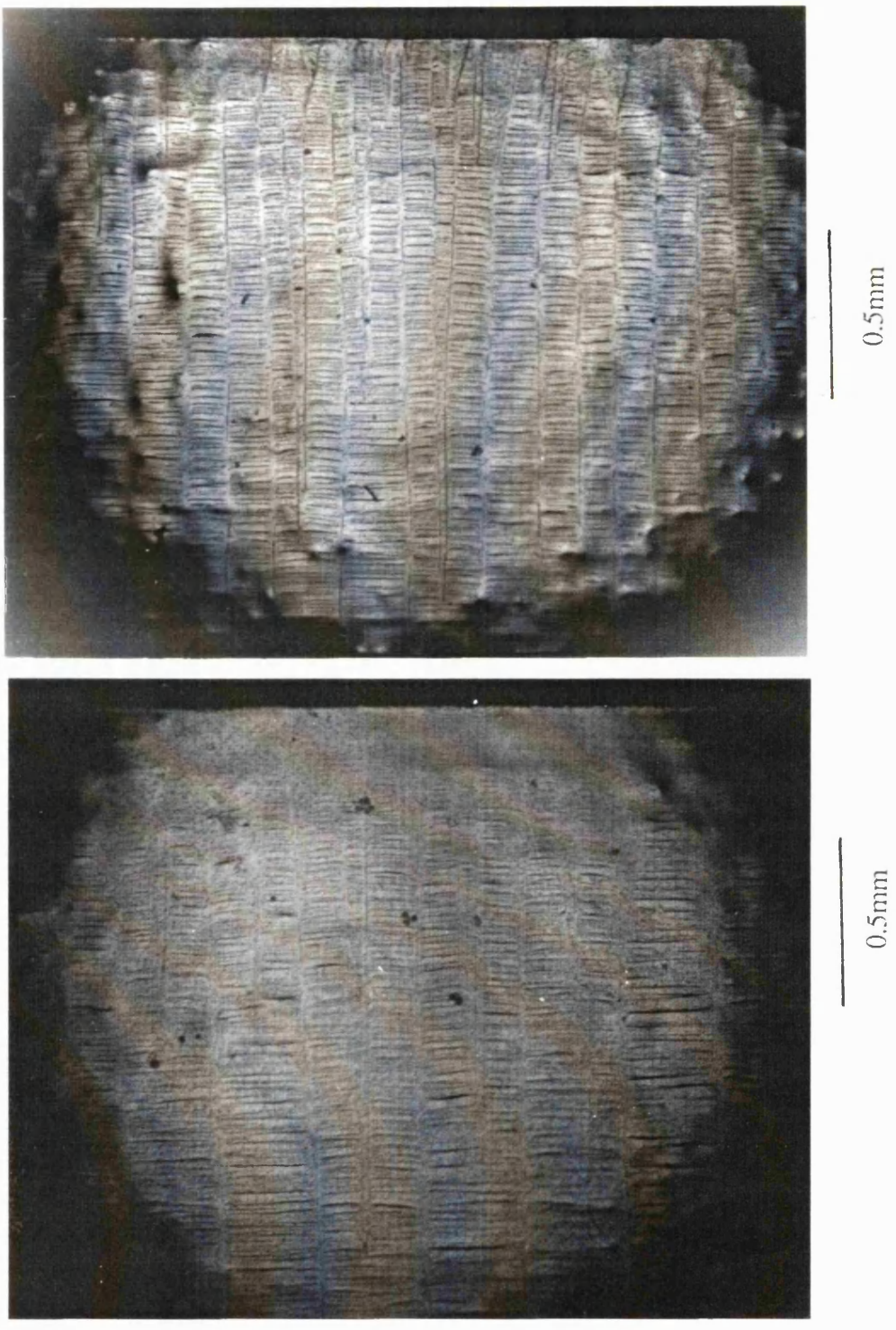

Figure 5.8: Photgraphs of typical domain structures on transversely field annealed VAC0040. a) T_a=250°C, b) T_a=300°C. Both exhibit clear transverse stripe domain patterns. Secondary domain walls are also visible.

(a)

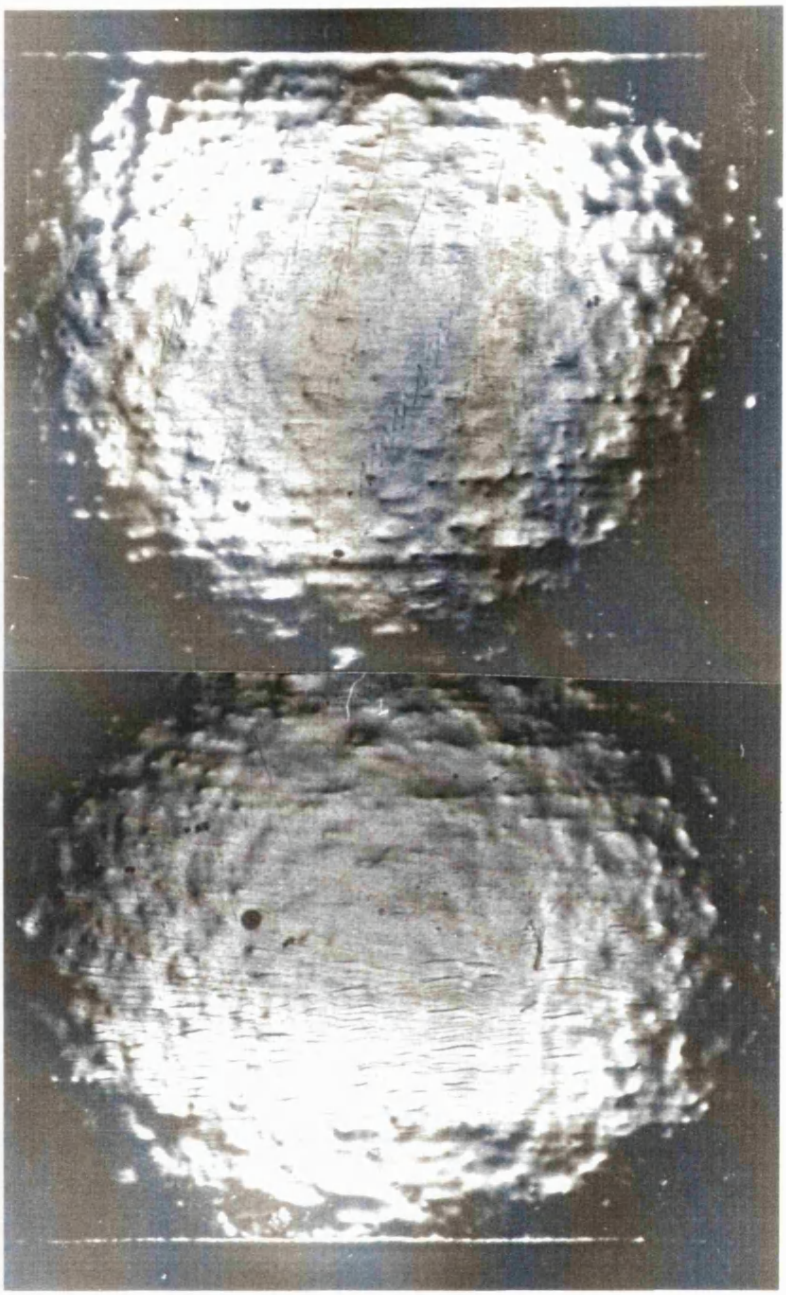

Figure 5.9: Photographs of typical domain structure of a VAC0040 sample with uniaxial anisotropy not fully developed. a) T_a=300°C, t_a=60 mins. b) T_a=300°C, t_a=20 mins. Near the edges the stripe pattern is fairly well developed, but the wall deviates away from the transverse direction towards the centre of the ribbon, and the walls become less distinct. Where this occurs, the wall becomes zigzagged on one half of the ribbon.

(b)

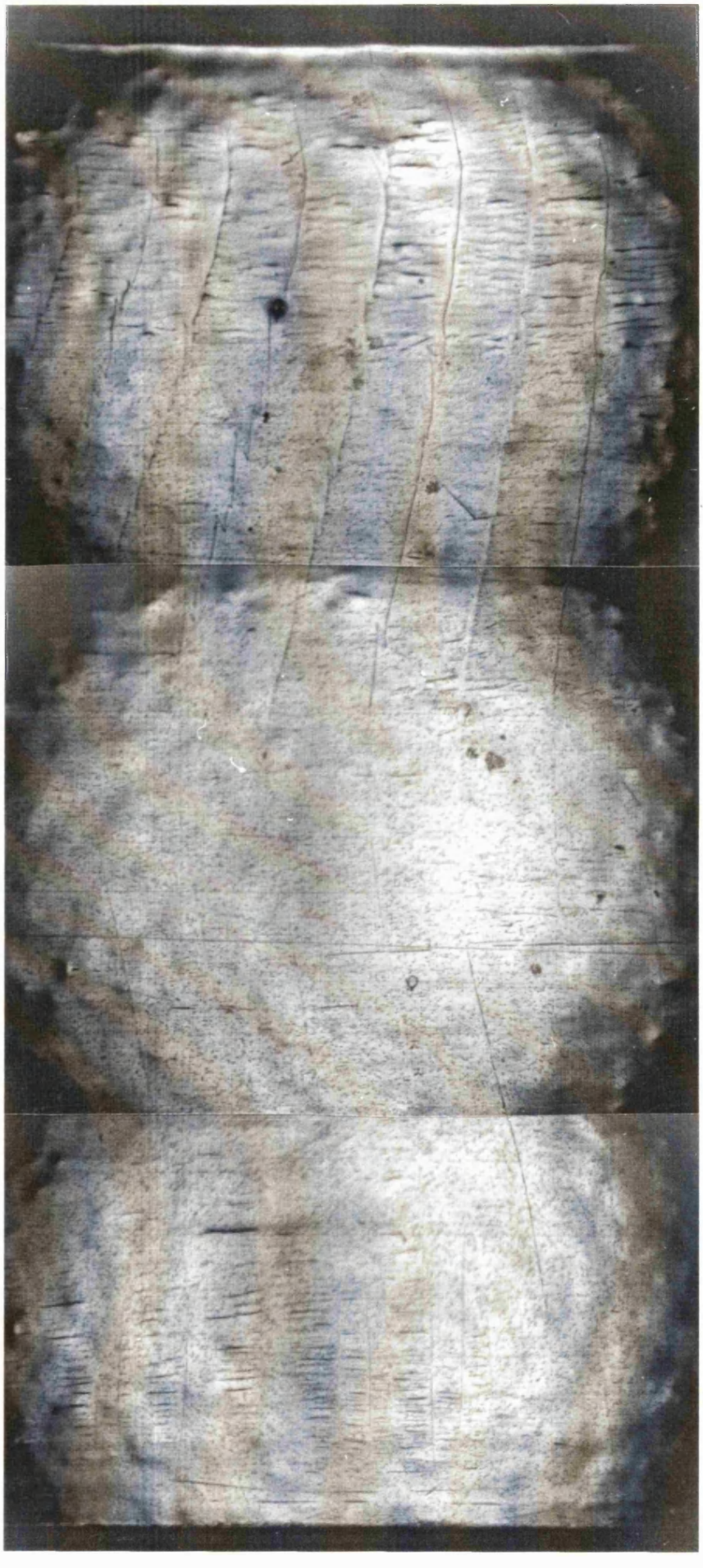

1mm

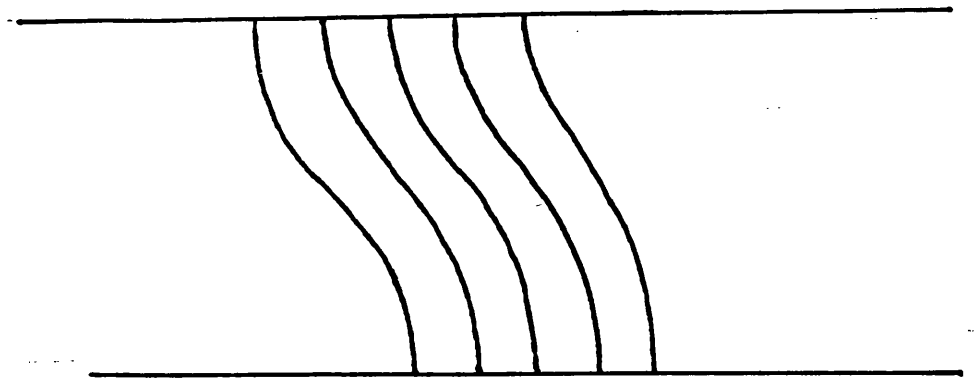

(a)

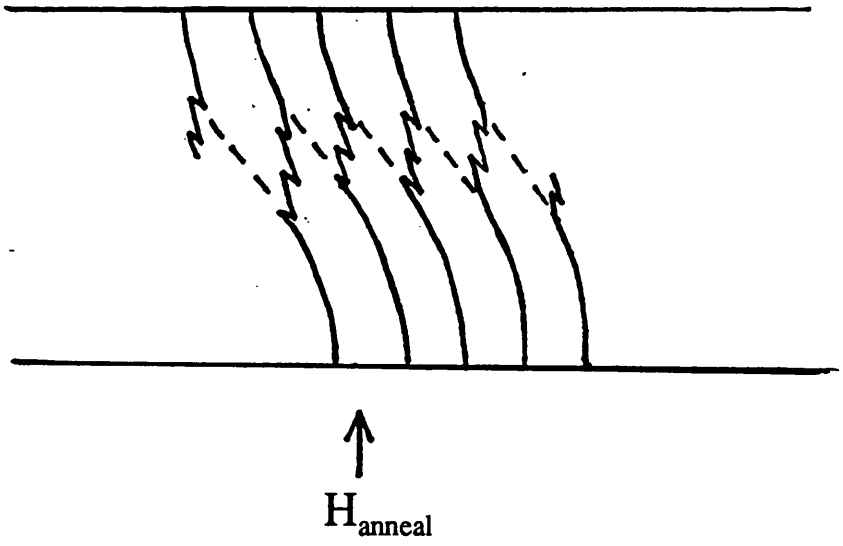

(b)

Figure 5.10: Schematic representation of the domain structure seen in the previous figure. a) Domain structure of a twisted ribbon. b) Domain structure after partial induction of transverse anisotropy.

stress relief. It was then laid flat between aluminium plates for the field anneal, inducing a macroscopic easy axis pattern as shown in Livingston and Morris [1984] and figure 5.10a. Partial induction of uniaxial transverse anisotropy during the field anneal then had the effect of straightening the easy axis to some extent, and caused neighbouring domains to merge end to end. This resulted in the zigzagged domain wall patterns, due to the sample maintaining 180° domain walls as far as possible (as seen in Hasegawa *et al* [1978]), and the domain structure indicated in figure 5.10b and shown in figure 5.9.

This illustrates the importance of completely stress relieving the sample prior to the field anneal. The deviation in easy axis from the transverse direction can easily be avoided by performing the stress relief with the sample in an identical arrangement to the field anneal, preferably without disturbing it between heat treatments. In this way very low macroscopic anisotropy can be induced, which, in the absence of internal stresses, can show a high degree of alignment in the anneal field direction. Thus moments are aligned in this direction to a high degree, due to the exchange and anisotropy forces largely acting to orientate the moments in the same direction. This produces a sample with high λ_e and low K_u, hence high magnetostrictive response and magnetoelastic coupling constant.

6 Partial Crystallisation

6.1 Introduction

Controlled heat treatments near the crystallisation temperature, T_x, can induce partial crystallisation, which in the case of metallic glass ribbons is generally nucleated initially at the surfaces. Slight differences in composition and density of the crystalline and amorphous phases cause stress fields to be set up between the surfaces, so inducing a macroscopic perpendicular stress induced anisotropy as described in chapter 2 [Herzer and Hilzinger 1986]. This provides an alternate method for obtaining maximum λ_e.

The development of λ_e with respect to heat treatment conditions was investigated, together with that of K_u, quadratic coefficients and maximum λ-H gradient. Three alloys were studied; METGLAS 2605S2 and VAC0040, which allowed comparison with parameters obtained from transverse field annealing, and also VAC7505, the annealed samples of which were provided by J. Vincent and S. Ritchie of GEC Hirst Research Laboratories. The composition of the VAC7505 alloy is close to that of METGLAS 2605S2, as are the intrinsic parameters, such as M_s. Heat treatments used are given in table 6.1.

Alloy	Anneal Temperature (°C)	Anneal Time (min.)
METGLAS 2605S2	400 425 450	60,180,360 60,180,240,360 30-240
VAC0040	350 380	120,240,360 30-120
VAC7505	450	60-1440

Table 6.1:Partial crystallisation anneal conditions.

The data is mostly presented with respect to extent of crystallisation. The coercivity has been shown to give a good indication of this [Sheard *et al* 1989], due to increased pinning from the crystallites and the crystal-amorphous interfaces. X-ray diffraction traces were taken on the VAC7505 samples. There were significant differences between the air cooled and wheel cooled sides. The α-Fe <200> peak at $2\theta=60°$ was far larger on the air cooled side, while the <110> crystalline peak superposed over the amorphous "bump" at $2\theta=45°$ was less evident (figure 3.19), implying texturing of the crystallites in different orientations on the two surfaces, as seen by Herzer and Hilzinger [1986]. The sharpness of the <200> peak on the air cooled side and the fact that it was separate from amorphous peaks allowed it to be readily used as a measure of crystallisation, at least on the air side. Figure 6.1a and b shows the relationship between the relative peak areas and heights and the coercivity. Although these plots show significant scatter there is a rough linear correlation. The scatter might have arisen from the fact that the X-ray beam incident on the sample surface had a cross section of a few millimetres. This was thought to be sufficient to obtain macroscopic values, but there may have been a significant region to region variation in crystallisation. Because of constraints on space within the X-ray diffractor, it was not possible to take readings over the whole sample. The error bars in the X-ray data indicate inaccuracies in the height and area measurements.

Figure 6.1c shows the variation of X-ray peak area with peak height. The definite linear relationship implies very little variation in the peak widths. The widths are dependent on the crystallite size, so it could be concluded that in the samples measured, with $H_c<100Am^{-1}$, the crystallisation developed mainly by crystallite nucleation rather than growth.

Domain studies were attempted, but no domain patterns could be seen. It was expected that maze patterns would have arisen from closure domains at the surface due to the perpendicular easy axis. Stress induced anisotropy might also have been expected

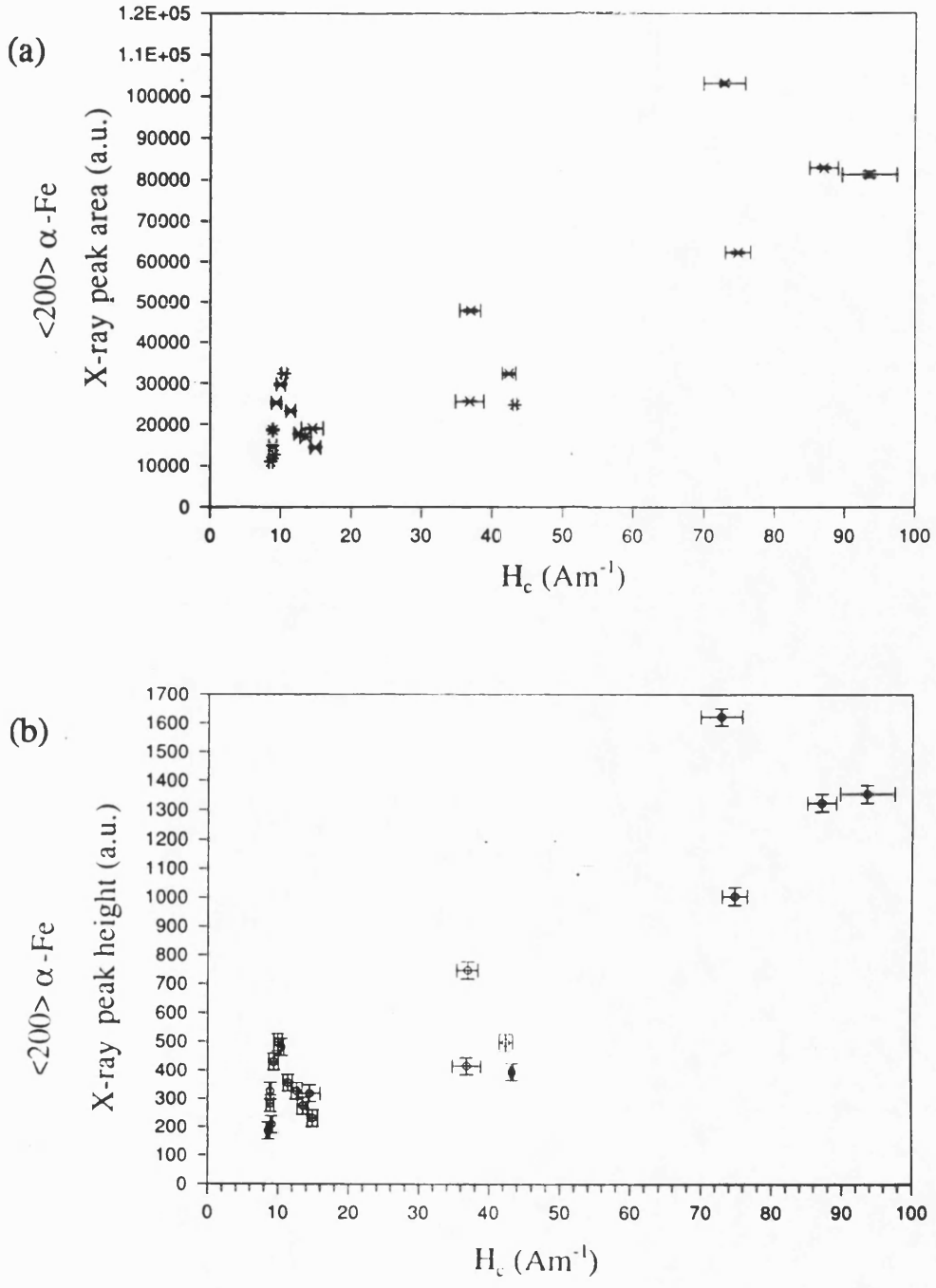

Figure 6.1: <200> α-Fe X-ray diffraction peak a) area and b) height versus coercivity of partially crystallised VAC7505 samples. c) Peak area versus peak height.

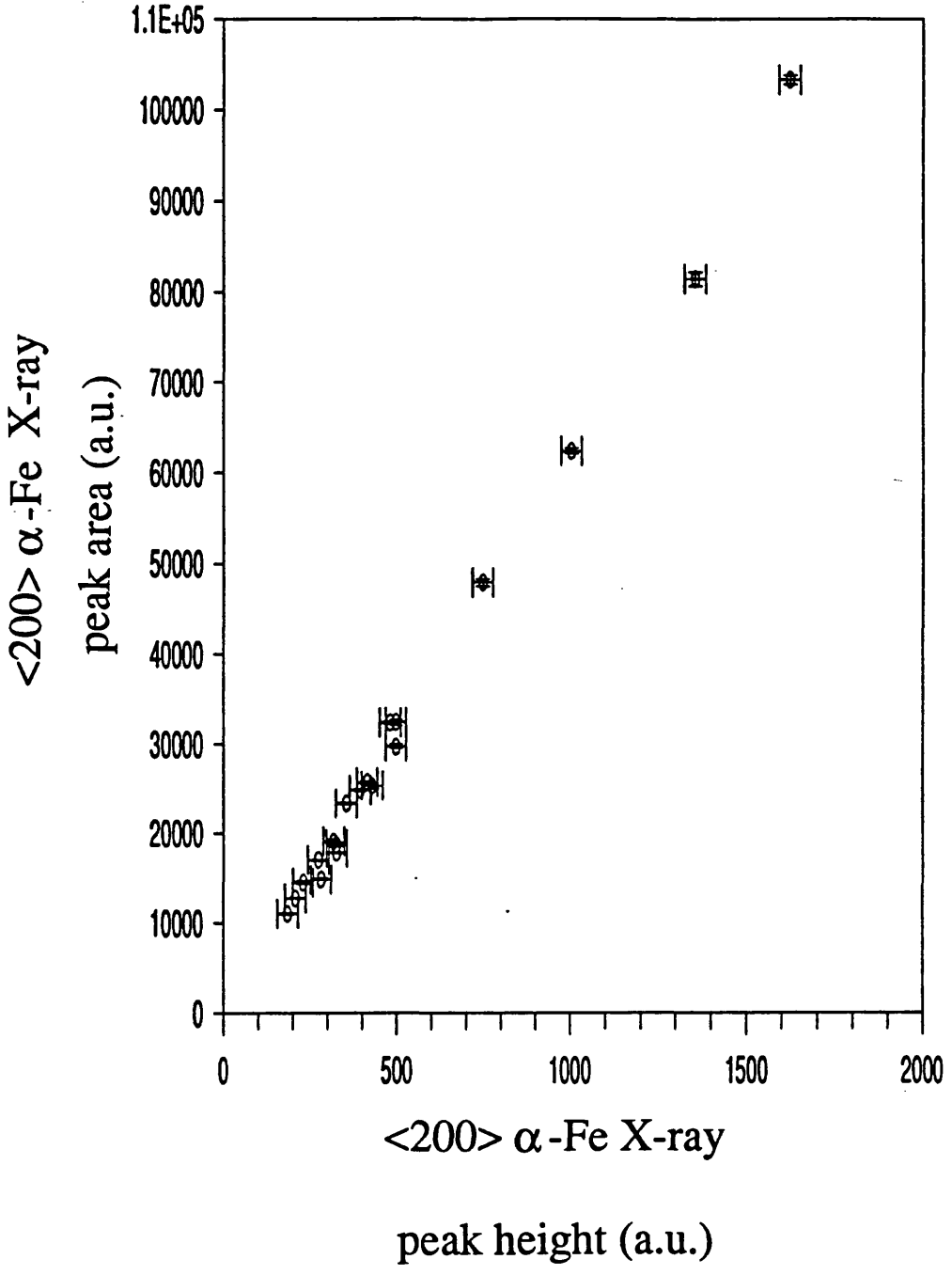
1.1E+05
100000
90000
80000
70000
60000
50000
40000
30000
20000
10000
0
0
500
1000
1500
2000
<200> α-Fe X-ray
peak area (a.u.)
<200> α-Fe X-ray
peak height (a.u.)

(c)

to produce radial patterns around crystallites. These would have given some qualitative indication of the extent of crystallisation, but not of the development of the anisotropy constant. It was thought that the absence of visible Bitter patterns was because the walls of the surface closure domains were probably too wide to cause colloid aggregation.

6.2 K_u and λ_e

K_u is plotted versus H_c for each alloy in figure 6.2. The main point to note is that K_u was far greater than those in the field annealed samples, and showed no sign of approaching an asymptote. For instance, where H_c was approximately $100Am^{-1}$, K_u was more than ten times the K_u(max) due to transverse field annealing in METGLAS 2605S2, although it was less in VAC0040 where it was approximately 1.5 times that from field annealing. K_u is proportional to the stress across the thickness of the ribbon. Thus, as stated in chapter 2, it increases with increasing surface crystallisation, until the material in the regions near the surfaces are close to fully crystallised and crystallisation proceeds in the bulk of the material, which was found to occur in TM-M alloys at approximately 20% crystallisation by volume [Sheard *et al* 1989]. In this paper it was stated that "the coherence of magnetisation vector is destroyed by bulk crystallisation", and the spread in anisotropy easy axis direction distribution would then increase. Judging from the data from Sheard *et al*, a coercive field in VAC0040 of $100Am^{-1}$ (which was approximately the maximum measured in this study) corresponded to approximately 20-30% crystallisation by volume, so K_u was some way from reaching its maximum.

The variation of K_u was approximately linear with H_c, which in turn was approximately linear with degree of crystallisation. This finding was in agreement with the prediction of the model by Herzer and Hilzinger [1986]. They stated that $K_u \propto \delta$, where δ denotes the total average thickness of the crystallised layers. According to this

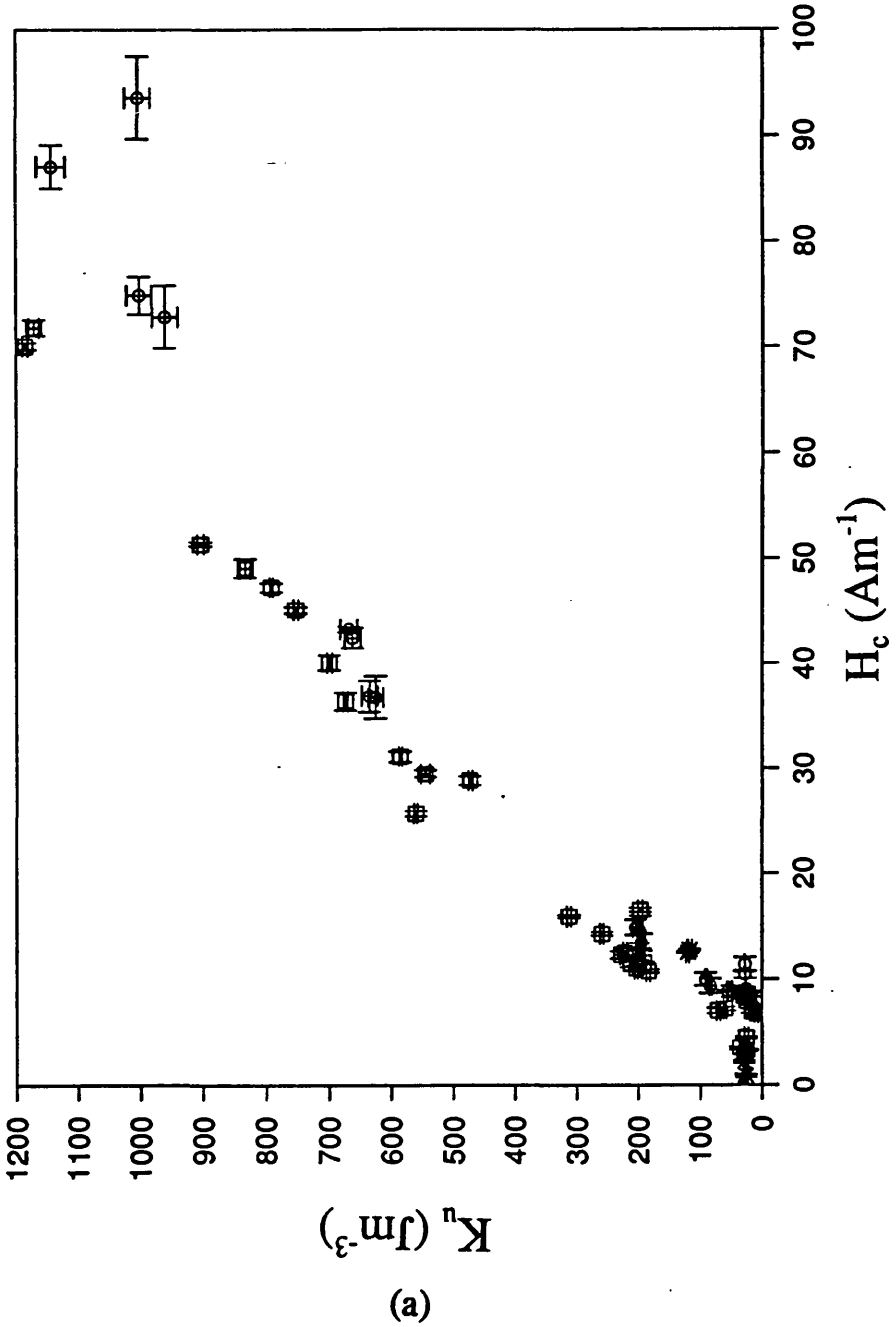

(a)

Figure 6.2: Anisotropy constant versus coercivity of partially crystallised a) METGLAS 2605S2 and VAC7505 (METGLAS 2605S2 T_a=400°C - ◇ , 425°C - × , 450°C - □ , VAC7505 T_a=450°C - ○), and b) VAC0040 (T_a=380°C).

(q)

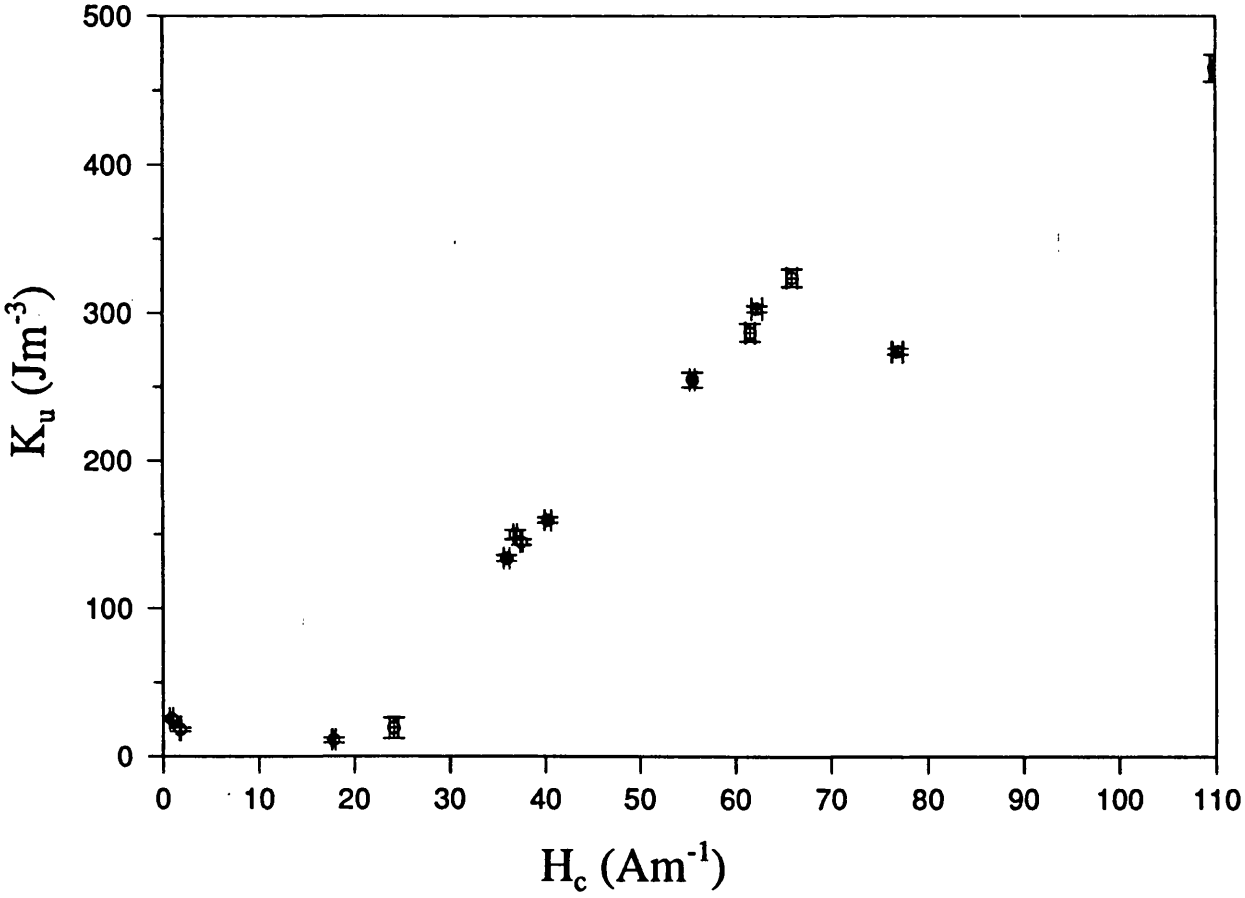
500
400
300
200
100
0
K_u (Jm^{-3})
0
10
20
30
40
50
60
70
80
90
100
110
H_c (Am^{-1})

model the maximum value measured in the METGLAS 2605S2 ribbon (thickness≈26μm), of $K_u \approx 1200 Jm^{-3}$, corresponds to approximately 2μm, which in turn gave a value of H_c of approximately $60 Am^{-1}$. Thus the agreement between the data in figure 6.2a and the model appears to be very good. However, the figures for δ and H_c become 1.3μm and $40 Am^{-1}$ when the figure for λ_s is altered from 30ppm to 40ppm, as obtained in this study. The errors in measurement of δ and areal fraction of the crystalline phase are probably at least as large as that of λ_s, so the agreement with data is good within error.

This linear relationship holds for samples with H_c above 5-$10 Am^{-1}$ in METGLAS 2605S2 and about $20 Am^{-1}$ in VAC0040. Samples with H_c below this were not subject to sufficient surface crystallisation to set up stress fields great enough to induce uniaxial anisotropy. This relationship is independent of anneal temperature. The development of K_u and H_c are shown in figure 6.3 for METGLAS 2605S2 for three different anneal temperatures, and for VAC7505 (T_a=450°C). After an initial decrease due to stress relief, both parameters increase steadily with increasing t_a, although the rate of this increase is lower for lower T_a due to the kinetics of the crystallisation processes.

The maximum χ_0 was of the order of 4×10^4 in all three alloys and decreased rapidly with the onset of crystallisation. It was of the order of 10^4 where λ_e became fully developed.

The linear relationship between H_c and both K_u (which was shown to be proportional to the thickness of the crystallised surface layers by Herzer and Hilzinger [1986, see section 2.5) and the X-ray diffraction peak areas indicates that it gives a good indication of the extent of crystallisation. It was possible to measure this more accurately and conveniently, and was shown to be more sensitive to the effect of shorter anneal times, than K_u. Consequently, the subsequent magnetostriction and magnetostrictive response data has been presented with respect to it.

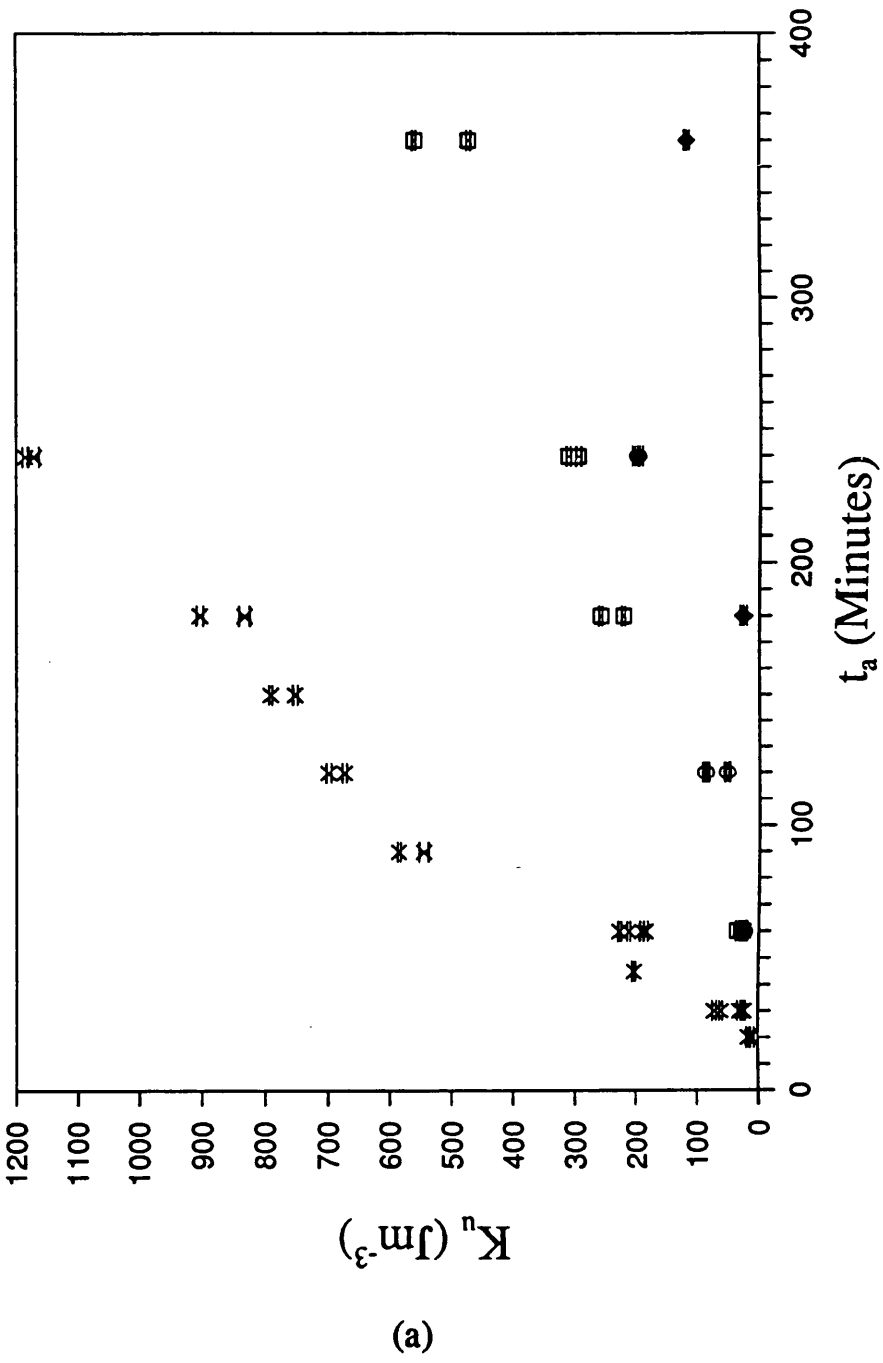

(a)

Figure 6.3: a) Anisotropy constant and b) coercivity versus anneal time of partially crystallised METGLAS 2605S2 and VAC7505 for different anneal temperatures. Key as figure 6.2.

(q)

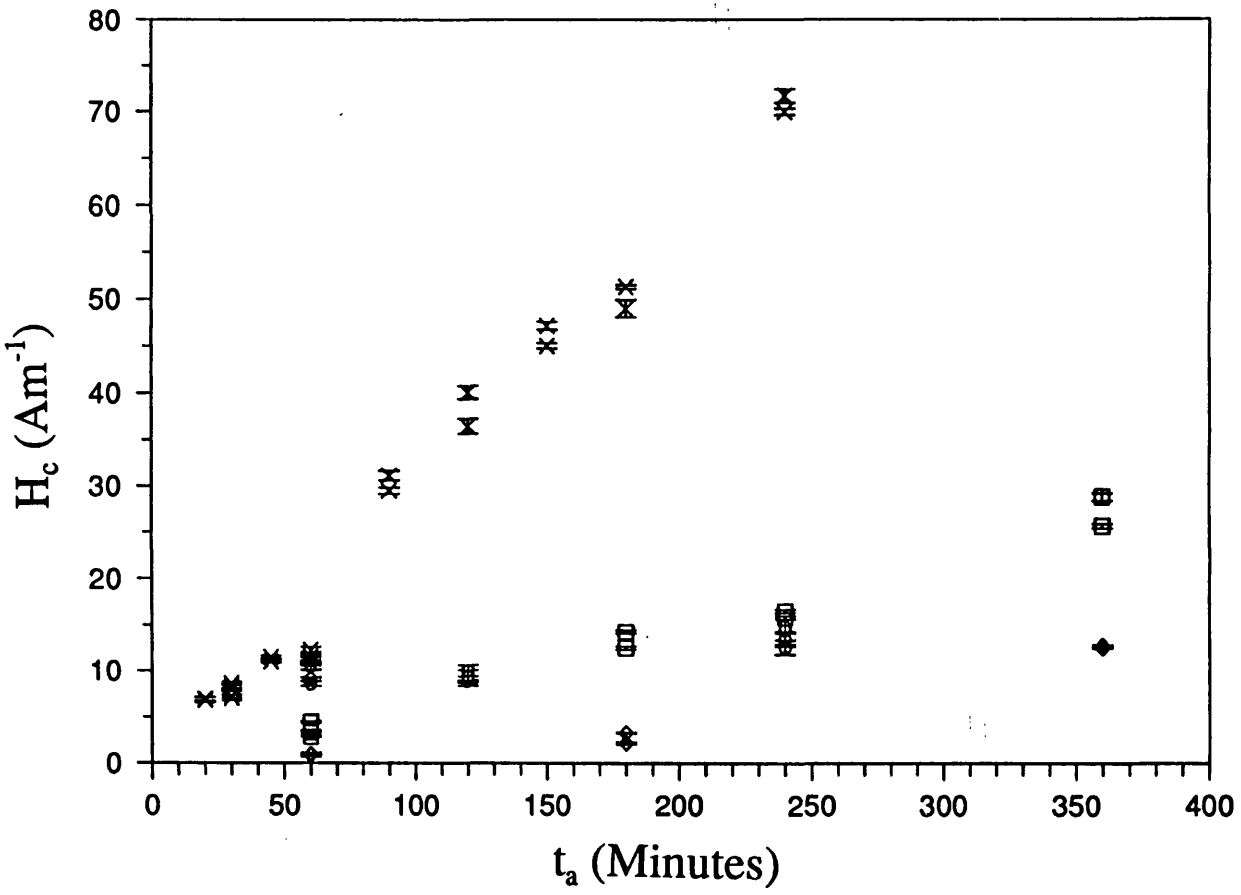
80
70
60
50
40
30
20
10
0
0
50
100
150
200
250
300
350
400
H_c (Am^{-1})
t_a (Minutes)

The variation of λ_e with H_c is shown in figure 6.4 for each alloy. The data from VAC7505 and METGLAS 2605S2 appear to lie on a similar curve. That is, λ_e increases from its as cast value to close to the maximum at $H_c \approx 10 Am^{-1}$. The VAC0040 follows a similar trend with the maximum λ_e occuring at $H_c \approx 20 Am^{-1}$. In both cases this corresponds to $K_u \approx 50\text{-}100 Am^{-1}$. This stage is approximately where the K_u starts to significantly increase with increasing coercivity, i.e. where the crystallisation is extensive enough to cause a uniform stress field great enough to induce a macroscopic uniaxial anisotropy. This occurs at higher H_c in VAC0040 because lower λ_s constants require that greater uniform stresses are required to induce an anisotropy great enough to turn the moments into the perpendicular direction, so requiring a greater degree of crystallisation.

Further crystallisation had little effect on the λ_e of the Fe-based alloys, which was very close to the maximum obtained using transverse field annealing. A slight decrease in λ_e with increasing H_c was attributed to the fact that the samples became harder to fully saturate, the mechanical loading of the crystalline layer restricted the sample strain, and that more of the sample volume was taken up by the crystallites, with their own magnetostrictive properties and non-perpendicular anisotropy. The average maximum λ_e measured on the crystallised samples was approximately 60ppm for METGLAS 2605S2 and 52ppm for VAC7505. In contrast, λ_e in VAC0040 did not reach the maximum value from field annealing, and decreased notably with increasing H_c. It is possible that the reasons for this are that the crystalline layers at the surfaces caused some mechanical loading and were subject to lower λ_e due to the higher K_u and wider spread in easy axis direction dictated by the crystal texture. Also it was possible that there was some bulk crystallisation in this alloy, degrading λ_e and K_u. It was found [Sheard *et al* 1989] that the point at which bulk crystallisation became significant corresponded roughly to the values of H_c over which the reduction in K_u was seen.

An attempt to investigate the nature of the crystallisation was made using the

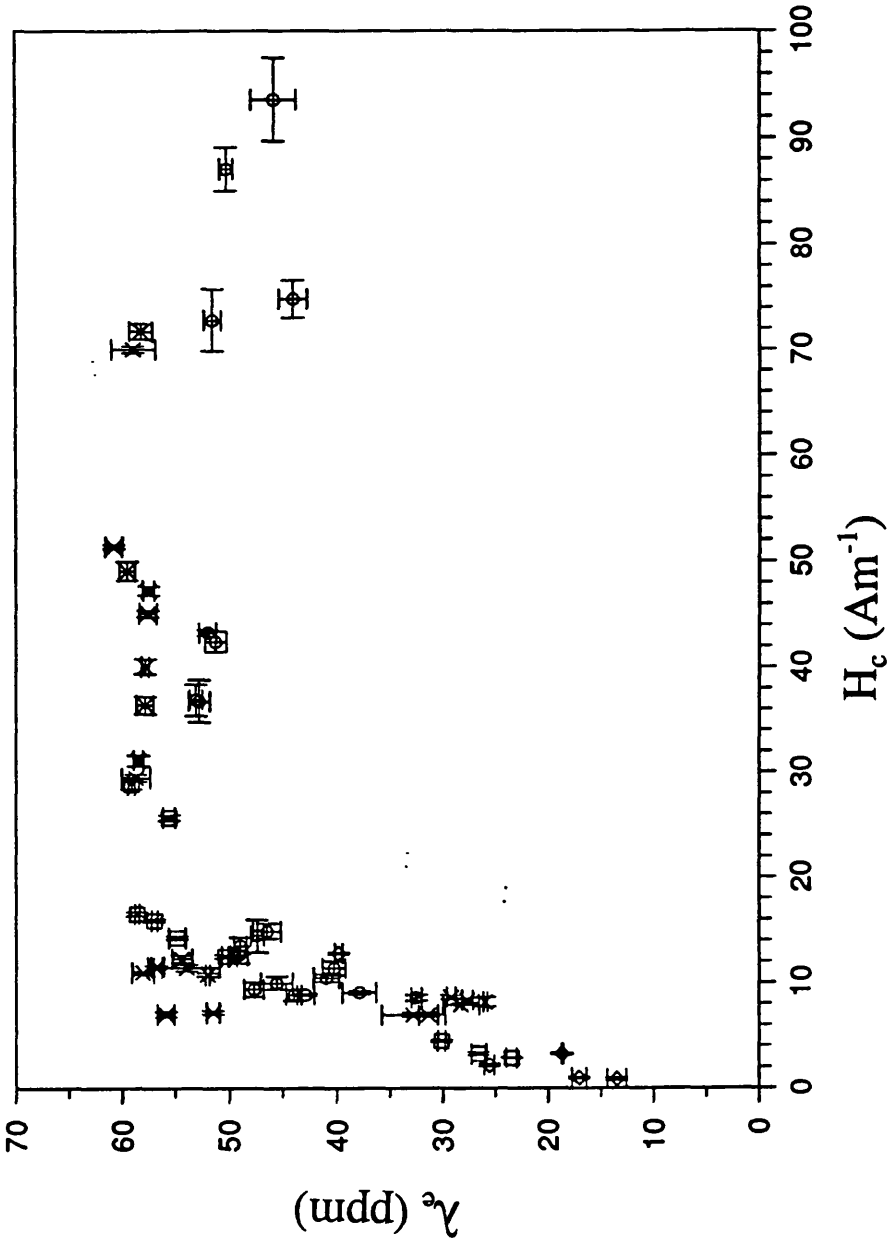

(a)

Figure 6.4: λ_e versus coercivity of partially crystallised a) METGLAS 2605S2 and VAC7505 (Key as figure 6.2) and b) VAC0040.

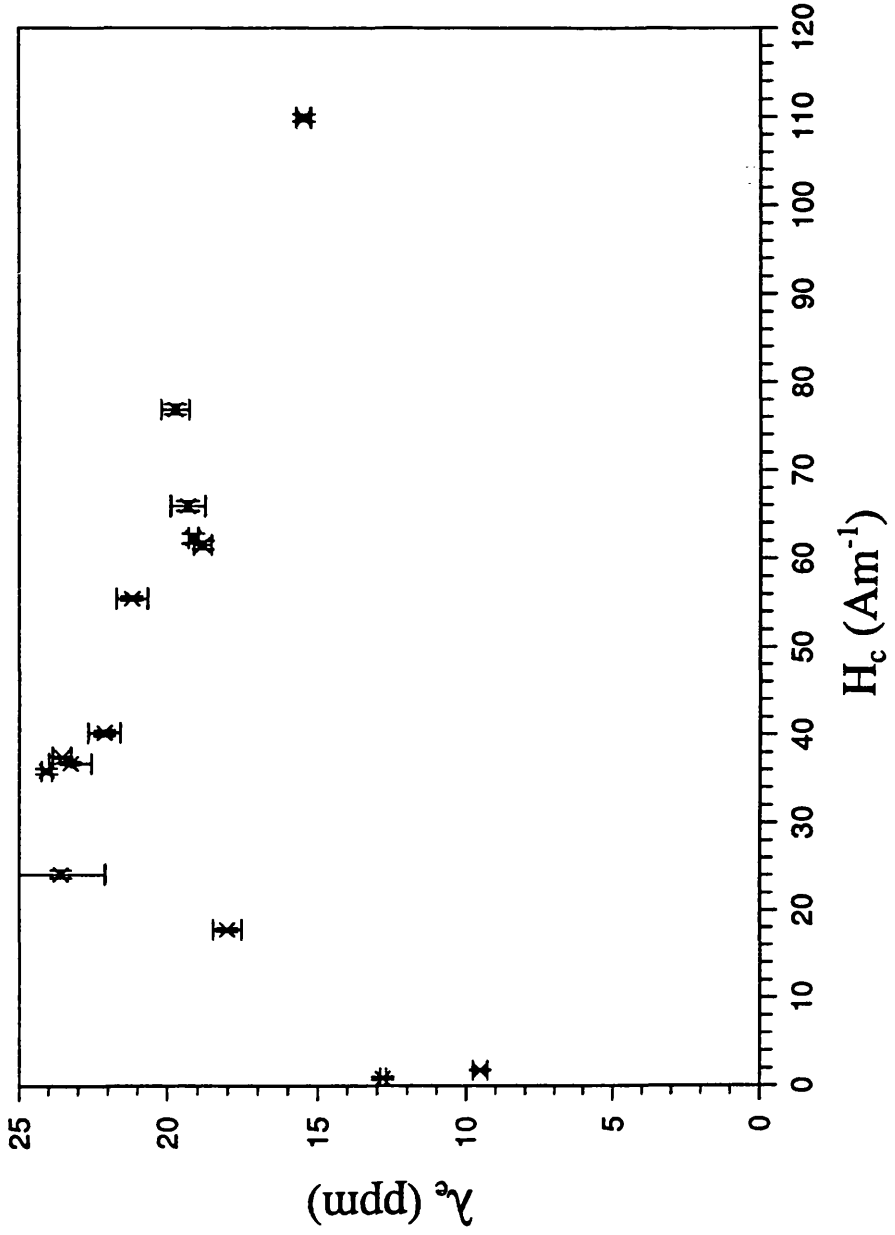
χ_g (ppm)
25
20
15
10
5
0
0
10
20
30
40
50
60
70
80
90
100
110
120
H_c (Am^{-1})

(b)

method that was used by Herzer and Hilzinger [1986]. The samples were mounted vertically in resin and polished down so that a section of the ribbon was visible. The sample was then lightly etched to show up grain boundaries, which could then be examined by optical or electron microscopy. The method of sample preparation is outlined by Lemcke [1989]. Unfortunately no features were seen on the prepared samples (using either metallographic optical microscopes or an SEM) and time did not permit a more extensive examination. A qualitative method of determining the type of crystallisation suggested was to polish thin layers from the surfaces and to measure the size of crystalline X-ray diffraction peaks. If the crystallisation was at the surfaces only, the peaks would disappear upon removal of the surface layers.

6.3 C_q, C_Q and $(d\lambda/dH)_{max}$

The variations of $\left|\frac{d\lambda}{dH}\right|_{max}$ with coercivity are shown in figure 6.5. The METGLAS 2605S2 and VAC7505 data lay on very similar curves, and the VAC0040 data was of a similar form. At low H_c, $\left|\frac{d\lambda}{dH}\right|_{max}$ increased due to the increase in λ_e. When λ_e reached its maximum value, further increase in coercivity, which is directly related to K_u, had the effect of magnetically hardening the material, so decreasing $\left|\frac{d\lambda}{dH}\right|_{max}$. Hence there existed a maximum in $\left|\frac{d\lambda}{dH}\right|_{max}$ which occurred at the stage where λ_e just reached its maximum with respect to H_c. As mentioned, this was where H_c is approximately $10Am^{-1}$ in METGLAS 2605S2 and VAC7505 and $20Am^{-1}$ in VAC0040. The maximum values were approximately $1.1\times10^{-6}A^{-1}m$ in both VAC7505 and METGLAS 2605S2 and $3.0\times10^{-7}A^{-1}m$ in VAC0040. This compared with corresponding values of $2.2\times10^{-6}A^{-1}m$ and $2.8\times10^{-7}A^{-1}m$ from the transverse field annealed data sets. Thus there was little difference between the two in VAC0040, while the values differed by a factor of 2 in METGLAS 2605S2. This difference in alloys was reflected by the anisotropies of the

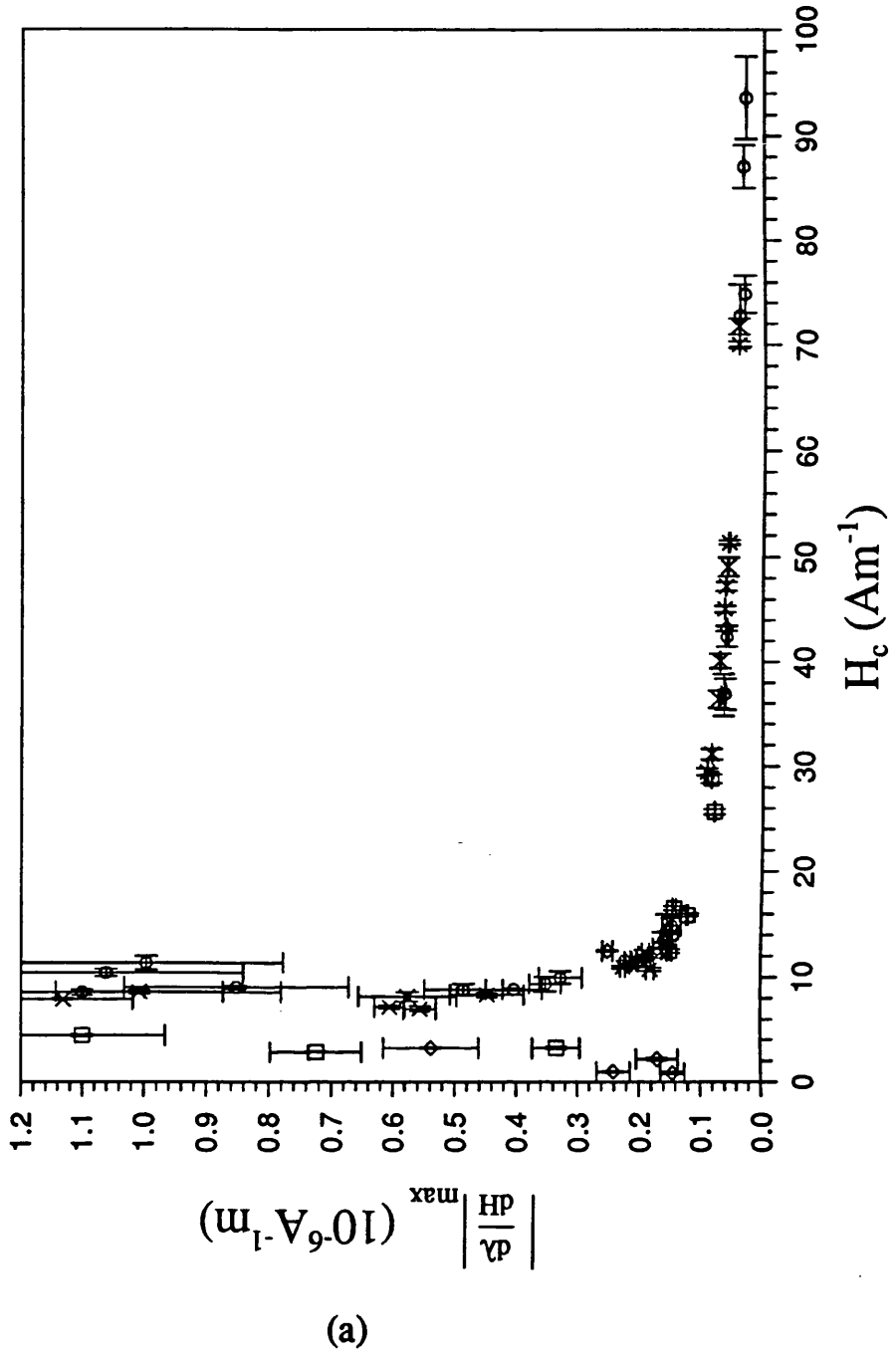

Figure 6.5: dλ/dH(max) versus coercivity of partially crystallised a) METGLAS 2605S2 and VAC7505 (Key as figure 6.2), b) with expanded y-scale, and c) VAC0040.

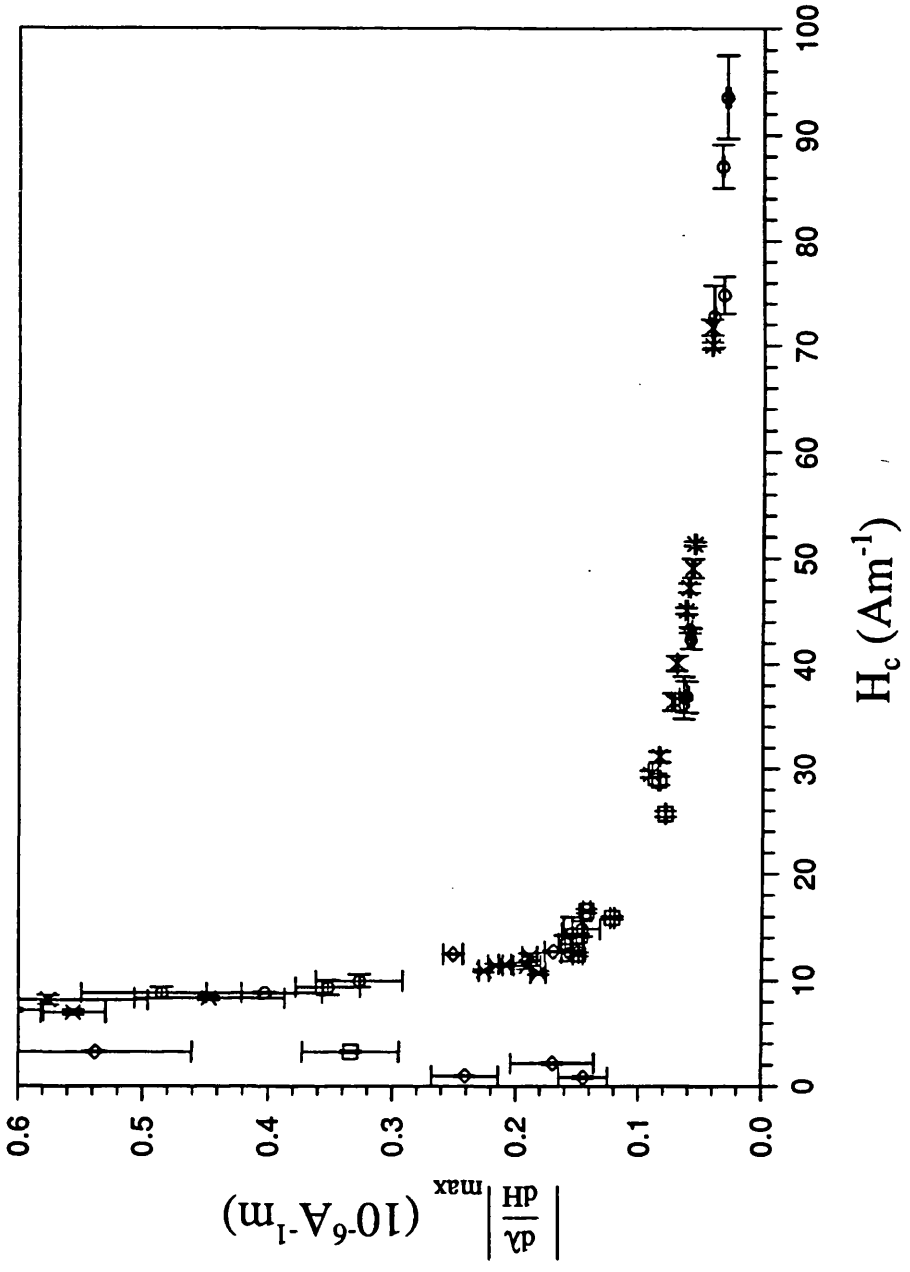
$\left|\frac{d\lambda}{dH}\right|_{max}$ ($10^{-6}A^{-1}m$)
0.0
0.1
0.2
0.3
0.4
0.5
0.6
0
10
20
30
40
50
60
70
80
90
100
H_c (Am^{-1})

(b)

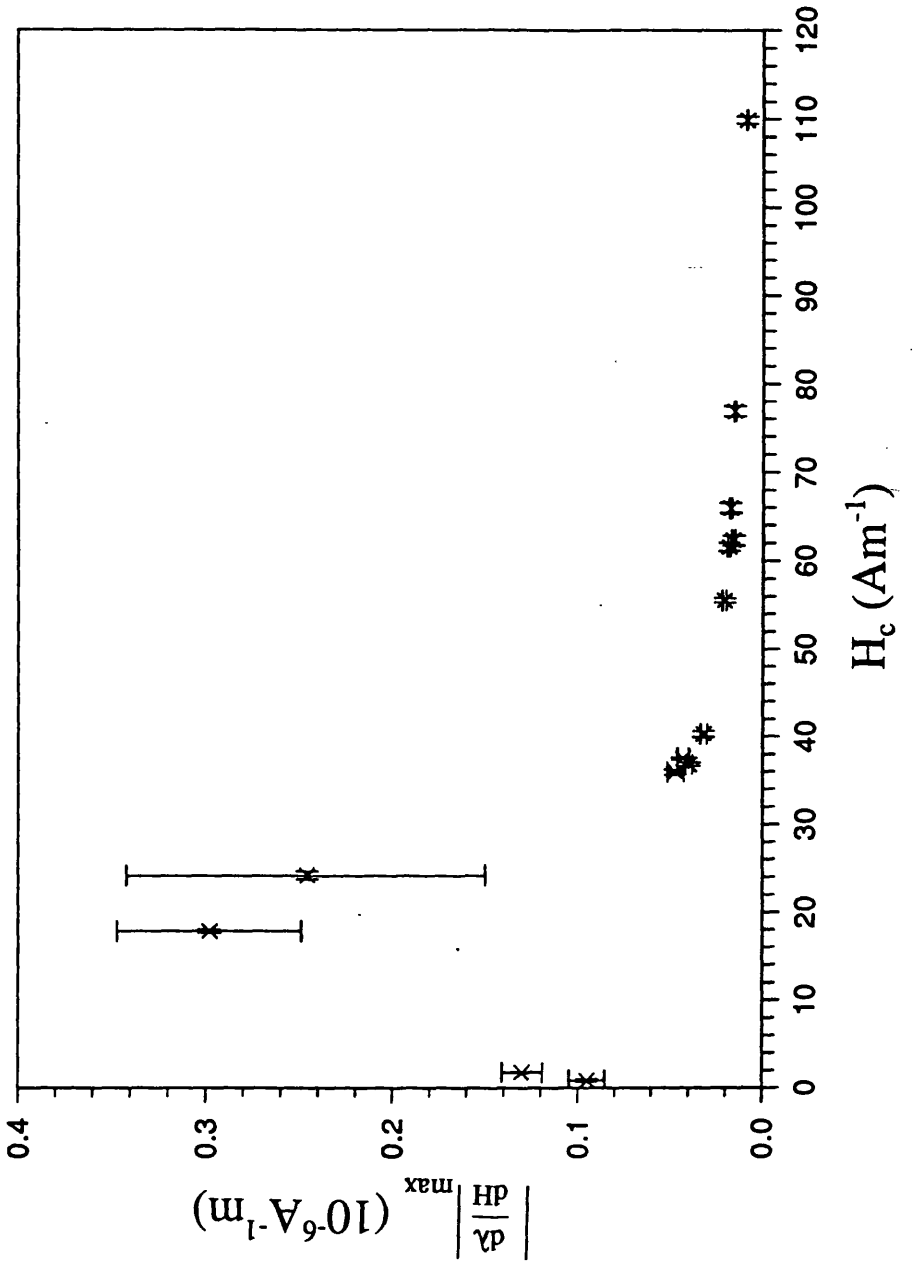
$\left|\frac{d\lambda}{dH}\right|_{max}$ ($10^{-6}A^{-1}m$)
0.0
0.1
0.2
0.3
0.4
0
10
20
30
40
50
60
70
80
90
100
110
120
H_c (Am^{-1})

(c)

materials. In field annealing the one-ion alloy has a lower induced K_u due to the absence of pair ordering. In surface crystallised samples the stress induced K_u is related to the magnetostriction constant, λ_s, and so is greater in the Fe-based alloy, since the stress fields are approximately equivalent in the two ribbons. It happens that K_u is of the same order of magnitude where λ_e approaches its maximum in VAC0040 in the two kinds of heat treatment (i.e. $\approx 100 Am^{-1}$), while it is significantly different in METGLAS 2605S2, with the stress induced K_u far higher than that induced by field anneal.

There was a similar trend in the variation in C_q with H_c for similar reasons. The maxima in the C_q values occurred at similar values of H_c as the $\left|\frac{d\lambda}{dH}\right|_{max}$ data sets. These variations were shown in figure 6.6. The data for samples whose H_c was less than that at which the maxima occurred are not shown. The values of C_q decreased rapidly with decreasing H_c below this point. They are not included, however, because the fit to a quadratic became severely degraded with decreasing H_c in this region. This was also the reason for the large error bars close to the maximum. This is covered further in the discussion of C_Q. The maximum values were approximately $1.3(\pm 0.2)\times 10^{-9} A^{-2}m^2$ and $1.0(\pm 0.4)\times 10^{-8} A^{-2}m^2$ in METGLAS 2605S2 and VAC0040, compared to corresponding values of $1.0(\pm 0.4)\times 10^{-7} A^{-2}m^2$ and $7.1(\pm 2)\times 10^{-9} A^{-2}m^2$ from the transverse field anneal data sets. Again the values were comparable for VAC0040 while the value due to field annealing in METGLAS 2605S2 was significantly higher that due to partial crystallisation.

A disadvantage of C_q of the partially crystallised samples was the large variation over a small range of H_c above the point at which it was at a maximum. Consequently small differences in heat treatment could result in significant variations in C_q, which would reduce consistency in transducers.

The variations of C_Q with H_c are shown in figure 6.7. The data sets of all three alloys follow a similar trend. C_Q increases with increasing λ_e. Further increase in H_c (and

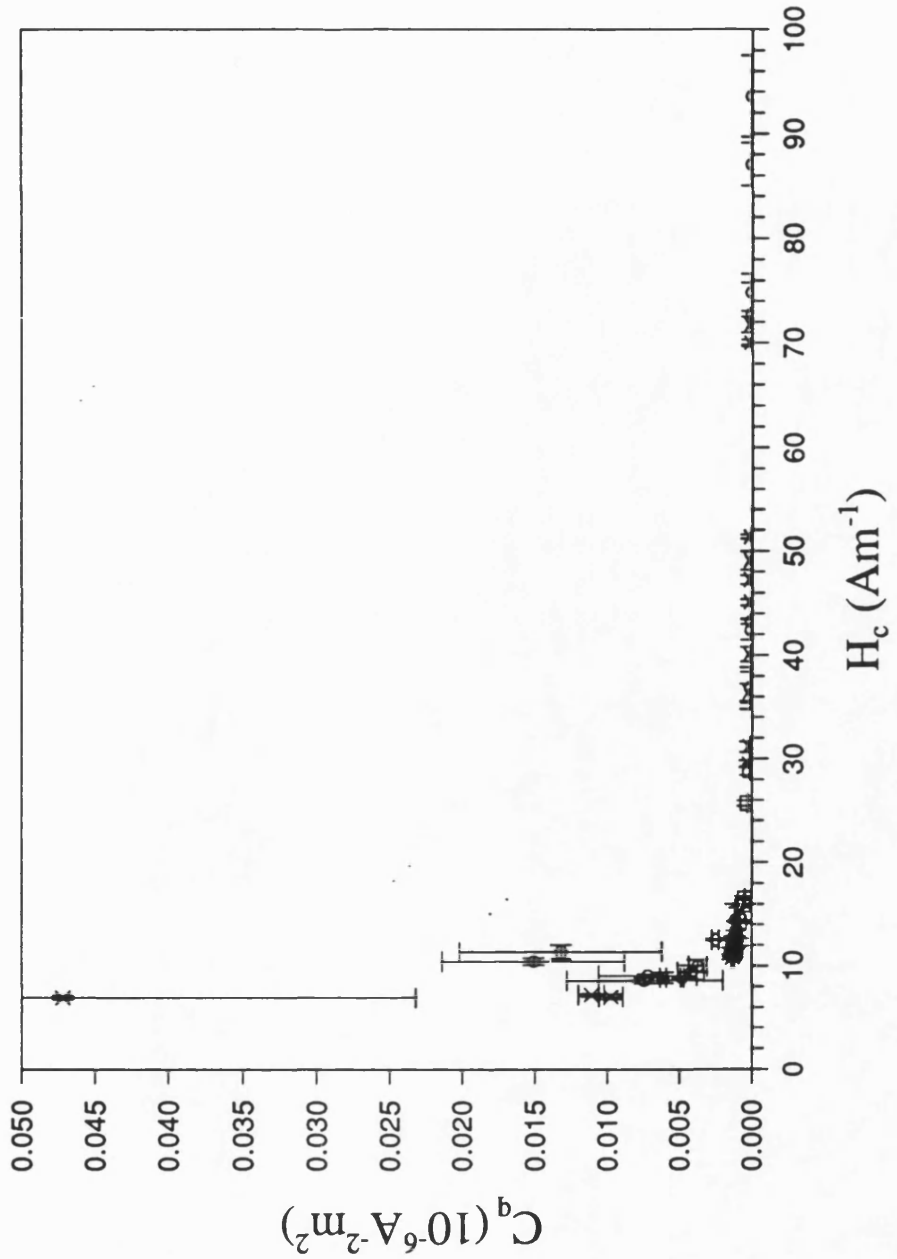

(a)

Figure 6.6: C_q versus coercivity of partially crystallised a) METGLAS 2605S2 and VAC7505 (Key as figure 6.2), b) with expanded y-scale, and c) VAC0040, d) with expanded y-scale.

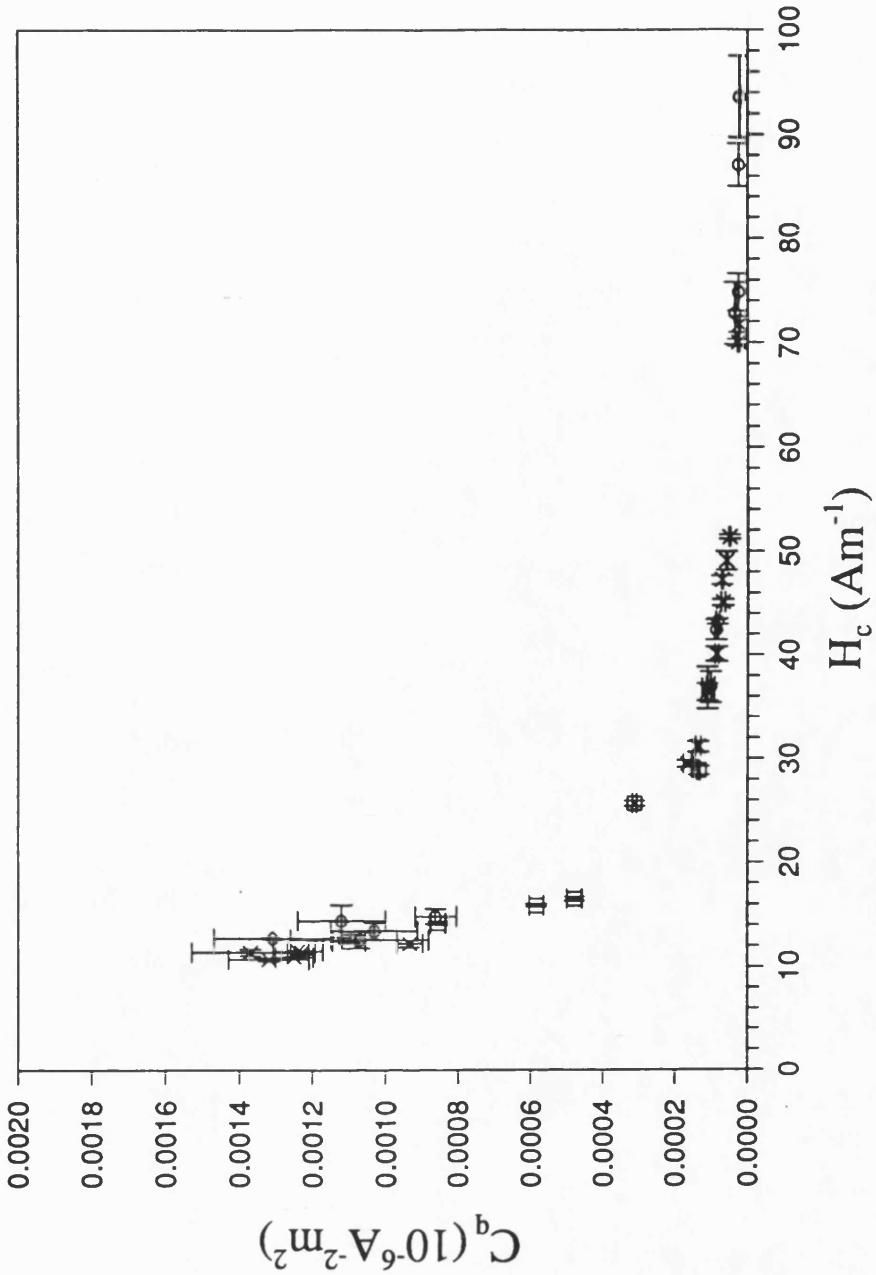
C_q ($10^{-6}A^{-2}m^2$)
0.0020
0.0018
0.0016
0.0014
0.0012
0.0010
0.0008
0.0006
0.0004
0.0002
0.0000
0
10
20
30
40
50
60
70
80
90
100
H_c (Am^{-1})

(b)

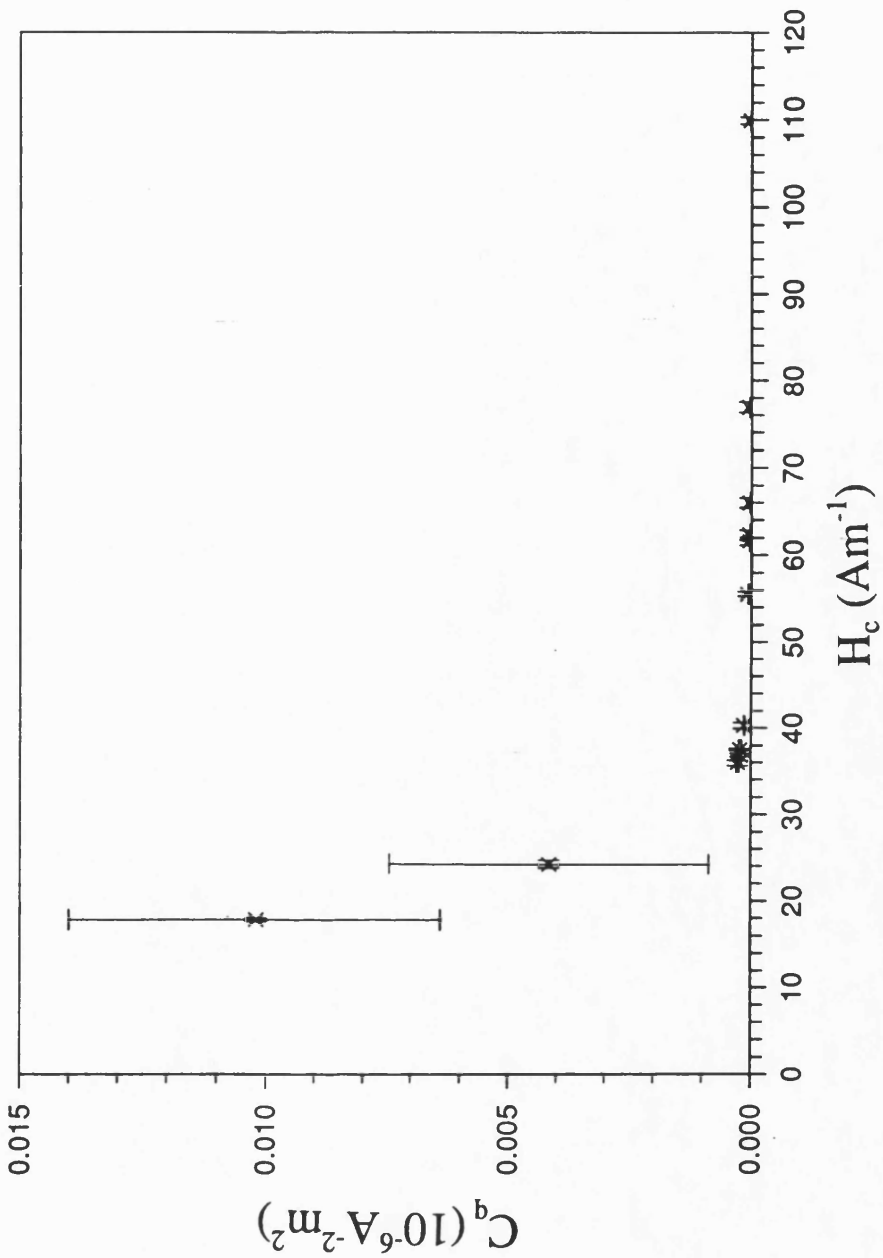
C_q ($10^{-6}A^{-2}m^2$)
0.015
0.010
0.005
0.000
0
10
20
30
40
50
60
70
80
90
100
110
120
H_c (Am^{-1})

(c)

(p)

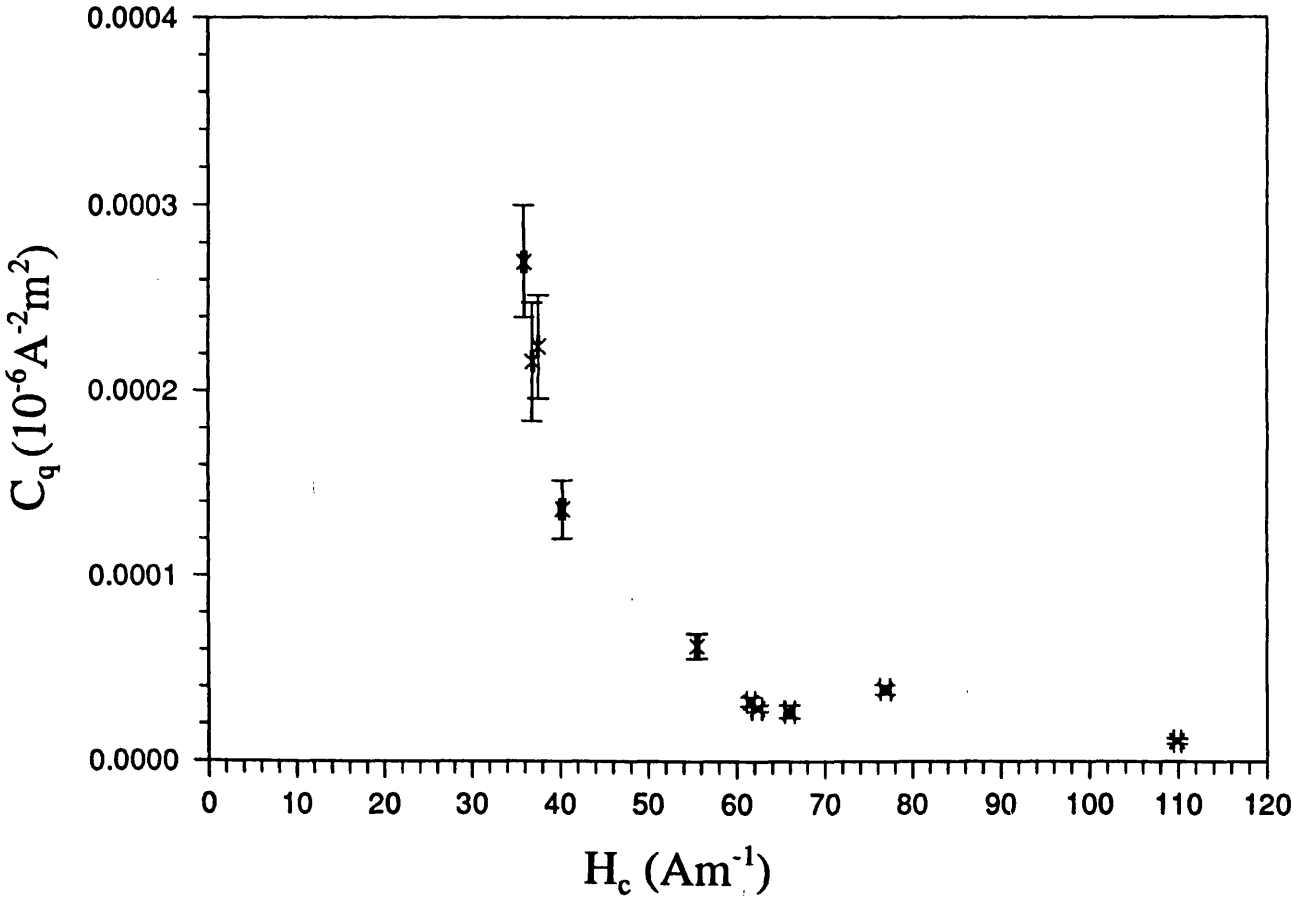
0.0004
0.0003
0.0002
0.0001
0.0000
C_q ($10^{-6}A^{-2}m^2$)
0
10
20
30
40
50
60
70
80
90
100
110
120
H_c (Am^{-1})

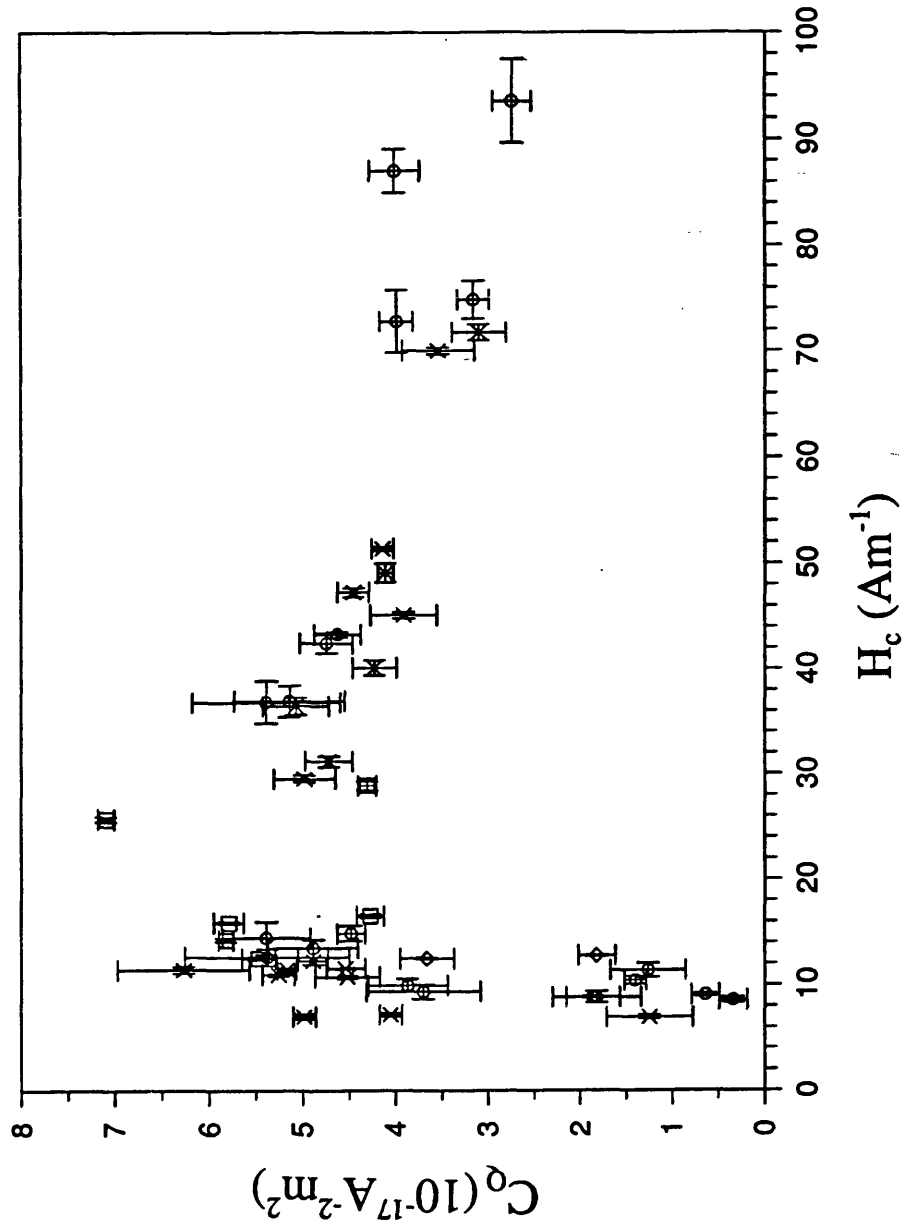

(a)

Figure 6.7: C_Q versus coercivity of partially crystallised a) METGLAS 2605S2 and VAC7505 (Key as figure 6.2) and b) VAC0040.

(q)

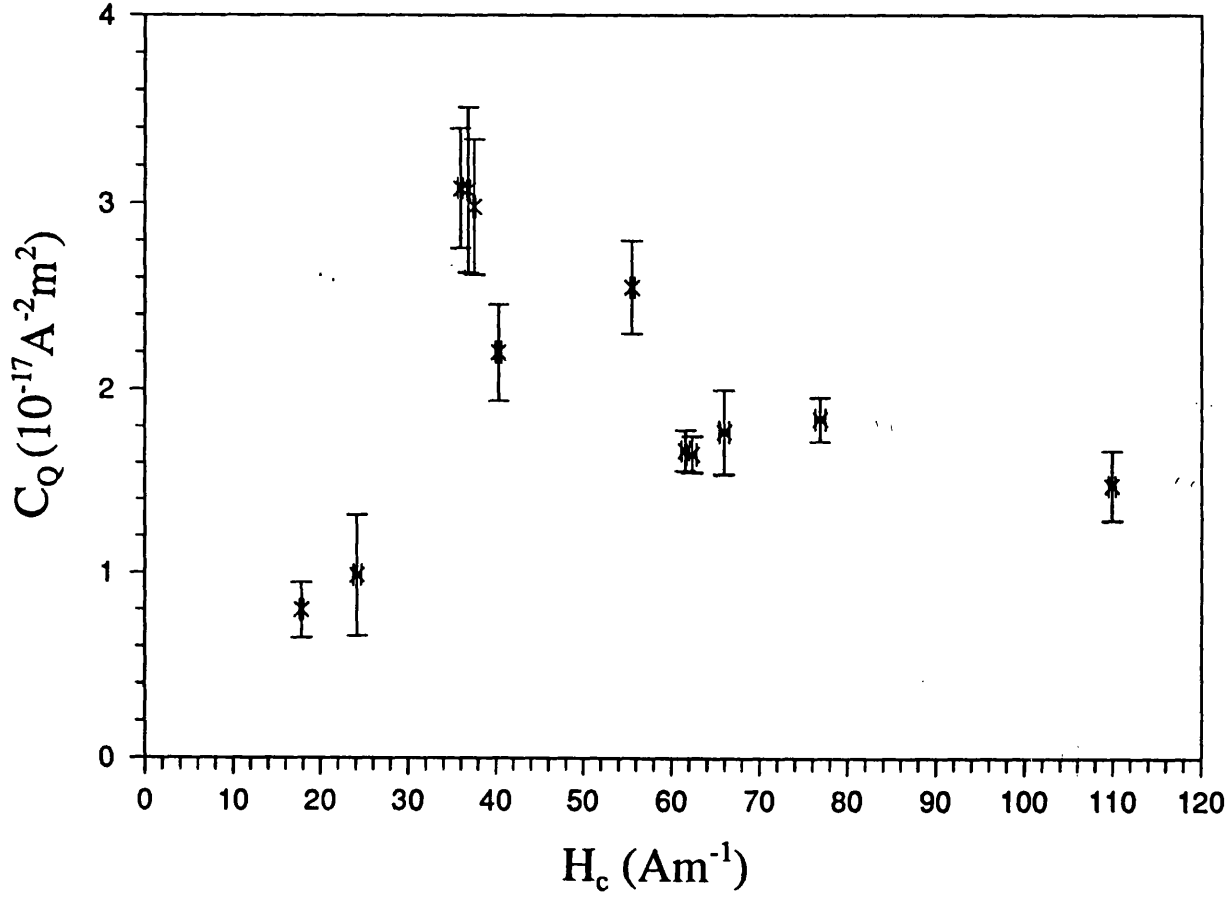

K_u) beyond the stage where λ_e became fully developed resulted in a decrease in C_Q. The maximum values were approximately $6\times10^{-17}A^{-2}m^2$ for METGLAS 2605S2 and VAC7505 and $3\times10^{-17}A^{-2}m^2$ for VAC0040, compared to $6\times10^{-17}A^{-2}m^2$ for both transverse field annealed METGLAS 2605S2 and VAC0040.

As with the λ-H data, the fit of the λ-M to a quadratic was poor at low H_c and improved with increasing crystallisation. Figure 6.8 shows typical λ-M plots of METGLAS 2605S2 and VAC0040 for various anneal times at constant values of T_a. At low H_c, where the samples are close to their as cast condition, the λ-M plots were flat over a wide range of M. Since magnetostriction occurs due to moment rotation only, it was inferred that the magnetisation proceeded mainly by way of domain wall movement rather than moment rotation, resulting in little magnetostrictive strain. Some strain occurred close to saturation due to rotation of the magnetisation once the domains had largely merged. As the degree of crystallisation increased, the perpendicular uniaxial anisotropy became stronger, causing greater alignment of moments in that direction, and so a greater degree of moment rotation. Thus the λ-M plots steadily developed from a fairly square shape with low λ_e to a quadratic with $\lambda_e=3\lambda_s/2$. The stage at which the plots became close to quadratic coincided with the full development of λ_e, where magnetisation became dominated by moment rotation. This therefore also coincided with the stage at which C_Q, C_q and $\left|\frac{d\lambda}{dI}\right|_{max}$ were approximately at their maximum.

6.4 Discussion

Optimum magnetostrictive response occurred at the point where λ_e reached its maximum value. Further crystallisation effected a decrease in the response due to increased K_u. Since magnetostriction occurs purely by moment rotation, it could be inferred that this stage was where the moments lay in the easy axis to a high degree. The

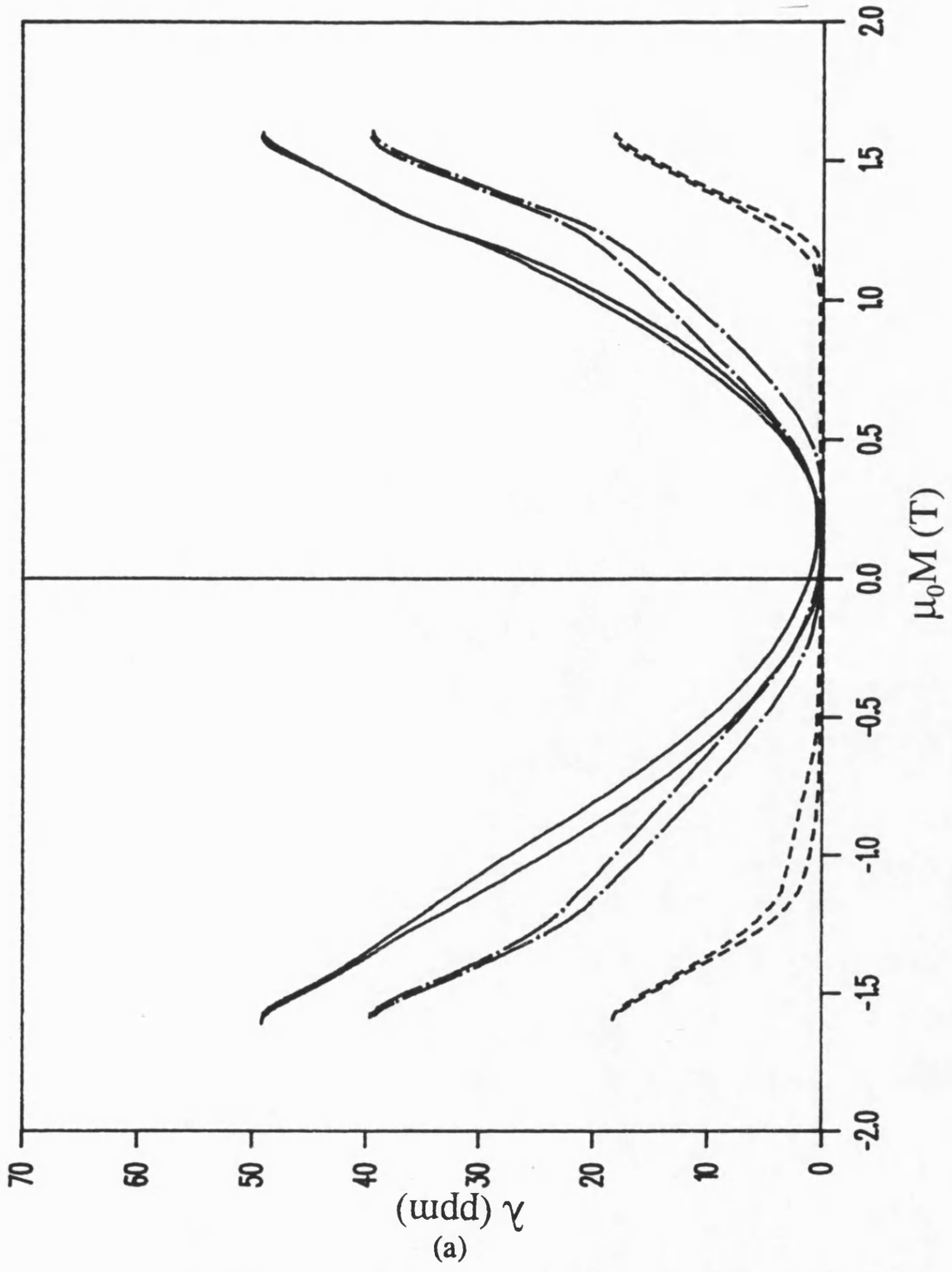

(a)

Figure 6.8a-e: Typical λ-M loops of partially crystallised samples of METGLAS 2605S2 and VAC0040.

METGLAS 2605S2; a) T_a=400°C (t_a=60mins - - - -, 360mins — · — and ———), b) T_a=425°C, (t_a=60mins - - - -, 180mins ———, 240mins — · —, 360mins — - —), c) T_a=450°C (t_a=20mins - - - -, 30mins ——— , 45mins —·—, 90mins — - —, 240mins — - - —).

(b)

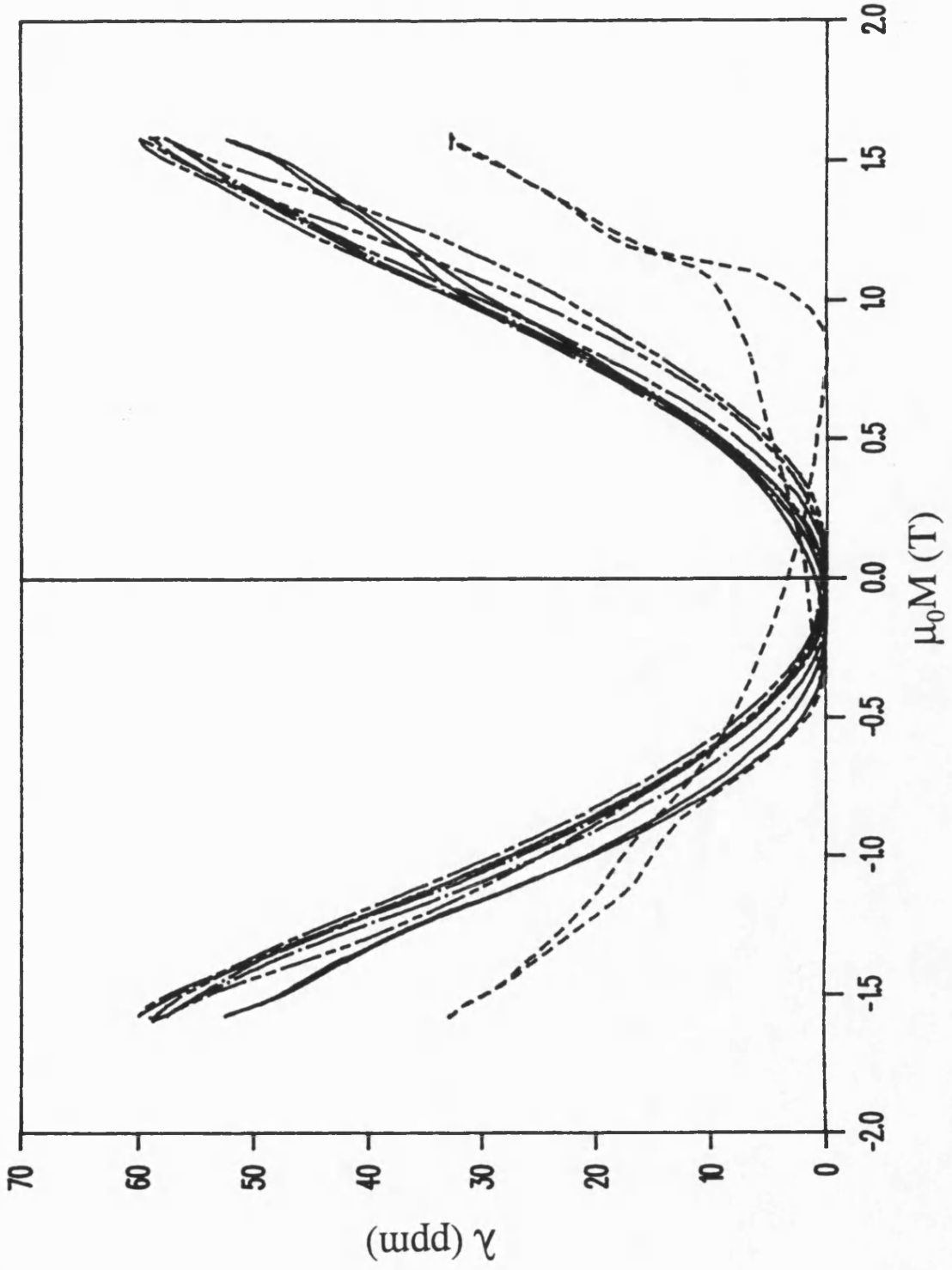

(c)

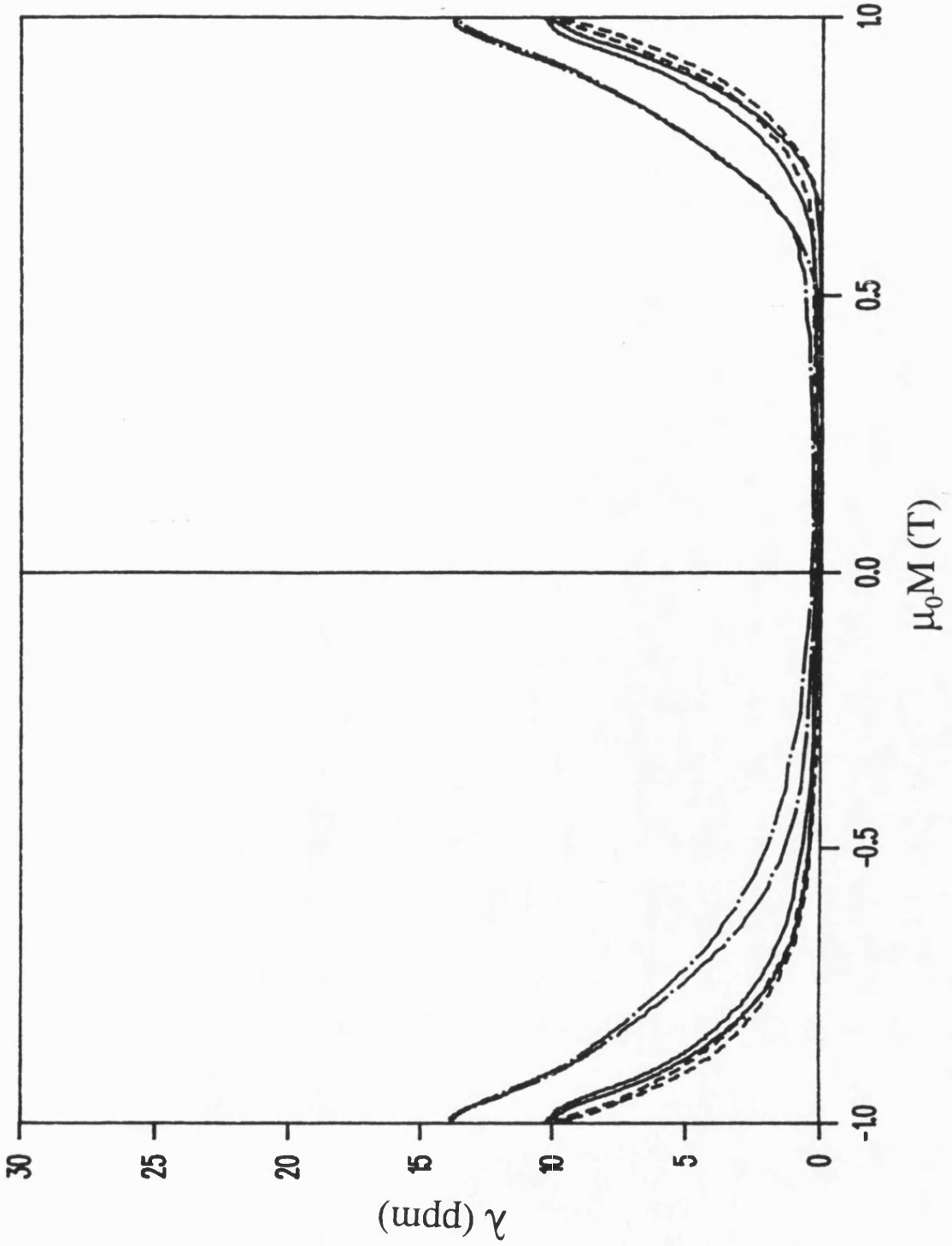

(d)

VAC0040; d) T_a=350°C (t_a=120mins- - - -, 360mins —— and —·—), e) T_a=380°C (t_a=30mins - - - -and —— , 60mins —·—, 90mins— - —, 105mins— - - —).

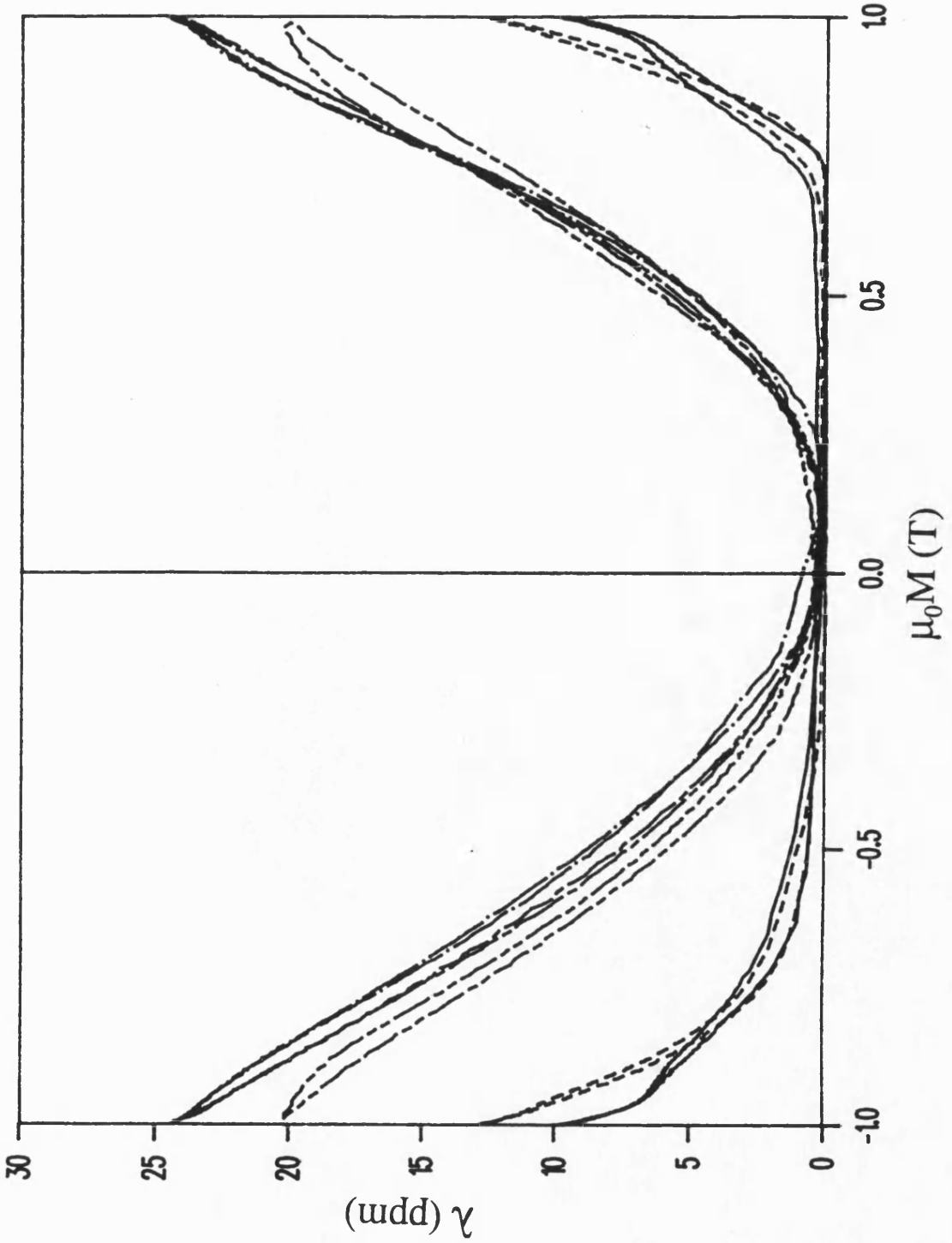

(e)

anisotropy causing the moment alignment was induced by tensile stress between the surfaces as a result of surface crystallisation.

Therefore the optimum parameters for transducer applications were obtained by introducing sufficient surface crystallisation to cause a uniform stress field which induced a perpendicular anisotropy just great enough to rotate moments into that direction to high degree, but before further crystallisation caused an increase in K_u, so decreasing the magnetostrictive response. This anisotropy was of the order of $10^2 Am^{-1}$ in the alloys studied. Care would have to be taken to ensure that the heat treatments on different samples were as consistent as possible because of the sensitivity of the magnetostrictive response to H_c and so to the extent of crystallisation at this stage.

The sensitivity and the fit of the data to the moment rotation model improved with a certain amount of additional crystallisation. It was thought that additional crystallisation, which was found to be predominantly in the form of additional crystallite nucleation (rather than growth) had the effect of increasing the uniformity of the surface crystallised layer, and the fraction of crystallisation within this layer. This would have the effect of making the interfaces between the amorphous phase in the bulk of the material and the crystallised layers more uniform and distinct. This enhanced the stress field between surfaces and so decreased the dispersion in the direction and magnitude of the anisotropy. The improvement in the readings were indicated by the collapse in the error bars and sample to sample scatter seen in the C_q, C_Q and $\left|\frac{d\lambda}{dH}\right|_{max}$ versus H_c plots, as well as a slight improvement in the shape and consistency of the λ-M plots. The resulting increase in K_u, however, resulted in a decrease in the response parameters by a factor of approximately 5-10.

The maximum values of C_q and $\left|\frac{d\lambda}{dI}\right|_{max}$ of the transverse field annealed Fe-based samples were greater than those of the partially crystallised samples, by factors of approximately eight and two respectively. The values of the Fe-Ni based alloy were

comparable. Since the values of λ_e(max) are approximately the same for the field annealed and partially crystallised samples, and M_s is not altered by the heat treatments, it was to be expected (from equation 2.21) that C_Q would be comparable. This was found to be the case for the Fe-based alloys, but was found to be low in the partially crystallised Fe-Ni based alloy. This was partly due to suppressed λ_e due to the mechanical loading and lower λ_e of the crystalline layers, as mentioned above. Another reason was thought to be that there was an appreciable contribution to magnetisation from domain wall movement, which generated no magnetostrictive strain, at low M.

Crystallisation generally occurs more readily in ribbons where some degree of nucleation of crystallites has occurred than in as cast material. A consequence of this is that the maximum operating temperature of a partially crystallised transducer must be lower than a purely amorphous one to ensure a long operating life. Allied-Signal recommend an operating temperature of the as cast material of less than 125°C for the alloys discussed here and Vacuumschmeltze recommend less than 200°C and 120°C for VAC0040 and VAC7505. The maximum operating temperatures for partially crystalline ribbons are therefore lower than this, although they have not been quantified.

6.5 Nanocrystallised Samples

A brief study was made on the effect of the introduction of nanocrystallisation on the magnetostriction as part of an investigation led by J. Vincent at GEC Hirst Research Labs. An introduction to nanocrystallisation is given in the following subsection, followed by experimental details and results.

6.5.1 Introduction

Nanocrystalline Fe-based alloys were first put forward by Yoshizawa *et al* [1988] as a class of material with potential in many applications such as transformers. Nanocrystalline materials contain polycrystalline structures with very small grain diameters, of the order of 10-300nm. They have been produced from Fe-based ferromagnetic amorphous alloys containing a few atomic percent Cu and an additive such as Nb, Mo, W or Ta. Crystallite nucleation during anneal is caused by the segregation of Cu and Fe, leading to Fe-Si and Fe rich regions. Crystal growth is suppressed by the Cu-Nb-B rich regions surrounding the crystallites, which are difficult to crystallise. This results in a polycrystalline structure with small grain size and random texture, with a proportionately high volume of an amorphous phase at the grain boundaries. In studies of $Fe_{73.5}Cu_1Nb_3Si_{13.5}B_9$ there were found to be two crystalline phases. The main one was α-FeSi which occupied a volume fraction of approximately 70-90%. At higher anneal temperatures (>600°C) a second crystalline phase, thought to be FeNbB, formed [Herzer 1989], while Müller *et al* [1991] identified another phase as Fe_2B in similar alloys. The fractional volume of the amorphous phase has been reported to be as high as 50% [Závêta 1991].

Herzer suggested that the very soft magnetic materials could be explained using the random anisotropy model of Alben *et al* [1978]. The randomly orientated grains are so small that they are of the same order of magnitude as the correlation length of the ferromagnetic exchange interactions, tending to align moments. This suppresses the effect of the crystal anisotropy within the grains, causing an effective anisotropy averaged over a number of grains, and hence partial cancelling of K_u. This, together with the existence of the amorphous phase with the structure allows the good soft magnetic parameters to be maintained after nanocrystallisation.

Yoshizawa *et al* [1988] found that the magnetostriction constant of the alloy decreased considerably upon nanocrystallisation. Herzer stated that "the high silicon content of the constituent α-FeSi grains leads to low or vanishing λ_s". Hernando *et al* [1991] attributed it to the different phases having different values of λ_s leading to a vanishing macroscopic value for certain volume fractions of the phases.

This then leads to material with soft magnetic parameters and λ_s. It has higher susceptibilities than Permalloys and other polycrystalline material and has the advantage of cost over Co-rich near zero magnetostriction glasses. Other advantages include high M_s and resistivity and good thermal stability, making it very useful for soft magnetic applications.

6.5.2 Experimental Details

The alloy used in this study was $Fe_{79}Si_{13}B_6Cu_1Nb_1$. The ribbon was melt spun and the samples were annealed at GEC Hirst. The sample dimensions were 50×10×0.025mm. Six samples were supplied; two as cast, one annealed at 560°C, two at 590°C, and one at 620°C. The anneal time was 60 minutes in each case. One of the as cast ribbons (termed sample "a") was coated in an etch resist which had not been fully removed. The coating stressed the sample so that it was not flat across its width and did not fit into a sample holder. λ_e was measured on the other as cast sample, but was not saturated by the maximum applied field. Therefore these samples were stress relieved for 60 minutes at 450°C, making them magnetically softer and flattening the coated sample.

λ_e was measured on the stress relieved (as cast) samples as described in chapter 3. However, the values of the annealed samples were too low to obtain accurate readings using this method. Therefore a similar program called "LOWLAM", written by P.T. Squire, was utilised. This worked by measuring the sample strain while stepping the

applied field from zero to maximum an (operator specified) number of times. The resulting strain reading was a square function superposed on the thermal drift. The steps occurred too fast for drift to have a significant effect, so λ_e was calculated simply from the mean of the step size.

The values of H_c, which was used to indicate the extent of crystallisation, were calculated as described in chapter 3 (using straight line fits of the M-H data near M=0 over 3,5,7... points) for the annealed samples. This was not suitable for the as cast samples because the M-H loops were subject to large Barkhausen jumps near M=0, and so the plots were not linear. The H_c in these cases was simply calculated as the difference between the zero crossing points of straight lines drawn between the data points either side of the M=0 axis on each branch of the loop. This value was in close agreement with the first method on the annealed samples.

6.5.3 Results

The measured values of H_c and λ_e are shown in table 6.2 and in figures 6.9 and 6.10. Also shown in the figure is data on $Fe_{73.5}Si_{13.5}B_9Cu_1Nb_3$ from Yoshizawa *et al* [1988]. The two data sets appear to be in good agreement, despite slight compositional differences. This fully illustrates the collapse in λ_s.

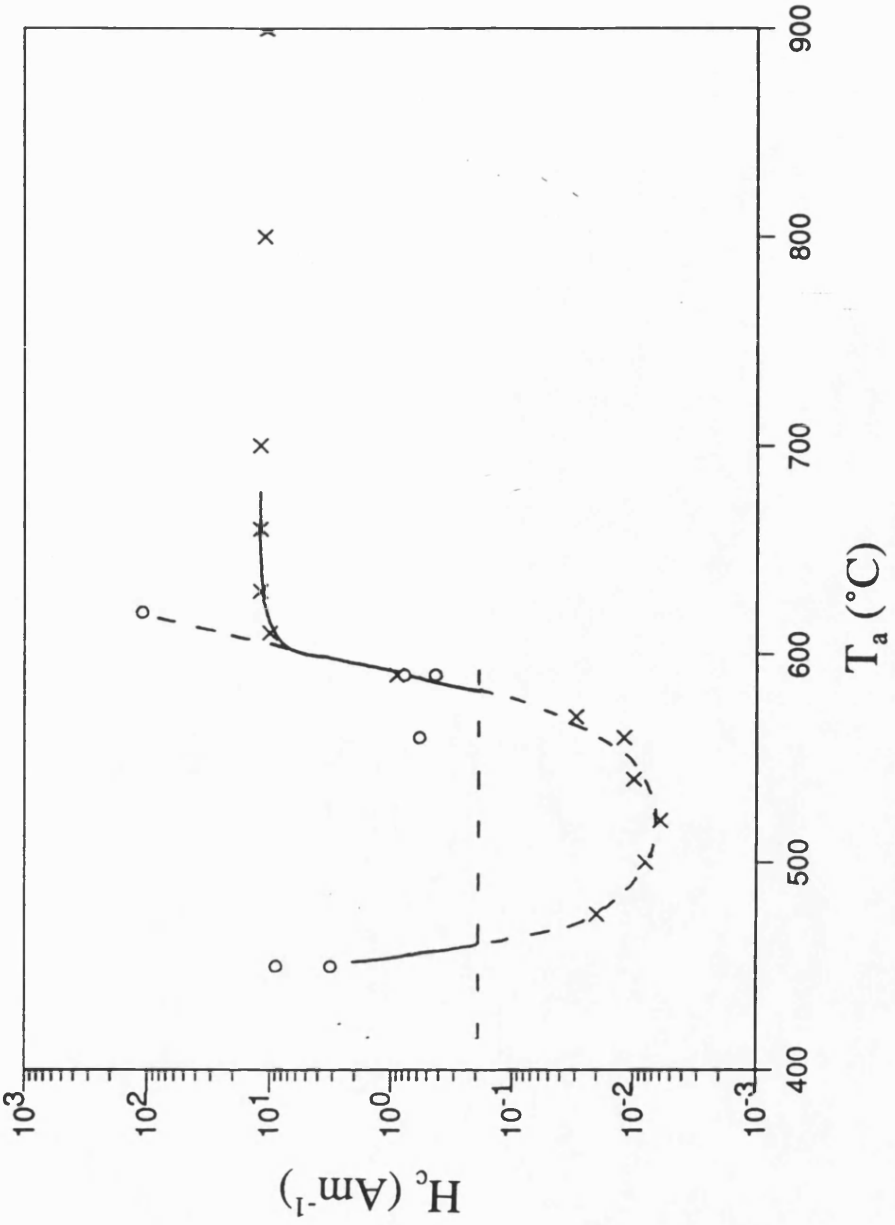

Figure 6.9: Coercivity versus anneal temperature of $Fe_{79}Si_{13}B_6Cu_1Nb_1$. This data is compared with corresponding data for $Fe_{73.5}Si_{13.5}B_9Cu_1Nb_1$ (from Herzer [1990]). Anneal time was 60 minutes. The dotted line represents the approximate limit of resolution of the magnetisation measurement rig. The data is in agreement with that of Herzer inasmuch as the coercivity increases rapidly with anneal temperature as T_a>600°C due crystallisation of the amorphous intergranular phase. (o - $Fe_{79}Si_{13}B_6Cu_1Nb_1$, × - $Fe_{73.5}Si_{13.5}B_9Cu_1Nb_1$, from Herzer [1989])

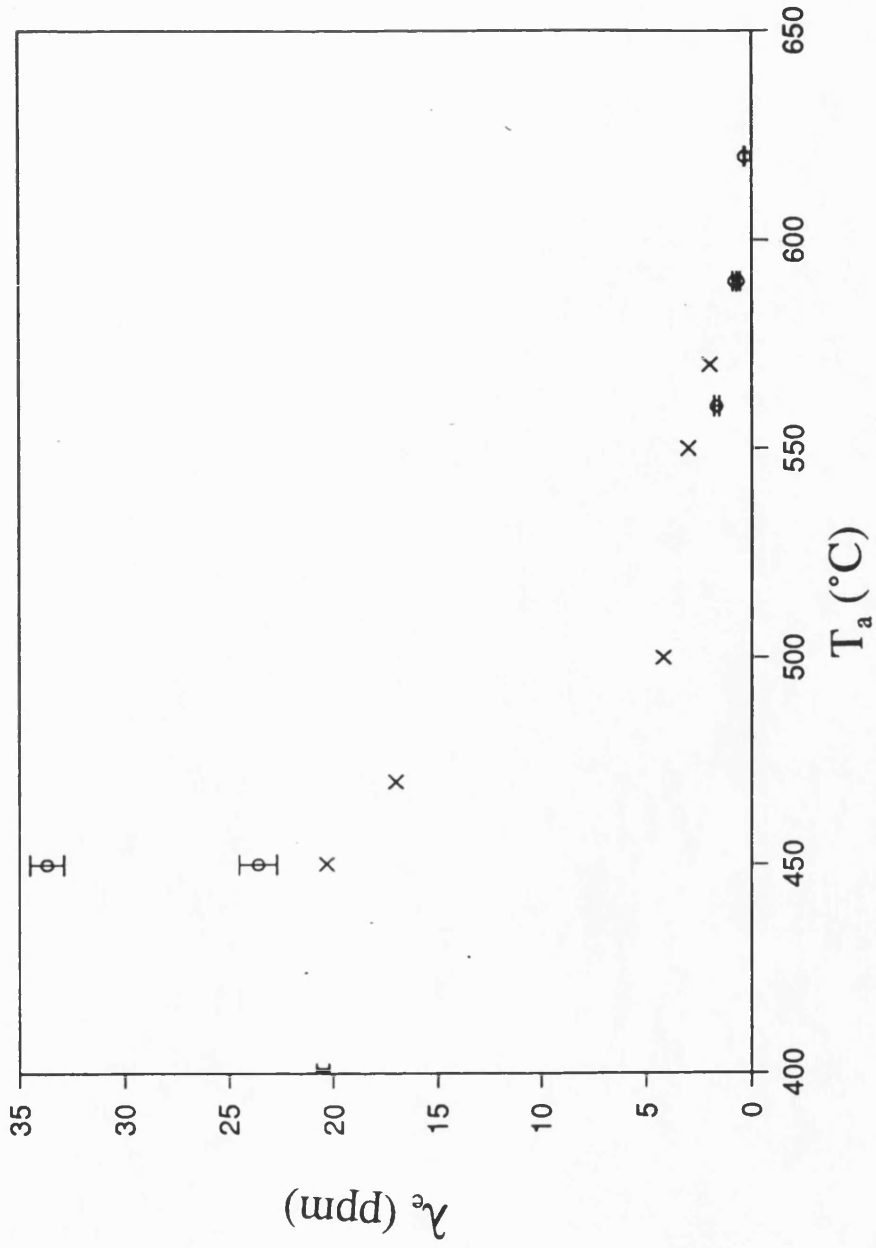

Figure 6.10: Engineering magnetostriction versus anneal temperature $Fe_{79}Si_{13}B_6Cu_1Nb_1$. This data is compared with corresponding data for $Fe_{73.5}Si_{13.5}B_9Cu_1Nb_1$ (from Yoshizawa *et al* [1988]), t_a=60 mins. Both sets of data illustrate the eduction of λ_e with the onset of nanocrystallisation. (o - $Fe_{79}Si_{13}B_6Cu_1Nb_1$, the datum point on the ordinate represents the value of the as cast sample, × - $Fe_{73.5}Si_{13.5}B_9Cu_1Nb_1$, from Yoshizawa *et al* [1988])

Anneal Temperature (°C)	λ_e (ppm)	H_c (Am^{-1})
As cast (a)		6.45 (0.26)
(b)	20.5 (0.3)	4.91 (0.29)
450 (a)	33.7 (0.8)	8.90 (0.14)
(b)	23.6 (0.9)	3.16 (0.12)
560	1.66 (0.12)	0.58 (0.09)
590 (a)	0.62 (0.07)	0.78 (0.07)
(b)	0.82 (0.09)	0.43 (0.08)
620	0.34 (0.03)	110.1 (0.2)

Table 6.2: λ_e and H_c for different T_a of nanocrystallisation anneals. The magnetostriction of the as cast samples were difficult to measure because they were not flat. The slight increase in λ_e of the "b" sample upon annealed at 450°C was due to the fact that saturation was not fully achieved in the as cast sample, but was when stress relieved. The increase in H_c of the as cast "a" sample after anneal at 450°C was thought to be due to the film of etch resist that had not been fully removed (see section 6.5.2)

The variation in H_c, in figure 6.9, is compared with similar data on the alloy mentioned above, from Herzer [1989]. The significant increase in H_c in the sample annealed at 620°C is thought to arise from the crystallisation of the NbB-rich phase to form some crystalline phase of FeNbB.

These results show the similarity between the alloy studied here and that by Yoshizawa *et al* and Herzer, and confirm the collapse of λ_s to near zero. Work is continuing in this area by J. Vincent and co-workers.

7 Discussion and Conclusions

7.1 Introduction

The results of each aspect of this project are summarised, and the conclusions arising from them are discussed. Each aspect of the study is considered in a separate section.

7.2 Comparison of Measured Values of λ_e and K_u

The value of λ_s for each alloy was obtained from the value of λ_e in material with fully developed transverse uniaxial anisotropy, where $\lambda_s=2\lambda_e/3$. These values are given in table 7.1.

Alloy	λ_s (ppm)
METGLAS 2605S2	41 (±0.7)
METGLAS 2605SC	41 (±0.7)
METGLAS 2826MB	16 (±0.5)
VAC0040	20 (±0.5)

Table 7.1: Measured values of λ_s.

These values are consistently higher than corresponding measurements on similar alloys using a variety of methods reviewed in chapter 2. Many of these measurements involved some degree of bonding of the sample, such as the strain gauge method where a strain gauge was bonded to the surface using an epoxy. One method involved no bonding but was calibrated using results obtained using strain gauges. Some methods

obtained λ_s from permeability measurements in ac varying applied fields. However, the permeability is less at ac frequencies than at dc because of the eddy currents have a greater effect on rapidly moving domain walls. Other measurements were taken on as cast ribbons, or stress relieved material.

The magnetic state of the material is far more consistent and analysed more easily when a uniaxial anisotropy is induced in it, so that can be clearly described by the Livingston or Squire models. It is therefore recommended that magnetostriction measurements are made on samples in this state.

A summary of some of these measurements is given in table 7.2.

It is thought that the reason for the discrepancies is reflected by the fact that the optical fibre dilatometer was a quasi-dc, direct strain measurement system that involved no loading of the sample. The only other system which fit this description was the tunneling-tip strain measurement detector [Brizzolara and Colton 1990]. A comparison of λ-H measurements on METGLAS 2605SC is discussed in chapter 2 and indicates good agreement between the two systems.

There was good agreement between the measured values of K_u of $Fe_{40}Ni_{40}B_{20}$ in this study and those of Luborsky and Walter [1977]. Also, the value of K_u of the METGLAS 2605SC $\theta=90°$ sample was found to be $34Jm^{-3}$, compared with $38Jm^{-3}$ obtained by Spano *et al* [1982] on the same alloy with an almost identical transverse field anneal. This, together with log time development of K_u of the field annealed material, gave added confidence to the method of calculating K_u from χ_0.

Alloy	λ_s ppm	Method of measurement	Remarks	Ref.
METGLAS 2605S2	27	Strain gauge	Manufacturer's data	Allied-Signal
METGLAS 2605S2	27	Piezoelectric transducer.	Transverse field annealed 400°C 2hours. Calibrated using strain gauge results.	Datta *et al* 1984
METGLAS 2605S2	24	Fibre-optic magnetometer transducer.	λ measured w.r.t. T_a and t_a. Involves bonding onto the sample.	Bucholtz *et al* 1986
METGLAS 2605S2	32	Measurement of permeability at constant stress and strain.	Heat treated near T_c. Freq.=10kHz.	Clark and Wun-Fogle 1989
METGLAS 2605SC	29.3	As above.	As above.	As above
METGLAS 2605SC	30	Strain gauge	Manufacturer's data	Allied-Signal
METGLAS 2605SC	27	Integrating magnetometer. Measurement of susceptibility w.r.t. stress.	T.F.A. 389°C 10min. Not well developed K_u (38J/m), similar anneal and K_u to that in this study.	Spano *et al* 1982
METGLAS 2605SC	28	Torsion-angle measurements	Transversely field annealed	Liniers *et al* 1985
METGLAS 2605SC	22	Torsion-angle measurements	Stress relieved 320°C 1 hour.	Núñez de V illavicencio *et al* 1986
METGLAS 2826MB	12	Strain gauge	Manufacturer's data	Allied-Signal
$Fe_{40}Ni_{40}B_{20}$	12	Strain gauge.	Same composition as VAC0040. Direct from the melt. Involves bonding onto the sample.	O'Handley 1977
$Fe_{40}Ni_{40}B_{20}$	13	Torsion-angle measurements	Stress relieved 320°C 1 hour.	Núñez de V illavicencio *et al* 1986

METGLAS 2605 ($Fe_{80}B_{20}$)	33	Piezoelectric transducer.	Calibrated using strain gauge results.	Datta *et al* 1984
METGLAS 2605	40	SAMR.	stress relieved 250°C 1 hour.	Narita *et al* 1979
METGLAS 2605	32	strain gauge.	Direct from the melt. Involves bonding onto the sample.	O'Handley 1977
$Fe_{80}B_{20}$	39	3-terminal capacitance	Direct from the melt.	Ishio and Kadowaki 1989
$Fe_{80}B_{20}$	39	3-terminal capacitance	Direct from the melt.	Tsuya *et al* 1978
$Fe_{80}B_{20}$	46	As above	Annealed 300°C for 3 hours.	As above
METGLAS 2826 ($Fe_{40}Ni_{40}P_{14}B_6$)	12.3	SAMR.		Narita *et al* 1980
METGLAS 2826	10	SAMR.	Stress relieved 300° 1.5 hours.	Sanchez *et al* 1988

Table 7.2: Comparison of some previously reported measurements of λ_s of alloys used in this study, or similar.

7.3 Magnetisation Rotation

The models used to predict the behaviour of the magnetoelastic parameters of metallic glass ribbons proposed by Livingston [1982] and Squire [1990] are both based on the premise that magnetisation proceeds by moment rotation alone in material with transverse uniaxial anisotropy. This has been shown in this study to be the case to a very high degree in the field annealed samples measured. Evidence for this arises from the following:

a) The magnetisation was predicted to be proportional to the applied field for $M<M_s$,

resulting in a linear M-H loop. The measured loops of transversely field annealed samples with well developed anisotropy were very close to linear, as illustrated in figure 5.1.

b) The engineering magnetostriction measured at saturation, λ_e, of samples field annealed at an oblique angle, θ, was predicted to be proportional to $\sin^2(\theta)$. The measured variation of λ_e with θ was found to be very close to this prediction, particularly when moment spread was accounted for.

c) The variation of magnetostriction with applied field was predicted to be quadratic. The best fit fourth order polynomials (even powers only) were found for the measured λ-H loops of transversely field annealed samples. It was found that the second order (quadratic) component was far larger than the fourth order at low H, and that best fit quadratic gave approximately as good a fit as the quartic without significant change in the quadratic coefficient. Hence the measured λ-H loops were very close to quadratic.

d) The variation of magnetostriction with magnetisation was also predicted to be quadratic. The generated λ-M plots were similarly found to be very close to quadratic at low M by finding the best fit even ordered polynomial to the λ-M data. Also, the normalised λ-M curves from samples of all the alloys measured were compared and were found to be similar, indicating that magnetisation occurred by the same processes in each alloy.

7.4 Moment Spread

It has been shown that there is inherent angular spread in the local magnetisation in amorphous ferromagnets, even with uniaxial induced macroscopic anisotropy. This spread is thought to be due to competition between the local anisotropy and exchange interactions. In RE-TM amorphous alloys, this spread can be large due to the magnitude of the local anisotropy, leading to speromagnetism in these materials. The spread is far

smaller in TM based alloys. Nevertheless, significant spread has been measured in field annealed Fe based amorphous alloys using Mössbauer studies. Since magnetostriction and other magnetoelastic phenomena occur due to moment rotation, angular moment spread has a direct effect on them. However, since the majority of these moments are strongly quenched into position by local anisotropy, they do not rotate appreciably, even in high applied fields, and so do not contribute towards the magnetostriction. Thus the apparent spread in the moments which have an effect on the magnetostriction, i.e. those that are able to rotate noticeably within the applied fields, is generally significantly less than the actual spread. It was this spread which was determined by the magnetostriction measurements in this study. This spread can be reduced by partial alignment of the local easy axes by suitable field annealing.

The angular distribution of moments was assumed to be Gaussian, with standard deviation, δ, and the normalised variation of λ_e with θ was derived for a range of δ. By altering the normalising factor to get a good fit to the measured λ_e-θ variation, the value of δ could be estimated, and hence the value of λ_e for $\delta=0$. A similar method could be used with the $\Delta E(H=0)$ data.

Using this method the spread was estimated to be less than 20° in all alloys measured and close to zero in some cases. Judging from the study of λ_e with respect to transverse field annealing conditions, the spread can be reduced to almost zero with sufficient development of the macroscopic anisotropy.

7.5 Comparison of Data with Predictions of Squire Model

The variation of the λ_e data agreed well with the predicted $\sin^2\theta$ relationship. The fit was improved by allowing a distribution in θ. As a result of the random nature of the amorphous structure, all material parameters are better described by distributions rather

than single values. The predictions of the model would therefore be improved by accounting for this. The model is currently being developed to allow for such distributions.

There was a clear discrepancy between the measured and predicted variations of χ_0 with θ. The increase in measured susceptibility with decreasing θ was significantly greater than predicted at low θ. This in turn caused a discrepancy between the measured and predicted values of C_Q. The main reason for this was that the model had assumed a single domain wall movement parameter for all θ. This was not the case. It was found that the walls moved more readily in the samples field annealed at low θ, so increasing the susceptibility. The domain wall parameter was assumed to be a quadratic with respect to distance across the wall. The increased ease of wall movement is due to a lower wall potential quadratic coefficient, *w*. It is possible that this is related to the domain width, which varies depending on the shape demagnetisation factor in the direction of the domain magnetisation.

Another reason for the discrepancy was that the model had not accounted for the coupling of the magnetisation directions between adjacent domains. This coupling meant that the rate of rotation of the domains were the same. This was measured in this study using photographs of Bitter domain patterns and was found to hold in practice. It inherently affected the rate of domain magnetisation rotation and therefore also χ_0. It also suppressed domain moment flipping, which had been permitted in the model and was the cause of the large discontinuities in the predicted E-H variations at high θ. Modifications to the model will be published by P.T. Squire at a later date.

7.6 Development of λ_e with Transverse Anisotropy

The variations of the engineering magnetostriction and magnetostrictive response parameters of transversely field annealed samples of METGLAS 2605S2 and VAC0040 were measured as a function of anneal time for a series of anneal temperatures. The corresponding anisotropy constant was also measured. λ_e and K_u were found to increase to an asymptotic value with increasing t_a for any given T_a. The asymptote, where the parameter becomes fully developed with t_a, is reached faster at higher temperatures, due to the kinetics of the processes of atomic rearrangement. It is well established that the fully developed induced anisotropy constant in field and/or stress annealed amorphous alloys is dependent on the anneal temperature. Higher T_a results in lower K_u due to increased entropy during the anneal. The anneal temperature dependence of K_u is particularly significant in binary alloys where the pair ordering has a predominant effect, but is also seen in single metal materials due to pair ordering of the metalloids.

This temperature dependence was seen in VAC0040, and was in good agreement with that measured by Luborsky and Walter [1977]. The corresponding variation of METGLAS 2605S2 could not be ascertained because the field anneal had to be performed below the Curie temperature, which was so far below the crystallisation temperature that the kinetics were too slow to fully develop K_u within the anneal times used in this study.

As expected, the development of λ_e was also faster at higher anneal temperatures. However, the fully developed value of λ_e at the asymptote was the same for all anneal temperatures. It can therefore be inferred that since λ_e is independent of T_a it is also independent of $K_u(max)$ and therefore of the extent of thermally activated structural disorder. Full moment rotation (of those moments that contribute to the magnetostriction) can be achieved in material with well developed uniaxial anisotropy largely regardless of the degree of SRO.

It was found that for any given anneal temperature, the maximum value of λ_e was attained well before the full development of K_u(max). This implies that there are two kinds of thermally activated processes of structural rearrangement occurring during the field anneal. Both have the effect of inducing anisotropy in the field direction, while only one increases λ_e, i.e. induces moment alignment. The fact that maximum λ_e is attained before maximum K_u points to the fact that the processes which effect change in λ_e generally have a lower activation energy spectrum than the other (although there may be some overlap of the spectra). Since the degree of angular moment spread is thought to arise from competition between local anisotropy and exchange interactions, it can further be inferred that these processes, which result in moment alignment, must therefore cause reduction in the angular spread of local easy axes.

The model for magnetostriction in amorphous ferromagnets proposed by Fähnle *et al* [e.g. 1987, 1990], discussed in chapter 2, was based on the volume average of λ of atomic scale structural units, each with its own anisotropy constant and easy axis direction. In such a structure the macroscopic K_u is developed by two processes. The first is by rotation of the easy axes of the structural units. This does not, of course, entail rotation of the units themselves (which is impossible due to elastic constraints), but occurs due to atomic rearrangements similar to shear transformations, as illustrated in figure 2.2. These atomic rearrangements are generally of the form of small shear deformations, which only cause small changes in the TSRO, and as such tend to have comparatively low activation energies, as discussed in chapter 2. The second process is the increase in the magnitude of the component of K_u in the anneal field direction, mainly due to directional ordering [Luborsky and Walter 1977a and b]. These tend to involve interdiffusion of atoms, involving higher activation energy changes in the CSRO and TSRO.

The value of λ_e reaches its maximum when the measurable moment spread has

been reduced as far as possible. If this spread is due to competition between local anisotropy and magnetisation then this occurs when the spread in easy axis has also reduced, so that the anisotropy and exchange forces act coincidentally to align the moments into the anneal field direction, and it is therefore insensitive to the distribution of magnitude of the local anisotropy constants, and so to K_u. It is thought, therefore, that λ_e was fully developed before K_u because the spread in anisotropy reduced due to rotation of structural unit easy axes. K_u was further increased due to additional increase in directional ordering, which was temperature dependent, especially in the binary alloy. This occurred at a slower rate because of the higher activation energy deformations involved. The value of λ_e(max) occurs at the maximum moment collinearity attainable and so is insensitive to the magnitude of K_u, and therefore it is also independent of T_a.

This provides evidence that the moment spread in amorphous alloys, such as that measured in chapter 4, occurs as a result of competition between anisotropy and exchange forces at a local scale.

The field dependent magnetostrictive response parameters, namely C_q and $\left|\frac{d\lambda}{dH}\right|_{max}$ in this study, are related directly to λ_e and inversely to K_u. The response increases as λ_e approaches its asymptote. After maximum λ_e is attained, continued transverse field annealing has the effect of further increasing K_u, reducing the magnetostrictive response. Hence both C_q and $\left|\frac{d\lambda}{dH}\right|_{max}$ reach a maximum with respect to anneal time, and thereafter decrease to a steady value dictated by the asymptotic values of K_u and λ_e. The optimum response occurs at approximately the stage at which maximum λ_e is attained, before further development of K_u.

The λ-M response parameters, such as C_Q, are not dependent on K_u. These parameters approach an asymptote at notionally the same rate as λ_e, since it is dependent only on this and M_s, which is altered by a negligible amount by the anneals.

7.7 Domain Studies

Domain patterns were obtained using both the Bitter and Kerr methods. Field annealing was shown to produce clear stripe domain patterns. The Bitter technique also showed up secondary domain structures within the main domains, which indicated some angular spread within the domains, implying that the moment correlation length was definitely less than the scale of these domains, ~40μm, in contradiction to the prediction by O'Handley [1987] from the model by Alben *et al* [1978] of a correlation length in TM based amorphous alloys of ~1mm.

Since the secondary walls lay normal to the domain magnetisation direction, it was possible to measure domain surface area and direction of magnetisation, and so calculate the magnetisation in the applied field direction of the photographed region of the ribbon surface. This was done for a series of applied fields enabling a comparison to be made with the measured M-H loops. The agreement was good, although the data from the domain photographs gave higher values of χ by factors of up to 20%. This agreement indicated that the surface domain structure also represented that in the bulk of the material, confirming the basis of the phenomenological model by Squire [1990], as illustrated in figure 2.5. It was also possible, by utilising the orientation of the secondary domain walls, to confirm experimentally that the magnetisation directions of adjacent domains are coupled, so that their rate of rotation of magnetisations, $d\phi/dH$, are constant and equal.

The rate of change of relative area of the domains was measured with respect to applied field using both Kerr and Bitter domain photographs. After accounting for differences in ambient fields and sample shape demagnetisation factors, the two sets of measurements were found to be in close agreement, giving added confidence to the data from the Bitter studies.

7.8 Partial Crystallisation

The manner of the induction of macroscopic anisotropy within the bulk of metallic glass ribbon, perpendicular to the ribbon plane, by the crystallisation of the surface layers was proposed by Ok and Morrish [1981]. This was used as the basis of a model by Herzer and Hilzinger [1986] which predicted the relationship between both the induced anisotropy and the coercivity with the extent of crystallisation, and compared these predictions with measurements on METGLAS 2605S2. It predicted that K_u is proportional to it, and that H_c varies quadratically for very small amounts of crystallisation, but then deviates from this at increased crystallisation, to approximately a linear relationship.

Samples of METGLAS 2605S2, VAC7505 and VAC0040 were subjected to anneals to induce partial crystallisation. The extent of crystallisation was gauged by the height and area of the <200> α-Fe X-ray diffraction peak on the wheel cooled side of the ribbon. Both K_u and H_c were found to vary approximately linearly with the degree of crystallisation in fully stress relieved samples, implying surface crystallised layers of up to approximately 2-3μm thick in ribbons of ~25μm thickness. The high degree of proportionality between X-ray peak height and area in the samples measured implied that crystallisation proceeded predominantly by crystallite nucleation rather than growth. The crystallites were highly textured and occurred mainly on the air-cooled side of the ribbon, in contrast to the finding of Ok and Morrish [1981] where crystallisation was seen to occur mainly on the wheel-cooled side.

The variation of magnetostriction and magnetostrictive response parameters were presented as functions of coercivity, representing the degree of crystallisation. λ_e was found to increase rapidly with increase in H_c, reaching its maximum value at ~20Am^{-1}. A slight decrease was seen with additional increase, but this was because the anisotropy

became so high that the magnetostriction measurement rig was unable to fully saturate the samples. Maxima were seen in the variations of C_q and $\left|\frac{d\lambda}{dH}\right|_{max}$ with respect to H_c for similar reasons to those for the transversely field annealed samples. That is, maximum λ_e was attained after a relatively small degree of crystallisation, at which K_u was of the order of $300Jm^{-3}$ and $100Jm^{-3}$ in METGLAS 2605S2 and VAC0040 respectively. Thereafter, further crystallisation induced higher K_u, reducing the response. The maximum response approximately coincided with the attainment of maximum λ_e.

It should be stressed that the moment alignment in these samples was caused by the reduction of angular spread of easy axes of structural units by the introduction of a tensile stress within the material, rather than by thermally activated structural rearrangement within an applied field.

λ-M loops showed that the point at which maximum λ_e was achieved also coincided with the stage at which magnetisation by way of domain wall movement became insignificant, and that the magnetisation occurred predominantly by moment rotation. At this stage the moments had become fully aligned perpendicular to the ribbon plane due to the anisotropy induced by the stress field set up between the crystallised surface layers.

The maximum λ_e achieved by this method was very close to that attained by transverse field annealing, particularly in the case of METGLAS 2605S2. The anisotropy was higher a factor of the order of five. It was concluded that controlled partial crystallisation is a viable method for controlling and optimising the magnetostriction and magnetostrictive response in these materials (see also section 7.9).

7.8.1 Nanocrystallisation

Measurements of λ_e and K_u were made on samples of $Fe_{79}Si_{13}B_6Cu_1Nb_1$ with respect to anneal temperature (t_a=60 mins.). Anneals performed on this alloy produce crystallisation with very small grain size, i.e. nanocrystallisation. These measurements ascertained that λ_e is reduced to less than 0.5ppm (compared with ~30ppm in the as cast state) when nanocrystallisation is induced. It was also found that H_c is increased slightly by the nucleation of the nanocrystallites from that of the stress relieved state. However, H_c increases dramatically when annealed at T_a>600°C, due to crystallisation of the amorphous Fe-Nb-B phase between the nanocrystallites. These findings were in general agreement with those on $Fe_{73.5}Si_{13.5}B_9Cu_1Nb_3$ by Yoshizawa *et al* [1988] and Herzer [1990].

7.9 Optimum Route for Transducer Applications

The maximum magnetostrictive response was achieved on the transversely field annealed Fe-based samples (METGLAS 2605SC and 2605S2). This was a direct result of their high magnetostriction and very low K_u. In the case of METGLAS 2605S2, the maximum λ-H response parameters resulted from a transverse field anneal which attained a value of λ_e of approximately 45ppm and a K_u of $20Jm^{-3}$, i.e. the engineering magnetostriction was relatively high, but below the maximum that was attainable because the optimum conditions were a trade off between development of λ_e and K_u, which had opposite effects on the response. (This is not the case with the maximum λ-M response. Hence the maximum coincided with that of λ_e). A disadvantage with this heat treatment was that the response was highly sensitive to slight variations in it. Annealing for a long time, where both λ_e and K_u have reached their asymptotic values would have the effect

of improving consistency and stability. The optimum anneal temperature would then be the maximum possible, due to the decrease in K_u with increase in T_a, although this would have a small effect in the case of Fe-only, single-metal glasses. This temperature would normally be just below T_c, except in alloys where T_c and T_x are so close that annealing near T_c would cause partial crystallisation and a degradation of the soft magnetic properties of the material. In METGLAS 2605S2 this entailed a reduction in the values of $\left|\frac{d\lambda}{dH}\right|_{max}$ and C_q from the maximum values by a factor of approximately 2 and 10 respectively.

For similar reasons to the field annealed material, the highest magnetostrictive response of the partially crystallised material was measured on the Fe-based alloys, namely METGLAS 2605S2 and VAC7505. Again, this maximum occurred before the maximum value of λ_e had been attained. Both C_q and $\left|\frac{d\lambda}{dH}\right|_{max}$ were of the order of half the corresponding maximum values of the field annealed material. However, both parameters were highly sensitive to variations in H_c, which can be very difficult to control when annealing. The response parameters decreased rapidly with increasing H_c, as did their sensitivity to variations in it. Measurements of the parameters had good repeatability and low errors at the stage where H_c was approximately $30Am^{-1}$. The reduction in C_q and $\left|\frac{d\lambda}{dH}\right|_{max}$ from the maximum values where of the order of 10-20 in both cases.

Consequently, transverse field annealing near T_c long enough to fully develop both λ_e and K_u at that temperature is considered to be the heat treatment to achieve the optimum stable magnetostrictive response parameters, for maximum transducer sensitivity.

A disadvantage of the very low K_u is that the response of the material becomes very sensitive to stresses. In practice, the samples must be fixed down in a practical transducer system. It would be likely that the stresses caused by this constraint could seriously degrade the response parameters of the material. Bucholtz *et al* [1987] measured the effective λ-H quadratic coefficient of METGLAS 2605S2 in their bulk optic

Michelson interferometer magnetostriction measurement system. This involved winding and bonding the ribbon into a multilayered toroid, and bonding an optical fibre around it's circumference, as shown in figure 2.10, followed by a field anneal along the toroid axis. They obtained a maximum value of $\sim 3\times10^{-10}A^{-2}m^2$ after field annealing at 400°C for 30 minutes. The value of C_q measured on an unconstrained sample in this study after a similar heat treatment was $\sim 1\times10^{-8}A^{-2}m^2$. Thus, the process of forming the ribbon into a transducer configuration can have a serious effect on its response parameters.

The stress induced anisotropy in the partially crystallised samples was approximately an order of magnitude greater than that in the field annealed samples, so the stresses due to bonding of the samples are expected to have a proportionately smaller effect on the susceptibility, and on the magnetostrictive response. M-H loops were measured on a typical transversely field annealed and a partially crystallised sample of VAC7505. The samples were then bonded to a glass slide and the M-H loops were remeasured, shown in figure 7.1. It can be seen that although the susceptibility is lower in the partially crystallised sample, the bonding of the sample has little effect on it, whereas the change in the bonded field annealed sample is more pronounced. Although this illustration does not account for the reduction in C_q of a factor of 300 (from the measurements in this study and in Bucholtz *et al*), it acts as an illustration of the stability of partially crystallised TM-M bonded samples.

This is a method for obtaining a magnetostrictive strain close to the maximum attainable in samples of Fe-based alloys, with K_u greater than that attainable by field annealing any TM-M alloy, so greater stability to bonding. RE-TM alloys exhibit higher λ_e and K_u, but lower magnetostrictive response, particularly at low applied fields. Partially crystallised samples therefore provide the highest magnetostrictive response in low field transducer applications where this degree of stability is required.

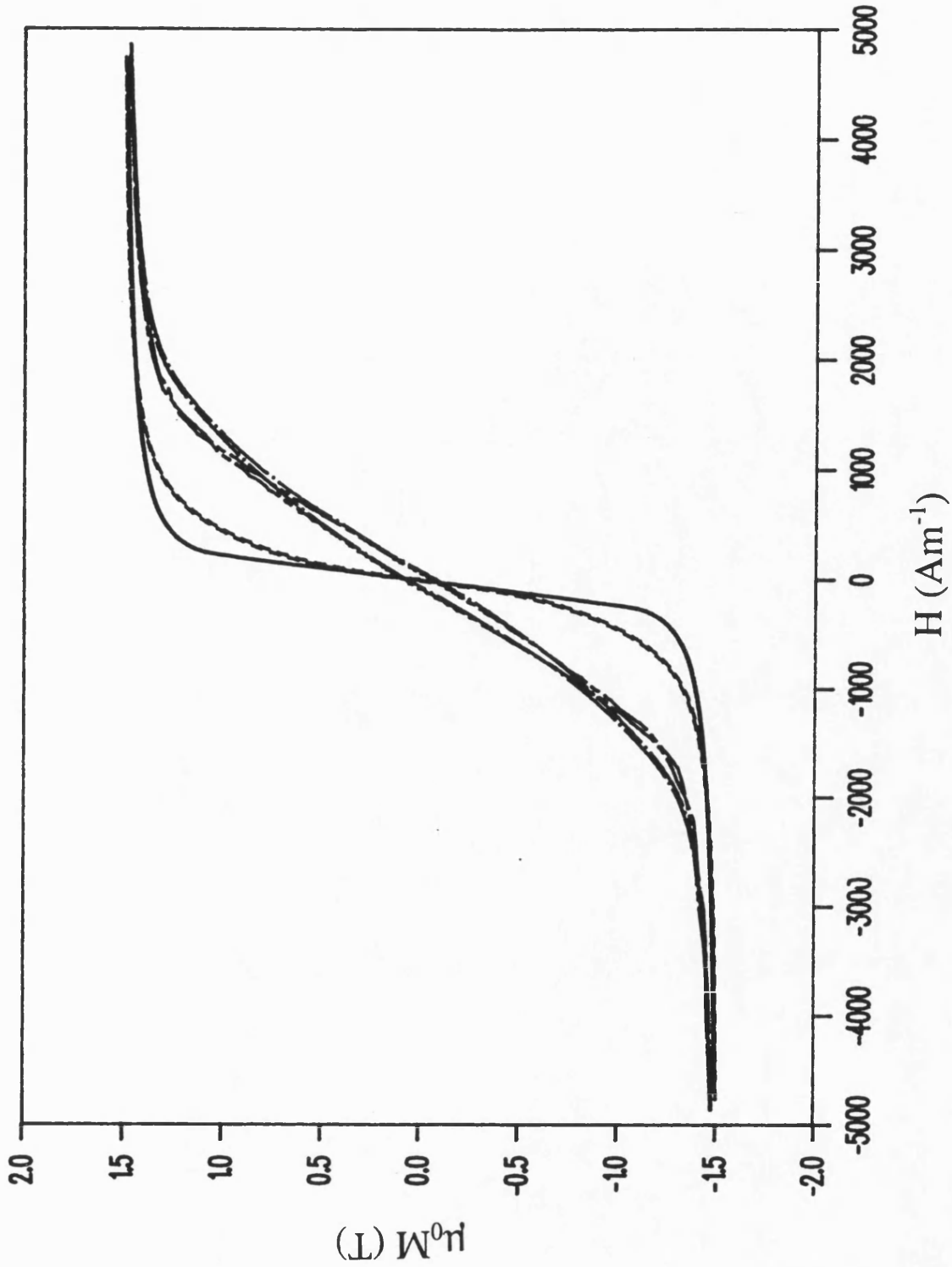

Figure 7.1: M-H loops for transversely field annealed and partially crystallised VAC7505, before and after bonding the samples to glass slides.

(Field annealed; unbonded - ——, bonded - - - - -. Partially crystallised; unbonded - — - —, bonded - — · —)

7.10 Summary

The magnetostriction and magnetostrictive parameters of samples of several Fe and Fe-Ni based amorphous alloys have been measured using an optical fibre dilatometer system. The values of λ_e obtained were significantly higher than corresponding measurements by other workers using a variety of methods.

It is established that magnetostriction occurs by distortion of the structure by rotation of the electron shells due to moment rotation of the unpaired electrons. It was shown that magnetisation occurs predominantly by moment rotation, rather than by domain wall movement, in material with transverse uniaxial anisotropy induced by field annealing, so enabling maximum λ_e to occur.

Maximum λ_e is achieved by coherent rotation of all moments into the applied field direction from some direction normal to it. This occurs when all moments are aligned normal to this direction by the induction of a macroscopic anisotropic magnetic easy axis. The spread of moments about this axis at a local level was discussed, and evidence was presented indicating that this spread is greater, and the moment correlation length is shorter, than previously predicted. The effect of moment spread on the magnetostriction was discussed. The apparent spread in moments contributing to the magnetostriction is significantly less than the actual spread, which has been shown to be substantial, even at low temperatures and high applied fields. It was shown that this apparent spread can be reduced to almost zero by suitable heat treatment, such as field annealing, maximising the magnetostriction.

The variation of λ_e and K_u were measured with respect to field annealing conditions. It was concluded that K_u was developed by both the alignment of local easy axes by shear deformations of the local structural units, and by increased directional pair ordering. The former process caused moment alignment, so increasing λ_e in material with

transversely induced anisotropy. This process had a lower activation energy spectrum than the latter, so λ_e was fully developed before K_u.

Magnetostrictive response parameters, namely λ-H and λ-M quadratic coefficients, and $\left|\frac{d\lambda}{dH}\right|_{max}$ were measured with respect to field anneal conditions, and the optimum heat treatments ascertained. Attainment of maximum response in field annealed material was found to be a trade off between the development of λ_e and K_u, which have opposite effects on it.

Partial crystallisation of the surface layers of metallic glasses induced a macroscopic magnetic anisotropy perpendicular to the ribbon plane due to tensile stress fields set up between the crystallised surface layers. This was shown to maximise λ_e, without having significantly detrimental effect on the magnetic softness. Moreover, the magnetostrictive response of partially crystallised material is less sensitive to external stresses, and so potentially more stable in a practical transducer configuration than other field annealed TM-M glasses. Therefore partial crystallisation was shown to be a viable alternative to field annealing as a route to treatment of metallic glass for transducer applications.

Measurements were made that confirmed the findings that nanocrystallisation of Fe based glasses (with Nb and Cu additives to suppress crystallite growth) caused significant decrease in λ_e, while maintaining very low coercivity and other soft magnetic properties.

References

Alben R., J.J. Becker and M.C. Chi, "Random anisotropy in amorphous ferromagnets", *J. Appl. Phys.*, 49 (1978) 1653.

Allia P. and F. Vinai, "New approach to the study of the magnetic permeability aftereffect of amorphous ferromagnetic alloys", *Phys. Rev. B*, 26 (1982) 6141.

Allia P., G.P. Soardo and F. Vinai, "Magnetic permeability after-effect and structural defects of amorphous ferromagnetic alloys", *J. Magn. Magn. Mat.*, 31-34 (1983) 1571.

Anderson P.M., "Magnetomechanical Coupling, ΔE effect, and permeability in FeSiB and FeNiMoB alloys", *J. Appl. Phys.*, 53 (1982) 8101.

Arai K.I. and N. Tsuya, "Magnetomechanical coupling and variable delay characteristics by means of giant ΔE effect in iron rich amorphous ribbon", *J. Appl. Phys.*, 49 (1978) 1718.

Aur S., T. Egami, A.E. Berkowitz and J.L..Walter, "Atomic structure of amorphous particles produced by spark erosion", *Phys. Rev. B*, 26 (1982) 6355.

Barandiarán J.M., M. Vazquez, A. Hernando, J. Gonzalez and G. Rivero, "Distribution of the magnetic anisotropy in amorphous alloys ribbons", *IEEE Trans. Magn.*, MAG-25 (1989) 3330.

Becker J.J., "A new mechanism for magnetic annealing in amorphous metals", *IEEE Trans. Magn.*, MAG-14 (1978) 938.

Berger L., "Magnetostriction in nickel alloys", *Phys. Rev.*, 138A (1965) 1083.

Bernal J.D. and J. Mason, "Coordination of randomly packed spheres", *Nature*, 188 (1960) 910.

Berry B.S. and W.C. Pritchet, "Vibrating reed internal friction apparatus for films and foils", *IBM J. Res. Develop.*, 19 (1975) 334.

Berry B.S. and W.C. Pritchet, "Magnetoelastic phenomena in amorphous alloys", *A.I.P. Conf. Proc.*, 34 (1976) 292.

Berry B.S. and W.C. Pritchet, "Influence of the magnetomechanical pole effect on the behaviour of thin vibrating reeds", *J. Appl. Phys.*, 50 (1979) 1630.

Beuerle T. and M. Fähnle, "Theory of magnetostriction in amorphous ferromagnets: Influence of non-local elastic behaviour", *J. Magn. Magn. Mat.*, 88 (1990) 7.

Brizzolara R.A., R.J. Colton, M. Wun-Fogle, H.T. Savage, "A tunneling-tip magnetometer", *Sensors and Actuators*, 20 (1989) 199.

Brizzolara R.A. and R.J. Colton, "Magnetostriction measurements using a tunneling-tip strain detector", *J. Magn. Magn. Mat.*, 88 (1990) 343.

Bucholtz F., K.P. Koo, G.H. Sigel and A. Dandridge, "Optimisation of the fibre/metallic glass bond in fibre-optic magnetic sensors", *J. Lightwave Technol.*, LT-3 (1985) 814.

Bucholtz F., K.P. Koo, A. Dandridge and G.H. Sigel, "Easy axis distributions in transversely annealed Metgles 2605S2", *J. Magn. Magn. Mat.*, 54-57 (1986) 1607.

Bucholtz F., K.P. Koo, A.M. Yurek, J.A. McVicker and A. Dandridge, "Preparation of amorphous metallic glass transducers for use in fibre optic magnetic sensors", *J. Appl. Phys.*, 61 (1987) 3790.

Butler D., R.D. Greenough and K.C. Pitman, "Magnetisation and magnetostriction of rapidly quenched rare earth-iron-boron alloys", *J. de Phys.*, 49 (1988) C8-1341.

Callen E. and H.B. Callen, "Static magnetoelastic coupling in cubic crystals", *Phys. Rev. B*, 129 (1963) 578; "Magnetostriction, forced magnetostriction, and anomalous thermal expansion in ferromagnets", *Phys. Rev. A*, 139 (1965) 455.

Cargill G.S., "Structural investigation of noncrystalline nickel-phosphorus alloys", *J. Appl. Phys.*, 41 (1970) 12.

Cargill G.S., "Structure of metallic alloy glasses", *Solid St. Phys.*, 30 (1975) 227.

Cargill G.S. and T. Mizoguchi, "Dipolar mechanisms for magnetic anisotropy in amorphous ferrimagnetic alloys", *J. Appl. Phys.*, 49 (1978) 1753.

Chambron W. and A. Chamberod, "Kinetics of induced magnetic directional order in a $Fe_{40}Ni_{40}P_{14}B_6$ amorphous alloy", *Solid St. Comm.*, 33 (1980) 157; "Reversible enhancement of magnetic directional ordering rate associated with quenched-in defects, in an amorphous $Fe_{40}Ni_{38}Mo_{41}B_8$ alloy", *Solid St. Comm.*, 35 (1980) 61.

Chen C.-W., Magnetism and Metallurgy of Soft Magnetic Materials, (Dover Publications, New York, 1986).

Clark A.E. and M. Wun-Fogle, "A new method of magnetostrictivity and magnetostriction measurement", *IEEE Trans. Magn.*, MAG-25 (1989) 3611.

Coey J.M.D., "Amorphous Magnetic Order", *J. Appl. Phys.*, 49 (1978) 1646.

Cowley R.A., N. Cowlam and L.D. Cussens, "A non-collinear magnetic structure for the amorphous ferromagnet, $Fe_{83}B_{17}$", *J. de Phys.*, 49 (1988) C8-1285.

Cowley R.A. ILL Annual Report, 1988; Private Communication to M.R.J. Gibbs (1990).

Cullity B.D., Introduction to Magnetic Materials (Addison-Wesley, Reading, MA, USA, 1972).

Datta A., D. Nathasingh, R.J. Martis, P.J. Flanders and C.D. Graham Jr., "Saturation and engineering magnetostriction of an iron-base amorphous alloy for power applications", *J. Appl. Phys.*, 55 (1984) 1784.

Durand J., *J. de Phys.*, 41 (1980) C8-609.

Durand J. and P. Panissod, "Investigations of the atomic-scale structure of amorphous metallic alloys by means of bulk and local magnetic measurements", *IEEE Trans. Magn.*, MAG-17 (1981) 2595.

Egami T., "Structural relaxation in amorphous $Fe_{40}Ni_{40}P_{14}B_6$ studied by energy dispersive X-ray diffraction", *J. Mat. Sci.*,13 (1978) 2587.

Egami T., "Structure and Magnetism of amorphous alloys", *IEEE Trans. Magn.*, MAG-17 (1981) 2600.

Egami T., "Magnetic amorphous alloys: physics and technological applications", *Rep. Prog. Phys.*, 47 (1984) 1601.

Fähnle M., Private Communication to M.R.J. Gibbs (1990).

Fähnle M. and H. Kronmüller, "The influence of spatially random magnetostatic, magnetocrystalline, magnetostrictive and exchange fluctuations on the law of approach to ferromagnetic saturation of amorphous ferromagnets", *J. Magn. Magn. Mat.*, 8 (1978) 149.

Fähnle M. and Egami T., "Phenomenological theory of magnetostriction in amorphous ferromagnets", *J. Appl. Phys.*, 53 (1982) 2319.

Fähnle M. and J. Furthmüller, "Various contributions to magnetostriction in amorphous and polycrystalline ferromagnets", *J. Magn. Magn. Mat.*, 72 (1988) 6.

Fähnle M. and J. Furthmüller, "On the change of magnetostriction by field annealing of amorphous ferromagnetic alloys", *Phys. Stat. Sol. (a)*, 117 (1990) K71.

Fähnle M., J. Furthmüller, R. Pawellek, T. Beuerle and C. Elsässer, "Magnetostriction in amorphous ferromagnets: theory and interpretation of experiments", *Proc. 5th Int. Conf. Physics of Magnetic Materials*, Madralin near Warsaw, Poland (World Scientific, 1990) 204.

Fujimori H., Y. Obi, T. Masumoto and H. Saito, "Soft ferromagnetic properties of some amorphous alloys", *Mater. Sci. Engng.*, 23 (1976) 281.

Furthmüller J., M. Fähnle and G. Herzer, "Theory of magnetostriction in amorphous and polycrystalline ferromagnets", *J. Phys. F*, 16 (1986) L255.

Furthmüller J., M. Fähnle and G. Herzer, "Theory of magnetostriction in amorphous and polycrystalline ferromagnets", *J. Magn. Magn. Mat.*, 69 (1987) 79, 89.

Gang Xiao and C.L. Chien, "Nonuniqueness of the state of amorphous pure iron", *Phys. Rev. B*, 35 (1987) 8763.

Garoche P. and A.P. Malozemoff, "Approach to magnetic saturation in sputtered amorphous films: Effects of structural defects, microscopic anisotropy, and surface roughness", *Phys. Rev. B*, 29 (1984) 226.

Gibbs M.R.J., "Anisotropy and magnetostriction in amorphous compounds", *J. Magn. Magn. Mat.*, 83 (1990a) 329.

Gibbs M.R.J., "The effect of large spread in moment directions on anisotropy and magnetostriction in amorphous alloys", *Proc. 5th Int. Conf. Physics of Magnetic Materials*, Madralin near Warsaw, Poland (World Scientific, 1990b) 242.

Gibbs M.R.J., J.E. Evetts and J.A. Leake, "Activation energy spectra and relaxation in amorphous materials", *J. Mat. Sci.*, 18 (1983) 278.

Gibbs M.R.J., N.G. Pace and D.W. Rees, "Metallic glasses for sonar applications", *Proc. IEE Colloquium - New Materials for Sonar Transducers* IEE Digest No. 1986/60 (1986) 2/1.

Gibbs M.R.J., P.T. Squire, D. Brugel, S.C. Hardy and J. Willson, "Magnetostrictive response of metallic glasses", *J. Appl. Phys.*, 61 (1987) 3784.

Gibbs M.R.J., P.T. Squire, A. Hayes and J.H. Vincent, "Optimisation of magnetostriction in metallic glasses", *J. Appl. Phys.*, 64 (1988) 5419.

Gibbs M.R.J. and P.T. Squire, (Chapter 11 - Applications) Sensors vol.5; Magnetic Sensors (Ed. R. Boll and K.J. Overshott) (VCH Publishers Inc., New York, 1989)

Gyorgy E.M., Metallic glasses, Eds. J.J. Gilman and H.J. Leamy (ASM, Metals Park, OH, USA) (1978) 275.

Hasegawa R., R.C. O'Handley, L.E.Tanner, R. Ray and S. Kavesh, "Magnetisation, magnetic anisotropy, and domain patterns of $Fe_{80}B_{20}$ glass", *Appl. Phys. Lett.*, 29 (1976) 219.

Hasegawa R. and R. Ray, "Iron-boron metallic glasses", *J. Appl. Phys.*, 49 (1978) 4174.

Hernando A., M. Vázquez, V. Madurga, E. Ascasibar and M. Liniers, "Influence of the anisotropy on the SAMR method for measuring magnetostriction in amorphous ribbons", *J. Magn. Magn. Mat.*, 61 (1986) 39.

Hernando A., M. Vázquez and J.M. Barandiarán, "Metallic glasses and sensing applications", *J. Phys. E*, 21 (1988) 1129.

Hernando A., M. Vázquez and G. Rivero, "Amorphous soft magnetic materials: Magnetostriction and induced anisotropies", *IEEE Trans. Magn.*, MAG-27, to be published (1991).

Herzer G., "Grain structure and magnetism of nanocrystalline ferromagnets", *IEEE Trans. Magn.*, MAG-25 (1989) 3327.

Herzer G., "Grain size dependence of coercivity and permeability in nanocrystalline ferromagnets", *IEEE Trans. Magn.*, MAG-26 (1990) 1397.

Herzer G. and H.R. Hilzinger, "Surface crystallisation and magnetic properties in amorphous iron rich alloys", *J. Magn. Magn. Mat.*, 62 (1986) 143.

Hodson P.D., "Magnetic property control in ferromagnetic amorphous alloys" PhD Thesis, University of Cambridge (1986)

Hygate G. and M.R.J. Gibbs, "Structural relaxation in metallic glasses: reversible and irreversible changes in a two-level systems model", *J. Phys. F*, 17 (1987) 815.

Ishio S. and F. Sato, *Japan J. Magn. Soc.*, 12 (1988) 259.

Ishio S. and S. Kadowaki, "magnetostriction of amorphous rare-earth-iron alloys", *J. Magn. Magn. Mat.*, 79 (1989) 358.

Ito A., E. Torika, S. Morimoto, K. Shiiki and M. Kudo, "Mössbauer study of the directional distribution of the local magnetisation axis in amorphous $(Co_{0.94}Fe_{0.06})_{74.5}Si_{13.51}B_2$ alloy", *Proc. 4th Int. Conf. on Rapidly Quenched Metals*, (1981) 1101.

Jagielinski T., "Magnetostriction and magnetoelastic effects in certain amorphous alloys", *IEEE Trans. Magn.*, MAG-17 (1981) 2825.

Jagielinski T., "Elimination of disaccomodation in zero-magnetostrictive FeCoSiB amorphous alloys", *J. Appl. Phys.*, 53, (1982) 7852.

Jergel M., G. Vlasak and P. Duhaj, "Magnetostriction study of some Co-based and Fe-based amorphous alloys", *Phys. Stat. Sol. (a)*, 111 (1989) 597.

Kabacoff L.T., "Thermal,magnetic, and magnetomechanical properties of METGLAS 2605 S2 and S3", *J. Appl. Phys.*, 53 (1982) 8098.

Kaneyoshi T. and I. Tamura, "The distribution of magnetic moments and the temperature dependence of reduced hyperfine fields in amorphous ferromagnets", *Phys. Stat. Sol. (b)*, 123 (1984) 525.

Kittel C., "Physical theory of ferromagnetic domains", *Rev. Mod. Phys.*, 21 (1949) 541.

Klokholm E., "The measurement of magnetostriction in ferrommagnetic thin films", *IEEE Trans. Magn.*, MAG-12 (1976) 819.

Kraus L.,"A novel method for measurement of the saturation magnetostriction of amorphous ribbons", *J. Phys. E*, 22 (1989) 943.

Krey U., S. Krompiewski and U. Krauss, "Itinerant magnetism and spin glass states of iron rich amorphous alloys", *J. Magn. Magn. Mat.*, 86 (1990).

Kronmüller H., "Theory of the coercive field in amorphous ferromagnetic alloys", *J. Magn. Magn. Mat.*, 24 (1981a) 159.

Kronmüller H., "Micromagnetism and microstructure of amorphous alloys", *J. Appl. Phys.*, 52 (1981b) 1859.

Kronmüller H., H.-Q. Guo, W. Fernengel, A. Hofmann and N. Moser, "Activation energy spectra of induced anisotropy and coercive field in amorphous ferromagnetic $Co_{58}Ni_{10}Fe_5Si_{11}B_{16}$", *Cryst Latt. Def. and Amorph. Mat.*, 11 (1984) 135.

Lachowicz H.K. and H. Szymczak, "Magnetostriction of amorphous magnetic material", *J. Magn. Magn. Mat.*, 41 (1984) 327.

Leamy H.J., S.D. Ferris, G. Norman, D.C. Joy, R.C. Sherwood, E.M. Gyorgy and H.S. Chen, "Ferromagnetic domain structure of metallic glasses", *Appl. Phys. Lett.*, 26 (1975) 259.

Lemcke M., "Metallographic examination of soft magnetic glasses", *Struers Metallographic News* (Copenhagen), 3/89 (1989) 13.

Liniers M., V. Madurga, M Vázquez and A. Hernando, "Magnetostrictive torsional strain in transverse field annealed METGLAS 2605", *Phys. Rev. B*, 31 (1985) 4425.

Livingston J.D., "Stresses and magnetic domains in amorphous metal ribbons", *Phys. Stat. Sol. (a)*, 56 (1979) 637.

Livingston J.D., "Magnetomechanical properties of amorphous metals", *Phys. Stat. Sol. (a)*, 70 (1982) 591.

Livingston J.D., "Magnetic domains, anisotropies, and properties of amorphous metals", Amorphous Metals and Semiconductors, Acta-Scripta Metallurgica Proc. Vol. 3, Ed. P. Haasen and R.I. Jaffee (Pergamon Press, Oxford) (1985) 212.

Livingston J.D., W.G. Morris and F.E. Luborsky, "Domain studies on amorphous ribbons with transverse or oblique magnetic anisotropy", *J. Appl. Phys.*, 53 (1982) 7837.

Livingston J.D. and W.G. Morris, "Magnetic domains in twisted amorphous ribbons", *IEEE Trans. Magn.*, MAG-20 (1984) 1379.

Livingston J.D. and W.G. Morris, "Magnetic domains in amorphous metal ribbons", *J. Appl. Phys.*, 57 (1985) 3555.

Lord D., Private Communication (IEE current research meeting, Preston, November 1988).

Luborsky F.E.(Ed.), Amorphous Metallic Alloys, (Butterworths, London) (1983).

Luborsky F.E. and J.L. Walter, "Magnetic anneal anisotropy in amorphous alloys", *IEEE Trans. Magn.*, MAG-13 (1977a) 953.

Luborsky F.E. and J.L. Walter, "Magnetically induced anisotropy in amorphous alloys of Fe-Ni-P-B", *IEEE Trans. Magn.*, MAG-13 (1977b) 1635.

Melamud M., L.J. Swartzendruber, L.H. Bennet, J. Cullen and M. Wun-Fogle, "Moment distribution in amorphous magnetic ribbons by Mössbauer measurements", *J. Appl. Phys.*, 61 (1987) 3644.

Methasiri T. and I.M. Tang, "Mössbauer studies on annealed $Fe_{81}B_{13.5}Si_{3.5}C_2$ amorphous ribbons", *Physica*, 133B (1985) 37.

Methasiri T., J.R. Cullen and I.M. Tang, "Mössbauer study of the in-plane anisotropy in annealed amorphous $Fe_{81}B_{13.5}Si_{3.5}C_2$ (METGLAS 2605SC) ribbons", *J. Magn. Magn. Mat.*, 53 (1985) 229.

Modzelewski C., H.T. Savage, L.T. Kabacoff and A.E. Clark, "Magnetomechanical coupling and permeability in transversely annealed METGLAS 2605 alloys", *IEEE Trans. Magn.*, MAG-17 (1981) 2837.

Moorjani K. and J.M.D. Coey, Magnetic glasses (Elsevier, Amsterdam) (1984).

Müller M., L. Illgen, H. Grahl, M. Barth and N. Mattern, "The influence of the composition of nanocrystalline FeSiB-CuNb soft magnetic alloys", *IEEE Trans. Magn.*, MAG-27, to be published (1991).

Narita K., J. Yamasaki and H. Fukunaga, "Saturation magnetostriction and its behaviour of $Fe_{100-x}B_x$ $Co_{100-x}B_x$ amorphous alloys", *J. Appl. Phys.*, 50 (1979) 7591.

Narita K., J. Yamasaki and H. Fukunaga, "Measurement of saturation magnetostriction of a thin amorphous ribbon by means of small-angle magnetisation rotation", *IEEE Trans. Magn.*, MAG-16 (1980) 435.

Nayar P.K.K. and I.S. Batra, "On the structural aspects of magnetism in transition metal-metalloid amorphous alloy", *J. Magn. Magn. Mat.*, 87 (1990) 357.

Néel L., *J. Phys. Rad.*, 15 (1954) 225.

Nielson O.V., "Effects of longitudinal and torsional stress annealing on the magnetic anisotropy in amorphous ribbon materials", *IEEE Trans. Magn.*, MAG-21 (1985) 2008.

Nowick A.S. and B.S. Berry, Anelastic Relaxation in Crystalline Solids (Academic Press, New York, 1972).

Núñez de Villavivencio C., M. Vázquez, V. Madurga and A. Hernando, "A new, simple measurement of the magnetostriction constant in metallic glass ribbons", *J. Magn. Magn. Mat.*, 59 (1986) 333.

O'Dell T.H., "Measurement of magnetomechanical coupling factor in amorphous ribbons", *Phys. Stat. Sol. (a)*, 74 (1982) 565.

O'Handley R.C., "Domain wall kinetics in soft ferromagnetic metallic glasses", *J. Appl. Phys.*, 46 (1975) 4996.

O'Handley R.C., "Magnetostriction of ferromagnetic metallic glasses", *Solid State Comm.*, 21 (1977a) 1119.

O'Handley R.C., "Temperature dependence of magnetostriction in $Fe_{80}B_{20}$ glass", *Solid State Comm.*, 22 (1977b) 485.

O'Handley R.C., "Magnetostriction of transition-metal-metalloid glasses: Temperature dependence", *Phys. Rev. B*, 18 (1978) 930.

O'Handley R.C., "Physics of ferromagnetic amorphous alloys", *J. Appl. Phys.*, 62 (1987) R15.

O'Handley R.C., R. Hasegawa, R. Ray and C.-P. Chou, "Ferromagnetic properties of some new metallic glasses", *Appl. Phys. Lett.*, 29 (1976) 330.

O'Handley R.C. and L. Berger, "Evidence supporting the split-band model from magnetostrictions of transition metal/metalloid glasses", *Inst. Phys. Conf. Ser. No. 39* (1978) 477.

O'Handley R.C. and M.O. Sullivan, "Magnetostriction of $Co_{80-x}T_xB_{20}$ (T=Fe, Mn, Cr, or V) glasses", *J. Appl. Phys.*, 52 (1981) 1841.

O'Handley R.C. and N.J. Grant, "Magnetostriction and short-range order of amorphous alloys", Rapidly Quenched Metals, Ed. S. Steeb and H. Warlimont (Elsevier) (1985) 1125.

Hang Nam Ok and A.H. Morrish, "Origin of the perpendicular anisotropy in amorphous $Fe_{82}B_{12}Si_6$ ribbons", *Phys. Rev. B*, 23 (1981) 2257.

Hang Nam Ok and A.H. Morrish, "Surface crystallisation and magnetic anisotropy in amorphous $Fe_{40}Ni_{38}Mo_4B_{18}$ ribbons", *J. Appl. Phys.*, 52 (1981) 1835.

Osborn J.A., "Demagnetising factors of the general ellipsoid", *Phys. Rev.*, 67 (1945) 351.

Pregger B.A. and J.J. Kramer, "Surface crystallisation of amorphous alloy METGLAS 2826", *IEEE Trans. Magn.*, MAG-25 (1989) 3333.

Rado G.T. and H. Suhl (Eds.), Magnetism I, (Academic press, 1963).

Rees D.W., M.R.J. Gibbs and N.G. Pace, "The use of a metallic glass scroll as an acoustic transducer element", *IEEE Trans. Ultrasonics, ferroelectrics and frequency control*, 36 (1989) 332.

Ryan D.H., J.M.D. Coey, E. Batalla, Z. Altounian and J.O. Ström-Olsen, "Magnetic properties of iron rich Fe-Zr glasses", *Phys. Rev. B*, 35 (1987) 8630.

Sanchez P., E. Lopez, M.C. Sanchez Trujillo and C. Aroca, "Application of the SAMR method to high magnetostrictive samples", *J. Magn. Magn. Mat.*, 75 (1988) 233.

Savage H.T. and M.L. Spano, "Theory and application of highly magnetoelastic METGLAS 2605SC", *J. Appl. Phys.*, 53 (1982) 8092.

Schroeder G., R. Schäfer and H. Kronmüller "Magneto-optical investigation of the domain structure of amorphous $Fe_{80}B_{20}$ alloys", *Phys. Stat. Sol. (a)*, 50 (1978) 475.

Sheard S.M., "Metallic glasses for pulse compression", PhD Thesis, University of Bath (1989).

Sheard S.M., Gao Wei, M.R.J. Gibbs and B. Cantor, "The effects of controlled crystallisation on the magnetic properties of $Fe_{40}Ni_{40}B_{20}$, $Fe_{78}Si_9B_{13}$ and $Co_{58}Ni_{10}Fe_5Si_{11}B_{16}$ metallic glasses", *J. Magn. Magn. Mat.*, 78 (1989) 347.

Smith R.H., G.A. Jones and D.G. Lord, "Domain structures in rapidly annealed $Fe_{67}Co_{18}B_{14}Si_1$", *IEEE Trans. Magn.*, MAG-24 (1988) 1868.

Spano M.L., K.B. Hathaway and H.T. Savage, "Magnetostriction and magnetic anisotropy of field annealed METGLAS 2605 alloys via dc M-H loop measurements under stress", *J. Appl. Phys.*, 53 (1982) 2667.

Squire P.T., "Phenomenological model for magnetisation, magnetostriction and ΔE effect in field annealed amorphous ribbons", *J. Magn. Magn. Mat.*, 87 (1990) 299.

Squire P.T. and M.R.J. Gibbs, "Fibre-optic dilatometer for measuring magnetostriction in ribbon samples", *J. Phys. E*, 20 (1987) 499.

Squire P.T. and M.R.J. Gibbs, "Shear-wave magnetometry using metallic glass ribbon", *Electron Lett.*, 23 (1987) 147.

Squire P.T., S.M. Sheard, C.H. Carter and M.R.J. Gibbs,"Digital M-H plotter for low-coercivity metallic glasses", *J. Phys E*, 21 (1988) 1167.

Squire P.T. and M.R.J. Gibbs, "ΔE effect in obliquely field annealed METGLAS 2605SC", *IEEE Trans. Magn.*, MAG-25 (1989) 3614.

Squire P.T., M.R.J. Gibbs and A.P.Thomas, "Magnetostriction of obliquely annealed metallic glass", *J. Magn. Magn. Mat.*, 83 (1990) 179.

Squire P.T., A.P. Thomas, M.R.J. Gibbs and M. Kuźminski, "Domain studies of field annealed amorphous ribbon", *Proc. Int. Conf. on Magnetism*, to be published (1991).

Suzuki Y. and T. Egami, "Single-ion anisotropy and magnetostriction of amorphous alloys", *J. Magn. Magn. Mat.*, 31-34 (1983) 1549.

Szymczak H., "Dipolar mechanism for magnetostriction in amorphous ferrimagnetic alloys", *IEEE Trans. Magn.*, MAG-14 (1978) 847.

Szymczak H., "Mechanism of stress dependence of saturation magnetostriction in amorphous alloys", *J. Magn. Magn. Mat.*, 67 (1987) 227.

Szymczak H. and R. Zuberek, "Effect of random anisotropy on magnetoelastic properties of amorphous ferromagnetic alloys", *IEEE Trans. Magn.*, MAG-17 (1981) 2843.

Szymczak H. and R. Zuberek, "Field dependence of forced magnetostriction in amorphous alloys", *J. Phys. F*, 12 (1982) 1841.

Szymczak H. and R. Zuberek, "Temperature and field dependence of magnetostriction in amorphous thin films", *J. Magn. Magn. Mat.*, 35 (1983) 149.

Tam A.C. and H. Schroeder, "A new high-precision optical technique to measure magnetostriction of a thin magnetic film deposited on a substrate", *IEEE Trans. Magn.*, MAG-25 (1989) 2629.

Taniguchi S. And M. Yamamoto, *Sci. Rept. Res. Inst. Tokohu Univ.*, A6 (1954) 330; A6 (1955) 269.

Tebble R.S., Magnetic Domains (Methuens, London) (1969) 15.

Tsuei C.C. and H. Lilienthal, "Magnetisation distribution in an amorphous ferromagnet", *Phys. Rev. B*, 13 (1976) 4899.

Tsuya N., K.L. Arai, Y. Shiraga, M. Yamada and T. Masumoto, "Magnetostriction of amorphous $Fe_{0.80}P_{0.13}C_{0.07}$ ribbon", *Phys. Stat. Sol. (a)*, 31 (1975) 557.

Vázquez M., A. Hernando and H. Kronmüller, "Critical exponents of the magnetostriction in amorphous alloys", *Phys. Stat. Sol. (b)*, 133 (1986) 167.

Vázquez M., E. Ascasibar, A. Hernando and O.V. Nielson, "Co-Si-B and Fe-Co-B amorphous alloys: Induced anisotropy and various magnetic properties", *J. Magn. Magn. Mat.*, 66 (1987) 37.

Vázquez M., W. Fernengel and H. Kronmüller, "Approach to magnetic saturation in rapidly quenched amorphous alloys", *Phys. Stat. Sol.*, 115 (1989) 547.

Vonsovsky S.V., *J. Phys. (USSR)*, 3 (1940) 181.

Warlimont H. and H.R. Hilzinger, "Structural interpretation of changes in K_u and λ_s of metallic glasses by annealing", *Proc. 4th Int. Conf. on Rapidly Quenched Metals*, (Sendai, 1981).

Wun-Fogle M., A.E. Clark and K.B. Hathaway, "Permeability in "frozen" high magnetomechanical coupling amorphous ribbons", *J. Magn. Magn. Mat.*, 54-57 (1986) 893.

Yoshizawa Y., S. Ogguma and K. Yamauchi, "New Fe-based soft magnetic alloys composed of ultrafine grain structure", *J. Appl. Phys.*, 64 (1988) 6044.

Závêta K., "Domain structure and magnetic properties of magnetically soft nanocrystalline materials", *IEEE Trans. Magn.*, MAG-27, to be published (1991).

Zijlstra H., Experimental Methods in Magnetism II (North Holland, Amsterdam, 1967).

Appendix - Combination of Errors

Errors in the measurement of variables were generally quoted as the standard deviation of a series of such measurements in this study. Where this was not the case, the method for determining the error in the measured parameter was described in the relevant section.

Where a parameter, z, was obtained by the combination of other parameters, x_1, x_2..., such that

$$z = fn(x_1, x_2 \ldots x_n), \qquad \text{A.1}$$

the error in z, δz, was obtained by using the expression

$$\delta z^2 = \sum_n \delta x_n^2 \left(\frac{\partial z}{\partial x_n} \right)^2 . \qquad \text{A.2}$$

The initial susceptibility was given by the combination of the measured initial susceptibility, χ_{eff} and the demagnetisation susceptibility, χ_d (equation 3.14):

$$\chi_0 = \left(\frac{1}{\chi_{eff}} - \frac{1}{\chi_d} \right)^{-1} . \qquad \text{A.3}$$

Therefore the error in χ_0 was therefore given by

$$\delta\chi_0 = \chi_0^2 \left[\frac{\delta\chi_{eff}^2}{\chi_{eff}^4} + \frac{\delta\chi_d^2}{\chi_d^4} \right]^{\frac{1}{2}} . \qquad \text{A.4}$$

The λ-M quadratic coefficient, C_Q, was given by (equation 3.23)

$$C_Q = \frac{C_{eff}}{\chi_{eff}^2}. \qquad \text{A.5}$$

Therefore the error in C_Q was given by

$$\delta C_Q = C_Q\left[\left(\frac{\delta C_{eff}}{C_{eff}}\right)^2 + \left(\frac{2\delta\chi_{eff}}{\chi_{eff}}\right)^2\right]^{\frac{1}{2}}. \qquad \text{A.6}$$

The maximum λ-H gradient, $\left|\frac{d\lambda}{dH}\right|_{max}$, was given by

$$\left|\frac{d\lambda}{dH}\right|_{max} = \frac{\chi_0}{\chi_{eff}}\left(\left|\frac{d\lambda}{dH}\right|_{max}\right)_{eff}. \qquad \text{A.7}$$

Therefore the error in $\left|\frac{d\lambda}{dH}\right|_{max}$ was given by

$$\delta\left|\frac{d\lambda}{dH}\right|_{max} = \left|\frac{d\lambda}{dH}\right|_{max}\left[\left(\frac{\delta\chi_0}{\chi_0}\right)^2 + \left(\frac{\delta\chi_{eff}}{\chi_{eff}}\right)^2 + \left(\frac{\delta\left(\left|\frac{d\lambda}{dH}\right|_{max}\right)_{eff}}{\left(\left|\frac{d\lambda}{dH}\right|_{max}\right)_{eff}}\right)^2\right]^{\frac{1}{2}}. \qquad \text{A.8}$$

The λ-H quadratic coefficient, C_q, was given in equation 3.22. The error, δC_q, was given by

$$\delta C_q = C_q\left[\left(\frac{\delta C_{eff}}{C_{eff}}\right)^2 + \left(\frac{2\delta\chi_{eff}}{\chi_{eff}}\right)^2 + \left(\frac{2\delta\chi_0}{\chi_0}\right)^2\right]^{\frac{1}{2}}. \qquad \text{A.9}$$